Technische Universität München

TUM School of Life Sciences

Mitochondrial calcium uniporter (MCU), mitochondrial redox biology and polyphenols: a metabolic triad for skeletal muscle health.

Anna Weiser

Vollständiger Abdruck der von der TUM School of Life Sciences der Technischen Universität München zur Erlangung des akademischen Grades einer

Doktorin der Naturwissenschaften (Dr. rer. nat.)

genehmigten Dissertation.

Vorsitz: Prof. Dr. Harald Luksch

Prüfer*innen der Dissertation:
1. Prof. Dr. Hannelore Daniel
2. Prof. Dr. Martin Klingenspor
3. Prof. Dr. Luc van Loon

Die Dissertation wurde am 02.09.2022 bei der Technischen Universität München eingereicht und durch die TUM School of Life Sciences der Technischen Universität München am 28.11.2022 angenommen.

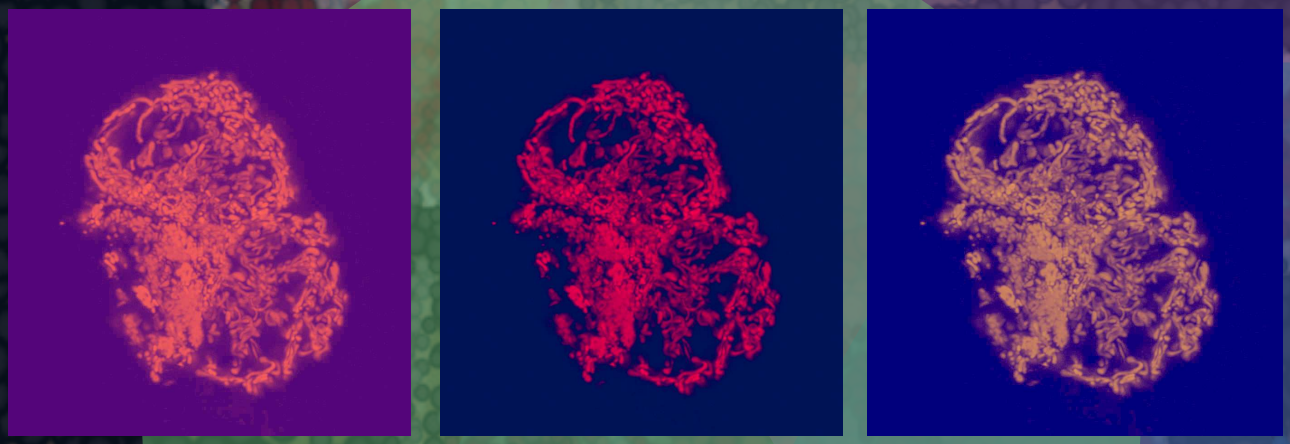

The Mitochondrial Calcium Uniporter (MCU), redox biology and polyphenols: a metabolic triad for skeletal muscle health.

- Anna Weiser -

Preface

The thesis was carried out as part of a cooperation between the Technical University of Munich (TUM) and Nestlé Research Lausanne. The dissertation was supervised by Prof. Hannelore Daniel (TUM) and Dr. Umberto De Marchi (Nestlé Research, Muscle Bioenergetics team). The main work took place at the Nestlé Institute of Health Sciences (NIHS) in Lausanne, with a short stay at the TUM School of Life Sciences under the supervision of Dr. Britta Spanier.

Acknowledgement

A PhD is much more than a written thesis and therefore I would like to thank several people for their incredible support over the years and express my sincere gratitude to you, as this work would not have been possible without you.

Prof. Hannelore Daniel, thank you for your great support before and during the PhD. You are a great source of inspiration and motivation, not only because of your impressive knowledge, but especially because of your genuine integrity, sense of fairness and humor. I will always be grateful to you for giving me the opportunity to go to UCD and participate in the NuGO conference in Bulgaria, and for accepting me as your final PhD student. I have learnt immeasurably from you and although I wish you well in your retirement, I wish you could teach at the university forever. Herzlichen Dank!

Umberto, you taught me to love mitochondrial calcium and redox signaling and were always available for great scientific discussions. I couldn't have found a better supervisor at NIHS than you! Thank you for your patience and confidence in accepting me as a PhD student. Grazie mille!

Britta, you are a great mentor and always a pleasure to talk to about *C.elegans* and other scientific curiosities. Your way of communicating research is very motivating and inspires to think beyond a particular research field. Thank you for letting me come to your lab and enjoy science!

Aurélie, you are a great colleague and great team player. And also, it was always fun to run with you and Astrid. Mercie beaucoup!

Sonia, you are the good soul of the lab. Thank you for your help and for always finding a solution, no matter what the problem is. Merci!

Joris, you often shared the human myoblasts with me. Thanks for being such a great team player!

Flavien, thank you so much for your support, especially during my first year! Mitochondrial isolation will always remind me of you.

Mathieu, mercie for all the discussions about everything in the lab: HSMM, qPCR, Licor, Western blots, Ponceau staining, etc....

Michaël, thank you for being a great colleague and your support in the lab.

Vincenzo, you were a great group leader and brought academic flair to NIHS. It is a shame you have left us, but I am sure you will enjoy your research in Singapore or the Netherlands. Grazie!

Helene, du bist einfach klasse und ich werde dir immer dankbar sein, dass du mich so oft schon unterstützt hast. Danke!

Ambrose, Astrid and Maria, you are by far the best friends anyone could have! I want to thank you from the bottom of my heart for all your support over the years. I have learned so much from you and have had

great adventures with each of you. I look forward to all the adventures that await us in the mountains. Go Raibh Maith Agaibh, hartelijk dank and muchas gracias.

A big thanks goes to the collaborators from the University of Padova. Especially Gaia, who did all the *in vivo* experiments in mice. It was a pleasure to meet you at the EMBO conference in Girona and I hope we will meet again. And thanks to Mattia and Professor Moro for the scientific discussions on protein-ligand interactions.

Thanks to the NIHS team for performing the different screenings of natural bioactive compounds which formed the base of my work.

Thanks to Federico, Eugenia, Robin and Patricia, all of whom were involved in one way or another in the experiments I did during my PhD. And thanks to the entire department.

Thanks to the examination committee with Prof. Martin Klingenspor and Prof. Luc van Loon and thanks to the chairman Prof. Harald Luksch.

Ich danke meiner ganzen Familie für die unglaubliche Unterstützung, die sie mir im Laufe meines Studiums und der Doktorarbeit gegeben hat.

And last but not least, I thank you Lukáš for your incredible support and patience. Ďakujem!

Abstract

Mitochondrial calcium uniporter (MCU), mitochondrial redox biology and polyphenols: a metabolic triad for skeletal muscle health.

Calcium (Ca^{2+}) is a widespread intracellular signaling element that controls many processes such as fertilization, proliferation, development, cognitive functions, contraction and secretion. The universality and versatility of Ca^{2+} signaling relies on an extensive molecular and cellular repertoire of signaling components that generate a broad spectrum of spatial and temporal signals. In particular, Ca^{2+} accumulation in energized mitochondria has been shown to be a biological process of utmost physiological relevance in controlling intracellular Ca^{2+} signaling, metabolism, cell survival and a number of cell type-specific functionalities. All these individual processes appear to be regulated by the recently discovered mitochondrial calcium uniporter (MCU). MCU is particularly important in tissues with high energy demands. This is the case in skeletal muscle, where mitochondrial Ca^{2+} import via MCU links contraction to mitochondrial energy production. However, the role of MCU in skeletal muscle ageing remains poorly described and the effects of MCU-targeting nutritional interventions need to be explored. Although it is known that the regulation of mitochondrial Ca^{2+} signaling is closely linked to the redox state of mitochondrial thiol groups a causal relationship between these two types of signal transduction has not been demonstrated.

Here, it is described that activation of the evolutionarily conserved MCU modulates the mitochondrial redox state by promoting a net reduction of mitochondrial thiol groups. Redox modulation of these groups by MCU activation improved respiratory capacity in primary human myotubes and *C. elegans* and increased mobility in worms. Overall, these results show that MCU regulates redox balance in mitochondria, which is required to promote MCU-dependent effects on bioenergetics and mobility.

The second aim of this thesis was to elucidate the role of MCU in skeletal muscle ageing and the biological effect of MCU-targeted interventions with natural bioactive compounds. By examining mitochondrial and muscle function in human and animal models of skeletal muscle ageing, we found impaired mitochondrial energy metabolism, reduced mitochondrial Ca^{2+} uptake and downregulation of the MCU regulator MCUR1 associated with impaired muscle function. Moreover, we identified the olive leaf-derived polyphenol oleuropein as direct activator of MCU. Supplementation with oleuropein activated pyruvate dehydrogenase (PDH) and mitochondrial respiration in muscles of both young and aged mice and reduced physical fatigue, whereas all effects were lost in MCU-KO mice. The obtained results highlight the central role of MCU in

regulating energy metabolism and muscle performance in healthy models and in aged models with a decline in muscle health.

Finally, the molecular mechanism of MCU activation by specific polyphenolic MCU activators was elucidated. It was discovered that two distinct mechanisms are involved in MCU activation by these compounds: one MICU1-dependent and one MICU1-independent.
In summary, a novel function of MCU as a mitochondrial redox regulator was discovered *in vitro* and *in vivo* at the interface between Ca^{2+} and redox signaling and its effects on skeletal muscle energy metabolism and mobility. Furthermore, administration of oleuropein demonstrated beneficial effects and its mechanism of action to promote skeletal muscle health in adults and the elderly by targeting the MCU was elucidated.

Zusammenfassung

Calcium (Ca^{2+}) ist ein ubiquitäres intrazelluläres Signal, das für die Steuerung zahlreicher Prozesse wie Befruchtung, Proliferation, Entwicklung, Lernen und Gedächtnis, Kontraktion und Sekretion verantwortlich ist. Die Universalität und Vielseitigkeit der Ca^{2+}-Signalübertragung beruht auf einem umfangreichen molekularen und zellulären Repertoire an Signalkomponenten, die ein breites Spektrum an räumlichen und zeitlichen Signalen erzeugen. Insbesondere die Ca^{2+}-Akkumulation in energetisierten Mitochondrien hat sich als biologischer Prozess von höchster physiologischer Relevanz für die Steuerung der intrazellulären Ca^{2+}-Signalübertragung, des Zellstoffwechsels, des Zellüberlebens und anderer zelltypspezifischer Funktionen erwiesen. Alle diese einzelnen Prozesse scheinen durch den kürzlich entdeckten mitochondrialen Calcium-Uniporter (MCU) reguliert zu werden. MCU ist besonders wichtig in Geweben mit hohem Energiebedarf. Dies ist der Fall in der Skelettmuskulatur, wo der mitochondriale Ca^{2+}-Import über MCU die Kontraktion mit der mitochondrialen Energieproduktion verbindet. Die Rolle von MCU bei der Alterung der Skelettmuskulatur ist jedoch nur unzureichend beschrieben, und die Auswirkungen von Ernährungsmaßnahmen, die auf MCU abzielen, müssen noch erforscht werden. Obwohl bekannt ist, dass die Regulierung der mitochondrialen Ca^{2+}-Signalgebung eng mit dem Redox-Zustand der mitochondrialen Thiol-Gruppen verknüpft ist, konnte ein kausaler Zusammenhang zwischen diesen beiden Arten der Signaltransduktion bisher nicht nachgewiesen werden.

In der vorliegenden Arbeit wird beschrieben, dass die Aktivierung des evolutionär konservierten MCU den mitochondrialen Redoxzustand moduliert, indem er eine Nettoreduktion der mitochondrialen Thiolgruppen fördert. Die Redox-Modulation dieser Gruppen durch die MCU-Aktivierung verbesserte in der Folge die Atmungskapazität in primären menschlichen Myotubes und in *C. elegans* und erhöhte dadurch auch die Mobilität der Würmer. Insgesamt zeigen diese Ergebnisse, dass MCU das Redox-Gleichgewicht in Mitochondrien reguliert, was erforderlich ist, um MCU-abhängige Effekte auf Bioenergetik und Mobilität zu fördern.

Das zweite Ziel dieser Arbeit war es, die Rolle von MCU bei der Alterung der Skelettmuskulatur und die biologische Wirkung von MCU-gerichteten Interventionen mit natürlichen bioaktiven Verbindungen zu untersuchen. Durch die Charakterisierung der Mitochondrien- und Muskelfunktion in menschlichen Zellen und tierischen Modellen der Skelettmuskelalterung konnte ein beeinträchtigter mitochondrialer Energiestoffwechsel, eine verringerte mitochondriale Ca^{2+}-Aufnahme und eine Herunterregulierung der MCU-Untereinheit MCUR1, die mit einer beeinträchtigten Muskelfunktion einhergeht, nachgewiesen werden. Darüber hinaus wurde das

aus Olivenblättern gewonnene Polyphenol Oleuropein als direkter Aktivator von MCU identifiziert. Eine Supplementierung mit Oleuropein aktivierte die Pyruvatdehydrogenase (PDH) und die mitochondriale Atmung in Muskeln junger wie auch älterer Mäuse und verringerte die körperliche Ermüdung, Diese Effekte gingen alle bei MCU-KO-Mäusen verloren. Die erzielten Ergebnisse unterstreichen damit die zentrale Rolle von MCU bei der Regulierung des Energiestoffwechsels und der Muskelleistung in gesunden Modellen sowie in Modellen mit altersbedingter Abnahme der Muskelgesundheit. Schließlich wurde der molekulare Mechanismus einer MCU-Aktivierung durch zwei andere spezifische polyphenolische MCU-Aktivatoren aufgeklärt. Dabei wurde gezeigt, dass zwei verschiedene Mechanismen an der MCU-Aktivierung durch diese Verbindungen beteiligt sind: ein MICU1-abhängiger und ein MICU1-unabhängiger Weg.

Zusammenfassend lässt sich feststellen, dass *in vitro* und *in vivo* eine neue Funktion von MCU als mitochondrialer Redox-Regulator an der Schnittstelle zwischen Ca^{2+} und Redox-Signalen mit profunden positiven Auswirkungen auf den Energiestoffwechsel der Skelettmuskulatur und die Mobilität entdeckt wurde, die offenbar durch Oleuropein gesteigert werden kann.

List of contributed articles during the PhD & contribution statement

The list below contains 4 manuscripts that are currently under revision or have been accepted in peer-reviewed journals. Manuscripts (1) and (2) represent the main publications of the dissertation and are described in detail in the first and second part of the results section. A third manuscript (not yet completed and not yet included in this list) is described in the third part of the results section. Manuscript (3) is an invited review paper on MCU and pancreatic cells. In manuscript (4), I had the opportunity to contribute to a paper during my Master's studies, which was completed during the PhD.

(1) **Weiser A**, Hermant A, Bermont F, Sizzano F, Karaz S, Sorrentino V, Feige J, De March U. *The mitochondrial calcium uniporter (MCU) promotes muscle energy metabolism and mobility by regulating mitochondrial redox state.* Redox Biology. Under revision.

(2) Gherardi G***** and **Weiser A***, Bermont F, Brinon B, Jacot G, Hermant A, Migliavacca E, Coulon P, Sturlese M, Nogara L, Barron D, Moro S, Blaauw B, Rizzuto R, Feige J, Mammucari C, De Marchi U. *The natural MCU activator Oleuropein increases skeletal muscle energy metabolism and* performance during aging and in adulthood, via MICU1. Manuscript in preparation. ***Shared first authorship**

(3) **Weiser A**, Feige JN, De Marchi U. *Mitochondrial Calcium Signaling in Pancreatic β-Cell*. *Int. J. Mol. Sci.* 2021, *22*(5), 2515; https://doi.org/10.3390/ijms22052515

(4) Spanier B, Laurençon A, **Weiser A**, Pujol N, Omi S, Barsch A, Korf A, Meyer SW, Ewbank JJ, Paladino F, Garvis S, Aguilaniu H, Witting M. *Comparison of lipidome profiles of Caenorhabditis elegans-results from an inter-laboratory ring trial.* Metabolomics: Official Journal of the Metabolomic Society. 2021 Feb;17(3):25. DOI: 10.1007/s11306-021-01775-6. PMID: 33594638; PMCID: PMC7886748

Contribution Statement:

Manuscript (1) represents the first part of the dissertation. The paper was written in coordination with my supervisor Umberto De Marchi and all respective experiments were performed by myself, including mitochondrial Ca^{2+} measurements in human leukemia cells and primary human myotubes with an adenoviral-induced MCU-knockdown, as well as measurement of oxygen consumption rate (OCR) under treatment with redox-active chemicals. To solve the problem of myotubes detaching under the microscope while measuring the mitochondrial redox state, I implemented an automated method to measure the fluorescence signal in a plate reader in a 96-

well plate, which solved the problem. Finally, I wanted to test whether my findings could also be applied *in vivo* in *C. elegans*. For this purpose, I started to bring *C. elegans* into our lab. Dr. Britta Spanier shared her knowledge about worm maintenance and genetic modifications through RNAi. I measured respiration in worms by modifying a protocol from the literature by changing the preparation of the worms and using carbachol instead of FCCP which proved to be efficient. In a final experiment, I measured the mobility of the worms across different treatments.

Manuscript (2) corresponds to the second part of the thesis: here I performed all the presented *in vitro* experiments including mitochondrial Ca^{2+} measurements and OCR in genetically modified human myotubes treated with the natural MCU activator oleuropein in adulthood and old age. Based on the literature and my own results in a MICU1-knockout model, I asked whether the mechanism of oleuropein is related to the MCU subunit MICU1. To answer this question, I used embryonic mouse fibroblasts with a MICU1-knockout and measured mitochondrial Ca^{2+} uptake upon treatment with oleuropein. As this was found to be a MICU1-dependent mechanism, I proposed to perform *in silico* binding studies to identify potential binding sites. Therefore, Prof. Moro and Mattia Sturlese from the Department of Pharmaceutical and Pharmacological Sciences of the University of Padua agreed to collaborate and provided the relevant binding sites. To support my *in vitro* results, Gaia Gherardi from the Department of Biomedical Sciences at the University of Padua performed the corresponding mouse studies.

Another manuscript is currently in progress and corresponds to the third part of this thesis. Here I drew on an earlier discovery of mine in human leukemia cells with a MICU1-knockout, where I measured mitochondrial Ca^{2+} uptake after treatment with the polyphenols kaempferol and fisetin, which were positive hits from an earlier screening at Nestlé Research. I tested these polyphenols in different knockout cell lines lacking different subunits of the MCU complex. Finally, I tested the proposed MICU1 mechanism of the polyphenols *in vivo* in *C. elegans* and measured the OCR.

Table of Contents

Section 1: Introduction

Ca^{2+} is one of the major second messengers in cell metabolism (Clapham, 2007). It regulates a plethora of dynamic processes from life sustaining pathways – such as stimulation of cell growth, muscle contraction, endocrine secretion, gene expression, neurotransmission and phosphorylation and dephosphorylation reactions - to the initiation of cell death (Pallafacchina et al., 2018). Impaired Ca^{2+} signaling dynamics are a major contributor to pathologies such as sarcopenia, myopathies, diabetes, neurodegenerative diseases and heart disease (Berridge et al., 2003, Dhanasekaran et al., 2020). The complexity underlying the coordination of Ca^{2+} signaling dynamics is of greatest interest, as its regulation promotes the optimal function of various tissues under healthy conditions and could provide therapeutic targets to prevent pathological conditions due to impaired Ca^{2+} signaling.

Intracellular Ca^{2+} signaling dynamics are characterized by spatiotemporal properties; for instance, Ca^{2+} concentrations vary significantly among cellular compartments and while muscle contraction and exocytosis at the synaptic cleft rely on fast Ca^{2+} sparks (µs to ms), processes like cell proliferation or gene expression require longer Ca^{2+} exposure (min to h) which can be achieved via Ca^{2+} oscillations (Berridge et al., 1998, Berridge et al., 2003). Because of the differing Ca^{2+} concentrations among extra- and intracellular Ca^{2+} storages as compared to the cytosolic space, it is possible to encode extracellular information into cytosolic Ca^{2+} signals. These signals are modulated by adjusting the frequency, duration and amplitude of incoming Ca^{2+} signals via Ca^{2+} buffering systems including cytosolic Ca^{2+} buffering proteins and mitochondrial activation. In this context, mitochondrial Ca^{2+} regulation emerges as a key player in controlling intracellular Ca^{2+} signaling, metabolism, cell survival and a number of cell type-specific functionalities (Rizzuto et al., 2012). Mitochondrial Ca^{2+} uptake is regulated by the mitochondrial Ca^{2+} uniporter (MCU) (Baughman et al., 2011, De Stefani et al., 2011), a mitochondrial inner membrane channel discovered at the molecular level in 2011. The MCU is involved in the fulfilment of three crucial tasks of mitochondria in handling Ca^{2+}: Buffering cytosolic Ca^{2+} signals, activating Ca^{2+}-sensitive dehydrogenases of the tricarboxylic acid cycle (TCA) and regulating cell death (Mammucari et al., 2017).

Ca^{2+} is an essential signaling molecule and can affect the conformation and charge of hundreds of mitochondrial proteins, depending on the different Ca^{2+} binding affinities of the proteins (Clapham, 2007). The change in a protein's shape and charge ultimately determines its function, highlighting the physiological importance of homeostatic mitochondrial Ca^{2+} signaling. Disruption of mitochondrial Ca^{2+} signaling cascades has been associated with detrimental effects on tissues such as heart, skeletal muscle and brain (Alevriadou et al., 2021). The common denominator of

these pathologies is mitochondrial dysfunction, which is essentially caused by three interrelated axes: Ca^{2+} dyshomeostasis, oxidative damage and impaired ATP generation (Smith et al., 2012). In addition, mitochondrial Ca^{2+} modulates cellular energetics and boosts energy metabolism by activating matrix dehydrogenases and stimulating the downstream respiratory chain (Glancy and Balaban, 2012). As a result, Ca^{2+} signaling in mitochondria alters the mitochondrial NAD(P)H/NAD(P)$^+$ ratio and simultaneously leads to an increase in ROS production (Clapham, 2007). Reducing equivalents such as NAD(P)H/NAD(P)$^+$ and ROS exert opposite effects (reducing and oxidizing) on the mitochondrial redox state and are difficult to dissect. This research gap has been addressed in the first part of this thesis to investigate the net effect of mitochondrial Ca^{2+} regulation on mitochondrial redox state, and its implication for cellular function. The results establish a new causal link between MCU activation and modulation of mitochondrial redox state, linking Ca^{2+} signaling to redox signaling at the mitochondrial level. Subsequently, skeletal muscle models were used to determine the physiological implications of this discovery (see below).

Given the importance of MCU modulation for skeletal muscle function, the Nestlé Institute of Health Sciences (NIHS) conducted a high-throughput screening of MCU activators to develop a potential MCU-targeted nutritional intervention for skeletal muscle health. A library of more than 5000 all-natural bioactive compounds found in foods was evaluated, and the natural compound oleuropein was identified as a potent MCU activator. In the second part of this thesis, the health benefits of using oleuropein on skeletal muscle physiology were investigated and the molecular mechanism determined. For this purpose, a collaboration with the Department of Biomedical Sciences of the University of Padova was established to validate *in vivo* the results obtained in primary human myotubes. The beneficial effects of oleuropein on skeletal muscle were found in both adult and elderly patients/animals.

The third and final part of the dissertation, focused on the study of a specific family of polyphenols that was most prominent in the screening of natural MCU activators: flavones and flavonols. Specifically, the molecular mechanism of kaempferol and fisetin in activating mitochondrial Ca^{2+} uptake via MCU was studied. As a result, the MCU subunit MICU1 was identified as a crucial binding partner for these polyphenols. Subsequently, the mechanism was investigated in an *in vivo* model of *C. elegans*. This revealed significant impairments in bioenergetics in worms with defective MICU1 expression.

All three parts are currently being prepared for submission or have already been submitted to relevant journals. The current findings will help to elucidate the complex regulation and physiopathological implications of Ca^{2+}-dependent mitochondrial signaling dynamics. These findings will contribute to the development of a new nutritional strategy for skeletal muscle health and in the context of diseases or conditions associated with impaired mitochondrial redox state.

In order to describe the importance of mitochondrial Ca^{2+} regulation in the context of cellular Ca^{2+} homeostasis and, in particular, for skeletal muscle function, and to highlight the possible interactions with mitochondrial redox signaling and the potential importance of specific polyphenols, the relevant knowledge on these topics will be summarized in the following subsections of the introduction.

1.1. Influx and efflux pathways for cytosolic and mitochondrial Ca^{2+}

Mitochondrial Ca^{2+} uptake starts by crossing the outer mitochondrial membrane (OMM) via the voltage dependent anion carrier (VDAC, **Figure 1**) which sets a first kinetic threshold for Ca^{2+} to regulate Ca^{2+} entry into the intermembrane space (IMS) (Patron et al., 2013). Ca^{2+} ions can subsequently pass the inner mitochondrial membrane (IMM) via the electrochemically driven MCU. To counteract an accumulation of Ca^{2+} inside the mitochondrial matrix, the sodium-calcium exchanger (NCLX) and the proton-calcium exchanger (HCX) shuffle back Ca^{2+} ions into the IMS where they can enter the cytosol via VDAC (O-Uchi et al., 2012). Back in the cytosol, sarco-/endoplasmic reticulum calcium ATPases (SERCA) and plasma membrane calcium ATPases (PMCA) pump back Ca^{2+} ions into the sarco-/endoplasmic reticulum (SR/ER) and extracellular environment, respectively (Boyman et al., 2013). Unlike the ER/SR, mitochondria cannot store high Ca^{2+} concentrations for long without opening the mitochondrial permeability transition pore (MPTP) which increases the permeability of the IMM and causes a final disruption of the mitochondrial membrane potential ($\Delta\Psi m$) irreversibly leading to cell death (Halestrap, 2009). To protect mitochondria from excessive Ca^{2+} influx, the major uniporter for rapid and extensive Ca^{2+} uptake, MCU, has a low Ca^{2+} affinity, in the micromolar range (Rizzuto et al., 2012). This means that an elevated Ca^{2+} level is required to activate the MCU. To address this issue, mitochondria use so called mitochondrial associated membranes (MAMs) which are microdomains that create quasi-synaptic junctions between mitochondria and the ER/SR membrane, nucleic membrane and the plasma membrane where high Ca^{2+} fluxes are reached to activate a MCU mediated Ca^{2+} exchange (Pinton, 2018). For mitochondrial Ca^{2+} uptake at a cytosolic Ca^{2+} concentration in the nanomolar range, some transport mechanisms have been described which are still under discussion. These include the leucine-zipper-EF hand-containing transmembrane region (Letm1), a Ca^{2+}/H^{+} antiporter, the rapid mode of calcium uptake (RaM), the mitochondrial type 1 ryanodine receptor (mRyR1) and the reversed activity of the NCLX (Santo-Domingo and Demaurex, 2010, Ryu et al., 2010).

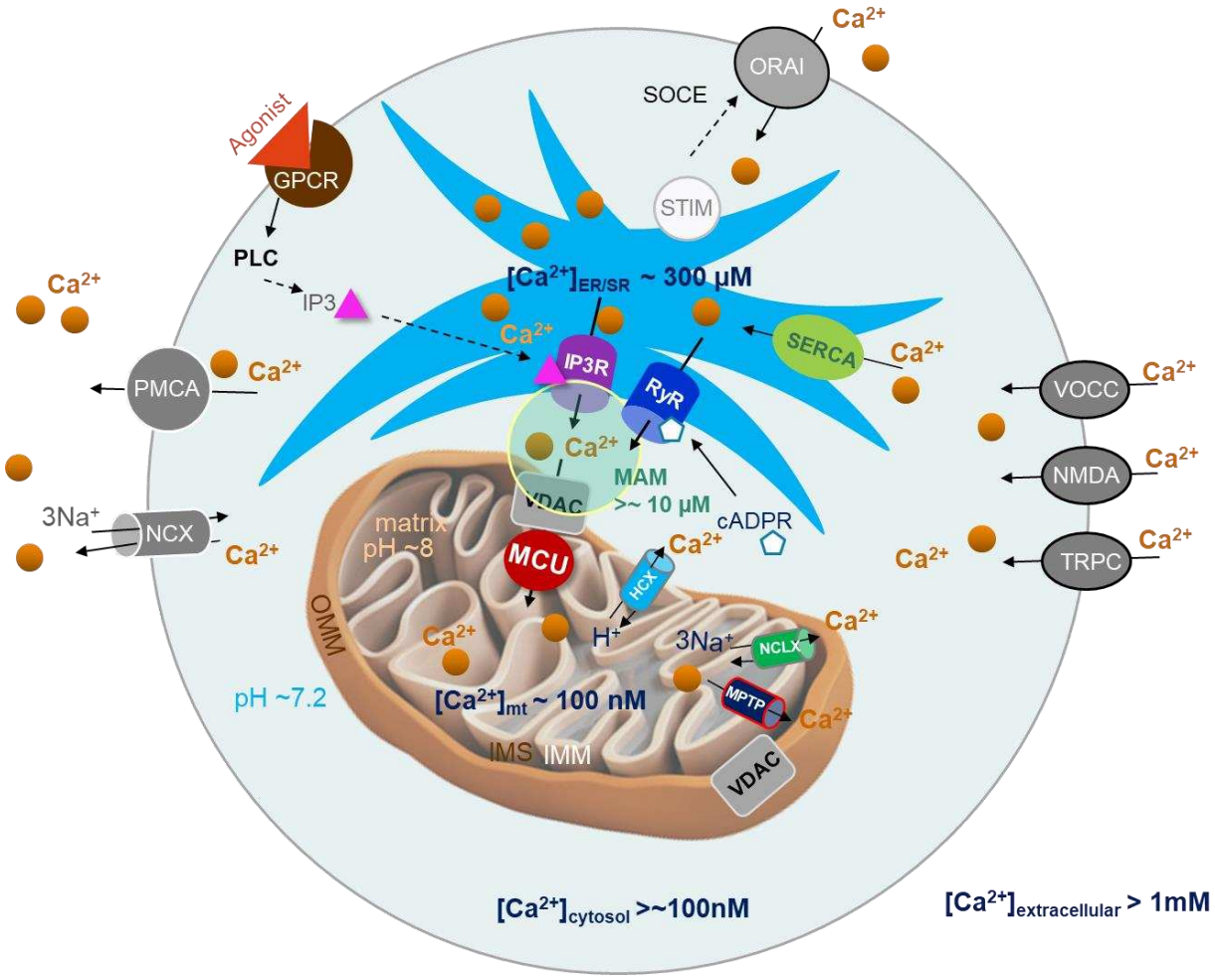

Figure 1. General model for multiple cellular Ca^{2+} entry and exit sites for Ca^{2+} signal transduction pathways (Krebs et al., 2015).
Binding of a G-protein coupled receptor (GPCR) agonist to its receptor releases inositol-triphosphate (IP3) which binds to its ER located receptor (IP3R) and triggers Ca^{2+} release. In SR, the IP3R homologue, ryanodine receptor (RyR) can be activated by cyclic ADP ribose (cADPR) to release Ca^{2+} from the SR. Plasma membrane Ca^{2+} ATPases (PMCA) pump back Ca^{2+} into the extracellular space while various plasma membrane based channels (voltage-operated Ca^{2+} channel, VOCC; receptor-operated Ca^{2+} channels such as NMDA; transient receptor potential channel, TRPC) allow extracellular Ca^{2+} to enter the cytosol for maintaining a stable Ca^{2+} concentration of approximately 100 nM. If the ER Ca^{2+} storage is depleted, storage-operated Ca^{2+} entry (SOCE) is activated by the luminal ER Ca^{2+} sensor STIM which leads to the stimulation of the ORAI Ca^{2+} channel, allowing Ca^{2+} to enter the cytosol. Mitochondria are in close proximity to other membranes via mitochondrial associated membrane (MAMs) allowing them to quickly take up high concentrations of cytosolic Ca^{2}. Mitochondrial Ca^{2+} uptake is mediated via the mitochondrial Ca^{2+} uniporter (MCU). Mitochondrial Ca^{2+} extrusion is regulated vie sodium-calcium exchanger (NCLX) and proton-calcium exchanger (HCX). A huge increase in mitochondrial Ca^{2+} leads to the opening of the mitochondrial permeability transition pore (MPTP). The different Ca^{2+} concentrations among extra- and intracellular as well as among cytosolic organelles make Ca^{2+} suitable to act as cellular master messenger.

Once Ca^{2+} has entered the mitochondria via the MCU complex, it activates a cascade of pathways, which contribute to drive cellular respiration. The TCA cycle needs three Ca^{2+}

dependent dehydrogenases including the two direct TCA dehydrogenases isocitrate dehydrogenase (IC-DH) and alpha-ketoglutarate dehydrogenase (αKG-DH) and the indirect TCA enzyme pyruvate dehydrogenase phosphatase isoform 1 (PDP1) which dephosphorylates and activates pyruvate dehydrogenase (PDH) (Kumari, 2018). PDH controls the pyruvate to acetyl-CoA supply for the TCA and therefore represents the rate limiting enzyme for glucose oxidation (Gherardi et al., 2019b). Furthermore, its control by the Ca^{2+} dependent PDP1 decides about the substance preference in skeletal muscle tissue favoring glucose oxidation over an increase in glycolysis (Gherardi et al., 2019b). This Ca^{2+}-induced shift towards oxidative metabolism ensures an adequate fueling of the TCA cycle where PDH, IC-DH and αKG-DH strip electrons from nutrients and provide NADH as electron carrier that feeds the electron transport chain (ETC) with electrons to drive ATP generation.

Mitochondria can buffer incoming Ca^{2+} signals from extracellular medium as well as Ca^{2+} signals released from the ER after G-protein coupled receptor (GPCR) stimulation which liberates inositol-trisphosphate (IP3) and allows its binding to the ER located IP3-Receptor (IP3R) leading to Ca^{2+} extrusion (Harrington and Murphy, 2015). A homologue of the IP3R in the ER, is the ryanodine receptor (RyR) in the SR which can be activated via cyclic ADP ribose (cADPR). When Ca^{2+} in the ER is depleted, the so-called store-operated calcium entry (SOCE) becomes activated, including the ER luminal Ca^{2+} sensor called stromal interaction molecule (STIM) and the plasma membrane Ca^{2+} channel ORAI1 through which Ca^{2+} can enter from the extracellular space into the cytosol where SERCA can refill the ER Ca^{2+} stores. Furthermore, Ca^{2+} can enter the cytosol from the extracellular space via various plasma membrane located channels such as voltage-operated calcium channels (VOCC), receptor-operated Ca^{2+} channels (e.g. N-methyl-D-aspartate receptor, NMDA) and transient receptor potential channels (TRPC) (Krebs et al., 2015).

As Ca^{2+} is among the most widespread signaling molecules in the human organism and is involved in a multitude of life-sustaining processes, the study of the Ca^{2+} signaling network in the cell together with its associated regulatory mechanisms is of utmost interest as it holds great potential for identifying causes of pathologies (Karlstad et al., 2012). This work particularly focuses on mitochondrial Ca^{2+} signaling pathways with the key player MCU, whose molecular structure is described in detail in the following section.

1.1.1. The MCU and its structural complexity

The molecular identification of the MCU transporter in 2011 deciphered the key player in the regulation of mitochondrial Ca^{2+} signaling and established that it operates in the delicate interphase of physiology and disease pathogenesis, making it a suitable target for the modulation

of mitochondrial Ca^{2+} signaling (De Stefani et al., 2011, Baughman et al., 2011). The MCU complex is an electrochemically driven uniporter, residing in the IMM, where it exerts a low-affinity but high-capacity for Ca^{2+} uptake. The complex consists of several subunits including: MCU, MCUb, essential mitochondrial Ca^{2+} uniporter regulator (EMRE), mitochondrial calcium uptake 1 (MICU1), MICU1.1 (skeletal muscle specific splice variant of MICU1) (Vecellio Reane et al., 2022), mitochondrial calcium uptake 2 (MICU2), mitochondrial calcium uptake 3 (MICU3) (tissue specific expression in brain and skeletal muscle) (Patron et al., 2019) and mitochondrial calcium uniporter regulator 1 (MCUR1), each contributing to orchestrate incoming Ca^{2+} signals (**Figure 2**).

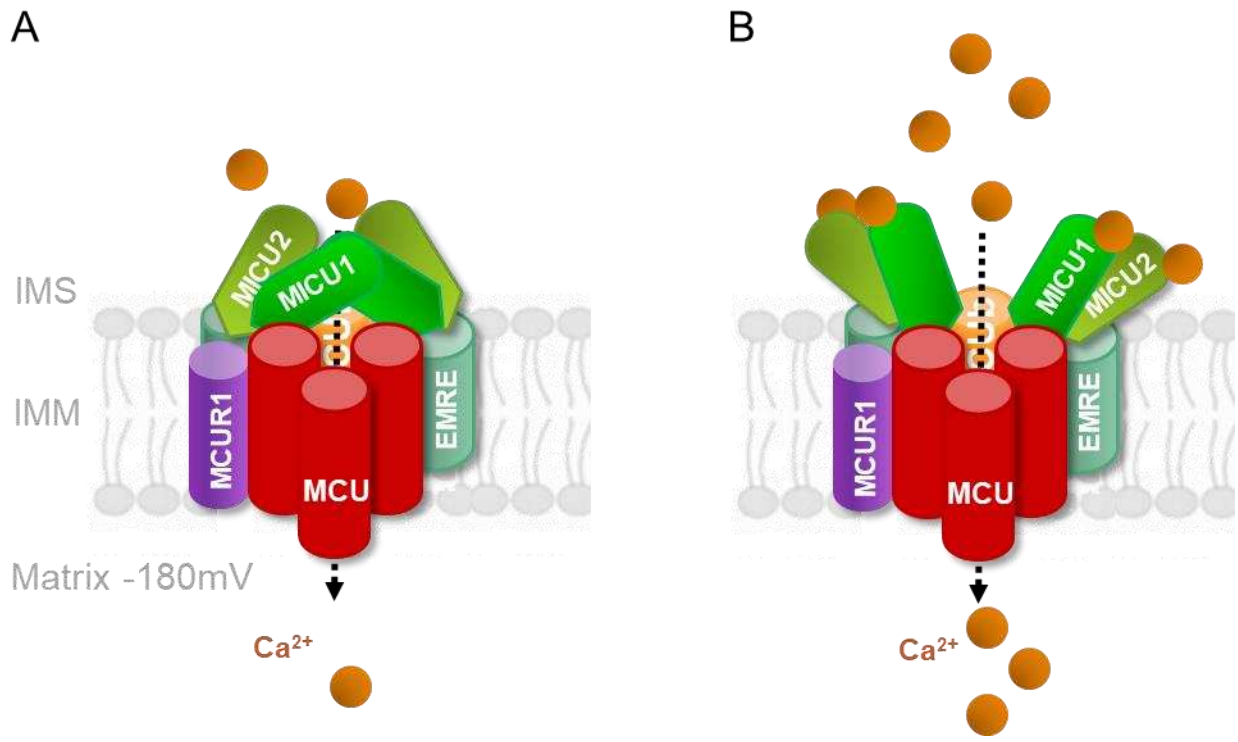

Figure 2. Proposed model for resting and active mode of MCU complex (Feno et al., 2019).
The MCU-complex is proposed to consist of 6 different subunits. MCU and MCUb form a pore which together with EMRE can transport Ca^{2+} from the inner mitochondrial space (IMS) into mitochondria. MICU1 and MICU2 fulfill gatekeeper functions by modulating the Ca^{2+} threshold for MCU activation. In skeletal muscle tissue a new splice variant of MICU1, called MICU1.1. was identified (Raffaello et al., 2020, Vecellio Reane et al., 2022). MCUR1 has a regulatory role of the MCU complex and it has been shown in several publications that silencing of MCUR1 leads to a decrease in mitochondrial Ca^{2+} uptake. What remains open is if MCUR1 is a direct modulator of the MCU complex or an indirect one acting on the complex IV of the respiratory chain. (A) Shows the MCU complex during resting conditions where MICU1 and MICU2 act as MCU gatekeepers by preventing Ca^{2+} from entering mitochondria. (B) Depicts the activated MCU complex via a rise in Ca^{2+} signal which causes Ca^{2+} binding to the EF hands of MICU1 and MICU2 leading to Ca^{2+} transportation into mitochondria.

The Ca^{2+} affinity of MCU varies across tissues and has been reported to range from 10 to 50 µM (De Stefani et al., 2015, Mishra et al., 2017, Foskett and Madesh, 2014b, Mallilankaraman et al., 2012b, Bernardi, 1999).The tetramer-forming subunits include the 40 kDa MCU and its paralog MCUb, which share 50% sequence identity and form the actual channel through which Ca^{2+} is transported into the mitochondria. MCUb is a negative regulator of MCU activity, and depending on the tissue, the ratio of MCU to MCUb changes significantly (**Figure 3**) (Pallafacchina et al., 2021). In cardiac tissue, it is essential to limit Ca^{2+} fluxes, which is why the rate of MCUb subunits is relatively high compared to MCU subunits, whereas in skeletal muscle tissue, MCU subunits dominate MCUb expression (Pallafacchina et al., 2018, Harrington and Murphy, 2015).

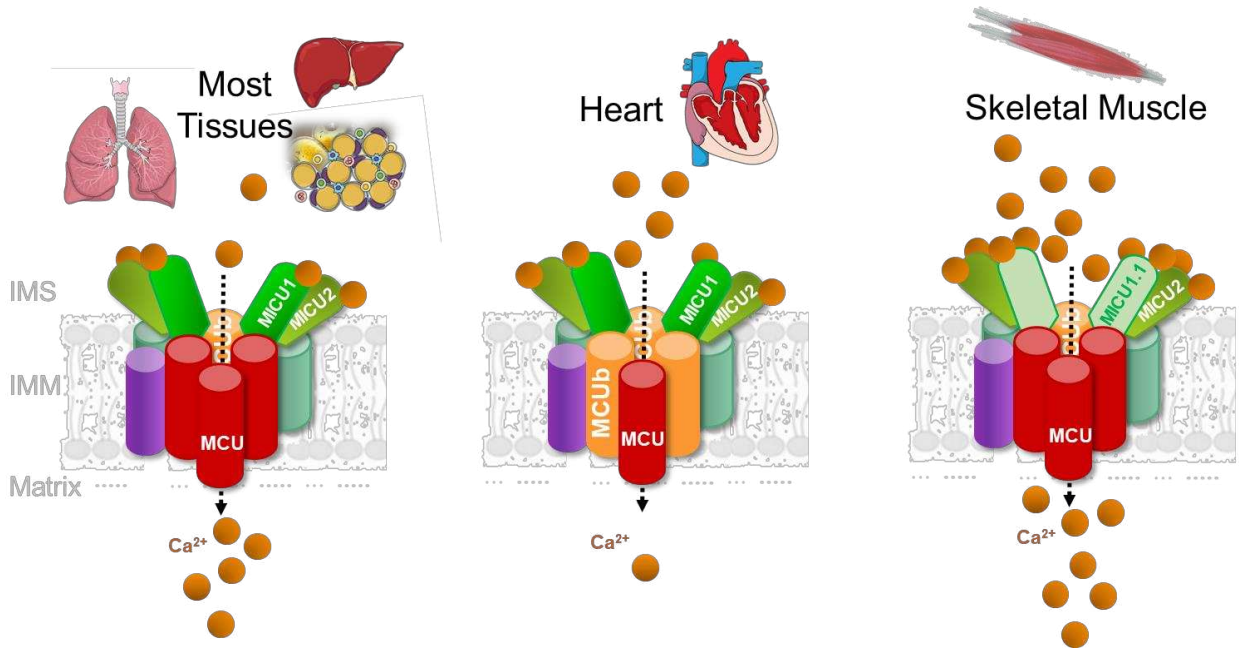

Figure 3. Different MCU holocomplex composition across tissues (Pallafacchina et al., 2021).
Different compositions of the MCU complex across tissues. In heart the MCUb:MCU ration is relatively high to ensure a tight regulation of Ca^{2+} to prevent tetanic reactions. However, in skeletal muscle tissue the composition of MCU is characterized by a lower MCUb:MCU ratio and additionally equipped with the MCIU1.1 splice variant which binds Ca^{2+} more effectively and increases mitochondrial Ca^{2+} uptake.

The pore alone is not sufficient to transport Ca^{2+}, but together with the 10 kDa EMRE the key subunits are present to enable Ca^{2+} transport (Kamer et al., 2019). The single-transmembrane subunit EMRE may be a crucial regulator electrostatically linking the MCU subunit to the 54 kDa MICU1 subunit (Phillips et al., 2019, Kamer et al., 2017), which is one of the identified MCU gatekeepers (Foskett and Madesh, 2014a). Other proposed mechanisms include direct binding of MICU1 to the MCU subunit (Paillard et al., 2018) or an interplay between the gatekeepers

MICU1 and MICU2 and cardiolipin (Kamer et al., 2017). MICU1 and its 50 kDa paralog MICU2 show 25% sequence identity and face the IMS (Mishra et al., 2017). Both gatekeeper proteins harbor two pairs of EF hands derived from specific parvalbumin sites E and F (Nakayama and Kretsinger, 1994), one of which is a canonical pair and the other a pseudo-pair (Mazumder et al., 2014). Ca^{2+} can only bind to the canonical EF hands and shows an estimated affinity of 0.3 µM for MICU1 and 0.6 µM for the dimer MICU1/MICU2 (Kamer et al., 2017). The binding of Ca^{2+} subsequently triggers a conformational change of the MICU1/MICU2 dimer, leading to the activation of MCU (Kamer et al., 2017). Similar to the expression patterns of MCUb, MICU1 is relatively low expressed in cardiac muscle compared to other tissues to prevent tetanic Ca^{2+} signaling. In skeletal muscle, the splice variant MICU1.1 (Raffaello et al., 2020) is predominant and characterized by stronger binding of Ca^{2+} (Vecellio Reane et al., 2016, Vecellio Reane et al., 2022), which occurs at lower Ca^{2+} concentrations compared to MICU1 (**Figure 3**) (Pallafacchina et al., 2018, Pallafacchina et al., 2021). The exact function of MICU2 is not yet known, but it has been shown that MICU2 increases the Ca^{2+} threshold at which the MICU1/MICU2 dimer triggers MCU activation (Kamer et al., 2019). Furthermore, introduction of mutations in either MICU1 or MICU2 leads to inhibition of MCU, while knockout of MICU1 leads to uncontrolled Ca^{2+} uptake (ibid). In the absence of MICU1, MICU2 mRNA can still be detected, but proper folding and function of MICU2 is no longer possible, lowering the Ca^{2+} threshold for MICU1 to activate Ca^{2+} uptake via MCU (De Stefani et al., 2015).

The next subunit of the MCU complex is MCUR1, which has been suggested to interfere with MCU but not MICU1, and whose function is still debated (Mallilankaraman et al., 2012a). On the one hand, several research groups have established a direct regulatory function of MCUR1 on MCU activity and have referred to MCUR1 as a scaffold factor of the MCU complex that, when silenced impedes mitochondrial Ca^{2+} uptake (Vais et al., 2015, Tomar et al., 2016, Lee et al., 2015, Mallilankaraman et al., 2012a). On the other hand, MCUR1 was found to function as an indirect MCU regulator by acting as a complex IV assembly factor, contributing to the maintenance of a stable $\Delta\Psi m$, whereas knockdown of MCUR1 would lead to an impaired $\Delta\Psi m$ and thus a decrease in the electrochemically driven activity of MCU (Paupe et al., 2015). Further investigation led to the discovery of MCUR1 as a regulator of the Ca^{2+} threshold for MPTP opening (Chaudhuri et al., 2016). To determine the exact function of MCUR1 in relation to the activity of the MCU complex, further studies are required that either support or challenge the previous findings.

Importantly, the ratio and stoichiometry of the individual subunits of the MCU complex can differ greatly depending on the cell type and tissue, which in turn can influence the Ca^{2+} affinity of the channel and thus its activity (**Figure 3**). The central theme of this thesis is the role of the MCU in

relation to skeletal muscle health, and the following section will provide scientific evidence to support this theme.

1.1.2. MCU and skeletal muscle health

The musculoskeletal system includes smooth muscle and skeletal muscle, the latter of which accounts for about 40% of total human body mass (Frontera and Ochala, 2015) and consumes about 20-30% of muscle O_2 at rest and up to 90% during intense exercise (Zurlo et al., 1990). To meet the high energy demands of skeletal muscle, its mitochondria have a very high capacity to take up mitochondrial Ca^{2+} to increase ATP production (Pallafacchina et al., 2021) and facilitate muscle contraction (Gherardi et al., 2019b, Vecellio Reane et al., 2016). The molecular identification of the MCU has thus contributed significantly to the study of the role of the MCU in the skeletal muscle system, indicating a crucial influence of mitochondrial Ca^{2+} uptake on muscle function.

An animal study using a tissue specific MCU-knockout (MCU-KO) revealed that the absence of mitochondrial Ca^{2+} signaling led to increased skeletal muscle atrophy while the overexpression of MCU elicited hypertrophy (Mammucari et al., 2015). Moreover, MCU expression was not only linked to improved muscle function but also to oxidative metabolism, which is essential to prevent a shortage in ATP synthesis especially during physical exercise (Gherardi et al., 2019b). Furthermore, physical exercise was shown to increase MCU expression, which might partially explain previously stated beneficial effects of exercise in preventing an age-related decline in muscle mass (Zampieri et al., 2016, Huertas et al., 2019). Very recently MICU3 expression in aged skeletal muscle tissue of mice was shown to be impaired, which is associated with a drastic decline in mitochondrial Ca^{2+} uptake and myogenesis as well as an increase in ROS production and cell death (Yang et al., 2021). Another study investigated the impact of mitochondrial fusion rates and showed a positive correlation between fusion rates and the oxidative capacity of muscle fibers (Mishra et al., 2015). Debattisti and coworkers, highlighted the role of MICU1 in muscle health and showed that impaired MICU1 function lowers the threshold for MCU driven Ca^{2+} uptake leading to an impaired aerobic metabolism, muscle weakness, fatigue, hampered excitation and contraction cycles and injured myofibers during exercise (Debattisti et al., 2019). In accordance, MICU1 mutations in humans and mice are not only linked to impairments such as fatigue and lethargy in muscle tissue, but also to cognitive changes including ataxia (Lewis-Smith et al., 2016, Logan et al., 2014). Mice with a MICU1-knockout (MICU1-KO) in a pure C57BL6 showed perinatal mortality while a MICU1-KO in C57BL6N or a mixed background of C57BL6NxJF1 partially

survived with a phenotype marked by severely impaired neurological and muscular functions (Antony et al., 2016, Liu et al., 2016).

While the relationship between mitochondrial Ca^{2+} signaling and muscle function is the core topic of this thesis, the effects of impaired mitochondrial Ca^{2+} signaling are not limited to muscle-related pathologies as described in this chapter, but rather affect a wide range of pathologies (Arduino and Perocchi, 2018), which are briefly mentioned in the following section.

1.1.3. MCU and associated pathologies

Ca^{2+} accumulation in energized mitochondria has been shown to be a biological phenomenon of great physiological importance (Rizzuto et al., 2012). Therefore, the uptake of Ca^{2+} in the mitochondrial matrix has been demonstrated to influence Ca^{2+} signaling, cell metabolism, cell survival and additional cell type-specific mechanisms through buffering of cytosolic Ca^{2+} concentrations and modulation of mitochondrial effectors. Numerous studies have successfully shown that an impaired mitochondrial Ca^{2+} machinery is associated with pathologies such as various cancers, sarcopenia, neurodegenerative, cardiovascular, airway diseases and diabetes (Granatiero et al., 2017, Jadiya et al., 2019, Mammucari et al., 2015, Santulli and Marks, 2015, Prakash et al., 2017).

Diabetes mellitus is one of the biggest global health challenges and is characterized by an impaired pancreatic insulin production and/or increasing insulin resistance leading to elevated blood glucose levels (Weyer et al., 1999). Main forms of Diabetes mellitus include type 1 diabetes, Gestational Diabetes and type 2 diabetes (T2D) of which the latter one represents the most frequent form (Chen et al., 2011). Diabetes Type 1 is an auto immune reaction directed against pancreatic β-cells of children or young adults whereas T2D is more dominant in middle age and old individuals (Notkins and Lernmark, 2001). Especially obesity, dyslipidemia and lifestyle habits are considered to significantly increase the risk for an early onset of T2D as well as cardiovascular diseases (Dutton and Lewis, 2015). Mitochondrial Ca^{2+} signaling has been demonstrated to affect insulin release from pancreatic β-cells, while silencing MCU decreases a glucose-stimulated increase in ATP which is essential for insulin secretion (Tarasov et al., 2012, Allen and Tessem, 2022). In another study, the flavonol kaempferol was used as a natural MCU activator to further increase insulin secretion (Bermont et al., 2020). These results make the MCU a popular target in the context of diabetes treatment (Weiser et al., 2021).

Phenotypes of genetically altered models of defective MCU have been described (Arduino and Perocchi, 2018) and showed that whole-body MCU-KO on a pure C57BL/6 background was embryonic lethal, while a mixed background with C57BL6xCD1 resulted in increased intolerance

to physical activity and reduced mouse size (Pan et al., 2013). A heart-specific MCU-KO resulted in loss of the fight-or-flight effect and similarly prevented ischemia/reperfusion injury (Luongo et al., 2015, Kwong et al., 2015). MCU-KO in the nematode *C. elegans* resulted in impaired wound healing in *mcu-1* mutants (Xu and Chisholm, 2014). Tissue specific knockdown of MICU1 in mouse liver resulted in tissue destruction and increased inflammation (Antony et al., 2016). Knockout of EMRE in mice showed no viability (Arduino and Perocchi, 2018).

While it is evident that impaired mitochondrial Ca^{2+} signaling is associated with muscle-specific, but also other tissue-specific pathologies, it is not yet clear which crucial signaling pathways are affected by impaired mitochondrial Ca^{2+} signaling causing the pathologies and how they can be regulated. This thesis examines how MCU regulation affects muscle physiology and pathology and incorporates mitochondrial redox signaling into the analysis. Importantly, mitochondrial Ca^{2+} homeostasis is closely linked to mitochondrial redox signaling, which in turn influences energy metabolism and plays a crucial role in muscle function. Therefore, the first part of this thesis explores the possibility that the modulation of mitochondrial redox biology could be regulated by MCU (see section 4.1), which could help bridge the gap between mitochondrial Ca^{2+} signaling and muscle health.

1.2. The link between MCU and mitochondrial redox signaling

Redox regulation of mitochondrial proteins is an increasingly relevant subject in cell physiology and pathology, as many mitochondrial features are associated with redox responses, comprising nutrient oxidation, oxidative phosphorylation, reactive oxygen species (ROS) production, mitochondrial permeability transition (Korotkov and Novozhilov, 2022), mitochondrial morphology and cell death (Mailloux et al., 2014). Redox responses and related alterations can act as cellular signals, e.g. metabolites and proteins can turn on specific cellular signaling pathways in a redox state-dependent way (Deponte and Lillig, 2015, Riemer et al., 2015). Moreover, various diseases are associated with defective redox signaling, among them cardiovascular and neurodegenerative diseases, insulin resistance, obesity, diabetes and aging (Mailloux et al., 2014). Notably, oxidation of protein thiol groups is associated with mitochondrial dysfunction, which impedes respiration and induces MPTP opening (Netto et al., 2002). Proteins located in the IMM are particularly at risk of oxidation as they are preferential targets of mitochondrial ROS. Many of the proteins located in the IMM therefore have antioxidant thiol switches to protect themselves by reversing the oxidation reaction. In this context, mitochondrial reduced glutathione (GSH) content has been shown to be the major defense mechanism for maintaining an adequate mitochondrial redox milieu to prevent or restore oxidative changes that otherwise lead to

mitochondrial dysfunction and subsequent cell death. At the skeletal muscle level, it has been shown that mitochondrial damage occurs after marked depletion of GSH and is prevented by supplementing GSH monoester (Mårtensson and Meister, 1989). In addition, an intervention with mitochondria-targeted antioxidants appears to have positive outcomes on mitochondrial function, insulin sensitivity and age-dependent decrease in muscle function (Broome et al., 2018). The net impact (reduction or oxidation) of mitochondrial Ca^{2+} rise, on matrix redox state, following a stimulation, is poorly defined (**Figure 4**).

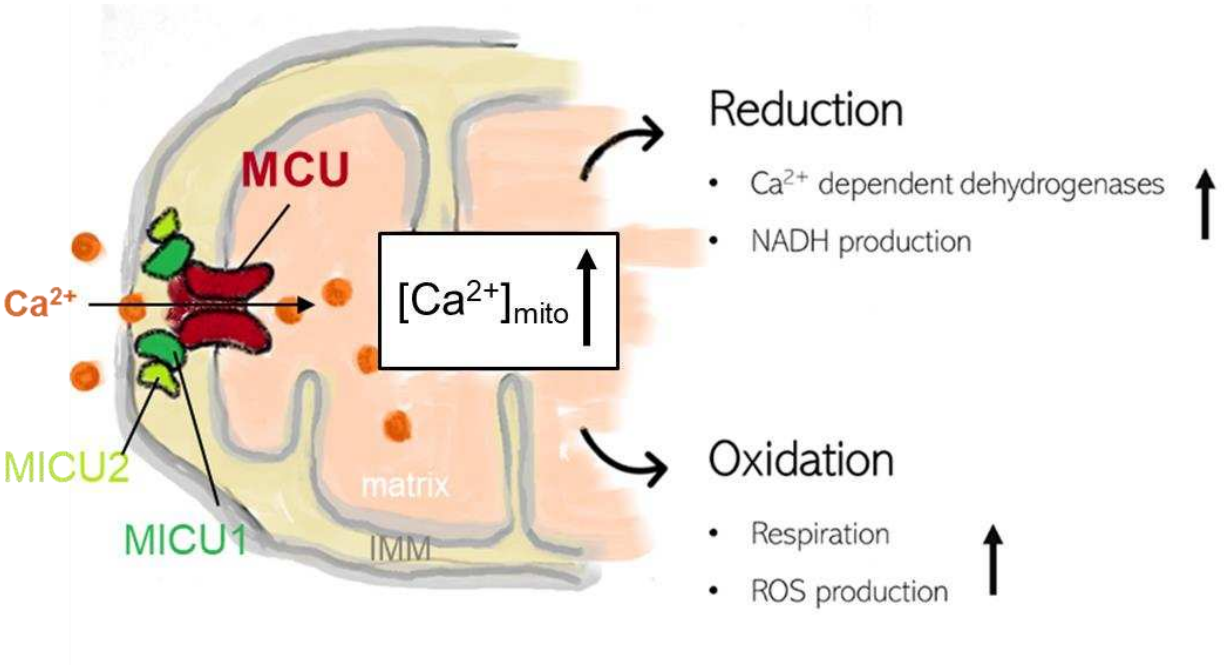

Figure 4. Activation of MCU simultaneously drives reducing and oxidizing reactions.
Representation of the mitochondrial oxidation and reduction steps, which are stimulated in parallel by mitochondrial Ca^{2+} (mt-Ca^{2+}) uptake through MCU complex (MCU subunit: red, MICU1/2 subunits: green, other subunits are not shown to simplify the scheme). The reduction is primarily caused by the stimulation of mitochondrial Ca^{2+} dependent dehydrogenases, which in turn increase the generation of reduced NAD(P)H (Glancy and Balaban, 2012). Concomitantly, elevated levels of mitochondrial Ca^{2+} stimulated respiration drive oxidative processes. Oxidation takes place upon oxidative phosphorylation where electrons leak from the electron transport chain (ETC) creating superoxide anions ready to be converted to different species of ROS like hydrogen peroxide.

The key channel for rapid mitochondrial Ca^{2+} uptake is the previously discussed MCU (Baughman et al., 2011, De Stefani et al., 2011). If causality could be established between MCU modulation and matrix redox state, MCU could be a good target to promote muscle health, via regulation of thiol groups.

To investigate potential MCU activators, the Muscle Bioenergetics team at the NIHS developed a project to identify natural bioactive compounds that increase MCU activation in the skeletal muscle system to promote muscle health. These data and the effect of selected natural bioactive

MCU activators are presented in the second and third part of the results section (sections 4.2 and 4.3).

1.3. Role of mitochondrial redox biology in skeletal muscle

Mitochondrial redox reactions are central to life and research into the biology involved is of the utmost interest, as many mitochondrial functions depend on a physiological redox state (Mailloux et al., 2014, Riemer et al., 2015). A disturbed redox state, in turn, appears to play a key role in numerous pathologies, such as cardiovascular diseases, diabetes, cancer, Alzheimer's disease, Parkinson's disease and skeletal muscular diseases (Mailloux et al., 2014, Riemer et al., 2015, Cooper et al., 2011).

With the discovery of the electron in 1897, then called the corpuscle, J. J. Thomson laid the groundwork for the known redox biology of today (Griffiths, 1997). Later in the 1950's it was reported that hydrogen peroxide (H_2O_2), a key redox molecule in physiological oxidative stress (Sies, 2017) is generated by respiring mitochondria (Chance and Williams, 1956). At that time, many important findings were made in relation to skeletal muscle under exercise conditions. Although the focus of this work is not on mitochondrial Ca^{2+} and redox biology during exercise, but on mitochondrial Ca^{2+} and redox biology in skeletal muscle health, there are historical achievements that are critical to understanding skeletal muscle metabolism. In the 1960's, it was first shown by John Holloszy that physical exercise increases mitochondrial content (Holloszy, 1967). In the early 1980's, exercise was reported to increase the number of free radicals in skeletal muscle, which may act as a stimulus for mitochondrial biogenesis (Davies et al., 1982, Jenkins, 1988). Over time and with advancing technical knowledge, exercise has been shown to induce free radicals and ROS, which include non-radical oxygen derivates. In the 1990's, literature emerged showing beneficial functions of ROS, for instance, in inducing transcription factors and triggering wound healing (Sen, 1995). In the same decade, oxidative stress, which is an imbalance between pro-and antioxidants in favor of the former, was associated with muscle fatigue (Barclay and Hansel, 1991) and muscle atrophy (Kondo et al., 1993). Today it is known that H_2O_2 and ROS in general are important signaling molecules, just like their reducing counterparts, which include the cell's antioxidant defense mechanisms (Murphy et al., 2011, Espinosa-Diez et al., 2015). This signaling function of ROS plays a key role in mediating exercise-induced adaptations of the skeletal muscles, while antioxidant supplementation attenuates this effect (Ristow et al., 2009, Jackson et al., 2022). Redox-active molecules carry out their signaling function by reversible oxidation/reduction of thiols present in proteins, which leads to their conformational and functional changes. Strikingly it has been shown that exercise itself activates

antioxidant mechanism by inducing transcription of antioxidant enzymes, modulating diverse signaling pathways. Among these redox-sensitive pathways are, adenosine monophosphate-activated protein kinase (AMPK), mitogen activated protein kinase (MAPK), nuclear respiratory factor2 (NRF2), and peroxisome proliferator-activated receptor gamma coactivator-1 alpha (PGC-1α), which is known to increase mitochondrial biogenesis in skeletal muscle and increase transcription and protein expression of antioxidant enzymes such as the selenoprotein glutathione-peroxidase (GPx) and mitochondrial superoxide dismutase (SOD2) (Lin et al., 2002, St-Pierre et al., 2006). The three main sources of ROS in muscle tissue are NADPH oxidase enzymes (NOX/DUOX), xanthine oxidase (XO) and mitochondria (Murphy, 2009). This mitochondrial crosstalk between ROS and Ca^{2+} will be further discussed in the subsequent chapter. There have been several reports in the literature, proposing that cytosolic ROS production predominates during exercise and mitochondrial ROS production prevails after exercise (Sakellariou et al., 2013, Pearson et al., 2014). The latter has been suggested to be important for the elimination of dysfunctional mitochondria through mitophagy (Henríquez-Olguin et al., 2019). Functional mitochondria have been shown to preserve a highly reduced redox state with an approximate midpoint potential of -300 mV (Hanson et al., 2004). Furthermore, mitochondrial redox signaling has been demonstrated to be critical for skeletal muscle fiber plasma membrane repair and that its impairment can induce and exacerbate Duchenne muscular dystrophy in mouse models (Horn et al., 2017). The same study discovered that the MCU is also essential in mediating this plasma repair mechanism. Although ROS and oxidative stress are frequently used, they are generic terms and do not provide insight into the actual chemistry within a cell (Herrmann and Dick, 2012). Over time, technology has improved and made it possible to perform compartmentalized redox measurements. This is important because redox changes are associated with their cellular compartment or even domains within a compartment (Mishina et al., 2011). Genetically encoded probes that target specific subcellular compartments have paved the way for tracking redox processes *in vitro* and *in vivo* (Hanson et al., 2004). Most probes are constantly being improved so that they are becoming more precise and distinct.

1.3.1. Mitochondrial ROS production

Mitochondria are commonly referred to as power plants, as they supply the cell with more than 60 % ATP through oxidative phosphorylation (Kim, 2014). This bioenergetic process is tightly coupled to mitochondrial Ca^{2+} uptake, which causes mitochondrial ROS production predominantly at complex I, either from its flavin mononucleotide (FMN) site during elevated ratios of $NADH/NAD^+$ or through respiratory complex I-mediated reverse electron transport (RET),

measured *in vitro*, and to a lesser extent at complex III (Denton, 2009, Territo et al., 2000, Lane, 2011, Murphy, 2009).

Due to the low redox potential of NADH ($E^{0'}$ = -340 mV), the electron is taken by redox pairs within the ETC with higher redox potentials until the electron reaches its final electron acceptor O_2 ($E^{0'}$ = +810 mV), reducing it to H_2O (Mailloux et al., 2014). Those redox reactions are used to pump protons out of the matrix into the IMS via ETC complex I, III and IV to generate a proton gradient for the phosphorylation of ADP to synthesize ATP at complex V. Even though ATP-synthesis is one of the central pathways in bioenergetics, it also generates about 0.1-2 % ROS based on the consumed amount of O_2 (Li, 2019, Murphy, 2009, Zhao et al., 2017). Out of 32 known cellular ROS sources, 16 are located in mitochondria (Mailloux, 2020) and best studied are αKG-DH, NOX4 and the ETC (Henriquez-Olguin et al., 2020, Sabens Liedhegner et al., 2012) where electrons can prematurely "spin off" at complex I and complex III to react with O_2, creating superoxide radical anion ($O_2^{\bullet-}$), a highly reactive oxygen derivative (**Figure 5**). Within the IMM, $O_2^{\bullet-}$ can be produced and released either into the mitochondrial matrix or the IMS (Kotiadis et al., 2014). In mitochondria, the SOD2 reduces $O_2^{\bullet-}$ to H_2O_2 which can freely pass membranes and act as an important mitochondrial or cytosolic signaling molecule by reversibly oxidizing thiol groups (-SH) to sulfenic acid (-SOH). Oxidizing such a thiol switch of a protein with a redox active cysteine residue can then alter its function or activity (Herrmann and Dick, 2012). As dynamic thiol switches are the heart of redox biology, they will be discussed in more detail in the following section. $O_2^{\bullet-}$ produced at complex III and released into the IMS can be reduced to H_2O_2 by the cytosolic and IMS protein sodium dismutase 1 (SOD1). Inside mitochondria, H_2O_2 can be further reduced to H_2O via ROS scavenging enzymes like GPx1 or peroxiredoxin 3 (Prx3) (Handy and Loscalzo, 2012). If Fe^{2+} is available, the Fenton reaction can take place and transform H_2O_2 into a hydroxyl radical ($OH^{\bullet}$). Another radical, peroxynitrite anion ($ONOO^{\bullet-}$), can be formed if nitric oxide (NO) reacts with $O_2^{\bullet}$.

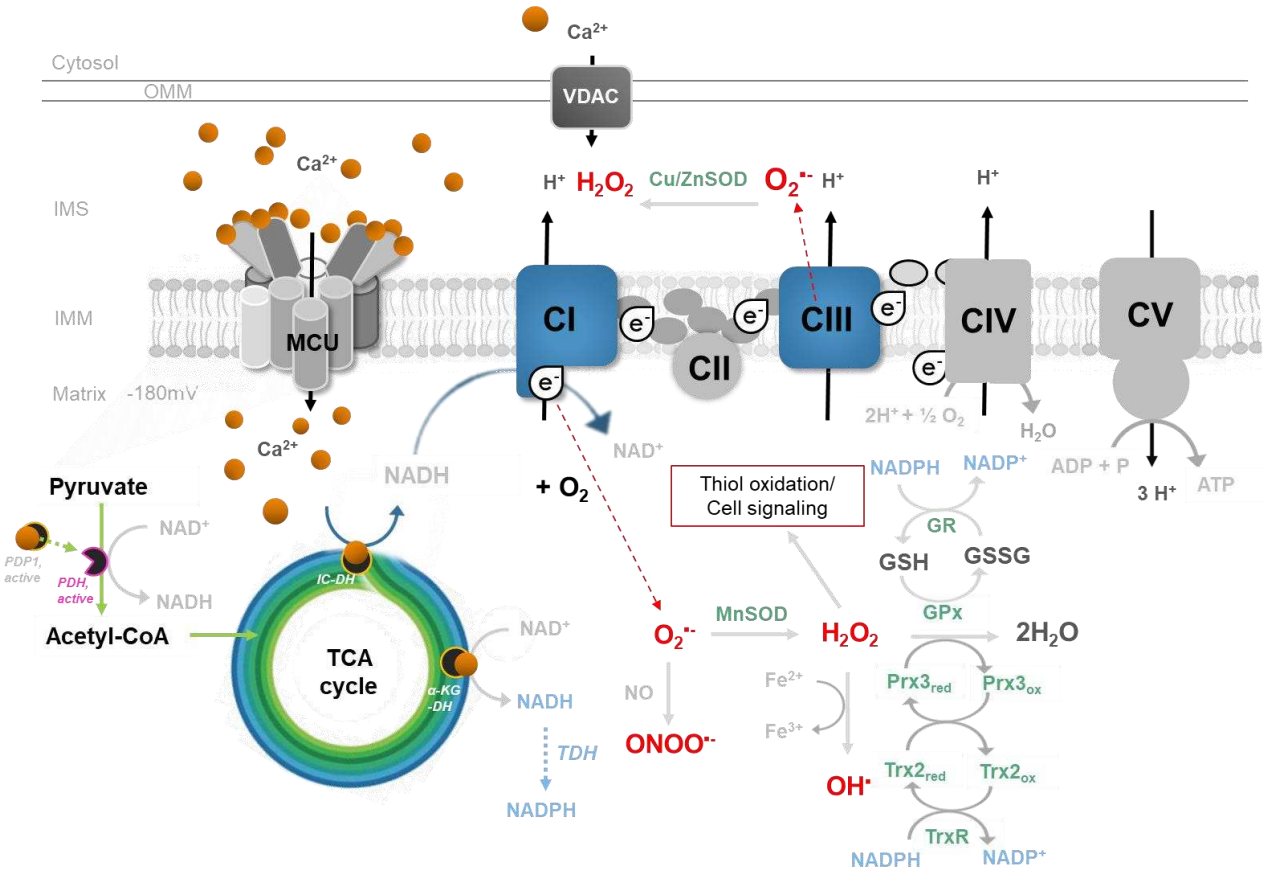

Figure 5 Model for the effect of mitochondrial Ca^{2+} uptake on mitochondrial matrix redox state.
After Ca^{2+} ions have passed the voltage dependent anion carrier (VDAC) to activate the MCU complex, Ca^{2+} can enter the mitochondrial matrix to bind and activate three Ca^{2+}-sensitive dehydrogenases which lead to the activation of the TCA cycle (pyruvate-dehydrogenase-phosphatase PDP; isocitrate-dehydrogenase IC-DH; alpha-ketoglutarate-dehydrogenase (α-KG-DH). Although PDP is not part of the TCA cycle however it dephosphorylates and activates the pyruvate-DH (PDH) which is a key enzyme transforming pyruvate into acetyl-CoA which is a prerequisite to initiate the TCA cycle. All three enzymes catalyze reactions where NADH is created and used to carry electrons to complex I (CI) of the ETC to trigger ATP-synthesis. If O_2 binds an electron that has escaped from the electron transport chain (ETC) before complex IV (CIV), it forms superoxide radical anion ($O_2^{\bullet-}$). $O_2^{\bullet-}$ produced at CI is mainly released into the matrix while $O_2^{\bullet-}$ released from CIII can also enter the IMS and subsequently the cytosol. In the IMS and cytosol the sodium dismutase 1 (SOD1) can reduce $O_2^{\bullet-}$ to hydrogen peroxide (H_2O_2) while in mitochondria, the sodium dismutase 2 (SOD2) transforms $O_2^{\bullet-}$ into H_2O_2 which can either freely pass membranes and act as cellular signaling molecule or it can be reduced to H_2O by the different ROS scavengers like glutathione-peroxidase (GPx) or peroxiredoxin 3 (Prx3). If Fe^{2+} is present, H_2O_2 can undergo the Fenton reaction which generates a hydroxyl radical ($OH^{\bullet}$). In the presence of nitric oxide (NO), $O_2^{\bullet-}$ can react to peroxynitrite radical anion ($ONOO^{\bullet-}$). In addition, mitochondria own defense mechanisms to target ROS by using thiol redox couples like $glutathione_{ox}$/$glutathione_{red}$ (GSSG/GSH) or $thioredoxin2_{ox}$/$thioredoxin2_{red}$ ($Trx2_{ox}$/$Trx2_{red}$) which reduce the ROS scavengers GPx and Prx3. GSSG and $Trx2_{ox}$ are recovered by glutathione reductase (GR) and thioredoxin reductase (TrxR) respectively, using NADPH as electron source. Besides other pathways, NADPH can be synthesized from NADH catalyzed by the proton translocating transhydrogenase (TDH) to recover the entities of the mitochondrial ROS defense system.

The effects of ROS cover many essential cellular pathways and may even contribute to lifespan extending reactions, to the initiation of harmful oxidative reactions including detrimental mutations in the mitochondrial DNA (mtDNA) that can lead to pathophysiological conditions like cancer (Santos et al., 2018). In the mitochondrial matrix are approximately 5 to 10 copies of mtDNA which

are not protected by histones or repaired by restriction enzymes making the mtDNA rather vulnerable towards ROS as compared to the nuclear DNA (Li, 2019).

1.3.2. Redox-active thiols as regulators of mitochondrial function

The mitochondrial redox state is controlled mainly through oxidation and reduction of mitochondrial thiol groups. The mitochondrial proteome contains a huge pool of exposed protein cysteine residues whose thiol groups can easily be modified and used for signal transduction (Mailloux et al., 2014). Modification of redox-active protein thiols by ROS and reducing molecules such as GSH is a key signaling mechanism in redox biology and crucial for maintaining mitochondrial function (Murphy, 2011, Riemer et al., 2015). Mitochondria can quickly respond to environmental and biochemical changes to neutralize H_2O_2 using redox-active protein thiols (**Figure 6**) which can reversibly undergo several modifications e.g. S-oxidation including sulfenic (-SOH) and sulfinic acid (-SO_2H), S-nitrosylation, or S-glutahionylation which plays an important role in preventing sulfenic acid (-SOH) from further and therefore increasingly irreversible oxidation steps (sulfonic acid -SO_3H) by generating a protein glutathione disulfide (-PSSG) (Mailloux et al., 2014). S-glutahionylation therefore plays two important roles, first in redox mediated cell signaling and second as a protective mechanism to prevent irreversible oxidation and subsequent degradation of important protein thiol switches. The oxidation of -SOH to -SO_2H can be reversed by sulfiredoxin (Srx) (Noh et al., 2009), while further oxidation to -SO_3H, is irreversible and an indicator of oxidative stress (Cho et al., 2010). Thiol groups contain a highly reactive sulfur (Lindahl et al., 2011) and are mainly present in GSH, cysteine and other low-molecular weight thiols. It is estimated that the mitochondrial proteome harbors 60-90 mM of exposed protein cysteine thiols, reflecting the mitochondrial "redoxome" that could potentially be modified, showing the huge potential of redox modulation in mitochondria (Mailloux and Treberg, 2016). In a proteome-wide study, 19 of the 50 most reactive cysteine thiols were found in mitochondria, including proteins such as aldehyde dehydrogenase 2 (Aldh2), mitochondrial thiolases such as acetoacetyl-CoA, the mitochondrial isoform of creatine kinase that uses ATP to phosphorylate creatine, aconitase, which catalyzes the conversion of citrate to isocitrate within the TCA, and mitochondrial branched-chain amino transferase (BCATm), which catalyzes the first step of the degradation of branched-chain amino acids (leucine, isoleucine, valine) (Riemer et al., 2015). Furthermore, mitochondria contain high concentrations of GSH from 1 to 12 mM (Cooper et al., 2011), representing the major cellular non-protein thiol defense mechanism against oxidants. The ratio of reduced and oxidized thiol groups of glutathione (2GSH/GSSG) during resting conditions shows a highly reduced midpoint potential around -300 mV (Kemp et al., 2008)

and is a reliable indicator of the mitochondrial redox state (Jones, 2002, Santo-Domingo et al., 2015). Another important thiol-redox couple is thioredoxin$_{ox}$/thioredoxin$_{red}$ (Trx$_{ox}$/Trx$_{red}$), which is used by ROS scavenging enzymes like GPx and peroxiredoxin (Prx) to catalyze the reaction of H_2O_2 to H_2O (Schwarzlander et al., 2016). The enzymes glutathione reductase (GR) and the selenoprotein thioredoxin reductase (TrxR) restore the GSH and Trx$_{red}$ pool in mitochondria using NADPH, which can be derived from NADH via the proton translocating transhydrogenase (TDH), also known as nicotinamide-nucleotide-transhydrogenase (NNT) (Rydström, 2006, Handy and Loscalzo, 2012). NADPH is crucial for the recovery of the reducing power of ROS scavengers, while NADH is more like an electron sink and important for oxidative phosphorylation and involved in ROS production. Their ratios are very contrasting: NADPH/NADP$^+$ is 100:1 (similar to 2GSH/GSSG), while NADH:NAD$^+$ is 1:10-1000 (Cooper et al., 2011). Glutaredoxin (Grx) reduces disulfides between proteins and between proteins and GSH (-PSSG) and thereby re-activates the thiol switch (-SH). To do so, Grx requires GSH, NADH or TrxR. These reversible thiol modifications play a crucial role in mitochondrial function as essential pathways are under redox regulation such as TCA with the redox-sensitive PDH (Yan et al., 2013), SDH (Chen et al., 2007) and aKG-DH (McLain et al., 2013) as well as oxidative phosphorylation with S-glutathionylation of complex I during increased concentrations of H_2O_2 e.g. during exercise, to reduce $O_2^{\bullet-}$ production and S-glutathionylation of ATP-synthase to stop ATP hydrolysis and reverse proton pumping (Mailloux et al., 2014). Further studies have highlighted a thiol-dependent regulation of the ETC (Dröse et al., 2014, Chouchani et al., 2013). Once H_2O_2 concentrations decrease, complex I and ATP-synthase activity can be restored by Grx. The regulatory role of Grx might be expanded to mitochondrial morphology and autophagy as shown in mouse skeletal muscle myoblasts (Liaghati et al., 2021). Absence of Grx in mitochondria led to a decrease in 2GSH/GSSG driven by an increase in GSSG, triggering hyperfusion by ongoing S-glutathionylation of mitofusin (Mfn) proteins (Shutt et al., 2012). Moreover, S-glutathionylation is potentially involved in MPTP opening by cysteine oxidation of adenine nucleotide translocase (ANT) which is involved in inducing cell death while S-glutathionylation of cyclophilin D (Cyp-D) may prevent docking and opening of MPTP (Kokoszka et al., 2004). Protein thiol modification has also been associated with regulating glycolysis favoring NADPH production (Mailloux, 2020). Thiols have been demonstrated to play a role in the first and second most common neurodegenerative diseases, Alzheimer's (Akterin et al., 2006) and Parkinson's (Sabens Liedhegner et al., 2012) where mitochondrial GSH levels from human postmortem frontal cortex were shown to be decreased (Ansari and Scheff, 2010) and where mitochondrial redox imbalance seems to play a major role in the progression of the diseases. Further publications have mentioned additional diseases associated with impaired thiol signaling in mitochondria such as

diabetes, obesity, non-alcoholic fatty liver disease and cataracts (Cooper et al., 2011, Mailloux and Treberg, 2016). Interestingly, S-glutathionylation can “switch-off” cancer-induced overexpression of uncoupling proteins (UCPs) (Mailloux and Treberg, 2016). UCPs (particularly UCP2 and UCP3) are members of the first line antioxidant defense mechanism as they uncouple respiration from ATP-synthase and prematurely let protons enter the matrix which lowers the mitochondrial membrane potential and therefore reduces the likelihood of electrons spinning off from complex I to produce ROS which otherwise happens during increased membrane potential. In cancer treatment, drug-induced increase of ROS concentrations is intended to kill oncogenic cells, therefore inactivation of the ROS-lowering UCPs is favored to increase the cells sensibility for chemotherapeutics (Pfefferle et al., 2013). A less studied but highly relevant effect of S-glutathionylation is its impact on mitochondrial Ca^{2+} homeostasis. The few studies, link depleted GSH pools with increased S-glutathionylation of SERCA pumps (Handy and Loscalzo, 2012, Xiong et al., 2011) and the RyR, the skeletal muscle Ca^{2+} release channel, which increases cytosolic and therefore mitochondrial Ca^{2+} and propose protein glutathionylation as a key player in mediating Ca^{2+} and redox signaling (Frosali et al., 2009, Aracena-Parks et al., 2006). Despite all the knowledge generated on thiol modulation in cellular physiology, it is a very complex machinery that decides which protein gets e.g. S-glutathionylated and what the impact on its function will be: activation or inactivation (Mieyal et al., 2008). With aging and associated physiological impairments, there is a generally reduced availability of mitochondrial GSH (Conde de la Rosa et al., 2014) which is linked to perturbed redox signaling, contributing to the progression of age-related diseases. Therefore, insights into the underlying molecular mechanisms that determine the coordination and precision of redox biology bear a huge potential for targeting thiol switches of key proteins involved in disease progression.

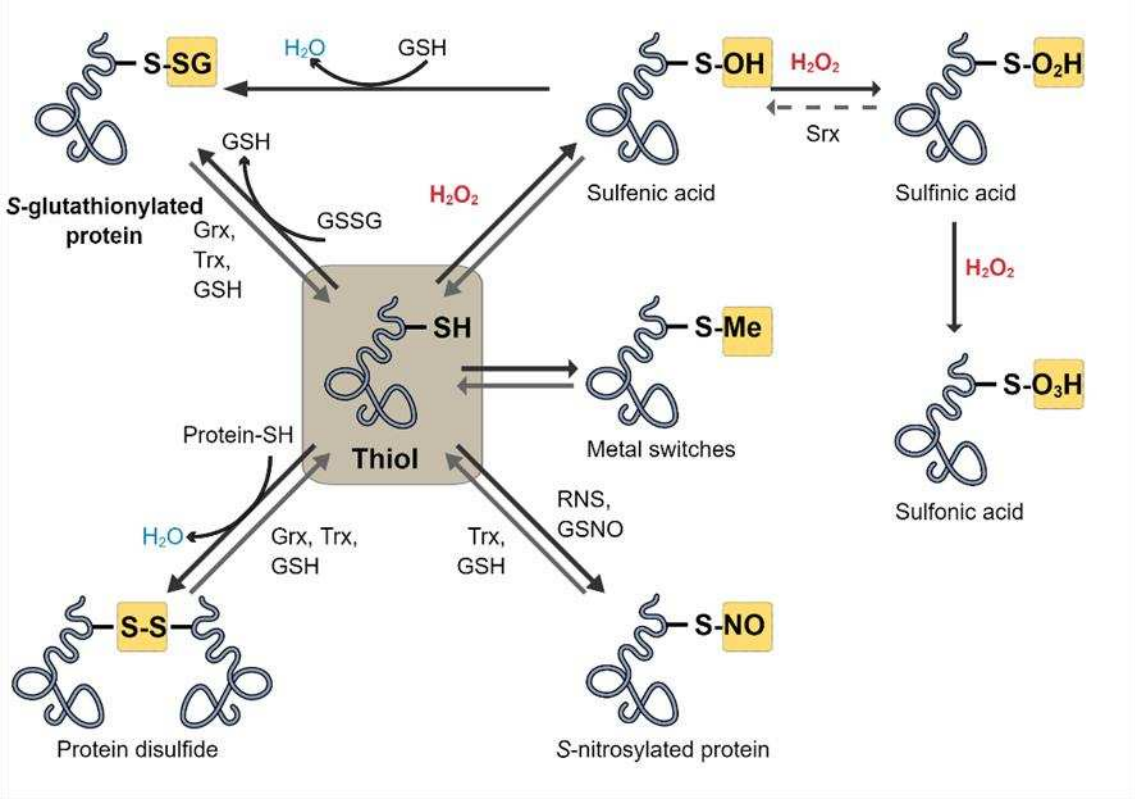

Figure 6. Scheme of physiological protein thiol switches (thiolswitches.de).
The sulfur in reduced protein thiols (-SH) has an oxidation state (OS) of -2, which can react dynamically with other thiols to form disulfide bonds (-S-S-) and set the OS of the sulfur to -1 (Lindahl et al., 2011). Thiols can also react with glutathione (GSH) and undergo glutathionylation (-PSSG). Both reactions are reversible by reduction by glutaredoxin (Grx), thioredoxin (Trx) or GSH to restore the reduced thiol group (-SH). Sulfenic acid (-SOH) is formed when hydrogen peroxide (H_2O_2) or other ROS react with a thiol and oxidize the thiol group (-SH), setting the OS from -2 to 0. This step is reversible by reduction by GSH and other reductants such as Grx and Trx to restore the reduced thiol group (-SH). Further oxidation of sulfenic acid to sulfonic acid ($-SO_2H$) sets the OS of sulfur to +2 and can still be reversed by sulfiredoxin (Srx), while further oxidation of sulfinic acid to sulfonic acid ($-SO_3H$) with an OS of sulfur of +4 is irreversible and is considered oxidative stress. Oxidation of thiols can also be triggered by reactive nitrogen species such as nitric oxide (NO) to form *S*-nitrosylated proteins (-S-NO) with an OS of -1. This reaction is reversible by Trx or the nitrosylated compound can nitrosylate further thiols by transnitrosylation with NO-containing species such as nitrosoglutathione (GSNO).

To detect changes in thiol switches, customized biosensors have been developed that can be targeted to specific cell compartments (Boss et al., 2018). One of the first redox-sensitive probes was the rxYFP (reduction-oxidation-sensitive yellow fluorescent protein), followed by the roGFP (reduction-oxidation-sensitive green fluorescent protein) (Meyer and Dick, 2010), which will be used in this thesis. The mechanism behind this lies in the two reversibly oxidized cysteine residues on the *Aequorea Victoria* GFP surface, which have two fluorescence excitation maxima at 400 (a rise of the excitation peak indicates cysteine oxidation) and 490 nm (a rise of the excitation peak indicates cysteine reduction) with emission collection at 510 nm (Hanson et al., 2004), allowing the sensor to respond to changes in the redox state in the environment (**Figure 7**). This is reflected in the formation of an intramolecular disulfide bridge that changes the conformation of the sensor,

resulting in a change in fluorescence that can be ratiometrically detected and quantified. Advantages of using roGFPs are their strong fluorescent signal, their pH stability and their independence from the probe concentration, as the ratio can be quantified based on the two excitation maxima (Schwarzlander et al., 2016).

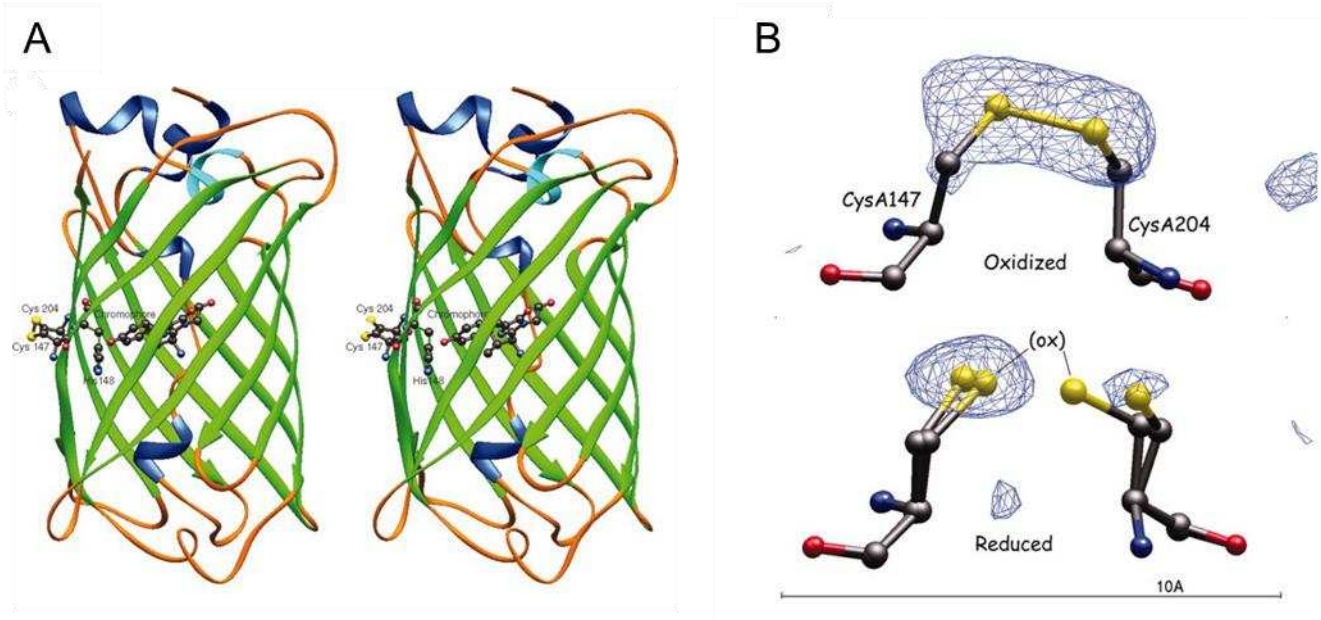

Figure 7. Crystal structure of the fluorescent redox sensitive probe roGFP (Hanson et al., 2004).
(A) Shows the atomic model of the first genetic redox-sensitive biosensor roGFP generated in 2004 for real-time analysis of changes in mitochondrial redox state. Redox alterations of relevant cysteines (here at 147 and 204) lead to a conformational change of the probe, which is accompanied by changes in fluorescence features that allow quantification of the redox change, which is proportional to the ratio F at 410/490. (B) Ball and stick model of cysteine residues which were introduced as reversibly oxidized thiol switches at two amino acid sites of GFP (here at 147 and 204) to detect oxidizing (disulphide formation, upper panel) and reducing (dithiol formation, lower panel) changes.

1.3.3. Dysregulated mitochondrial redox signaling in age-induced muscle decline

Organs and tissues possess different onsets for age-associated declines in functionality and health status. The involuntary and progressive decline in muscle mass and muscle function in elderly is defined as sarcopenia. Official data suggest a prevalence of sarcopenia between 8 to 40 % in people over 60 years (Abellan Van Kan, 2009). This age-induced muscle atrophy reduces muscle strength and increases morbidity, frailty, falls, muscle injury and overall mortality (Ziaaldini et al., 2017). At the muscle level, sarcopenia has been characterized by an equal loss of type 1 (slow twitch) and type 2 (fast twitch) fibers, with type 2 fibers losing size (Tanganelli et al., 2021). Risk factors for sarcopenia are low physical activity, malnutrition, high susceptibility to chronical inflammation, hormonal dysfunction especially due to downregulation of sex hormones and growth factors (Beas-Jiménez et al., 2011). The underlying metabolic processes that initiate and thrive sarcopenia are not fully understood which hampers the development of appropriate treatments. However, several hallmarks of sarcopenia are reported, such as chronic inflammation, dysfunctional mitochondria (Bratic and Larsson, 2013, Alway, 2019, Harper et al., 2021), reduced muscle stem-cell regeneration (García-Prat et al., 2016), protein aggregation, epigenetic changes combined with DNA impairments (Alway et al., 2014) and excess ROS production. Sustained high levels of ROS could weaken the responsiveness of muscle adaptation in aged muscles during exercise, which subsequently further drives muscle breakdown (Jackson et al., 2022). Since mitochondrial functionality plays a pivotal role not only in sarcopenia but also in multiple other age-related health impairments such as various cancers, diabetes, neurodegenerative, cardiovascular and airway diseases, obtaining a better understanding of the critical factors for mitochondrial homeostasis is essential for rational prevention and treatment options. Dysfunctional mitochondria are characterized by dysregulated redox signaling, impaired biogenesis, a reduction in the respiratory chain protein repertoire and ATP synthesis rate but also in the morphology and dynamics of the organelles (Boengler et al., 2017, Bhatti et al., 2017). These processes are linked to an increase in ROS levels, impaired mitochondrial Ca^{2+} signaling and the induction of cell death via the opening of the MPTP (Boengler et al., 2017). In the context of age-related muscle decline, dysfunctional redox signaling is furthermore associated with impaired satellite cells, reduced muscle regeneration and disturbed excitation-contraction coupling (**Figure 8**) (Szentesi et al., 2019).

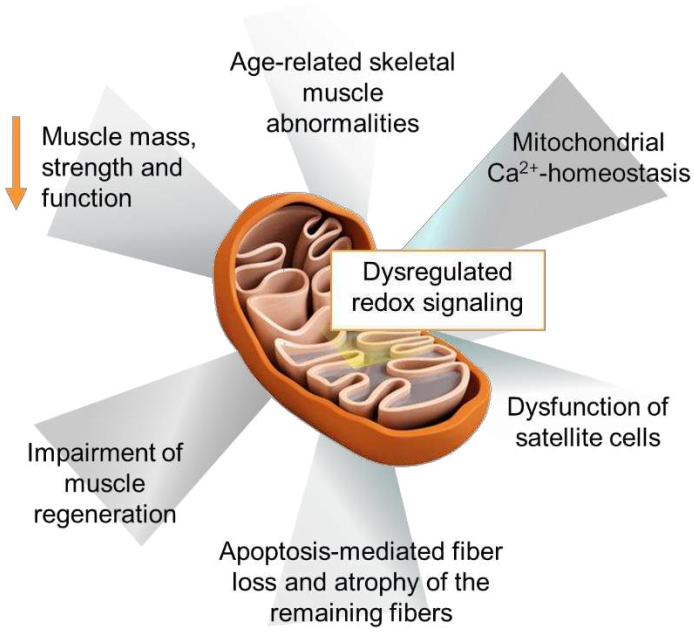

Figure 8. Reported effects of dysregulated mitochondrial redox signaling on age-related muscle decline (Szentesi et al., 2019).

Oxidative stress increases with age and is considered a major cause of mitochondrial dysfunction, causing multiple metabolic comorbidities. Particularly impaired mitochondrial redox signaling is thought to be a main driver of age-related muscle loss. If oxidative stress continues, muscle impairments are likely to increase, including decrease in muscle mass, strength and function, impaired muscle regeneration, apoptosis-mediated fiber loss and atrophy of remaining fibers, muscle stem cell dysfunction and altered mitochondrial Ca^{2+} homeostasis.

The idea that ROS play a role in aging was first postulated by Denham Harman in 1956 (Harman, 2002) stating that disrupted redox homeostasis due to increasing oxidative stress causes aging and age-related diseases. In mitochondria, unsaturated fatty acids and proteins with iron-sulphur clusters, as well as mtDNA, are susceptible to ROS (Smith et al., 2012) and become increasingly damaged during aging, impacting on skeletal muscle health if ROS are not kept in balance (Harper et al., 2021). Harman's theory has been challenged over time as ROS have been shown to be important signaling molecules e.g., in inducing muscle adaptations. It is now known that ROS play key roles in skeletal muscle-specific glucose uptake, mitochondrial biogenesis, excitation/contraction linkage, exercise adaptation and mitophagy (Le Moal et al., 2016, Henríquez-Olguin et al., 2019). Another series of studies that challenged Harman's theory showed that not only oxidants but also antioxidants increase during ageing (Dimauro et al., 2012, Ji et al., 1990). Further studies reported a link between skeletal muscle decline and decreased availability of redox-sensitive thiols leading to a limited redox flexibility and alterations in redox signaling (McDonagh et al., 2014, Le Moal et al., 2016). A recent human study with young and old subjects confirmed lower availability of reduced protein thiol groups in mitochondria of older subjects after exercise, suggesting that impaired redox signaling is the cause of reduced muscle adaptation during and after exercise (Pugh et al., 2021). While the exact molecular mechanisms of age-related muscle loss and sarcopenia need further investigation to decipher and identify the pathways involved (Calvani et al., 2013), physical exercise has proven to slow down age-related loss of muscle mass (Ji et al., 2016, Zampieri et al., 2016, Harper et al., 2021), suggesting that

an exercised muscle can - at least in part - overcome other factors associated with aging, such as nutritional status, chronic inflammation, changes in hormonal status, a decline in neuronal and mitochondrial function (Cruz-Jentoft and Sayer, 2019, Landi et al., 2014, Yoo et al., 2018). Another possibility to slow-down age-related muscle decline might be short-term nutritional interventions with mitochondria-targeted antioxidants (Calvani et al., 2013), including polyphenols through different mechanisms for example, attenuating death signaling coming from decreased removal of dysfunctional mitochondria which otherwise can augment loss of muscle fibers (Alway, 2019). Notably, polyphenols in foods have attracted a lot of interest since the 1990s, as there is growing evidence of their beneficial effects on human health (Visioli et al., 2011), and they will be covered in the next section.

1.4. Polyphenols and their effects on mitochondrial Ca^{2+}

Polyphenols are secondary compounds produced by plants and comprise a single or multiple phenol rings. According to their number of phenolic rings and the associated structure, polyphenols can be divided into different groups comprising phenolic acids, coumarins, stilbenes, lignans, isoflavonoids, phenolic polymers, and flavonoids. The latter group is subdivided into the most abundant flavonols (e.g. kaempferol, quercetin, fisetin) (**Figure 9**), and the less abundant flavones (e.g. luteolin, apigenin), flavanones (e.g. naringenin, hesperitin), flavanonols (e.g. taxifolin), flavanols (e.g. catechins) and anthocyanidins (e.g. cyanidin, delphinidin) (Barba et al., 2014). Polyphenols have been shown to exert anti-inflammatory, anti-microbial, anti-cancerous, and antioxidant functions. The reducing power of polyphenols depends on the amount and position of hydroxyl groups as their hydrogen is used to quench oxidants.

In 2004, Montero et al. tested the effect of some flavonoids and reported a direct effect of the flavonol kaempferol on mitochondrial Ca^{2+} uptake (Montero et al., 2004). The effect was blunted when mitochondrial Ca^{2+} uptake was inhibited using Ru360. In search of the underlying mechanism, the authors proposed that the activation of mitochondrial Ca^{2+} uptake by selected flavonoids is not restricted to their antioxidant effect by testing several antioxidants including α-tocopherol, lipoic acid, ascorbic acid and N-methyl-cysteine, which showed no impact on mitochondrial Ca^{2+} uptake. The fact, that quercetin and galangin showed less potent effects on mitochondrial Ca^{2+} uptake compared to kaempferol gives rise that the position of the individual hydroxy groups plays a significant role in MCU-activation. Finally, the authors hypothesized a direct interaction with the MCU, potentially dependent on the 4'hydroxy group of the B ring and the 3' hydroxy group of the C ring, which remained to be proven as the molecular identity of the MCU was only identified in 2011 (Baughman et al., 2011, De Stefani et al., 2011). Regarding the impact of kaempferol on mitochondrial Ca^{2+} signaling, a screening at the NIHS has identified several potent close analogues of kaempferol that stimulate mitochondrial Ca^{2+} uptake via the MCU.

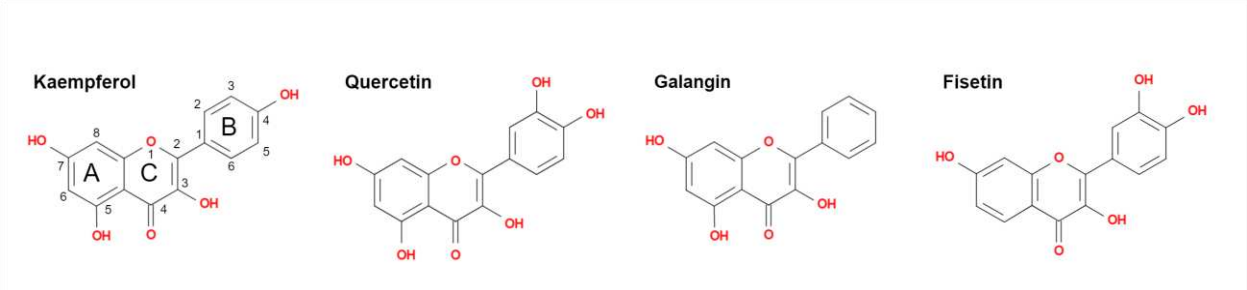

Figure 9. Chemical structures of selected flavonoids.
The first structure shows kaempferol and the general nomenclature for phenolic compounds.

It is important to mention oleuropein at this point, another polyphenol that is one of the central polyphenols in this thesis. In 1959, oleuropein (**Figure 10**) was for the first time isolated and chemically characterized (Shasha and Leibowitz, 1959) and has been demonstrated later as being the most abundant polyphenol in olive leaves, seed, pulp and peel of unripe olives (Barbaro et al., 2014). Oleuropein is a methyl ester of dimethyl-oleuropein, comprising the polyphenol hydroxytyrosol, the secoiridoid elenolic acid, and glucose (Ahamad et al., 2019). During the ripening process of olives, oleuropein is increasingly hydrolysed to oleuropein aglycone (**Figure 10**) and finally hydroxytyrosol (Wang et al., 2021). Additional studies, associated oleuropein with numerous health benefits linked to attenuating Alzheimer's and Parkinson's disease (Sarbishegi et al., 2014, Bazoti et al., 2006), decreased production of inflammatory cytokines, reducing oxidative burst after post-ischemic injury, anti-thrombotic, anti-atherosclerotic and anti-cancerous effects (Hamdi and Castellon, 2005, Casaburi et al., 2013). In the context of cancer, oleuropein might act through antioxidant mechanisms to prevent a pro-oxidative environment favoring oncogenesis and/or through an anti-angiogenic function in slowing down tumor progression (Barbaro et al., 2014). In primary chicken muscle cells, oleuropein was shown to decrease mitochondrial ROS production and increase mitochondrial biogenesis by stimulating PGC-1α protein expression (Muroi et al., 2022).

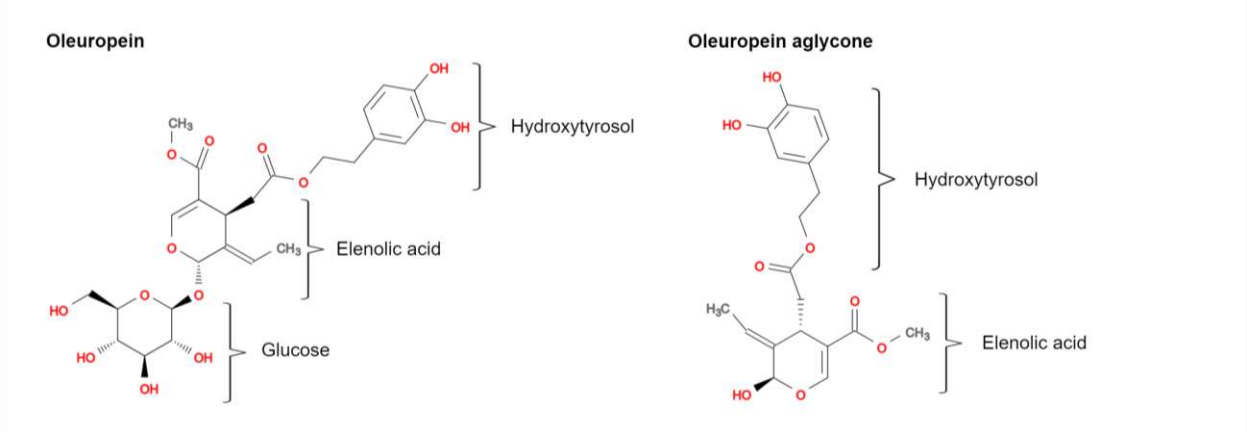

Figure 10. Chemical structure of oleuropein and oleuropein aglycone.
The left side shows the structure of the secoiridoid oleuropein identified by Panizzi et al. (Bianco & Ramunno, 2006) with its three components, the polyphenol hydroxytyrosol, the secoiridoid elenolic acid and glucose (Ahamad et al., 2019). On the right side is the aglycone form of oleuropein, which is formed by β-glucosidase-induced hydrolysis of the glucose moiety.

Section 2: Aim of the thesis

Over the last two decades, Ca^{2+} accumulation in energized mitochondria has been shown to be a biological event of paramount physiological importance (Rizzuto et al., 2012). MCU-mediated mitochondrial Ca^{2+} uptake has been demonstrated to regulate intracellular Ca^{2+} signaling, cell metabolism, cell survival and additional cell type-specific functionalities through buffering cytosolic Ca^{2+} concentrations and mediating regulation of mitochondrial effectors (Nemani et al., 2018, Rizzuto et al., 2012). In parallel, the redox state of mitochondrial thiol groups is emerging as a central process in cell physiology and pathology, as many mitochondrial functions are linked to matrix redox reactions (Mailloux et al., 2014, Riemer et al., 2015). Regulation of the redox state of mitochondrial thiol groups is intimately linked to mitochondrial Ca^{2+} signaling; however, no causal link has been demonstrated until now between these two types of signaling pathways.

All these reflections are particularly relevant for skeletal muscle tissue, a tissue with high energy demands. In skeletal muscle, MCU-mediated uptake of Ca^{2+} couples muscle contraction to mitochondrial energy metabolism. However, the role of MCU in the aging skeletal muscle in conjunction with an MCU-targeted intervention via a natural bioactive compound has not been investigated.

Given the above considerations, the overall aim of the present thesis is to better understand the crosstalk between mitochondrial Ca^{2+} and mitochondrial redox signaling and to assess the feasibility of an MCU-based intervention strategy, focusing on skeletal muscle systems. The 3 main objectives are described here:

(1) Establish the role of MCU in modulating the mitochondrial redox balance and show its impact on muscle energy metabolism and muscle function.
Considering the simultaneous oxidizing and reducing effects of MCU activation on the redox state of matrix thiol groups and the unknown net effect of MCU stimulation, a possible causal relationship between MCU activation and the regulation of the mitochondrial redox state needed to be explored. Given that several conditions and diseases are associated with deregulated redox signaling in mitochondria, the demonstration of a possible causality between MCU regulation and matrix redox state modulation would make MCU a novel pharmacological or nutritional target in such contexts.

(2) Clarify the role of MCU on skeletal muscle aging and determine the biological effect of an MCU-targeted intervention with natural bioactive compounds.

Based on the coupling between skeletal muscle contraction and energy production through mitochondrial activation, and in light of the known link between muscle aging and dysfunctional mitochondria, the role of the MCU in the context of muscle aging was investigated. In addition, the efficacy of an MCU-targeted intervention on mitochondrial energy production and muscle function was explored in both, control (adult) and aged muscle models.

(3) And finally, the mechanisms by which an MCU activation mediates its effects should be revealed.

Models in which specific subunits of the MCU complex are ablated are employed to study the mechanism of action of specific polyphenols that have been shown to be MCU activators. Moreover, the effect of these selected compounds on mitochondrial respiration *in vivo* in *C. elegans* was assessed.

Section 3: Materials and Methods

3.1. Part 1: MCU and mitochondrial redox biology in skeletal muscle (Weiser et al 2022)

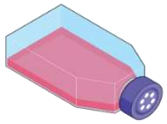

3.1.1. Cell lines and maintenance conditions

Control HAP1 cells and CRISPR/Cas9-edited knockout (KO) cell lines were purchased from Horizon and maintained in Iscove's Modified Dulbecco's Medium (IMDM) (Gibco Thermo Fisher, Scotland) containing 10 % heat-inactivated fetal bovine serum, 100 U/ml penicillin and 100 mg/ml streptomycin (Gibco, Thermo Fisher).

Human Skeletal Muscle cells (#CC-2580: 655307, Lonza) were kept in Skeletal Muscle Cell Growth Medium (AmsBio, SKM-M medium). Unless otherwise indicated, incubation conditions for all cell lines were maintained at 37 °C and 5 % CO_2. Primary human myoblasts from adult donors were obtained from Lonza after the supplier received informed consent from the donors and after consent was obtained from the Vaud ethics commission for human research (CER–VD) under protocol 281/14.

3.1.2. *C. elegans* strains and maintenance

C. elegans strains used in this paper are the wild-type Bristol N2 strain as control and the CZ19982 strain (Xu and Chisholm, 2014) as mutant mcu-1 (ju1154), characterized by dysfunctional MCU activity (Álvarez-Illera et al., 2020). All strains were purchased from the Caenorhabditis Genetics Center (University of Minnesota) and maintained at 20 °C on agar plates containing nematode growth media (NGM) spotted with *E. coli* strain HT115.

3.1.3. Western blot and antibodies

To detect MCU protein levels in HAP1 cells, mitochondria were isolated and resuspended in incubation buffer (300 mM sucrose, 10 mM Hepes, 0.5 mM EGTA, Complete EDTA-free protease inhibitor mixture, Roche, pH 7.4). Protein concentration was measured using BCA protein assay kit (Pierce, Thermo Fisher). Twenty µg of protein was separated by SDS-polyacrylamide gel electrophoresis using 4-12 % acrylamide gels (Invitrogen) and transferred to PVDF membranes (Mini format 0.2 µm PVDF, Bio-Rad) using a semi-dry blotting protein transfer (Bio-Rad, Trans Blot Turbo). Membranes were washed with TBS-tween buffer (0.5 M Tris, 1.5 M NaCl, 0.01 % Tween, pH 7.4) before blocking with 5 % BSA for 1-h at RT. The washed

membranes were incubated overnight with the primary antibodies MCU 1:1000 (Sigma Life Science, #HPA016480) and TOM20 1:1000 (Cell Signaling, #42406) diluted in 1 % BSA at 4 °C. The next day, the washed membranes were incubated for 1-h at RT with IRDye 800 CW goat anti rabbit IgG (LI-COR Biosciences, U.S.) 1:15000 diluted in 1 % BSA. For quantitative analysis of Western blot data, membranes were scanned using the Odyssey scanner (LI-COR Biosciences, U.S.).

To detect MCU protein in primary human myotubes, cells were lysed with RIPA buffer and proteins were quantified by BCA. The samples were processed using the Sally Sue automated capillary western blotting system (ProteinSimple, San Jose, CA, USA). Sample preparation was performed according to the manufacturer's protocol using the Anti-Rabbit Detection Module (ProteinSimple, #DM-001) and the 12-230 kDa Sally Sue Separation Module (ProteinSimple, #SM-S001). The loading concentration was adjusted to 0.2 µg/µl using RIPA buffer. Primary antibodies used were MCU 1:30 (Cell Signaling, #14997) and TOM20 1:100 (Cell Signaling, #42406) diluted in the manufacturer's antibody diluent (ProteinSimple).

3.1.4. Measurement of mitochondrial Ca^{2+} uptake in HAP1 cells and primary human myotubes

Per well, 35000 control HAP1 cells and 30000 MCU-KO HAP1 cells were seeded in a white 96 well plate with a clear bottom and incubated overnight. The mitochondrial Ca^{2+} uptake was measured with the bioluminescent genetically encoded mitochondrial mutant aequorin calcium indicator (Montero et al., 2004, Bonora et al., 2013), which was transferred from an adenovirus (Sirion Biotech, Germany). Infected HAP1 cells were incubated for 24-h prior to the measurement with the Cytation3 imaging reader (BioTek, Switzerland). For measurement, medium was removed, and cells were incubated with native coelenterazine 5 µM (Biotium, USA, #55779-48-1), diluted in aequorin buffer (145 mM NaCl, 1 mM $MgCl_2$, 5 mM KCl, 10 mM HEPES, 10 mM glucose, 1 mM $CaCl_2$, pH 7.4) for 2-h at RT in the dark. Then coelenterazine was aspired and aequorin buffer added. Basal luminescence was measured, followed by stimulation with 1 mM ATP (Merck, Germany, #A2383-10G). The experiment was ended by adding a solution containing 25 µM digitonin (Merck, Germany, #11024-24-1), 10 mM $CaCl_2$ (Merck, Germany, #10043-52-4) which calibrates the fluorescence signal as described by Montero and collaborators (Montero et al., 2004).

For experiments rescuing MCU expression in MCU-KO HAP1, MCU-KO cells were seeded as described above and incubated at 37 °C and 5 % CO_2 for 24-h. Then the cells were transfected with 0.75 g/well MCU plasmid (Origene, #MC212635), or with pcDNA3.1 (Thermo Fisher

Scientific, #V79020, control cells) using the jetPEI DNA transfection Kit (Polyplus transfection, USA). Cells were incubated for 24-h before infection with 200 MOI of the adenoviral vector carrying mitochondria-targeted aequorin. After 24-h, mitochondrial Ca^{2+} uptake was measured according to the general protocol previously described.

Human Skeletal Muscle cells (Lonza) were seeded in 96-well plate, coated with human fibronectin (Corning) at 20 µg/ml for 1-h at RT and washed twice with PBS 1 X (Thermo Fisher Scientific) before adding 12000 cells/well in growth medium (AmsBio, SKM-M medium). After 24-h of incubation at 37 °C, knockdown of MCU was induced by adenoviral infection with MCU shRNA (Sirion Biotech, Germany) at 100 MOI. Control cells were subjected to adenoviral infection with scrambled shRNA (Sirion Biotech, Germany) at 100 MOI and incubated for 48-h. Cells were then differentiated into myotubes by replacing the medium with Dulbecco's Modified Eagle Medium F-12 Nutrient Mixture (DMEM/F-12 (1:1) (1x) + GlutaMAX) (Gibco, Thermo Fisher), containing 2 % horse serum,100 U/ml penicillin and 100 mg/ml streptomycin (Gibco, Thermo Fisher). After 3 days of incubation, cells were subjected to adenoviral infection with mitochondria-targeted aequorin at 200 MOI and incubated for 24-h. Mitochondrial Ca^{2+} uptake was determined according to the general protocol, using 5 mM caffeine (Sigma Aldrich, #C0750) and 10 µM epibatidine (Sigma Aldrich, #E1145) as stimulants to trigger an increase in cytosolic Ca^{2+} that activates MCU. Caffeine causes Ca^{2+} release from the SR by binding to the RyR (Reggiani, 2021), while epibatidine is an alkaloid that binds to the muscle acetylcholine receptor (AChR), which is a protein complex that allows ion transduction of Na^{+} and Ca^{2+} across the postsynaptic membrane after binding of the agonist (Traynor, 1998, Prince and Sine, 1999).

For the analysis of mitochondrial Ca^{2+} uptake data, the raw data from the Cytation3 Imaging Reader (BioTek, Switzerland) were calibrated using the following equation (Bonora et al., 2013):

$$Ca^{2+}\,(M) = \frac{\left(\frac{L}{L_{max}} * \lambda\right)^{\frac{1}{n}} + \left(\left(\frac{L}{L_{max}} * \lambda\right)^{\frac{1}{n}} * K_{TR}\right) - 1}{K_R - \left(\left(\frac{L}{L_{max}} * \lambda\right)^{\frac{1}{n}} * K_R\right)}$$

L = light intensity at sampling time
L_{max} = total light emitted at sampling time
K_R = constant for calcium-bound state
K_{TR} = constant for calcium-unbound state
λ = rate constant for aequorin consumption at saturation [Ca^{2+}]
n = number of Ca^{2+} -binding sites

In HAP1 cell experiments, each calibrated calcium trace was used to calculate the area under the curve (AUC), using cubic smoothed splines. The final graphs show mitochondrial Ca^{2+} in AUC %. For this purpose, results from control cells were averaged and rescaled to a reference value of 100 % and then each AUC was normalized with this. In experiments with human myotubes, calibrated calcium traces were used to define the interval in which mitochondrial Ca^{2+} uptake increases and subjected to linear regression to determine slope values of mitochondrial Ca^{2+} uptake. Significant differences in mitochondrial Ca^{2+} uptake between two groups were calculated using the Student's t-test for parametric data and the Mann-Whitney-Wilcoxon test for non-parametric data. To investigate differences between more than two groups, a one-way ANOVA was applied.

3.1.5. Cellular NAD(P)H/NAD(P)$^+$ ratio in HAP1 cells

Cells were grown in 6-well plates at a density of 200000 cells of control HAP1 and 150000 cells of MCU-KO HAP1. One plate was prepared for each time point and incubated overnight. Cells were then stimulated with 1 mM ATP (Merck, Germany, #A2383-10G) and incubated at 37 °C according to the selected time points (10-s, 15-min) before plates were placed on ice to wash the cells twice with PBS 1X and add NAD(P)$^+$/NAD(P)H extraction buffer for 20-min. Cells were scraped and homogenized using a 1 ml syringe and transferred to 1.5 ml Eppendorf tubes. Samples were vortexed for 10-s and then centrifuged at 13000 g for 10-min. The supernatant was transferred to fresh tubes and NAD(P)$^+$/NADH concentrations were measured using the NAD(P)$^+$/NAD(P)H quantification kit (Sigma Aldrich, #MAK037) according to the manufacturer's protocol. Results were normalized to protein concentrations, determined by using BCA (Pierce Thermo Fisher).

3.1.6. Mitochondrial superoxide anion in HAP1 cells

To measure mitochondrial superoxide anion in HAP1 control and MCU-KO cells, HAP1 were washed, trypsinized, centrifuged and resuspended in IMDM medium before transferring 500000 cells in 1 ml of IMDM medium, into round-bottomed FACS tubes. Cells were then incubated with 2.5 µM MitoSOX (Thermo Fisher Scientific, #M36008) for 15-min at 37 °C and 5 % CO_2. Fluorescent signal of superoxide production was measured by flow cytometry at baseline, followed by addition of 1 mM ATP (Merck, Germany, #A2383-10G) or 1 ml of IMDM medium as control. Samples were acquired by means of a 5-laser Fortessa Cell Analyzer (Becton Dickinson, USA) using the 561 nm laser line excitation and collecting fluorescence emission with a 610/20

band pass filter. Cells were identified using scatter parameters, excluding debris and out-of-scale events. For data analysis, the results from the medium injected cells were subtracted from the ATP stimulated samples to derive the delta values of ATP evoked mitochondrial $O_2^{\bullet-}$ production.

3.1.7. Mitochondrial and cytosolic redox state in HAP1 cells

To determine the redox state in mitochondria and the cytosol, 800000 HAP1 control cells and 750000 HAP1 MCU-KO cells were seeded in 35 mm glass coverslips (MatTek, USA) and incubated with 2 ml IMDM medium for 24-h, followed by transfection with the jetPRIME transfection kit (Polyplus transfection, USA) to add 2 µg of either mitochondria-targeted or cytosol-targeted roGFP1-DNA (Hanson et al., 2004) (provided by S. James Remington, University of Oregon, Eugene, OR) per coverslip. The medium was changed after 24-h and the cells were incubated for additional 48-h. Before recording the mitochondrial and cytosolic redox state, cells were washed twice with Krebs–Ringer bicarbonate Hepes buffer (KRBH), containing (in mM): 140 NaCl, 3.6 KCl, 0.5 NaH_2PO_4, 0.5 $MgSO_4$, 1.5 $CaCl_2$, 10 Hepes, 5 $NaHCO_3$ pH 7.4, and 2.5 mM glucose. The coverslips were placed under the DMI6000 B inverted fluorescence microscope with a HCX PL APO 40×1.30 NA oil immersion objective (Leica Microsystems) and an Evolve 512 back-illuminated CCD with 16×16 µm pixel camera (Photometrics, Tucson, Arizona), and the cells were excited at 480 and 410 nm to record emission at 535 nm (535DF45, Omega Optical) using a 505DCXR (Omega Optical) dichroic mirror. Images for the mitochondrial and cytosolic redox state were acquired every 5-s before and after stimulation with 1 mM ATP (Merck, Germany, #A2383-10G). The 480/410 ratio traces obtained were normalized to both the minimum ratio fluorescence, by addition of 10 mM H_2O_2 (Sigma Aldrich, #16911), and the maximum of ratio fluorescence, by addition of 60 mM DTT, (Sigma Aldrich, #1610611). Traces were calculated using MetaFluor 7.0 and further analysed in Excel (Windows Microsoft) and GraphPad Prism 7.02.

For experiments rescuing MCU expression in MCU-KO cells, MCU-KO cells were seeded as above and co-transfected with the jetPRIME transfection kit (Polyplus, USA) with either 2 µg of MCU DNA (Origene, #MC212635) plus 2 µg of mitochondria-targeted roGFP1 DNA per coverslip or 2 µg pcDNA3.1 (Thermo Fisher Scientific, #V79020) plus 2 µg of mitochondria-targeted roGFP1 DNA per coverslip (control). The medium was changed after 24-h and the cells were incubated for 48-h before measurement.

3.1.8. Mitochondrial redox state in primary human myotubes

To measure mitochondrial redox state in primary human myotubes, 8000 cells per well were seeded in a black 96-well clear-bottomed plate, coated for 1-h at RT with human fibronectin (Corning) at 20 µg/ml and washed twice with PBS 1 X (Thermo Fisher). Then Skeletal Muscle Cell Growth Medium (AmsBio, SKM-M medium) was added and cells were incubated overnight. Cells were then subjected to adenoviral infection with MCU or scrambled shRNA (Sirion Biotech, Germany) at 100 MOI and incubated for 48-h. Cells were then differentiated into myotubes by medium exchange with DMEM/F-12 (1:1) (1x) + GlutaMAX (Gibco, Thermo Fisher) containing 2 % horse serum, penicillin (100 U/ml) and streptomycin (100 mg/ml) (Gibco, Thermo Fisher). After incubation for three days, cells were infected with an adenovirus containing a mitochondria-targeted roGFP1 at 150 MOI and incubated for 24-h before the mitochondrial matrix redox state was determined using the Cytation3 Imaging Reader (BioTek, Switzerland). Myotubes were excited at 480 and 410 nm and emission was recorded at 535 nm. Basal redox state was recorded for 3-min before myotubes were stimulated with 5 mM caffeine (Sigma Aldrich, #E1145) and 10 µM epibatidine (Sigma Aldrich, #E1145) and recorded for 3-min before adding a final injection with 60 mM DTT (Sigma Aldrich, #1610611) to normalized to the traces to the DTT induced maximum reduction.

3.1.9. RNA extraction and cDNA synthesis for RT-qPCR in *C. elegans*

RNA was extracted from L4 control and *mcu*-1 mutants by washing and pelleting worms in 15 ml falcons from well-populated 9-cm NGM plates until most of the bacteria had disappeared, as indicated by a clear supernatant. The falcons were placed on ice and 1 ml of QIAzol lysis reagent (Qiagen, #85300) was added. Worms were transferred to 1.5 ml tubes containing 1 Tungsten Carbide Bead 3 mm (Qiagen) and homogenized with the TissueLyser II (Qiagen) for 1-min. 200 µL of chloroform (Merck, #67-66-6) was added per sample and samples were mixed in the rack before centrifugation at 12000 rcf for 10-min at 4 °C. 600 µL of the upper clear phase was transferred to a new tube and 1 volume of isopropanol was added and mixed before the samples were transferred to the appropriate columns according to the manufacturer's instructions for the RNeasy Protect Mini Kit (Qiagen). Total RNA concentration and quality were determined using the Nanodrop spectrophotometer before reverse transcription was performed to obtain cDNA according to the manufacturer's protocol (High-Capacity cDNA Reverse Transcription Kit, Thermo Fisher). Applied conditions for reverse transcription: 10-min at 25 °C, followed by 120-min at 37 °C and 5-min at 85 °C. The LightCycler 1536 DNA Green Master System (Roche Applied Science)

was used for qPCR. Two assays were conducted with a total number of 4 biological specimens, which were measured in two technical replicates. *Ama*-1 was used as the housekeeping gene and relative gene expression data was analyzed using the $2^{-\Delta\Delta Ct}$ method. Primer sequences are as follows:

mcu-1: FW, 5'-CGCCGTGTATGGAACGAGTA-3'; RV, 5'-ATGACTCGATCCGTGTGAGC-3'

ama-1: FW, 5'-GAAAAGGCGAAGGATGTGTTG-3'; RV: 5'-TCCGGCATCTCGTAGAAAATC-3'

3.1.10. Oxygen consumption rate (OCR) in myotubes and *C. elegans*

OCR was measured using the Seahorse XF96 instrument (Seahorse bioscience Inc., North Billerica, MA, USA). For primary human myotubes, 8 000 myoblasts per well were seeded in Seahorse XF96 Cell Culture Microplates (Agilent) previously coated with human fibronectin (Corning) at 20 µg/ml for 1-h at RT and washed twice with PBS 1X (Thermo Fisher) before adding the cells and incubating them overnight. Subsequently, adenoviral infection with MCU shRNA (Sirion Biotech, Germany) at 100 MOI was performed to knockdown MCU. Adenoviral infection with scrambled shRNA (Sirion Biotech, Germany) was used as a control, and cells were incubated for 48-h before initiating differentiation into myotubes by replacing the medium with DMEM/F-12 (1:1) (1x) + GlutaMAX (Gibco, Thermo Fisher) containing 2 % horse serum, penicillin (100 U/ml) and streptomycin (100 mg/ml) (Gibco, Thermo Fisher). After 3 days of incubation, cells were washed with KRBH, containing 10 mM glucose, 1.5 mM $CaCl_2$ and 1 mM pyruvate and incubated at 37 °C without CO_2. For measurements with mitochondrial paraquat (mtPQ, Cayman, #CAY-188085), the chemical was added to the washed cells 15-min before acquisition at a concentration of 0.01 µM. The injection sequence includes the following chemicals: 10 mM DTT (Sigma Aldrich, #1610611), a mix of 5 mM caffeine (Sigma Aldrich, #E1145) and 10 µM epibatidine (Sigma Aldrich, #E1145), 2.5 µg/ml oligomycin (Sigma Aldrich, #75351), 3 µM FCCP (Sigma Aldrich, #C2920), a mix of 2 µM rotenone (Sigma Aldrich, #45656) and 2 µg/ml antimycinA (Sigma Aldrich, #A8674). The control vehicle used was Krebs buffer. The chemicals were injected during acquisition as shown in the figures. In contrast to cellular respiratory assays, oligomycin, rotenone and antimycinA are not used in *C. elegans* as they are not taken up across the cuticle (Koopman et al., 2016a).

For *C. elegans*, synchronized control and *mcu*-1 mutants were grown to day 4 of adulthood on NGM plates containing 10 µM 5-Fluorouracil (Sigma Aldrich, #F6627) to inhibit ovulation. Next, worms were washed with M9 buffer and centrifuged at 1200 rpm at 20 °C for 3-min. The worm pellet was resuspended in M9 buffer and 20-30 worms per well were transferred into a Seahorse

XF96 Cell Culture Microplate (Agilent), with the final volume adjusted to 200 µl with M9 buffer. The chemicals injected during acquisition of the OCR were 0.1 µM mtPQ (mtPQ, Cayman, #CAY-188085), 10 mM DTT (Sigma Aldrich, #1610611), 10 mM carbachol (Merck, #C4382) and 40 mM NaN3 (Sigma Aldrich, #S2002). The control vehicle used was M9 buffer.

3.1.11. Mobility in *C. elegans*

Synchronized worms were transferred on 35-mm Ø NGM agar plates with HT115 at 20 °C and recorded on day 4 of adulthood. A total of 4 conditions were compared: control N2 with M9 buffer, N2 treated with 0.1 µM mtPQ, control *mcu*-1 mutants with M9 buffer and *mcu*-1 mutants treated with 10 mM DTT (Sigma Aldrich, #1610611). For the treatment, 1 µl of M9 buffer, mtPQ (Cayman, #CAY-188085) or DTT solution were directly pipetted on the individual worms under the microscope and incubated for 20-min before recording the worms. Three plates of 10 worms each were recorded for 45-s per condition. Plates were recorded using a Leica M165 FC microscope with a DFC7000 T 2.8 MP camera (Leica Microsystems) connected to a computer. The recorded videos were used to calculate the distance covered by the worms according to the organism's center of gravity using the Parallel Worm Tracker for MATLAB (Ramot et al., 2008). Based on this, the average speeds of the worms per plate and condition were calculated with ObjectAnalyzer and further analysed with Excel and Graphpad Prism 7.02 (Mouchiroud et al., 2016).

3.1.12. Data analysis

Data analysis and statistical tests were performed using R version 3.5.2 and GraphPad Prism 9.3.1. All data were expressed as the mean ± SEM. Samples were tested for normality using the Shapiro-Wilk test. The results were statistically analyzed using parametric Student's *t*-test or non-parametric Mann-Whitney-Wilcoxon test for two groups and the parametric one-way ANOVA or non-parametric Kruskal Wallis test for multiple groups. Results were considered significant at an alpha level of 0.05; $*p < 0.05$.

3.2. Part 2: MCU and oleuropein in muscle ageing (Gherardi and Weiser et al 2023)

3.2.1. Cell lines and maintenance conditions

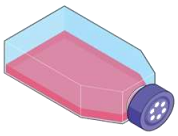

HeLa cells (ATCC, #CCL-2TM) were maintained in growth medium consisting of DMEM, GlutaMAX supplement Medium (MEM) (Gibco, Thermo Fisher) containing 10 % heat-inactivated fetal bovine serum, penicillin (100 U/ml) and streptomycin (100 mg/ml) (Gibco, Thermo Fisher).

Mouse Embryonic Fibroblasts (MEF) (MitoCare Center, department of pathology, USA) and C2C12 (ATCC, #CRL-1772) were cultured in growth medium comprising DMEM, high glucose, GlutaMAX™ Supplement, pyruvate (Gibco, Thermo Fisher) containing 10 % heat-inactivated fetal bovine serum, penicillin (100 U/ml) and streptomycin (100 mg/ml). C2C12 were differentiated using DMEM, high glucose, GlutaMAX™ Supplement, pyruvate (Gibco, Thermo Fisher) supplemented with 1 % heat-inactivated horse serum (Gibco, Thermo Fisher), penicillin (100 U/ml) and streptomycin (100 mg/ml).

Human Skeletal Muscle cells were purchased from different vendors (Lonza, Amsbio, and Cook Myosite) and kept in Skeletal Muscle Cell Growth Medium (Zen-Bio, SKM-M medium). Young donors were purchased from Lonza (#CC-2580: 655307, 639629) and Amsbio (#SKB-F: SKM070512A), and old donors from Amsbio (#SKB-F: SK120211, SKM062712B) and Cook Myosite (#SK1111: P01477, P01064, P01590). Differentiation of human myoblasts was initiated by adding DMEM/F-12 (1:1) (1x) + GlutaMAX (Gibco, Thermo Fisher) containing 2 % heat-inactivated horse serum, penicillin (100 U/ml) and streptomycin (100 mg/ml). All cell lines were maintained at 37 °C and 5 % CO_2 which represent standard incubation conditions. Changes of incubation conditions are indicated in the respective methods.

Primary human myoblasts from adult donors were obtained from Lonza, Amsbio and Cook Myosite after the supplier received informed consent from the donors and after consent was obtained from the Vaud ethics commission for human research (CER–VD) under protocol 281/14.

3.2.2. Animals

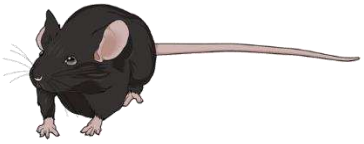

The animal experiments in this work were performed by our collaborators from the University of Padova and were approved and carried out in accordance with the Italian law D. L.vo n_26/2014. Wild-type C57Bl6J mice were purchased from Charles River or Janvier Lab. Mice with a skeletal muscle specific MCU knockout (skMCU-/-) were developed and generated in the laboratory of Prof. Mammucari; for more information see the corresponding paper (Gherardi et al., 2019b). Adult mice were 4 months old and the older animals

were 24 months old when the experiments were conducted. For all genotypes (WT, fl/fl, skMCU-KO and aged mice) a chronic treatment with oleuropein (20mg/kg/day) was done for 4 weeks. After 2 weeks, running capacity experiments were performed and after 4 weeks all remaining experiments were performed such as OCR, PDH activity and mitochondrial Ca^{2+} uptake.

3.2.3. *In vivo* DNA transfection of mouse skeletal muscle

The mice used in this work were adult males and anaesthetized before starting experimental procedures. A hyaluronidase solution (2 mg/ml) (Sigma) was injected under the foot pads of the hind limbs (Gherardi et al., 2019a). In the same way, but with a 30-min pause in between, 20 µg of plasmid DNA in 20 µl of physiological solution was injected. A gold-plated acupuncture needle was then positioned under the skin at the heel and a second needle at the base of the toe, parallel to each other and perpendicular to the long axis of the foot and connected to the BTX porator (Harvard apparatus). The muscles were electroporated with 20 pulses of 20 ms duration each and an interval of 1 s to generate an electric field of 100 V. Individual fiber cultures were made 7 days later.

3.2.3. Mouse exercise studies

Prior to the start of the acute concentric loading experiments, mice were acclimatized by training on a 10° uphill LE8700 treadmill (Harvard apparatus) for 2 days. On the first day, mice were exposed to a 5-min running sequence on the treadmill at a speed of 8 m min-1, and on the second day, the same sequence was followed with an additional 5-min speed of 10 m min-1. On the third day, mice were exposed to a single running sequence starting at a speed of 10 m min-1. After 10 minutes, the speed was continuously increased by 1 m min-1 every 5 minutes until the mice were exhausted. Exhaustion was defined as the state in which the mice stood on the electric shocker for more than 5 seconds without trying to run again. For each mouse, the total running time and the total running distance were recorded.

3.2.4. PDH activity

To assess PDH activity in TA muscles, the Pyruvate Dehydrogenase Enzyme Activity Microplate Assay Kit (Abcam) was used according to manufacturer's instructions.

3.2.5. Western blot and antibodies

To determine the expression level of MICU1 protein in control and MICU1-KO MEF cells, cells were washed twice using PBS and scraped from a 175 cm^2 flask to collect the lysate in 50 ml falcons on ice before centrifuging the cells at 1500 rpm for 4 min at 4 °C. The supernatant was discarded and cells were resuspended in Mito buffer (300 mM sucrose, 10 mM Hepes, 0.5 mM EGTA, Complete EDTA-free protease inhibitor mixture (Roche), pH 7.4) and incubated on ice for 30-min. Cells were transferred to a 2 ml glass potter for homogenization and transferred to a 2 ml Eppendorf tube and centrifuged at 600 g for 10-min at 4 °C. Supernatant was collected in a 1.5 ml Eppendorf tube and centrifuged at 6000 g for 10-min at 4 °C to pellet the mitochondria. Next, supernatant was discarded and the pellet was dissolved in 50 µl Mito buffer to measure protein concentration via BCA (Pierce Thermo Fisher). 20 µg of protein was separated by SDS- polyacrylamide gel electrophoresis using 4-12 % acrylamide gels (Invitrogen) and transferred to PVDF membranes (Mini format 0.2 µm PVDF, Bio-Rad) with a semi-dry blotting protein transfer (Bio-Rad, Trans Blot Turbo). TBS-tween-washed membranes (0.5 M Tris, 1.5 M NaCl, 0.01 % Tween, pH 7.4) were blocked with 5 % BSA for 1-h at RT. The washed membranes were incubated overnight with the primary antibodies MICU1 1:400 (Sigma Life Science) and TOM20 1:1000 (Cell Signaling) diluted in 1 % BSA at 4 °C. After 24-h, the washed membranes were incubated for 1-h at RT with IRDye 800 CW goat anti rabbit IgG (LI-COR Biosciences, U.S.) 1:15000 diluted in 1 % BSA. Membranes were scanned on the Odyssey scanner (LI-COR Biosciences, U.S.).

To determine MCU and MCUR1 protein levels in primary human myotubes (Lonza, #CC2580), cells were lysed with RIPA buffer (ThermoFischer, #89901) supplemented with Complete EDTA-free protease inhibitor mixture (Merck, #11836170001, Germany) and phosphoSTOP™ (Merck, #4906845001, Germany). Protein concentrations were measured via BCA. Because of limited quantities of MCU-knockdown and MCUR1-knockdown myotubes, the Sally Sue automated capillary Western blotting system (ProteinSimple, San Jose, CA, USA) was applied. Samples were prepared according to the manufacturer's protocol using the Anti-Rabbit Detection Module (DM-001, ProteinSimple) and the 12-230 kDa Sally Sue Separation Module (SM-S001, ProteinSimple). The loaded amount of protein was 1.6 µg at a concentration of 0.2 µg/µl using RIPA buffer. Primary antibodies used were MCU 1:30 (Cell Signaling), MCUR1 1:30 (Booster) and TOM20 1:100 (Cell Signaling) diluted in the manufacturer's antibody diluent (ProteinSimple).

To monitor protein levels in mouse skeletal muscles, frozen muscles were pulverized by means of Qiagen Tissue Lyser and protein extracts were prepared in an appropriate buffer containing 50 mM Tris pH 7.5, 150 mM NaCl, 5 mM $MgCl_2$, 1 mM DTT, 10 % glycerol, 2 % SDS, 1 % Triton X-

100, Complete EDTA-free protease inhibitor mixture (Roche), 1 mM PMSF, 1 mM $NaVO_3$, 5 mM NaF and 3 mM β-glycerophosphate. 40 µg of total proteins were loaded, according to BCA quantification. Proteins were separated by SDS-PAGE electrophoresis, in commercial 4-12 % acrylamide gels (Thermo Fisher Scientific) and transferred onto nitrocellulose membranes (Thermo Fisher Scientific) by semi-dry electrophoretic transfer. Blots were blocked 1-h at RT with 5 % non-fat dry milk (Bio-Rad) in TBS-tween (0.5 M Tris, 1.5 M NaCl, 0.01 % Tween) solution and incubated at 4 °C with primary antibodies. Secondary antibodies were incubated 1-h at RT. The following primary antibodies were used: MCU 1:1000 (Merck), phosphoPDH Ser293 1:5000 (Abcam), PDH 1:1000 (Cell Signaling), GRP75 1:1000 (Santa Cruz), TOM20 1:1000 (Santa Cruz).

3.2.6. RNA extraction, reverse transcription, and qPCR

Total RNA was extracted from mouse tissues by mechanical tissue homogenization in TRIZOL reagent (Thermo Fisher Scientific) according to the manufacturer's instructions. RNA samples were quantified using Nanodrop (Thermo Fisher Scientific) and 1 µg of total RNA from each sample was retro-transcribed with the cDNA synthesis kit SuperScript II (Thermo Fisher Scientific). Oligo(dT)12-18 primers (Thermo Fisher Scientific) were used for first-strand reverse transcriptase cDNA synthesis. The generated cDNA was analyzed by real-time PCR using QuantStudio5 Real-Time PCR System thermal cycler and SYBR green chemistry (Thermo Fisher). The corresponding primers were designed and analyzed using Primer3 (Rozen and Skaletsky, 2000). The efficiency of all primers was in the range of 90 % to 110 %. The housekeeping gene GAPDH served as an internal control for cDNA normalisation. The housekeeping gene GAPDH served as internal control for cDNA normalization. For quantification, expression values were calculated by using the $2^{-\Delta\Delta Ct}$ method.

Primer sequences used for real-time PCR:

MCU: FW, 5'-AAAGGAGCCAAAAAGTCACG-3'; RV, 5'-AACGGCGTGAGTTACAAACA-3'

GAPDH: FW, 5'-CACCATCTTCCAGGAGCGAG-3', RV, 5'-CCTTCTCCATGGTGGTGAAGAC-3'

MICU1 splice variant specific (NM_144822):

FW, 5'-GCGCTTTGATGGAAAGAAAATTGC-3', RV, 5'-TGTCTACCTCTCCGTCTCCA-3'

MICU1.1 splice variant specific (NM_001291443):

FW, 5'-CTTTGATGGAAAGGAGTTCTGGC-3', RV, 5'-CCTCCATGTCTACCTCTCCGT-3'

MICU2: FW, 5'-TGGAGCACGACGGAGAGTAT-3', RV, 5'-GCCAGCTTCTTGACCAGTGT-3'

3.2.7. Mitochondrial and cytosolic Ca^{2+} uptake in HeLa cells

For the measurements of mitochondrial and cytosolic Ca^{2+} levels in intact HeLa cells, 9000 cells/well were seeded in a 384-well plate (Corning) and 15000 cells/well in a 96 well plate containing respective growth medium. After 24-h, HeLa cells were infected with MOI 200 of the adenoviral vector carrying either mitochondria-targeted aequorin (Sirion Biotech, Germany) for primary and orthogonal screening or the cytosolic-targeted aequorin (Sirion Biotech, Germany) for counter screening. After 48-h, medium was removed and cells were incubated with 5 µM native coelenterazine (#10110-1 Biotium, USA) diluted in aequorin buffer (145 mM NaCl, 1 mM $MgCl_2$, 5 mM KCl, 10 mM HEPES, 10 mM glucose, 1 mM $CaCl_2$, pH 7.4) for 2-h at RT in the dark. Coelenterazine was aspired and compounds were added at 10 µM final concentration in DMSO 1 % for 2-h at RT in the dark. Basal luminescence was measured, followed by stimulation with 100 µM histamine (Merck, #7125, Germany) diluted in aequorin buffer with simultaneous luminescence detection. To measure and calibrate the bioluminescence of the remaining Ca^{2+}, HeLa cells were semi-permeabilized with a detergent solution containing 25 µM digitonin (#11024-24-1, Merck, Germany) and 10 mM $CaCl_2$ (#21115, Merck, Germany) in aequorin buffer. To detect bioluminescent signals, the bioluminescence plate readers FLIPR TETRAmax (Molecular Device,USA) and Cytation3 (Biotek, USA) were used for 384 well and 96 well plates respectively.

3.2.8. Mitochondrial Ca^{2+} uptake in semi-permeabilized HeLa cells

To measure mitochondrial Ca^{2+} uptake in semi-permeabilized HeLa (ATCC, #CCL-2^{TM}) and MEF cells 35000 cells/well and 15000 cells/well respectively were seeded in 96 well plates. After 24-h, cells were infected with the mitochondria-targeted aequorin probe (Sirion Biotech, Germany) using the same conditions as described in the previous section. After 2-h of incubation with native coelenterazine at 5 µM, cells were washed and first treated with a thapsigargin solution (0.2 µM) containing intracellular medium (IM: 140 mM KCl, 1 mM KH_2PO_4, 1 mM $MgCl_2$ and 20 mM Na-HEPES) supplemented with 10 mM Glucose and 0.1 mM EGTA at pH 7.2 for 15-min. 5-min before starting the measurement, a 60 µM digitonin solution with a final concentration of either DMSO 1 % for control or 10 µM of the selected compound for the treated samples, was added. Basal luminescence was measured before stimulating the cells with a 5X calcium solution (IM supplemented with 8 mM Na-Succinate, 4 mM Na-Pyruvate, 4 mM Mg-ATP, 5 mM Mg-EDTA and $3.12.10^{-4}$M $Ca^{2+}_{[total]}$) corresponding to specific concentrations of Ca^{2+} per well. This concentration

of free Ca^{2+} reflects the intracellular Ca^{2+} microdomains and promotes mitochondrial Ca^{2+} uptake which leads to a rise of the luminescent signal. Finally, a 6X calibration solution (final concentration in the well: 140 mM KCl and 10 mM $CaCl_2$) was added to calibrate the signal (Montero et al., 2004, Biochemical Journal, 384:19-24). Next, the slope values of mitochondrial Ca^{2+} uptake were analyzed using linear regression.

3.2.9. Mitochondrial Ca^{2+} uptake in primary human skeletal muscle myotubes

Human Skeletal Muscle cells (Lonza, #CC2580) were seeded in a previously prepared 96-well plate, coated with human fibronectin (Corning, #356008) at 20 µg/ml for 1-h at RT and washed twice with PBS 1 X (Thermo Fisher) before Skeletal Muscle Cell Growth Medium was added together with 12000 cells/well. After 24-h, knockdown of MCU or MCUR1 was induced by adenoviral infection with MCU shRNA or MCUR1 shRNA (Sirion Biotech, Germany) at MOI 100. Control cells were subjected to adenoviral infection with scrambled shRNA (Sirion Biotech, Germany) at MOI 100 and incubated for 48-h. Cells were then differentiated into myotubes by replacing the medium with Dulbecco's Modified Eagle Medium F-12 Nutrient Mixture (DMEM/F-12 (1:1) (1x) + GlutaMAX) (Gibco, Thermo Fisher) containing 2 % horse serum and, penicillin (100 U/ml) and streptomycin (100 mg/ml). After 3 days, cells were subjected to adenoviral infection with mitochondria-targeted aequorin at MOI 200 and incubated for 24-h. For experiments with oleuropein aglycone , myotubes were washed with aequorin buffer and incubated with native coelenterazine at 5 µM for 2-h at RT in the dark before removing coelenterazine and adding a final concentration of 10 µM oleuropein aglycone in 1 % DMSO with aequorin buffer and incubating the cells for 20-min at RT in the dark. Control myotubes were treated with DMSO 1 % in aequorin buffer. For experiments without oleuropein aglycone, myotubes were kept in aequorin buffer after 2-h of incubation with native coelenterazine and ready for acquisition according to the general protocol using 5 mM caffeine (#C0750, Sigma Aldrich) as stimulant to trigger Ca^{2+} release from the sarcoplasmic reticulum.

3.2.10. Mitochondrial Ca^{2+} uptake in C2C12 cells

Mouse Muscle Myoblast, C2C12 cells (ATCC, #CRL-1772) were seeded in a 96-well plate with 10000 cells/well, in respective growth medium. After 24-h, cells were differentiated into myotubes by replacing the medium with Dulbecco's Modified Eagle Medium GlutaMAX Supplement High Glucose + Pyruvate (Gibco, Thermo Fisher) containing 2 % horse serum (Gibco, #26050088), penicillin (100 U/ml) and streptomycin (100 mg/ml). After 3 days of incubation, cells were

subjected to adenoviral infection with mitochondria-targeted aequorin (Sirion Biotech, Germany) at MOI 200 and incubated for 24-h. Mitochondrial Ca^{2+} uptake was determined according to the general protocol using 5 mM caffeine (#C0750, Sigma Aldrich) as stimulant to trigger Ca^{2+} release from the sarcoplasmic reticulum.

3.2.11. Real time imaging of mitochondrial and cytosolic Ca^{2+} in FDB fibers

For real-time imaging experiments, muscles were digested using collagenase A (4 mg/ml) (Roche) diluted in Tyrode's salt solution (pH 7.4) (Sigma-Aldrich) containing 10 % fetal bovine serum (Thermo Fisher Scientific). Individual fibers were isolated, placed on laminin-coated glass coverslips and kept in DMEM with HEPES (42430 Thermo Fisher Scientific), containing 10 % fetal bovine serum, penicillin (100 U/ml) and streptomycin (100 µg/ml). Fibers were cultured at 37 °C with 5 % CO_2.

To measure mitochondrial Ca^{2+} uptake, myofibers were kept in Krebs-Ringer modified buffer (135 mM NaCl, 5 mM KCl, 1 mM $MgCl_2$, 20 mM HEPES, 1 mM $MgSO_4$, 0.4 mM KH_2PO_4, 1 mM $CaCl_2$, 5.5 mM glucose, pH 7.4) containing 0.02 % pluronic acid for 20-min at 37 °C and subsequently washed with Krebs-Ringer modified buffer in presence of 75 µM N-benzyl-P-toluenesulfonamide (BTS, Sigma-Aldrich) to prevent fiber contraction. For stimulation of mitochondrial Ca^{2+} uptake, 30 mM caffeine (Sigma-Aldrich) was added which triggered Ca^{2+} release from the SR. The experiments were conducted on a Zeiss Axiovert 200 microscope equipped with a 40×/1.3 N.A. PlanFluor objective and excitation was performed with a DeltaRAM V high-speed monochromator (Photon Technology International) equipped with a 75 W xenon arc lamp. Images were taken with a high-sensitivity Evolve 512 Delta EMCCD (Photometrics). The system was checked by MetaMorph 7.5 (Molecular Devices) and assembled by Crisel Instruments.

For measurements of mitochondrial Ca^{2+} uptake in young and old mice, fibers were dissected and treated with 2 µM mitofura-2/AM (Pendin et al., 2019). Images were taken by alternatively exciting the fluorophore at 340 and 380 nm and fluorescence emission recorded through a 515/30 nm band-pass filter (Semrock). Exposure time was set to 100-ms and acquisition was performed at binning 1 with 200 of EM gain. Image were analyzed with Fiji distribution of the ImageJ software (Schindelin et al., 2012). The background was subtracted from each image and changes in fluorescence (340/380 nm ratio) were expressed as R/R0, where R is the ratio at time t and R0 is the ratio at the beginning of the acquisition.

For measurements of mitochondrial Ca^{2+} uptake in oleuropein related experiments, FDB fibers were dissected 7 days after *in vivo* transfection with a plasmid encoding the sensor 4mtGCaMP6f (Gherardi et al., 2019b). Muscles were digested as previously described. 4mtGCaMP6f was

alternatively excited every second at 475 and 410 nm respectively and images were taken through an emission filter (535/30 nm) (Chroma). Exposure time was set to 50-ms. Acquisition was performed at binning 1 with 200 of EM gain. Images were analyzed with Fiji distribution of the ImageJ software (Schindelin et al., 2012). Images were corrected for the background frame by frame by subtracting the mean pixel value of a cell-free region of interest. Changes in Ca^{2+} levels (475/410 nm fluorescence ratio) were expressed as R/R0, where R is the ratio at time t and R0 is the ratio at the beginning of the experiment. Mitochondrial Ca^{2+} peak was expressed as (R-R0)/R0 and normalized for the control value.

For the cytosolic Ca^{2+} measurements, fibers were isolated and loaded with 2 µM fura-2/AM (Thermo Fisher Scientific) diluted in Krebs-Ringer modified buffer (described above) containing 0.02 % pluronic acid for 20-min at 37 °C and then washed with Krebs-Ringer modified buffer in presence of 75 µM N-benzyl-P-toluenesulfonamide (BTS, Sigma-Aldrich) to prevent fiber contraction. For mitochondrial Ca^{2+} stimulation, 30 mM caffeine (Sigma-Aldrich) were added as indicated on each graph to elicit Ca^{2+} release from intracellular stores. Experiments were performed on a Zeiss Axiovert 200 microscope equipped with a 40×/1.3 N.A. PlanFluor objective. Excitation was performed with a DeltaRAM V high-speed monochromator (Photon Technology International) equipped with a 75 W xenon arc lamp. Images were captured with a high-sensitivity Evolve 512 Delta EMCCD (Photometrics). The system was checked by MetaMorph 7.5 (Molecular Devices) and assembled by Crisel Instruments. Images were taken by alternatively exciting the fluorophore at 340 and 380 nm and fluorescence emission recorded through a 515/30 nm band-pass filter (Semrock). Exposure time was set to 100-ms. Acquisition was performed at binning 1 with 200 of EM gain. Images were analyzed with Fiji distribution of the ImageJ software (Schindelin et al., 2012). Images were background corrected. Changes in fluorescence (340/380 nm ratio) were expressed as R/R0, where R is the ratio at time t and R0 is the ratio at the beginning of the experiment.

3.2.12. High-throughput screening

The different screenings of mitochondrial Ca^{2+} and the identification of MCU activators were carried out by the NIHS before the start of this thesis and formed the starting point for the research conducted during the PhD.

To identify active compounds from an inhouse established library that are able to modulate MCU activity, a high-throughput screening assay was set up. The high-throughput screening was performed in a 384 well plate seeded with HeLa cells (ATCC, #CCL-2TM) and infected with the adenovirus carrying the mitochondria targeted Ca^{2+} probe aequorin. Expression of recombinant

aequorin in HeLa cells allows the precise measurement of Ca^{2+} in specific compartments such as mitochondria (Montero et al., 2004, Bonora et al., 2013). Using this cell-based assay, a library of 5571 natural compounds was screened. The high-throughput screening workflow contains 3 critical steps: In the first step, histamine (Merck, #H7125) induced increases in mitochondrial Ca^{2+} uptake in natural compound treated HeLa cells were measured. Based on this primary screening, all compounds that increased mitochondrial Ca^{2+} more than 35 %, were selected for the second step. Therefore, an orthogonal validation screening was applied on 78 natural compounds which returned 52 natural compounds. In the last step, 43 natural compounds were selected that were shown to not affect cytosolic but only mitochondrial Ca^{2+} concentrations. In conclusion, the workflow of the high-throughput screening is summarized in **Figure 29A** and contains three criteria for the selection of positive mitochondrial Ca^{2+} modulators: (1) In the primary screening, positive compounds have to increase mitochondrial Ca^{2+} uptake in intact HeLa cells by more than 35 % (**Figure 29B**). (2) In the orthogonal validation screening, positive compounds have to increase mitochondrial Ca^{2+} uptake in intact HeLa cells by more than 45 % (**Figure 29C**). (3) In the counter screening, positive compounds have to be specific in modulating mitochondrial but not cytosolic Ca^{2+} responses (to exclude compounds that affect intracellular calcium stores, **Figure 29D**). Based on these criteria, 43 natural compounds were found to positively modulate mitochondrial Ca^{2+} uptake.

3.2.13. Dose-response effect of oleuropein metabolites on mitochondrial Ca^{2+} uptake in C2C12 myotubes

To assess the dose response of oleuropein and its intermediates oleuropein aglycone and hydroxytyrosol in C2C12 (ATCC, #CRL-1772) myotubes, cells were infected with mitochondrial aequorine using the same conditions as previously described to measure mitochondrial Ca^{2+} uptake. After the 2-h incubation time with native coelenterazine at RT in the dark, latter one was removed and oleuropein and its metabolites (oleuropein aglycone and hydroxytyrosol) were added at 100, 33, 10, 3, 1, 0.3, 0.1 µM final concentration in DMSO 1 % in aequorin buffer and incubated for 15-min at RT in the dark before starting the acquisition.

3.2.14. OCR measurements in primary human myotubes

To measure the effect of oleuropein aglycone on oxygen consumption rate (OCR) in control and MCU-kd human myotubes, 8000 cells/well were seeded in a respective Seahorse XF96 Cell Culture Microplate (#101085-004, Agilent) previously coated with fibronectin (#356008, Corning)

at 20 mg/ml for 1-h at RT and washed twice with PBS 1 X (#10010023, Thermo Fisher) before adding the cells and incubating them overnight. The next day, cells were infected with 100 MOI of adenoviral MCU shRNA (Sirion Biotech, Germany) to induce knockdown of MCU. Control cells were infected with 100 MOI of scrambled shRNA (Sirion Biotech, Germany). After 48-h, cells were differentiated into myotubes by exchanging the medium with DMEM/F-12 (1:1) (1x) + GlutaMAX (Gibco, Thermo Fisher) containing 2 % horse serum, penicillin (100 U/ml) and streptomycin (100 mg/ml). After 72-h, cells were washed with KRBH, containing 10 mM glucose, 1.5 mM $CaCl_2$ and 1 mM pyruvate and incubated with 10 µM oleuropein aglycone in 1 % DMSO for 20-min at 37 °C without CO_2. For the acquisition, basal respiration was recorded before injecting caffeine with a final concentration of 5 mM to stimulate the myotubes followed by 2.5 µg/ml oligomycin (Oligo) and 2 µM rotenone (Rot) plus 2 µg/ml antimycin A (AntiA). Basal respiration of control and MCU-kd myotubes was used for normalization and expressed in % to see the effect of oleuropein aglycone on OCR.

3.2.15. OCR measurements in mouse FDB fibers, *ex-vivo*

To measure oxygen consumption rate (OCR), FDB fibers were isolated (Gherardi et al., 2019b). Muscles were digested in collagenase A (4 mg/ml) (Roche) dissolved in Tyrode's salt solution (pH 7.4) (Sigma-Aldrich) containing 10 % fetal bovine serum (Thermo Fisher Scientific). Individual fibers were isolated, placed on laminin-coated XF24 microplate wells and kept in DMEM (D5030 Sigma-Aldrich) with 1 mM NaPyr, 5 mM glucose, 33 mM NaCl, 15 mg phenol red, 25 mM HEPES and 1 mM of L-Glu. Fibers were kept for 2-h in culture at 37 °C in 5 % CO_2.

The OCR was measured in real-time with the XFe24 Extracellular Flux Analyzer (Agilent), capturing OCR changes after up to four sequential injections of compounds. Fibers were prepared as described above. Prior to starting the experiment, a titration with the uncoupler FCCP was done and returned the FCCP concentration (0.6 µM) that maximally increased OCR.

Results were then normalized to the fluorescence of calcein (Sigma-Aldrich). For this, fibers were treated with 2 µM calcein for 30-min. Fluorescence was acquired using a Perkin Elmer EnVision plate reader in well scan mode using 480/20 nm filter for excitation and 535/20 nm filter for emission.

3.2.16. Effect of oleuropein on muscle fatigue following tetanic stimulation, *ex-vivo*

First, the EDL muscles were cut from tendon to tendon under a stereomicroscope and placed between a force transducer (KG Scientific Instruments, Heidelberg, Germany) in a chamber

continuously perfused with oxygenated Krebs-Ringer buffer at 25 °C. Next, muscle force was measured using a force-frequency protocol with increasing pulses (20 Hz, 40 Hz, 55 Hz, 75 Hz, 100 Hz, 150 Hz) every 15-s. Subsequently, 10 µM oleuropein aglycone (n=10 EDL fibers) or DMSO (1%) was added as a control (n=10 EDL fibers) and force frequency was recorded every 10-min for 1-h. The fibers were then subjected to a fatigue protocol with 120 tetanic contractions (100 Hz) of 300-ms per second. The recorded drop in force compared to the basal force was used to assess fatigue. All results were normalized to muscle weight.

3.2.17. Transcriptomic data analysis and protein interactions

RNA sequencing data obtained from the Singapore sarcopenia study were described in detail (Migliavacca et al., 2019) and are available at the Gene Expression Omnibus (https://www.ncbi.nlm.nih.gov/geo/) under accession numbers GSE111016.
Briefly, after removing genes with a mean expression lower than 20 reads, data were normalized by the trimmed mean of M-values method as implemented in the edgeR function calcNormFactors67, and the voomWithQualityWeights function was used to model the mean-variance relationship and estimate the sample-specific quality weights68. P-values were corrected for multiple testing using the Benjamini–Hochberg method.

3.2.18. *In silico* binding mode investigation of oleuropein on MICU1 binding site

The 3D-model of human MICU1 (UNIPROT entry: Q9BPX6) was obtained from the experimentally solved structure of Ca^{2+}-free MICU1 in its hexameric form (PDB ID: 4NSC; Resolution: 3.2 Å) (Wang et al., 2014) similarly to recently reported work on mus musculus Orthologue. The monomeric unit used was obtained from the most complete chain (chain C), was selected to obtain a wider range in the MICU1 model (107-467). The Protein Preparation tool of MOE 2018 suite (Chemical Computing Group (CCG) Inc. Molecular Operating Environment (MOE) 2018) was applied to process the X-ray structure to add hydrogen atoms, incorporating missing atoms in 17 side chains, and modeling three missing loops. Protein partial charges were assigned using Amber2014 force field (Maier et al., 2015). The ligands were used from Pubchem (PubChem CID: 5281614; 5280863; 56842347; 5281544) and their partial charge assessed after semi-empirical (PM6) energy minimization applying MOE 2018 (Chemical Computing Group (CCG) Inc. Molecular Operating Environment (MOE) 2018) (Stewart, 2007). Molecular docking studies were performed with plants1.2 coupled to chemPLP scoring function (Korb et al., 2009) defining as binding site a sphere placed on the model center of the mass and using a radius of

20 Å. For each run 20 output conformations were produced and investigated by visual inspection. The ligand-protein complexes were prepared for MD simulations with AmberTools14, assigning Gasteiger charges and General Amber Force Field (GAFF) parameters to the ligands and Amber14 partial charges and parameters to the proteins. Each system was solvated with explicit waters (TIP3P model) resulting in a tetragonal box with boundaries at least 11 Å far from any atom of the complex. Each system was neutralized adding Na^+/Cl^- ions to a final concentration of 0.1 M. Each system was subjected to 300 steps of conjugate-gradient minimization followed by 100 ps NVE and 500 ps NPT equilibration applying harmonic positional constraints (1 kcal mol−1 Å−2) on protein and ligands atoms. The pressure was maintained to 1 atm by Berendsen barostat and the temperature to 310 K by a Langevin thermostat. Subsequently, three replicats of 10-ns classical MD simulations in the NVT ensemble were acquired to calculate MMGBSA energy and evaluate RMSD along the trajectory. All MD simulations were performed with the ACEMD engine, with a time-step of 2fs, by handling the nonbonded long-range Coulomb interactions with the particle mesh Ewald summation method (PME) (Essmann et al., 1995) with a cutoff distance of 9 Å and a switching distance of 7.5 Å.

3.2.19. Data analysis

Data analysis and statistical tests were performed using R version 3.5.2 and GraphPad Prism 9.3.1. All data were expressed as the mean ± SEM. Samples were tested for normality using the Shapiro-Wilk test. The results were statistically analyzed using parametric Student's *t*-test or non-parametric Mann-Whitney-Wilcoxon test for two groups and the parametric one-way ANOVA or non-parametric Kruskal Wallis test for multiple groups. Results were considered significant at an alpha level of 0.05; $*p < 0.05$. For the analysis of mitochondrial Ca^{2+} uptake data, the raw data from the Cytation3 Imaging Reader (BioTek, Switzerland) and FLIPR tetraMAX (Molecular Devices) were calibrated using the following equation.

$$Ca^{2+}\,(M) = \frac{\left(\frac{L}{L_{max}} * \lambda\right)^{\frac{1}{n}} + \left(\left(\frac{L}{L_{max}} * \lambda\right)^{\frac{1}{n}} * K_{TR}\right) - 1}{K_R - \left(\left(\frac{L}{L_{max}} * \lambda\right)^{\frac{1}{n}} * K_R\right)}$$

L = light intensity at sampling time
L_{max} = total light emitted at sampling time
K_R = constant for calcium-bound state
K_{TR} = constant for calcium-unbound state

λ = rate constant for aequorin consumption at saturation [Ca^{2+}]
n = number of Ca^{2+} -binding sites

For each calibrated calcium trace, either peak values or slope values using linear regression were analyzed.

3.3. Part 3: Molecular mechanisms of polyphenols in MCU activation

3.3.1. Cell lines and maintenance conditions

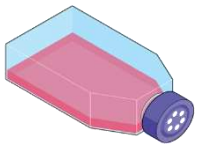

Control HAP1 cells and CRISPR/Cas9-edited knockout (KO) cell lines were purchased from Horizon and maintained in Iscove's Modified Dulbecco's Medium (IMDM) (Gibco Thermo Fisher, Scotland) containing 10 % heat-inactivated fetal bovine serum, penicillin (100 U/ml) and streptomycin (100 mg/ml) (Gibco, Thermo Fisher). Cell lines were maintained at 37 °C and 5 % CO_2.
HeLa cells (ATCC, #CCL-2TM) were maintained in growth medium consisting of DMEM, GlutaMAX supplement Medium (MEM) (Gibco, Thermo Fisher) containing 10 % heat-inactivated fetal bovine serum, penicillin (100 U/ml) and streptomycin (100 mg/ml) (Gibco, Thermo Fisher). Cells were maintained at 37 °C and 5 % CO_2.

3.3.2. Western blot and antibodies

To detect MCU, MICU1, MCUR1 and MCUb protein levels in the respective HAP1 KO cell lines, mitochondria were isolated and resuspended in incubation buffer (300 mM sucrose, 10 mM Hepes, 0.5 mM EGTA, Complete EDTA-free protease inhibitor mixture, Roche, pH 7.4). Protein concentration was measured using BCA protein assay kit (Pierce, Thermo Fisher). Twenty µg of protein was separated by SDS-polyacrylamide gel electrophoresis using 4-12 % acrylamide gels (Invitrogen) and transferred to PVDF membranes (Mini format 0.2 µm PVDF, Bio-Rad) using a semi-dry blotting protein transfer (Bio-Rad, Trans Blot Turbo). Membranes were washed with TBS-tween buffer (0.5 M Tris, 1.5 M NaCl, 0.01 % Tween, pH 7.4) before blocking with 5 % BSA for 1-h at RT. The washed membranes were incubated overnight with the respective primary antibodies MCU 1:1000 (Sigma Life Science, #HPA016480), anti-MICU1 1:1000 (Sigma Life Science, #HPA037480), anti-MCUR1 1:1000 (Thermo Fisher Scientific, Switzerland, #PA5-42641) and TOM20 1:1000 (Cell Signaling, #42406) diluted in 1 % BSA at 4 °C. The next day, the washed membranes were incubated for 1-h at RT with IRDye 800 CW goat anti rabbit IgG

(LI-COR Biosciences, U.S.) 1:15000 diluted in 1 % BSA. For quantitative analysis of Western blot data, membranes were scanned using the Odyssey scanner (LI-COR Biosciences, U.S.).

3.3.3. PCR for MCUb-KO validation

Since there is no high-quality validated MCUb antibody, MCUb-KO HAP1 cells were validated by PCR. 800000 cells from control and MCUb-KO cells were seeded in triplicates in 6 well plates and incubated in IMDM medium (Gibco Thermo Fisher, Scotland) containing 10 % heat-inactivated fetal bovine serum, penicillin (100 U/ml) and streptomycin (100 mg/ml) (Gibco, Thermo Fisher) for 2 days at 37 °C and 5 % CO_2. RNA was extracted using the RNeasy Mini Kit (Qiagen, Netherlands) and following the manufacturer's protocol. RNA extracts were quantified via Nanodrop (Thermo Fisher Scientific, Switzerland) and transcribed into cDNA using a high-capacity cDNA reverse transcription kit (High-Capacity cDNA Reverse Transcription Kit, Thermo Fisher) and a thermocycler (Bio-Rad, Switzerland) following the manufacturer's protocol using 1 µl of cDNA (200 µg/µl), running 35 cycles: 30-s at 95 °C, 30-s at 55 °C, 1-min at 72°C followed by 1 cycle of 10-min at 72 °C before cooling the temperature down to 8 °C until next step which is loading of a 1.5 % agarose gel. For this, 1.5 % agarose gel containing SYBR was prepared since the product length of the amplified product is approximately 300 bp. The gel cooled down for 20-min before loading 10 µl of each sample. After the run, gels were scanned.

MCUb: FW, 5'-GGGAGGATGCTCCAGAGGG-3'; RV, 5'-TGTTGCCATCTGCTGTGAAGA-3'

Further primer pairs for MCUb were tested, with a second primer pair giving good results (data not shown).

MCUb: FW, 5'-CGGGAGGATGCTCCAGAGG-3'; RV, 5'-TCATGTTGCCATCTGCTGTGA-3'

3.3.4. Screening of kaempferol-close analogues

The screening of kaempferol-close analogues to measure their effect on mitochondrial Ca^{2+} was performed at the NIHS before the start of this thesis.

For this, 50000 HeLa cells/well were seeded in a white 96 well plate with a clear bottom and incubated overnight. The mitochondrial Ca^{2+} uptake was measured with the bioluminescent genetically encoded mitochondrial mutant aequorin calcium indicator (Montero et al., 2004, Bonora et al., 2013), which was transferred from an adenovirus (Sirion Biotech, Germany). Infected HeLa cells were incubated for 48-h prior to the measurement with the Cytation3 imaging

reader (BioTek, Switzerland). For the measurement, medium was removed, and cells were incubated with native coelenterazine 5 µM (Biotium, USA, #55779-48-1), diluted in aequorin buffer (145 mM NaCl, 1 mM $MgCl_2$, 5 mM KCl, 10 mM HEPES, 10 mM glucose, 1 mM $CaCl_2$, pH 7.4) for 2-h at RT in the dark. Then coelenterazine was aspired and 100 µl of aequorin buffer containing 10 µM of kaempferol and its analogues were added. As control condition, 1 % DMSO was used and to ensure mitochondrial function, 1 µM FCCP was administered. Basal luminescence was measured, followed by stimulation with 100 µM histamine (Merck, #H7125). The experiment was ended by adding a solution containing 25 µM digitonin (Merck, Germany, #11024-24-1), 10 mM $CaCl_2$ (Merck, Germany, #10043-52-4) which calibrates the fluorescence signal as described by Montero and collaborators (Montero et al., 2004).

For the analysis of mitochondrial Ca^{2+} uptake data, the raw data from the Cytation3 Imaging Reader (BioTek, Switzerland) were calibrated using the following equation.

$$Ca^{2+}\,(M) = \frac{\left(\frac{L}{L_{max}} * \lambda\right)^{\frac{1}{n}} + \left(\left(\frac{L}{L_{max}} * \lambda\right)^{\frac{1}{n}} * K_{TR}\right) - 1}{K_R - \left(\left(\frac{L}{L_{max}} * \lambda\right)^{\frac{1}{n}} * K_R\right)}$$

L = light intensity at sampling time
L_{max} = total light emitted at sampling time
K_R = constant for calcium-bound state
K_{TR} = constant for calcium-unbound state
λ = rate constant for aequorin consumption at saturation [Ca^{2+}]
n = number of Ca^{2+} -binding sites

3.3.5. Mitochondrial Ca^{2+} uptake in HAP1 cells

Depending on the experiment, 35000 control HAP1 cells, 30000 MCU-KO HAP1 cells, 45000 MICU1-KO cells, 40000 MCU1-KO cells and 40000 MCUb-KO cells were seeded per well in a white 96 well plate with a clear bottom and incubated overnight. The mitochondrial Ca^{2+} uptake was measured with the bioluminescent genetically encoded mitochondrial mutant aequorin calcium indicator (Montero et al., 2004, Bonora et al., 2013), which was transferred from an adenovirus (Sirion Biotech, Germany). Infected HAP1 cells were incubated for 24-h prior to the measurement with the Cytation3 imaging reader (BioTek, Switzerland). For measurement, medium was removed, and cells were incubated with native coelenterazine 5 µM (Biotium, USA, #55779-48-1), diluted in aequorin buffer (145 mM NaCl, 1 mM $MgCl_2$, 5 mM KCl, 10 mM HEPES,

10 mM glucose, 1 mM $CaCl_2$, pH 7.4) for 2-h at RT in the dark. Then coelenterazine was aspired and 100 µl aequorin buffer added. For experiments with polyphenols, 100 µl of aequorin buffer containing 10 µM of the polyphenols kaempferol (Tocris, #3603) or fisetin (Santa Cruz, #sc-276440) (both from 1 mM stock solution in DMSO) or 1 % DMSO as control was added to the cells. Basal luminescence was measured, followed by stimulation with 1 mM ATP (Merck, Germany, #A2383-10G). The experiment was ended by adding a solution containing 25 µM digitonin (Merck, Germany, #11024-24-1), 10 mM $CaCl_2$ (Merck, Germany, #10043-52-4) which calibrates the fluorescence signal as described by Montero and collaborators (Montero et al., 2004).

For the analysis of mitochondrial Ca^{2+} uptake data, the raw data from the Cytation3 Imaging Reader (BioTek, Switzerland) were calibrated using the following equation:

$$Ca^{2+}(M) = \frac{\left(\frac{L}{L_{max}} * \lambda\right)^{\frac{1}{n}} + \left(\left(\frac{L}{L_{max}} * \lambda\right)^{\frac{1}{n}} * K_{TR}\right) - 1}{K_R - \left(\left(\frac{L}{L_{max}} * \lambda\right)^{\frac{1}{n}} * K_R\right)}$$

L = light intensity at sampling time
L_{max} = total light emitted at sampling time
K_R = constant for calcium-bound state
K_{TR} = constant for calcium-unbound state
λ = rate constant for aequorin consumption at saturation [Ca^{2+}]
n = number of Ca^{2+}-binding sites

In HAP1 cell experiments, each calibrated calcium trace was used to calculate the area under the curve (AUC), using cubic smoothed splines. The final graphs show mitochondrial Ca^{2+} in AUC %. For this purpose, results from control cells were averaged and rescaled to a reference value of 100 % and then each AUC was normalized with this. Significant differences in mitochondrial Ca^{2+} uptake between two groups were calculated using the Student's *t*-test for parametric data and the Mann-Whitney-Wilcoxon test for non-parametric data. To investigate differences between more than two groups, one-way ANOVA was used.

3.3.6. Molecular docking simulations for MICU1 interaction with polyphenols

See section 3.2.17. about *In silico* binding mode investigation of oleuropein on MICU1 binding site. The same approach was used for the polyphenols kaempferol and fisetin to investigate the corresponding binding sites of MICU1.

3.3.7. *C. elegans* strains and maintenance

The *C. elegans* strain used in this part of the thesis is the wild-type Bristol N2 strain. This strain was purchased from the Caenorhabditis Genetics Center (University of Minnesota) and maintained at 20 °C on agar plates containing nematode growth media (NGM) spotted with *E. coli* strain HT115.

3.3.8. RNAi feeding and qPCR

MICU1 RNAi clone was grown over night in 3 ml LB-Tetracycline medium (25 µg Tetracycline/ml) on a shaker at 37 °C. Next day, the overnight culture was diluted 1:50 in LB-Ampicillin for approximately 4-h on a shaker at 37 °C. NGM plates containing IPTG (MP Biomedicals, #114064102-CF) were spotted with MICU1 bacteria solution and incubated for at least 4-h to ensure generation of dsDNA.

For qPCR, RNA was extracted from L4 control and MICU1 knockdown worms by washing and pelleting worms in 15 ml falcons from well-populated 9-cm NGM plates until most of the bacteria had disappeared, as indicated by a clear supernatant. The falcons were placed on ice and 1 ml of QIAzol lysis reagent (Qiagen, #85300) was added. Worms were transferred to 1.5 ml tubes containing 1 Tungsten Carbide Bead 3 mm (Qiagen) and homogenized with the TissueLyser II (Qiagen) for 1-min. 200 µl of chloroform (Merck, #67-66-6) was added per sample and samples were mixed in the rack before centrifugation at 12000 rcf for 10-min at 4 °C. 600 µl of the upper clear phase was transferred to a new tube and 1 volume of isopropanol was added and mixed before the samples were transferred to the appropriate columns according to the manufacturer's instructions for the RNeasy Protect Mini Kit (Qiagen). Total RNA concentration and quality were determined using the Nanodrop spectrophotometer before reverse transcription was performed to obtain cDNA according to the manufacturer's protocol (High-Capacity cDNA Reverse Transcription Kit, Thermo Fisher). Applied conditions for reverse transcription: 10-min at 25 °C, followed by 120-min at 37 °C and 5-min at 85 °C. The LightCycler 1536 DNA Green Master System (Roche Applied Science) was used for qPCR. Two assays were conducted with a total number of 4 biological specimens, which were measured in two technical replicates. *Ama*-1 was

used as the housekeeping gene and relative gene expression data was analyzed using the $2^{-\Delta\Delta Ct}$ method. Primer sequences are as follows:

micu-1: FW, 5'-TGATCGCTGGAATGGTTATCC-3'; RV, 5'-CTTTTCTTTGACTTCCTCTACTTC-3'

ama-1: FW, 5'-GAAAAGGCGAAGGATGTGTTG-3'; RV, 5'-TCCGGCATCTCGTAGAAAATC-3'

3.3.9. OCR measurements in control and MICU1-kd

OCR was measured using the Seahorse XF96 instrument (Seahorse bioscience Inc., North Billerica, MA, USA). Synchronized control and micu-1 knockdown worms were grown to L4 stage on NGM plates. For experiments with polyphenols, NGM plates were spotted with bacteria (HT115 with and without MICU1-RNAi) containing 100 µM of kaempferol (Tocris, #3603) or fisetin (Santa Cruz, #sc-276440). Polyphenols were added from stock solutions (10 mM), prepared in EtOH (92%)/Tween80 (8%) (Merck, #P4780). As control treatment EtOH/Tween80 was mixed with bacteria to spot plates. Plates were dried overnight at RT and the next day, synchronized eggs were placed on the plates and worms were grown until L4. Next, worms were washed with M9 buffer and centrifuged at 1 200 rpm at 20 °C for 3-min. The worm pellet was resuspended in M9 buffer and 20-30 worms per well were transferred into a Seahorse XF96 Cell Culture Microplate (Agilent), with the final volume adjusted to 200 µl with M9 buffer. OCR was measured to capture basal respiration before injecting the parasympathomimetic carbachol (10 mM) to induce muscle contraction (Álvarez-Illera et al., 2020), followed by a second injection of sodium azide (NaN_3, 40 mM) to block complex IV and V (Koopman et al., 2016a).

3.3.11. Data analysis

Data analysis and statistical tests were performed using R version 3.5.2 and GraphPad Prism 9.3.1. All data were expressed as the mean ± SEM. Samples were tested for normality using the Shapiro-Wilk test. The results were statistically analyzed using parametric Student's *t*-test or non-parametric Mann-Whitney-Wilcoxon test for two groups and the parametric one-way ANOVA or non-parametric Kruskal Wallis test for multiple groups. Results were considered significant at an alpha level of 0.05; $*p < 0.05$.

Section 4: Results

4.1. Part I: MCU improves muscle energy metabolism and mobility by regulating the mitochondrial redox state

The first part of the thesis was devoted to the questions of how MCU modulates mitochondrial redox equilibrium and transmits the effects on energy metabolism and muscle function. The main discovery was that mitochondrial Ca^{2+} facilitates the net reduction of matrix thiol groups. This MCU-dependent reduction of matrix thiol groups stimulates energy metabolism in primary human myotubes and increases mitochondrial respiration and mobility in *C. elegans*, *in vivo*. Altogether, these results point to the importance of mitochondrial thiol group modulation for muscle bioenergetics and function and introduce MCU as a new target for modulation of mitochondrial redox homeostasis.

4.1.1. MCU activation is essential for mitochondrial Ca^{2+} uptake in HAP1 cells

To investigate the effects of MCU on the redox state of thiol groups in the mitochondrial matrix, an MCU-ablated model was created in human chronic myeloid leukaemia HAP1 cells in collaboration with Horizon Discovery using CRISPR/Cas9. Isolated mitochondria from control and MCU-KO cells were used to validate the model by Western blot (**Figure 11A**). For functional validation, mitochondrial Ca^{2+} uptake was measured in control and MCU-KO HAP1 cells after stimulation with ATP (**Figure 11B**). Calibrated total Ca^{2+} uptake during stimulation was calculated as area under the curve (AUC) using cubic smoothed splines. Data were normalized to the average mitochondrial Ca^{2+} uptake in control cells and presented as percentage (**Figure 11C**). Stimulation with an agonist (ATP) resulted in a robust mitochondrial Ca^{2+} increase in control cells but not in MCU-KO cells, demonstrating that MCU is the main transporter mediating the mitochondrial Ca^{2+} increase in HAP1 cells.

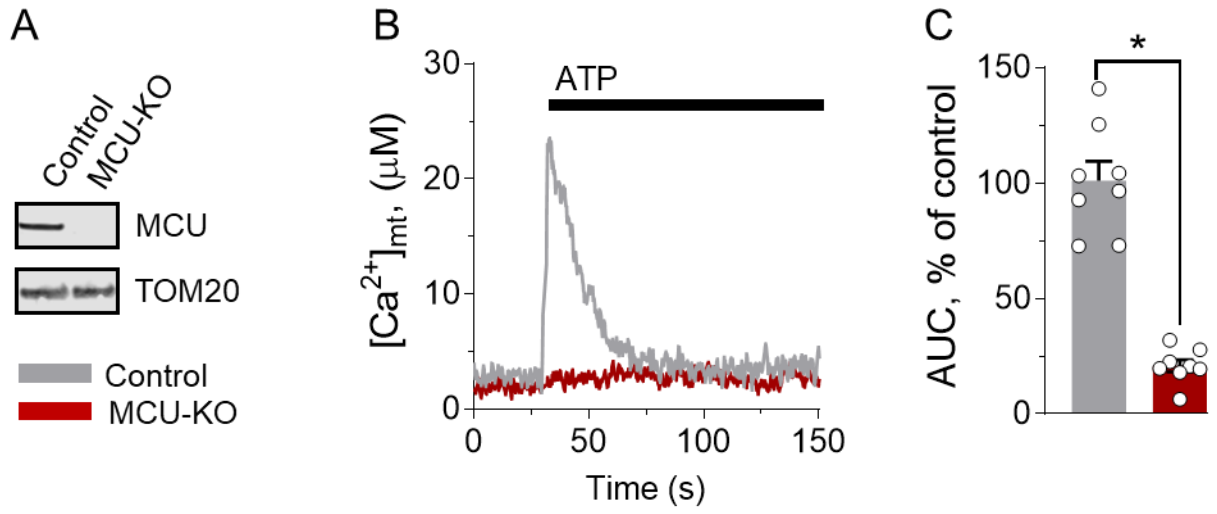

Figure 11. ATP stimulates mitochondrial Ca^{2+} elevation in control but not in MCU-KO HAP1 cells.
(A) WB of isolated mitochondria of control and MCU-KO HAP1 cells. (B) Shows calibrated mitochondrial Ca^{2+} traces of control (grey) and MCU-KO (red) HAP1 cells after stimulation with ATP. (C) Shows statistical analysis calculating the area under the curve (AUC), normalized to control cells and displayed in %. Data are expressed as mean±SEM. Results are considered significant at a significance threshold of $\alpha < 0.05$; *$p < 0.05$; (Student's *t*-test to compare two groups).

Activation of MCU stimulates mitochondrial Ca^{2+} uptake, which promotes reductive and oxidative signalling through activation of the TCA cycle, where electron carriers such as NAD^+ are reduced to NADH with the electrons fed into the ETC to undergo oxidative phosphorylation, in which electrons can be stripped from the ETC at complex I to generate $O_2^{\bullet-}$. To measure the effects of MCU activation on reduction, the ratio of NAD(P)H to $NAD(P)^+$ was measured at baseline and at two time points after stimulation with ATP (10-s, 15-min) (**Figure 12A**). To assess the oxidative response to ATP stimulation, mitochondrial $O_2^{\bullet-}$ concentrations were measured at different time points (0, 5, 15 and 30-min) using MitoSOX. Basal $O_2^{\bullet-}$ generation was measured by adding medium at the same time points (**Figure 12B**) and that revealed no difference between control and MCU-KO cells. Conversely, stimulation of MCU after ATP administration significantly increased $O_2^{\bullet-}$ production in control cells compared to MCU-KO cells (**Figure 12C**).

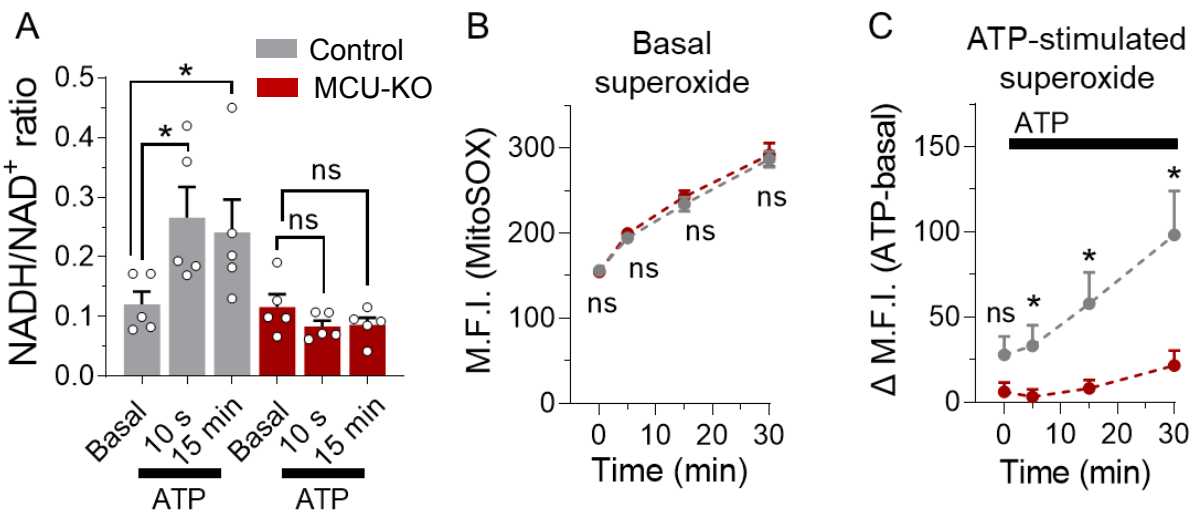

Figure 12. MCU-activation promotes oxidative and reducing effects in HAP1 cells.
(A) MCU dependent increase of NAD(P)H/NAD(P)+ in control (grey, n=8 experiments) but not MCU-KO (red, n=8 experiments) HAP1 cells after stimulation with ATP, measured at baseline and after MCU-activation. (B) Superoxide anion ($O_2^{\bullet-}$) production in medium injected control (grey, n=4 experiments) and MCU-KO (red, n=4 experiments) cells over time. (C) $O_2^{\bullet-}$ production in control (grey, n=4 experiments) and MCU-KO (red, n=4 experiments) cells at basal and at 5, 15 and 30-min after ATP-stimulation. Data are expressed as mean±SEM. Results are considered significant at a significance threshold of $\alpha < 0.05$; *$p < 0.05$; ns, not significant (Student's *t*-test to compare two groups and one-way ANOVA to compare more than 2 groups).

4.1.2. MCU activation promotes net reducing state of mitochondrial thiol groups

After functional validation of MCU-KO HAP1 cells was completed, the system was used to measure the net effect of MCU on the redox state of the mitochondrial matrix. The redox state of the matrix of HAP1 control and MCU-KO cells was assessed using the mitochondria-targeted roGFP1 (reduction-oxidation-sensitive green fluorescent protein 1) sensor (**Figure 13A**), which detects reduced thiol groups in mitochondria, including GSH (Schwarzlander et al., 2016, Santo-Domingo et al., 2015, Hanson et al., 2004). Single cell bioimaging analysis was performed by randomly selecting 10 cells per dish and measuring the baseline redox state for 3-min, followed by ATP stimulation and subsequent measurement of the fluorescent signal for 17-min. Then, H_2O_2 was added to completely oxidize the thiol groups present for 4-min (max oxidation = 0) before a final injection of dithiothreitol (DTT) to completely reduce the thiol groups for a further 4-min period (max reduction = 1) (**Figure 13B**). The injections of H_2O_2 and DTT were used to normalize the data (Hanson et al., 2004).

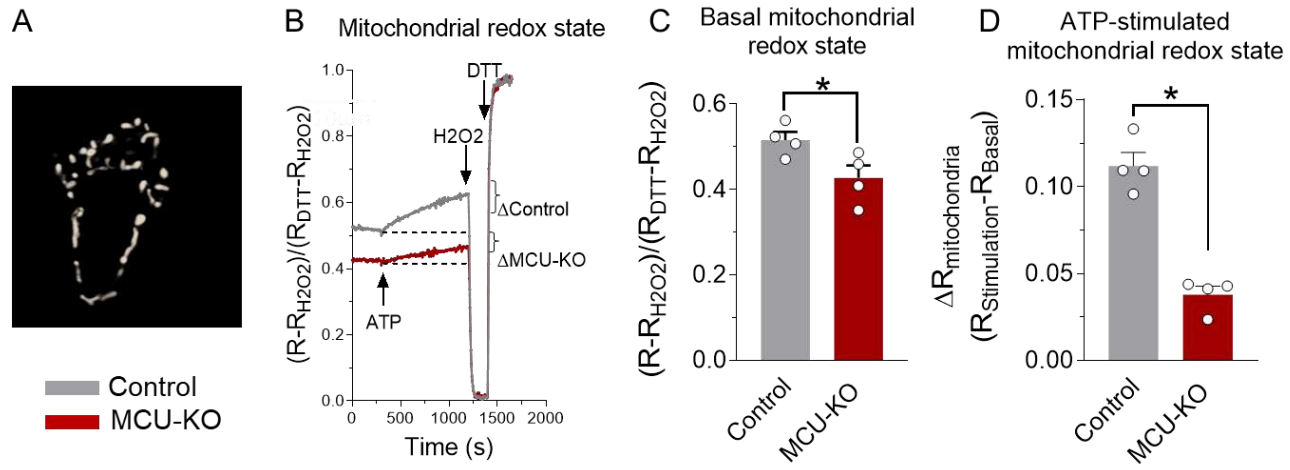

Figure 13. Mitochondrial matrix redox state in HAP1 control and MCU-KO cells.
(A) Shows transfected control HAP1 cells with the mitochondria targeted roGFP1 sensor. (B) The redox state of mitochondrial thiol groups was measured in control (grey) and MCU-KO (red) cells under basal conditions and after stimulation with 1 mM ATP. 10 mM H_2O_2 (ratio = 0) and 50 mM DTT (ratio = 1) were used to fully oxidize and reduce the traces respectively to calibrate each trace. (D) The ATP-stimulated delta redox state was determined by subtracting the basal redox state (C) from the redox state after 1 mM ATP stimulation in both control (grey, n=4; 10 cells/sample) and MCU-KO (red, n=4; 10 cells/sample) HAP1 cells. Data are expressed as mean±SEM. Results are considered significant at a significance threshold of $\alpha < 0.05$; *$p < 0.05$; (For C, Student's *t*-test and for D, Mann-Whitney test to compare two groups).

The baseline mitochondrial redox state was lower in MCU-KO cells compared to control cells (**Figure 13C**). The overall net redox effect of MCU activation, following stimulation with ATP, revealed a significantly increased reduction of matrix thiol groups in control cells (**Figure 13D**). Although mitochondrial Ca^{2+}-dependent activation of cellular respiration increased ROS production (**Figure 12C**) in control cells, the results obtained clearly showed that MCU-dependent increased production of reduced species (e.g. NADH by dehydrogenases) outweighs oxidative processes and determines an increased reduced net status of mitochondrial thiol groups. Importantly, the stimulus-dependent increase in reduced thiol groups was much smaller in MCU-ablated cells, suggesting that most of the mitochodrial thiol reduction is MCU-dependent.

To investigate the effect of ATP stimulation on cytosolic redox state, a control experiment was performed using a cytosolic roGFP1 sensor (**Figure 14A**). The change in cytosolic redox state after ATP stimulation showed delta values close to zero in both control and MCU-KO cells, with no significant differences between cell lines (**Figure 14B**). This result demonstrates that activation of MCU regulates mitochondrial but not cytosolic redox state.

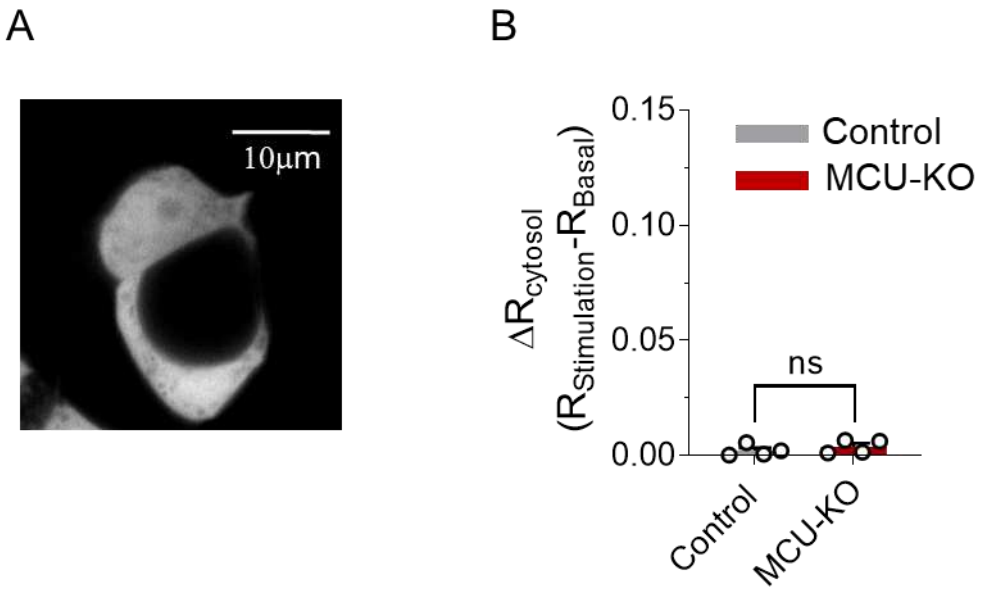

Figure 14. MCU activation is mitochondria specific and does not change cytosolic redox state.
(A) Shows HAP1 control cells transfected with the cytosolic targeted roGFP1 sensor. (B) Statistical analysis of effects of ATP (1mM) evoked MCU activation on changes in cytosolic roGFP1 fluorescence, in control (grey, n=4; 10 cells/sample) and MCU-KO (red, n=4; 10 cells/sample) cells. Data was analyzed in the same was as described in Figure 6D and expressed as mean±SEM. Results are considered significant at a significance threshold of $\alpha < 0.05$; *p < 0.05; ns, not significant (Student's *t*-test to compare two groups).

4.1.3. Proof of causality: MCU activation modulates matrix redox state in HAP1

To determine whether the change in matrix redox state is a specificity of MCU-ablated cells or more likely due to causality between MCU stimulation and changes in matrix redox state, MCU was rescued in MCU-ablated cells (**Figure 15A**). Both mitochondrial Ca^{2+} uptake and mitochondrial redox state were measured after stimulation with ATP (**Figures 15B and 16**). Rescue of the MCU transporter in MCU-KO cells was achieved by transfecting MCU-KO cells with an MCU-encoding-plasmid and control cells with the control plasmid pcDNA3.1. For statistical analysis, the AUCs of the obtained mitochondrial Ca^{2+} traces in control (grey), MCU-KO (red) and MCU-KO cells with reintroduced MCU (yellow) were normalized to the control cells and expressed as a percentage, demonstrating the functional rescue of the MCU (**Figure 15C**).

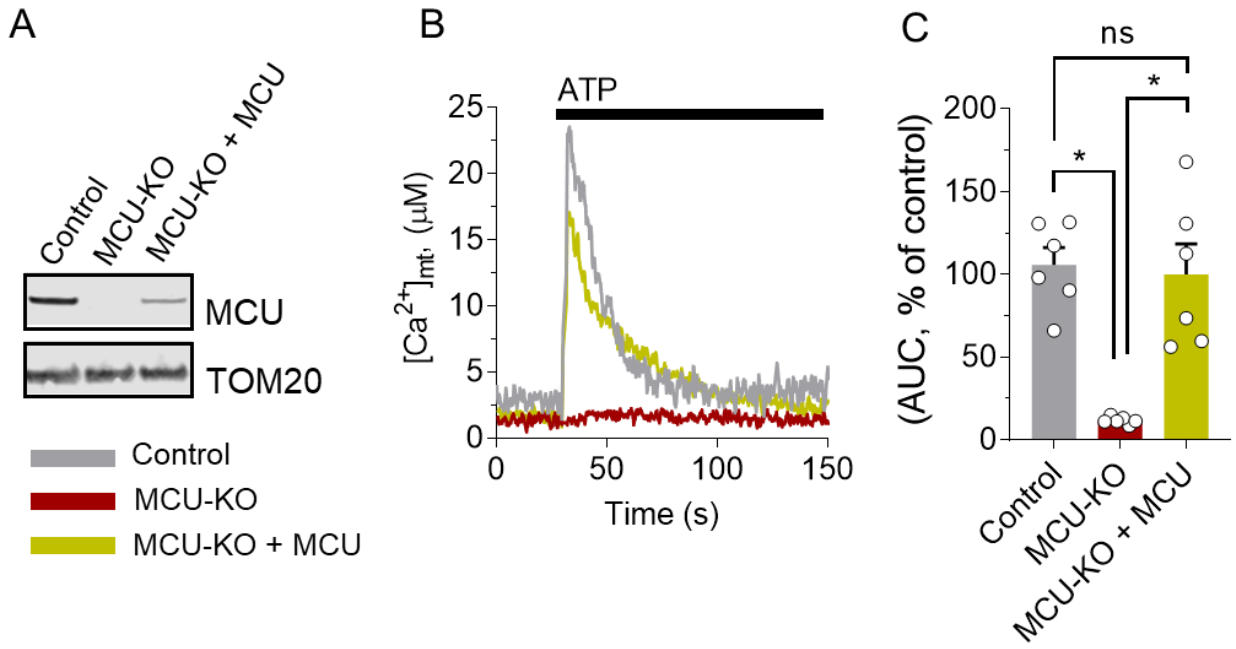

Figure 15. Transfection with the MCU-plasmid rescues mitochondrial Ca^{2+} signaling in MCU-KO cells.
(A) MCU expression in control, MCU-KO and MCU-KO cells with reintroduced MCU expression (MCU-KO+MCU) was validated by western blot using TOM20 as loading control. (B) Functional validation of MCU-KO+MCU (yellow) compared to control (grey) and MCU-KO (red) HAP1 cells by measuring ATP-induced mitochondrial Ca^{2+} uptake. (C) AUC values of mitochondrial Ca^{2+} uptake were measured in control cells (grey, n=6; 10 cells/sample), MCU-KO cells (red, n=6; 10 cells/sample) and MCU-KO+MCU cells (yellow, n=6; 10 cells/sample), and values for MCU-KO and MCU-KO+MCU cells were normalized to control cells and expressed as percentages. Data are expressed as mean±SEM. Results are considered significant at a significance threshold of $\alpha < 0.05$; *$p < 0.05$; ns, not significant (One-way ANOVA to compare more than 2 groups).

The same system was then used to measure the redox state of the matrix thiol groups in stimulated control, MCU-KO and MCU-KO cells with reintroduced MCU. The obtained traces were normalized to H_2O_2 and DTT as described in Figure 6B, and the average traces for MCU-KO and MCU-rescue were displayed (**Figure 16A**). Statistical evaluation of the basal redox state in MCU-KO and MCU-KO+MCU showed no difference between the groups (**Figure 16B**). However, MCU activation (with ATP) caused a significant increase in the ratio of reduced to oxidized mitochondrial thiol groups in the MCU-KO cells with reintroduced MCU, resulting in a significantly increased delta redox value compared to MCU-KO cells (**Figure 16C**). These results demonstrate that the change in thiol groups is not simply a specificity of MCU-ablated cells, and thus establish a causal relationship between the mitochondrial redox state and its modulation by mitochondrial Ca^{2+} increase via MCU, leading to a net reduction.

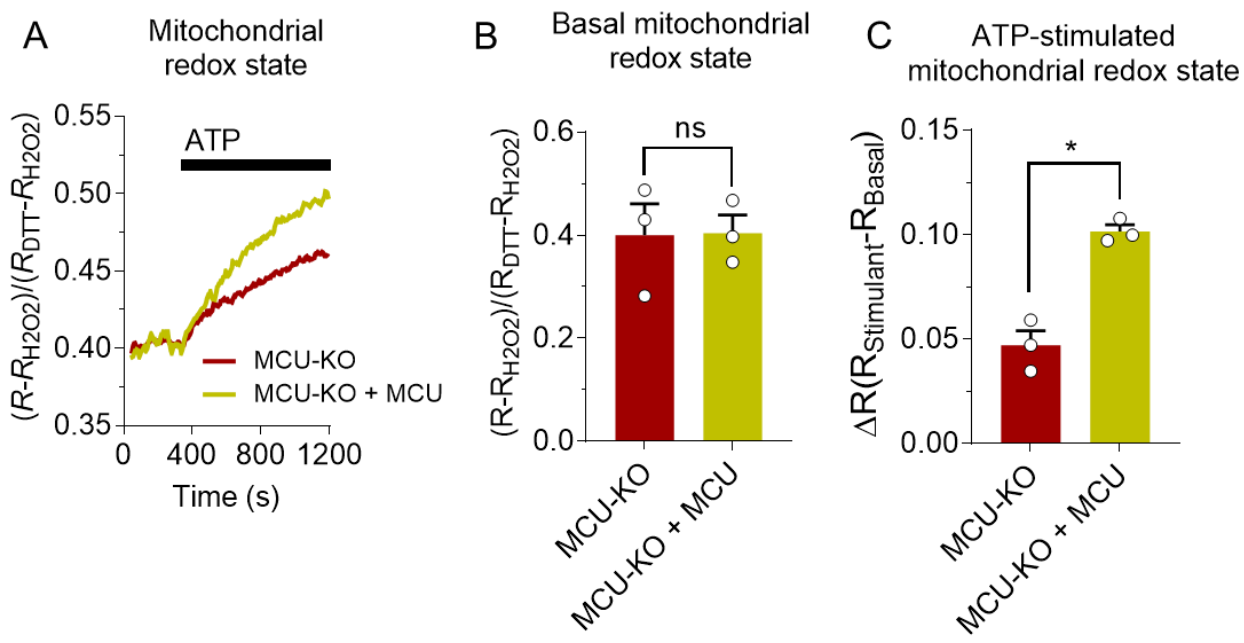

Figure 16. Mitochondrial matrix redox state in HAP1 MCU-KO and MCU-KO+MCU cells.
(A) Shows the average redox traces for MCU-KO and MCU-KO+MCU cells, each based on 3 dishes with in total 30 selected cells per group. (B) Basal redox state was measured for 3 min in MCU-KO (red, n=3 experiments; 10 cells/sample) and MCU-KO+MCU (yellow, n=3 experiments; 10 cells/sample) HAP1 cells. (C) Depicts the quantified increase of reduced thiol groups 15 min after ATP (1 mM) stimulation, by subtracting basal redox state. Each dot shows the average of one dish and each bar depicts the total average of 3 dishes with in total 30 cells of MCU-KO (red) or MCU-KO+MCU (yellow) HAP1 cells, respectively. Data are expressed as mean±SEM. Results are considered significant at a significance threshold of $\alpha < 0.05$; *$p < 0.05$; ns, not significant (Student's *t*-test to compare two groups).

4.1.4. MCU modulates matrix redox state in primary human myotubes

Given the importance of a balanced mitochondrial redox biology in skeletal muscle (Szentesi et al., 2019, Mailloux et al., 2012, Le Moal et al., 2017, Riemer et al., 2015), the next step was to investigate whether the previous findings in HAP1 cells could be found also in human skeletal muscle myotubes. For this purpose, primary human control myoblasts and myoblasts with an MCU-knockdown (MCU-kd) were generated using adenoviral control and MCU-shRNA and subsequently differentiated into human myotubes (**Figure 17A**). To obtain an optimal MCU-kd model, different concentrations of MCU-shRNA were tested in lysed myotubes and validated by capillary Western blot (**Figure 17B**). For functional validation, control and MCU-kd myotubes were infected with the mitochondria-targeted aequorin probe (Bonora et al., 2013) to measure mitochondrial Ca^{2+} uptake after stimulation with a mixture of caffeine and epibatidine (**Figure 17C**). Based on the calibrated Ca^{2+} traces, an interval from caffeine/epibatidine injection to peak mitochondrial Ca^{2+} uptake was used to calculate the slope values of each sample via linear regression (**Figure 17D**), which revealed a significant decrease in mitochondrial Ca^{2+} uptake in MCU-depleted myotubes.

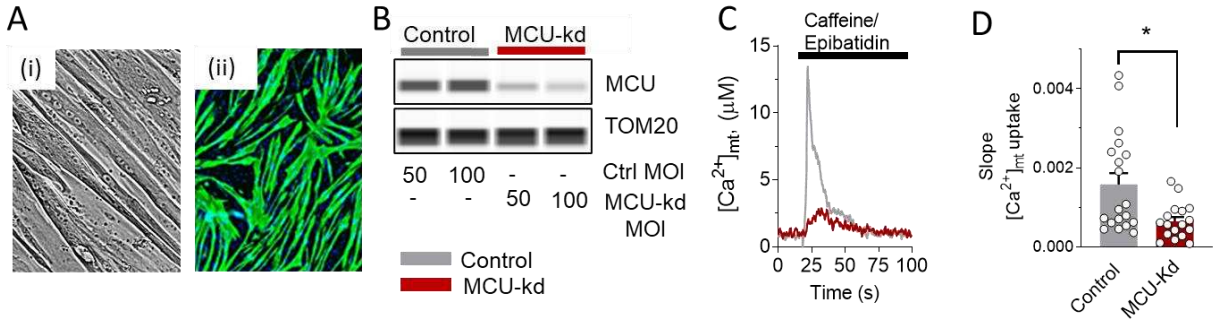

Figure 17. MCU activation regulates mitochondrial Ca^{2+} uptake in primary human myotubes.
(A) Microscopic images of differentiated myotubes under the brightfield (i) and fluorescence microscope, stained with troponin T and DAPI (ii). (B) Different expression levels of the MCU subunit in myotubes using 50 and 100 MOI of MCU shRNA (red) or scrambled control shRNA (grey) to optimize the knockdown of the MCU subunit. TOM20 antibody was used as loading control. (C) Mitochondrial Ca^{2+}, measured in control and MCU-knockdown (MCU-kd) myotubes after stimulation with 5 mM caffeine plus 10 µM epibatidine. (D) Statistical analysis of calculated slope values of mitochondrial Ca^{2+} traces to analyse the uptake in control (grey, n=19 experiments) and MCU-kd (red, n=17 experiments) myotubes. Data are expressed as mean±SEM. Results are considered significant at a significance threshold of $\alpha < 0.05$; *$p < 0.05$; ns, not significant (Mann-Whitney test to compare two groups).

In a next step, the effect of mitochondrial Ca^{2+} activation by caffeine/epibatidine on mitochondrial redox status was investigated in control and MCU-kd primary human myotubes using the mitochondria-targeted roGFP1 sensor (**Figure 18A**). Due to the high sensitivity of the differentiated myotubes, the experiment was automated using a fluorescence plate reader with two injection ports. For this reason, the cells were first stimulated by injection of a caffeine-

epibatidine mixture, followed by a second injection with DTT to normalize the traces. Statistical evaluation of the basal mitochondrial redox state showed no significant difference between control and MCU-kd myotubes (**Figure 18B**), while the calculated delta redox value, after MCU activation with caffeine/epibatidine, showed a significant increase in reduced versus oxidized mitochondrial thiol groups in control but not in MCU-kd myotubes (**Figure 18C**). Delta redox values were determined by taking the maximum value after stimulation with caffeine/epibatidine and subtracting the baseline redox state measured before the start of the first injection. These results show that MCU activation also promotes a net reduction of mitochondrial thiol groups in primary human myotubes.

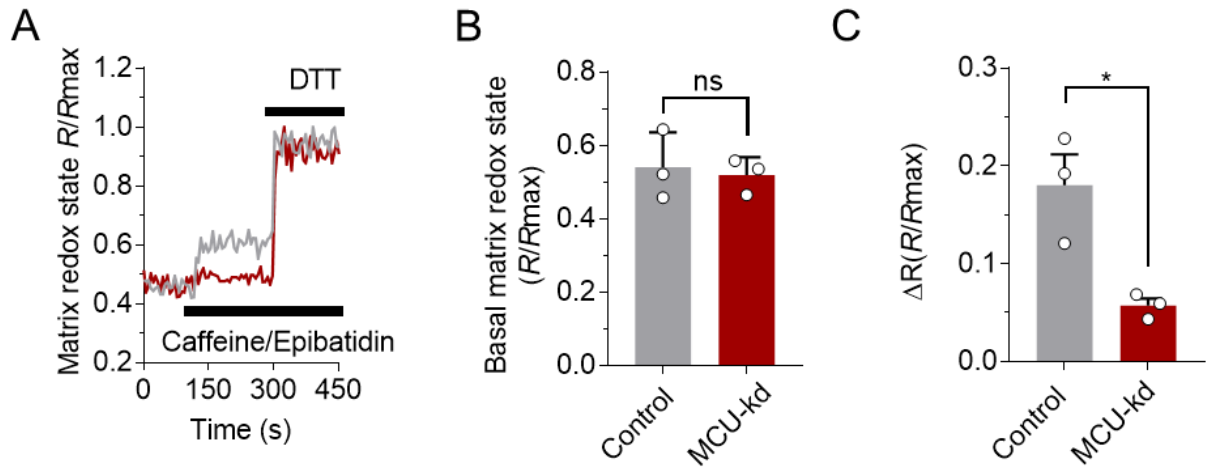

Figure 18. MCU activation modulates matrix redox state in primary human myotubes.
(A) Shows mitochondrial redox traces of control (grey) and MCU-kd (red) human myotubes infected with mitochondria targeted roGFP1 to measure effect of stimulation with caffeine (5 mM) and epibatidine (10 µM). Traces were normalized to maximum fluorescence reached by addition of DTT (60 mM). (B) Statistical analysis of basal redox state in control (grey, n=3 experiments) and MCU-kd (red, n=3 experiments) myotubes. (C) Delta redox values were calculated by subtracting basal redox values from stimulation induced maximum values for control (grey, n=3 experiments) and MCU-kd (red, n=3 experiments) myotubes. Data are expressed as mean±SEM. Results are considered significant at a significance threshold of $\alpha < 0.05$; *$p < 0.05$; ns, not significant (Student's *t*-test to compare two groups).

4.1.5. Modulation of mitochondrial thiols via MCU regulates respiration in human myotubes

To assess the role of MCU in mitochondrial energy metabolism of skeletal muscle myotubes, the effect of mitochondrial Ca^{2+} increase on oxygen consumption was measured in control and MCU-kd myotubes after stimulation with caffeine/epibatidine (**Figure 19A**, grey and red traces). Compared to MCU-kd myotubes, stimulation with the mitochondrial Ca^{2+} activators caffeine/epibatidine induced a significant increase in the oxygen consumption rate (OCR) in

control myotubes, confirming the promoting effect of mitochondrial Ca^{2+} in improving mitochondrial respiration.

Given the link between MCU modulation and mitochondrial redox signaling, the question arose whether mitochondrial redox signaling itself can modulate energy metabolism. To answer this question, pharmacological agents, capable of oxidizing and reducing mitochondrial thiol groups, were applied to human control and MCU-kd myotubes to measure their effect on OCR and to assess the link to MCU. First, the mitochondria-targeted oxidizing compound mitochondrial paraquat (mtPQ), a known redox cycler at complex I (Murphy, 2009) that promotes $O_2^{\bullet-}$ synthesis, was added to control myotubes and the agonist-induced OCR was evaluated (**Figure 19A**, orange trace).

The potent ROS inducer mtPQ completely attenuated the caffeine/epibatidine-induced increase in cellular respiration in control myotubes and exhibited a similar respiration profile than MCU-kd (**Figure 19A**, red trace). Statistical analysis confirmed the agonist-induced enhancement effect on ATP synthase-dependent respiration in control myotubes, an effect that was attenuated by MCU-kd but also by the application of the potent mitochondrial oxidant mtPQ to control myotubes (**Figure 19B**).

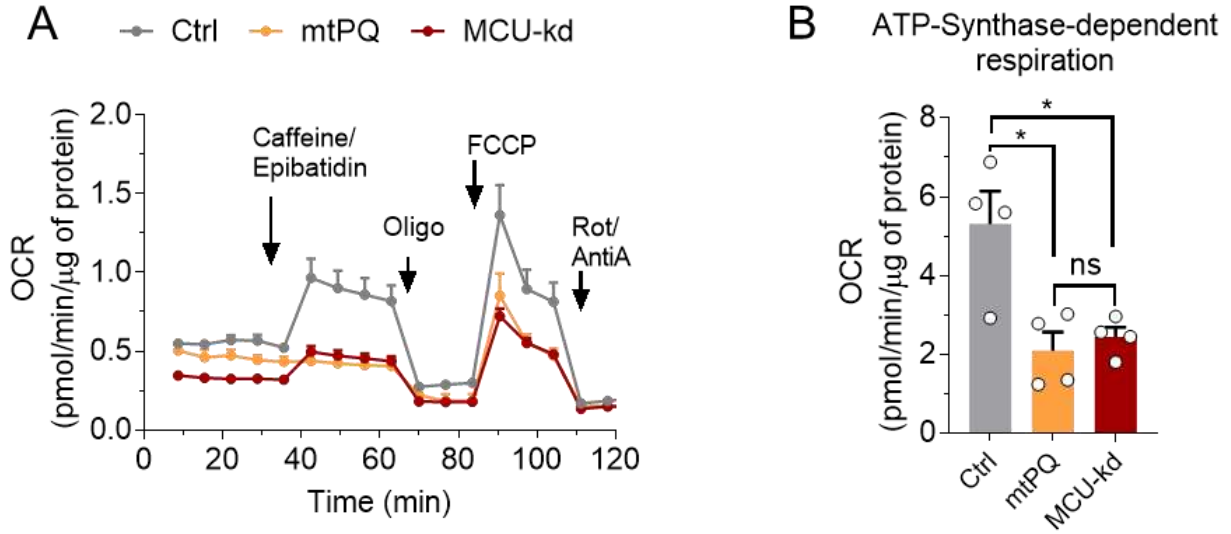

Figure 19. MCU activation promotes cellular respiration in primary human myotubes.
(A) Oxygen consumption rate (OCR) profiles of the control group without (Ctrl, grey, n=4 experiments) or with the addition of 0.01 µM mitochondria-targeted paraquat (mtPQ, orange, n=4; 8 000 cells/sample) and MCU-kd myotubes (MCU-kd, red, n=4 experiments). To evaluate the OCR profiles of the three groups, the effects of 5 mM caffeine/10 µM epibatidine, 2.5 µg/ml oligomycin (oligo), 3 µM FCCP and 2 µM rotenone (Rot) plus 2 µg/ml antimycin A (antiA) were tested. (B) Shows the respective statistical analysis of ATP synthase-dependent respiration calculated in control without (Ctrl, grey, n=4 experiments) or with addition of 0.01 µM mitochondria-targeted paraquat (mtPQ, orange, n=4; 8000 cells/sample) and in MCU-kd myotubes (MCU-kd, red, n=4 experiments). This parameter was calculated by by subtracting OCR data after oligomycin addition to the recorded values before oligomycin addition Data are expressed

as mean±SEM. Results are considered significant at a significance threshold of $\alpha < 0.05$; *p < 0.05; ns, not significant (One-way ANOVA for comparison of more than 2 groups).

These results suggest that mitochondrial redox signaling is directly coupled to bioenergetics in muscle physiology. This was further investigated by testing the effect of the thiol reducing agent DTT in primary human myotubes. For this purpose, OCR was measured in MCU-kd myotubes stimulated with caffeine/epibatidine, which did not cause a significant increase in mitochondrial respiration. Then the reducing agent DTT was injected to reduce the thiol groups (**Figure 20A**, blue trace). A vehicle containing Krebs buffer was used as a control (**Figure 20A**, red trace). Injection of DTT caused an immediate response in the respiration profile that resembled MCU activation in the control myotubes previously analyzed (**Figure 12A**, grey trace). Statistical analysis revealed an approximate 50 % increase in OCR in MCU-kd myotubes injected with DTT compared to control MCU-kd myotubes injected with the vehicle (**Figure 20B**). These results demonstrate that direct reduction of thiol groups can rescue mitochondrial respiration in MCU-depleted myotubes.

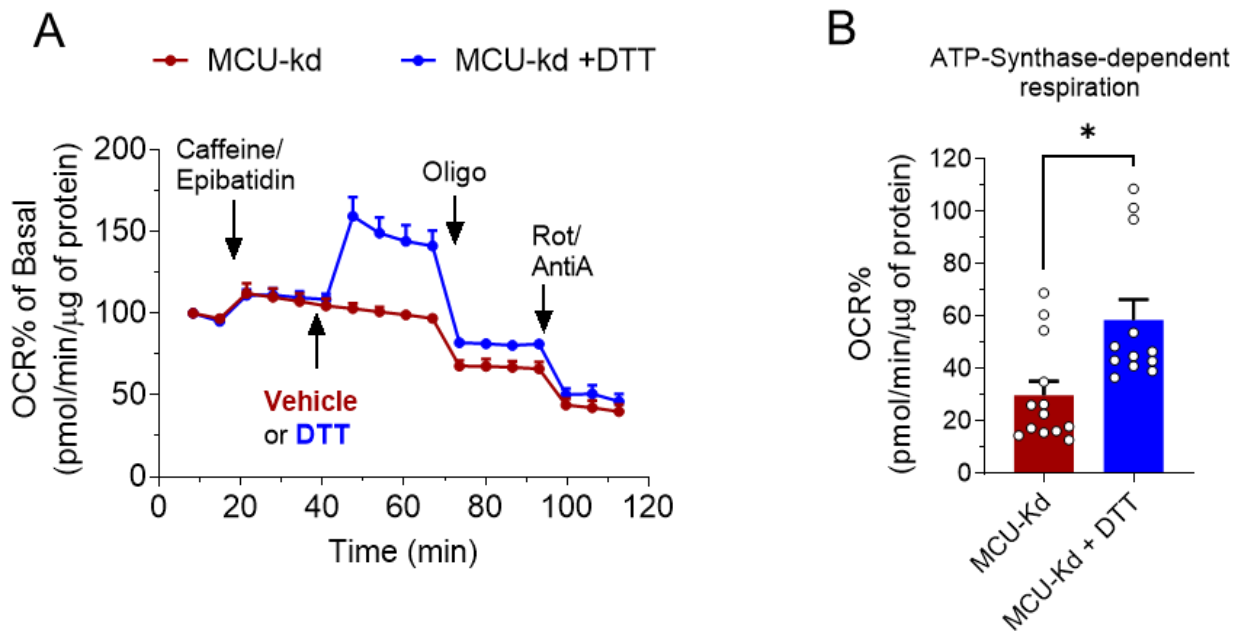

Figure 20. Pharmacological modulation of cellular respiration in primary human myotubes.
(A Shows respiration profiles with 5 mM caffeine/10 µM epibatidine stimulation of MCU-kd with (blue, n=12; 8000 cells/sample) and without (red, n=13, 8 000 cells/sample) injection of 10 mM of the thiol reducing agent DTT, followed by 2.5 µg/ml oligomycin (oligo) and 2 µM rotenone (Rot) plus 2 µg/ml antimycin A (antiA). Data was normalized to each individual basal OCR set to 100 % to evaluate the effect of DTT on cellular respiration. (B) Shows ATP-synthase dependent respiration in MCU-kd (red, n=12, 8 000 cells/sample) and DTT-treated MCU-kd (blue, n=12; 8 000 cells/sample) myotubes, after normalizing each sample to its basal OCR, set to 100 % to track the effect of DTT on

cellular respiration. Data are expressed as mean±SEM. Results are considered significant at a significance threshold of α < 0.05; *p < 0.05; (Student's *t*-test to compare two groups).

When mitochondrial thiol groups were oxidized, MCU-dependent activation of respiration was prevented. Conversely, pharmacologically mediated reduction of thiol groups was sufficient to increase mitochondrial energy metabolism even in MCU-depleted cells, indicating that MCU-dependent reduction of thiol groups is downstream of MCU activation. Collectively, these results suggest that MCU activation enhances energy metabolism via the reduction of mitochondrial thiol groups in human myotubes.

4.1.6. MCU activation increases bioenergetics and mobility in *C.elegans*, *in vivo*

The nematode *C. elegans* was used as a model to investigate *in vivo* the effects of thiol group regulation via MCU on mitochondrial respiration and locomotor activity. For this purpose, the MCU-KO strain *mcu-1* was validated by qPCR (**Figure 21A**) and OCR was measured in control and *mcu-1* mutant worms stimulated with carbachol to activate mitochondrial Ca^{2+} uptake (Álvarez-Illera et al., 2020). After stimulation with carbachol, sodium azide (NaN_3), a potent blocker of complex IV and V (Koopman et al., 2016b), was added to inhibit mitochondrial respiration (**Figure 21B**). The reason for choosing NaN_3 to block respiration instead of other standard chemicals (e.g. oligomycin, rotenone and antimycinA) used in mitochondrial respiration assays is that they are not sufficiently absorbed across the cuticle of *C. elegans* to promote efficient modulation of mitochondrial respiration in worms. Statistical analysis of carbachol-stimulated NaN_3-sensitive respiration was calculated by subtracting non-mitochondrial respiration (determined after addition of NaN_3) from carbachol evoked respiration. A significantly lower value was measured in MCU-defective worms compared to control worms (**Figure 21C**). These results highlight the role of MCU as a key component of stimulated mitochondrial respiration, *in vivo*.

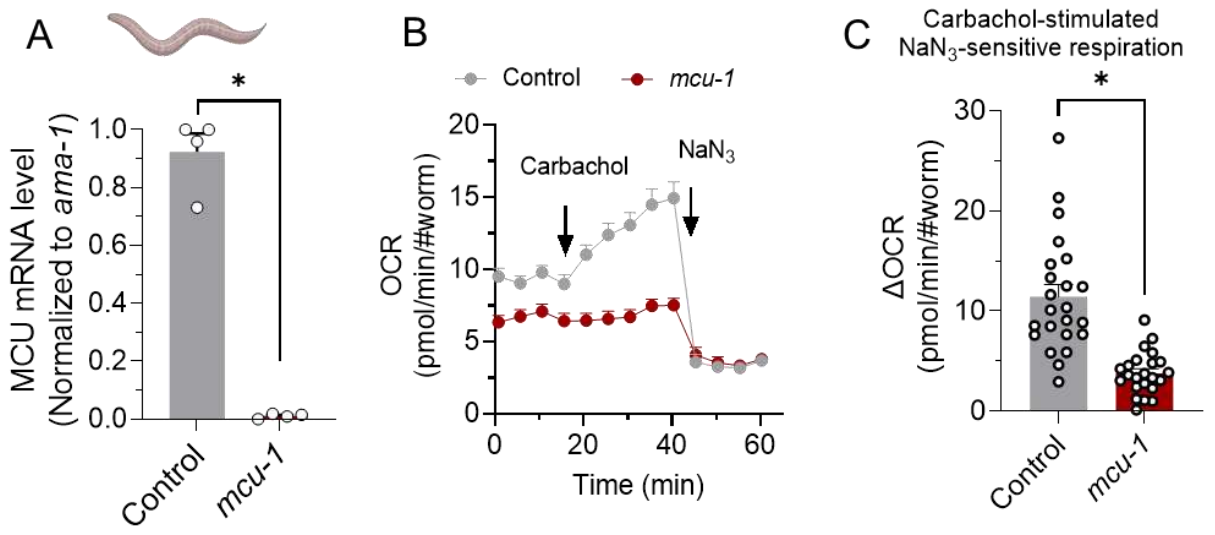

Figure 21. MCU activation promotes cellular respiration in *C. elegans, in vivo*.
(A Shows qPCR validation of the *mcu-1* mutant worm (red, n=4 experiments) compared to the control (grey, n=4 experiments). (B) Oxygen consumption rate (OCR) was measured in adult control (grey, n=8 samples each with 20-30 worms) and adult *mcu-1* mutants (red, n=6 samples each with 20-30 worms), after stimulation with 10 mM carbachol. (C) Carbachol-stimulated NaN_3-sensitive respiration was calculated by subtracting NaN_3-sensitive respiration from carbachol induced respiration in adult control (grey, n=3 experiments with 8 samples with 20-30 worms) and adult *mcu-1* (red, n=3 experiments with 6 samples with 20-30 worms) worms. Data are expressed as mean±SEM. Results are considered significant at a significance threshold of $\alpha < 0.05$; *$p < 0.05$; (For A, Mann-Whitney test and for C, Student's *t*-test to compare two groups).

To test whether redox-active compounds can influence bioenergetics *in vivo*, the respiratory profiles of control worms using a control vehicle were compared with worms injected with the oxidant mtPQ, which caused a slight but non-significant decrease in basal respiration (**Figure 22A-B**). However, after stimulation with carbachol, OCR increased only in the control worms but not in the mtPQ-treated worms, indicating a link between mitochondrial redox state and regulation of mitochondrial respiration (**Figure 22A**). Therefore, statistical evaluation of carbachol-induced and NaN_3-sensitive respiration showed a significant decrease in OCR after mtPQ treatment (**Figure 22C**).

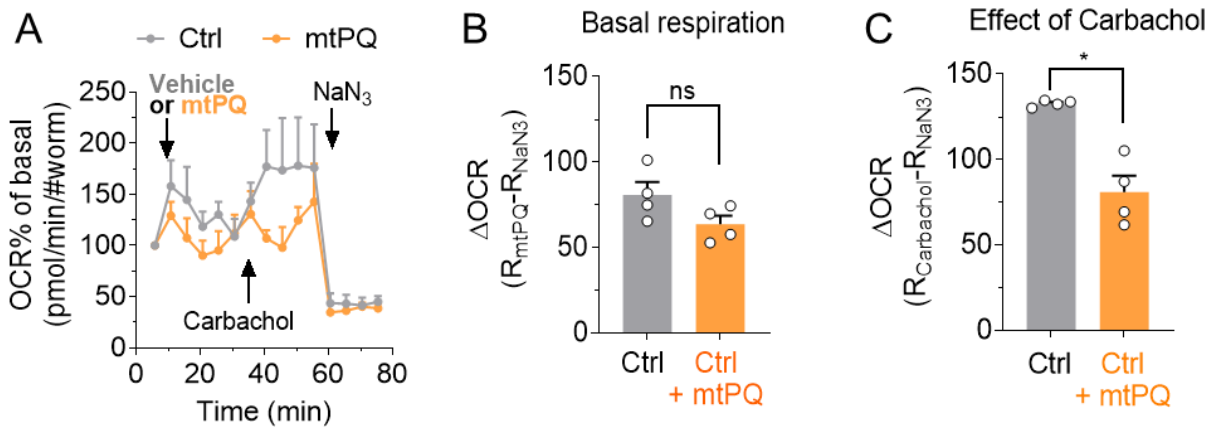

Figure 22. Mitochondrial paraquat blunts the carbachol-stimulated increase in cellular respiration in *C. elegans*. (A) Oxygen consumption rate (OCR) of adult control (grey, vehicle, n=6; 20-30 worms/experiment) and mitochondrial paraquat (mPQ, 0.1 µM) injected adult control worms (orange, mtPQ, orange, n=6; 20-30 worms/experiment), normalized to basal respiration and expressed in %. (B) Basal respiration of the control (grey) and mtPQ injected control worms (orange). (B) Basal OCR in control (grey, n=4 experiments with 6 samples) and mtPQ injected control worms (orange, n=4 experiments with 6 samples). (C) Effect of stimulation with the MCU activator carbachol (10 mM) on OCR in control (grey, n=4 experiments with 6 samples) and mtPQ treated control worms (orange, n=4, experiments with 6 samples). Carbachol-stimulated NaN_3-sensitive respiration was calculated by subtracting NaN_3-sensitive respiration from maximum respiration after stimulation with carbachol. Data are expressed as mean±SEM. Results are considered significant at a significance threshold of $\alpha < 0.05$; *$p < 0.05$; ns, not significant (For C, Mann-Whitney test and for B, Student's *t*-test to compare two groups).

The fact that mtPQ can attenuate the increase in respiration induced by carbachol in control worms suggests a link between redox modulation and bioenergetics *in vivo.* To evaluate the relationship between redox state modulation by MCU activation and oxygen consumption, the *C. elegans mcu-1* model was used and the effect of the reducing agent DTT on respiratory profiles was measured. Injection of DTT into the MCU-defective worms caused a significant increase in respiration (**Figure 23A-B**, blue), similar to the carbachol-induced increase in the control worms (**Figure 23A**, grey). However, the control vehicle did not cause an increase in OCR of the *mcu-1* worms. Injection of carbachol did not result in any further increase in respiration, either in the *mcu-1* worms injected with the vehicle or in those injected with DTT (**Figure 23C**).

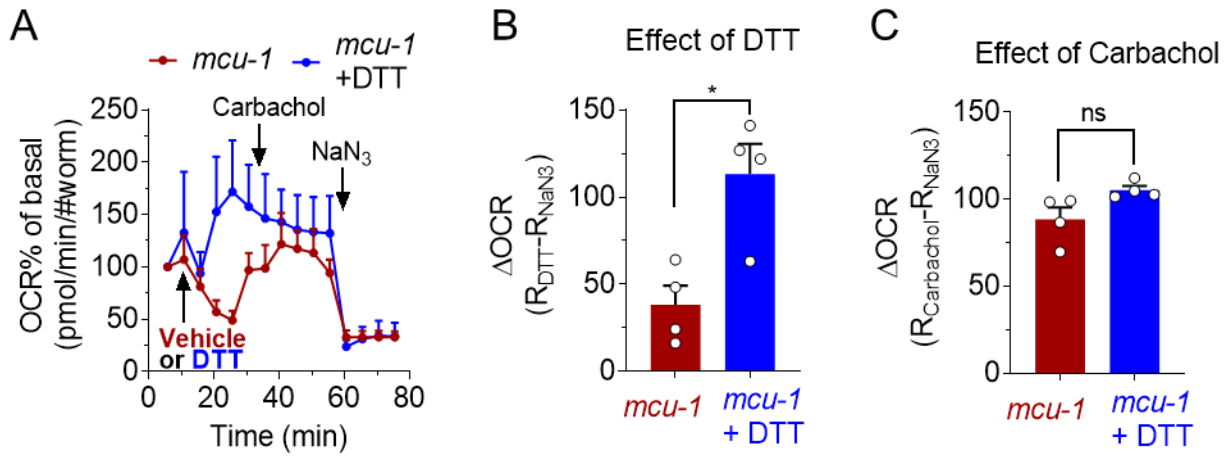

Figure 23. The reducing agent DTT but not carbachol increases respiration in MCU deficient worms.
(A) Oxygen consumption rate (OCR) of adult *mcu-1* control worms (red, vehicle, n=4; 20-30 worms/experiment) and DTT (10 mM) injected adult *mcu-1* worms (blue, n=4; 20-30 worms/experiment), normalized to basal respiration and expressed in %. (B) Basal respiration of the *mcu-1* mutant worms (red, n=4; 20-30 worms/experiment) compared to the DTT injected *mcu-1* worms (blue, n=4; 20-30 worms/experiment). (C) Effect of stimulation with the MCU activator carbachol (10 mM) on OCR in *mcu-1* control (red, n=4; 20-30 worms/experiment) and DTT injected *mcu-1* worms (blue, n=4; 20-30 worms/experiment). Carbachol-stimulated NaN_3-sensitive respiration was calculated by subtracting NaN_3-sensitive respiration from maximum respiration after stimulation with carbachol. Data are expressed as mean±SEM. Results are considered significant at a significance threshold of $\alpha < 0.05$; *$p < 0.05$; ns, not significant (For B, Mann-Whitney test and for C, Student's *t*-test to compare two groups).

These results suggest that mitochondrial redox management by MCU modulation (or by direct disruption of thiol groups) also regulates energy metabolism in *C. elegans*. Reduction of mitochondrial thiol groups is dominant over MCU mutation because it acts downstream of mitochondrial Ca^{2+}-sensitive dehydrogenases.

In a final experiment, the aim was to investigate the effect of MCU and pharmacological redox modulators on the healthspan of *C. elegans* by evaluating the effects on mobility. For this, plates with control worms either with or without acute treatment (20-min) of the oxidant mtPQ and *mcu-1* worms either with or without acute treatment (20-min) by the reducing agent DTT were recorded under the microscope with a camera connected to a laptop (**Figure 24A**). Subsequent analysis of the recorded movies was done in MATLAB and provided respective average velocities (**Figure 17B**). The results showed a clear MCU dysfunction-dependent decline in mobility, which could be rescued by adding the reducing agent DTT. This pharmacological agent increased mobility to a similar average speed as in the control worms (**Figure 24B**). On the contrary, the oxidant mtPQ reduced the mobility in control towards the level of *mcu-1* mutants.

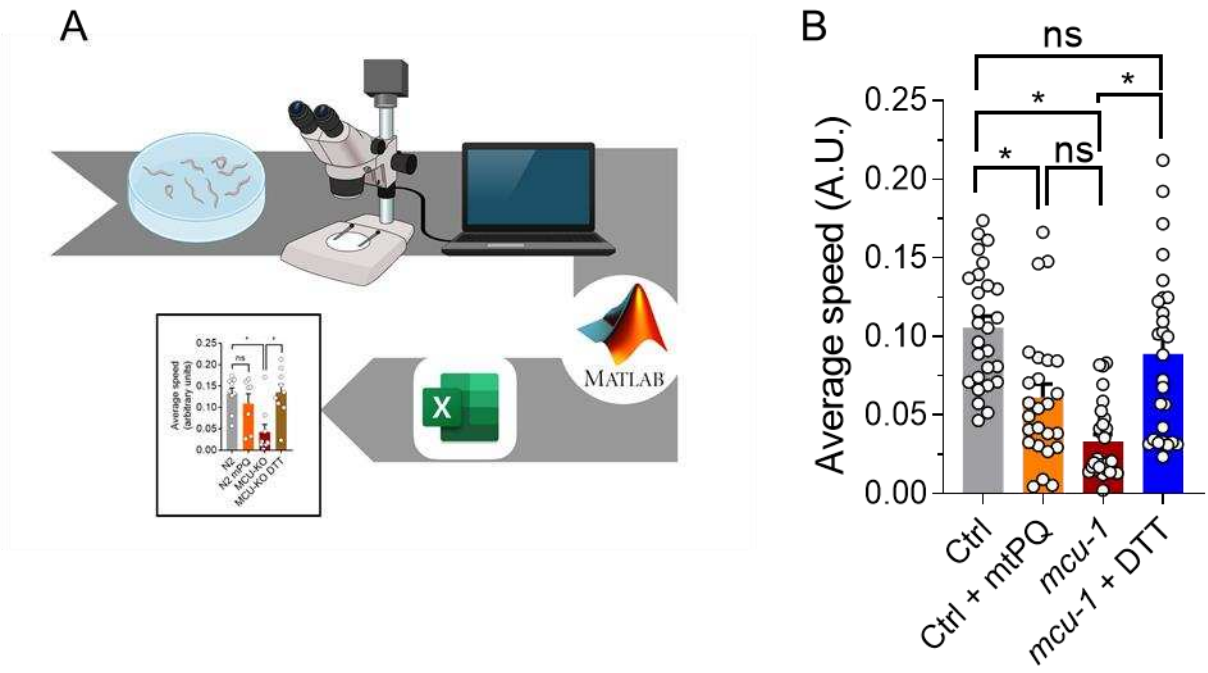

Figure 24. MCU regulates mobility in a redox dependent manner in *C. elegans.*
(A) Schematic workflow of the *C.elegans* movement tracker. First the lid is removed and the plate is placed under the microscope, which is connected to a camera and a laptop to record the movement of the worms for 90-s. The recordings are processed in Matlab with the Movement Tracker software (Koopman et al., 2016b) and finally exported to excel for further data analysis and statistical analysis. (B) Average speed of adult control (grey, n=27 worms), mtPQ (0.1 µM) treated control (orange, n=27 worms), adult *mcu-1* mutant (red, n=27) and DTT (10 mM) treated *mcu-1* worms (blue, n=28). Data are expressed as mean±SEM. Results are considered significant at a significance threshold of $\alpha < 0.05$; *$p < 0.05$; ns, not significant (Kruskall-Wallis test to compare more than 2 groups).

Overall, the *in vitro* and *in vivo* results show the significance of MCU in regulating bioenergetics and mobility through the mitochondrial redox state. In particular, MCU enhances a net reduction of redox-sensitive thiol groups in mitochondria, thus boosting energy metabolism in myotubes and in *C. elegans* and increasing worm mobility *in vivo.*

4.2. Part II: Oleuropein is a natural MCU activator that promotes energy metabolism and skeletal muscle performance in both adults and aged models

In the second part of the results section, data on the importance of MCU in the context of skeletal muscle aging are shown that also served as a concept for the development of an MCU-based intervention with expected positive effects on skeletal muscle mitochondrial energy metabolism and performance. The section focuses on the identified natural bioactive polyphenol and MCU activator oleuropein and its mechanism of action to promote skeletal muscle health through MCU.

4.2.1. MCUR1 mRNA and mitochondrial Ca^{2+} uptake decline in aged human muscle

To study the impact of mitochondrial Ca^{2+} signaling in skeletal muscle during aging, human myotubes from adult (**Figure 25A-B**) and aged donors were investigated by measuring mitochondrial Ca^{2+} uptake upon caffeine-induced Ca^{2+} release from the SR to activate the MCU and increase mitochondrial Ca^{2+} uptake (**Figure 25C**). In aged human myotubes the mitochondrial Ca^{2+} uptake was significantly decreased compared to non-aged controls (**Figure 25D**).

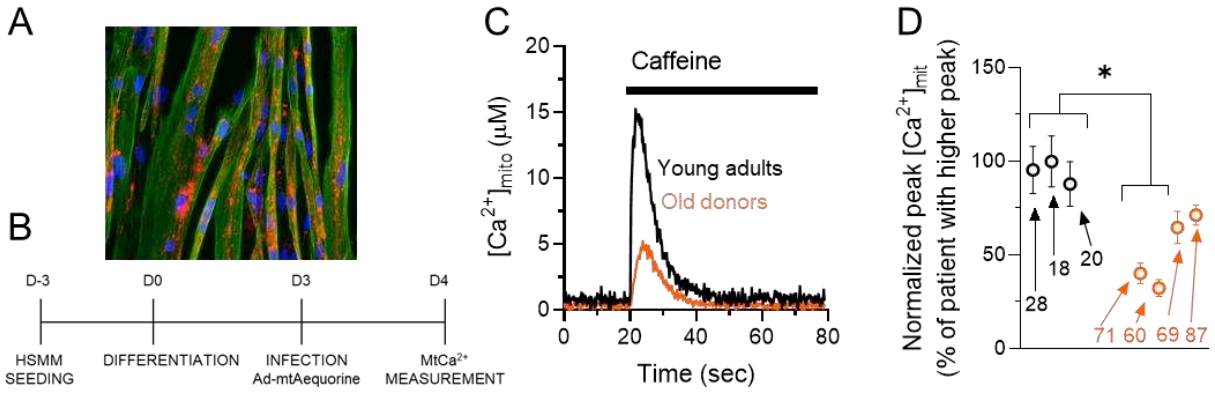

Figure 25. Mitochondrial Ca^{2+} uptake declines significantly with age.
Shows differentiated primary human myotubes stained with DAPI (blue, nuclei), MCU (red, mitochondria) and troponin (green, fibers) following the differentiation protocol in (B) where cells are seeded at D-3, differentiated at D0 using 2% horse serum, infected on D3 with the mitochondrial-targeted Ca^{2+} probe aequorin and measured at D4. (C) Calibrated Ca^{2+} traces, depicting mitochondrial Ca^{2+} uptake after stimulation with caffeine in young (black) and old (orange) primary human myotubes. (D) Statistical analysis of caffeine stimulated mitochondrial Ca^{2+} uptake in young (black, n=3) and old (orange, n=4) human myotubes normalized to the young 18-year-old donor and expressed in %. Data are expressed as mean±SEM. Results are considered significant at a significance threshold of $\alpha < 0.05$; *$p < 0.05$ (ANOVA).

To investigate the molecular link between aged muscle and mitochondrial Ca^{2+} regulation, biopsies were taken from the gastrocnemius muscle of 40 healthy elderly donors and 40 sarcopenic study participants. The transcriptomic profile of genes encoding proteins responsible

for mitochondrial Ca^{2+} transport was then evaluated. Among all measured genes associated with mitochondrial Ca^{2+} regulation (**Figure 26A**.), the MCUR1 mRNA expression was significantly lower in sarcopenic elderly compared to controls (**Figure 26A**, left panel).

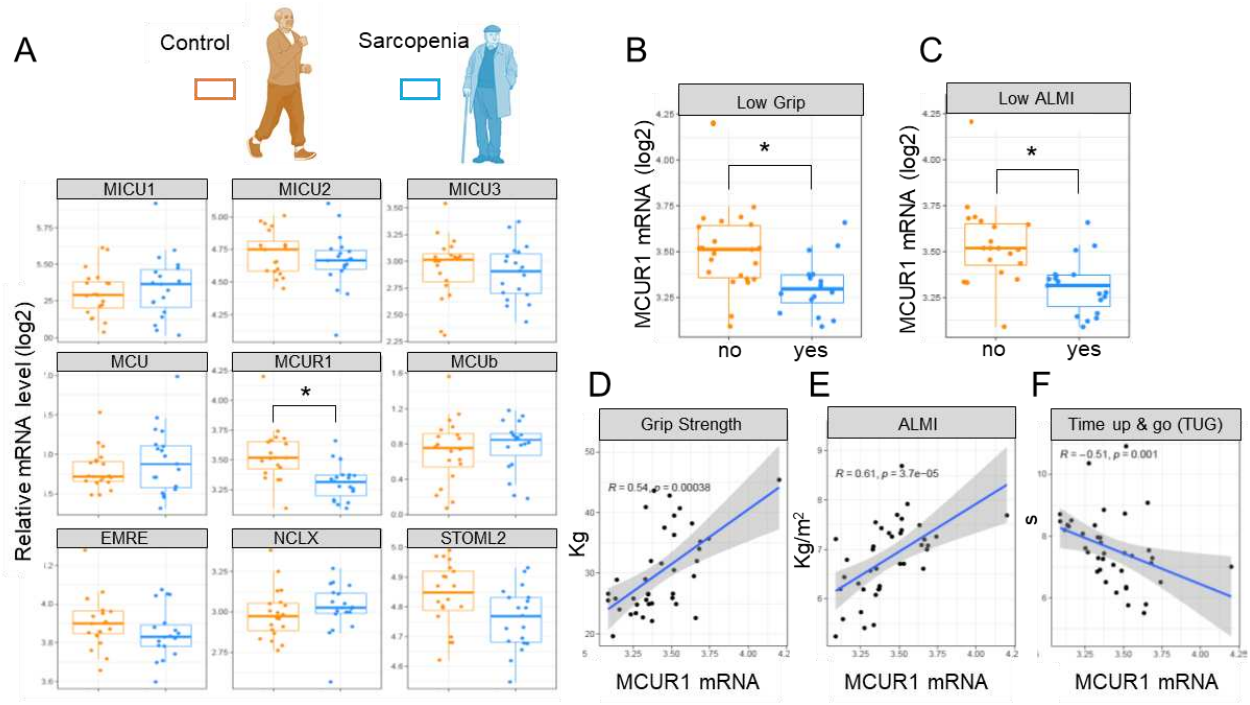

Figure 26. Impaired mitochondrial Ca^{2+} response in old people correlates with markers of sarcopenia.
(A) Shows gene expression data of proteins involved in mitochondrial Ca^{2+} import (MICU1, MICU2, MICU3, MCU, MCRUR1, MCUb and EMRE) and export (NCLX and STOML2) in muscle tissue from 40 old control men (orange) and 40 old sarcopenic men (blue). (B) Displays MCUR1 mRNA expression in old men with low grip strength and (C) shows MCUR1 mRNA expression in old men with low appendicular lean mass index (ALMI). Values were normalized using 10 housekeeping genes. For panel A two-tailed t-test was used for statistical testing and the non-parametric Wilcoxon test was used for panel B and C. (D) The linear relationships between MCUR1 mRNA expression and the variables Grip Strength, (E) ALMI, and (F) Stand up and walk were determined by calculating the *Pearson* correlation coefficient *R*. Individual samples are plotted (black) together with a fitted line (blue) and a grey polygon indicating the upper and lower thresholds of the predicted interval. Results are considered significant at a significance threshold of $\alpha < 0.05$; *p < 0.05 (p-values were adjusted for multiple testing using Benjamin-Hochberg method).

MCUR1 is a crucial regulatory subunit of the MCU complex, (Mallilankaraman et al., 2012a) and was shown to decline significantly in mRNA expression in individuals with impaired muscle health (**Figure 26A**, middle and right panel). To evaluate further the functional relationship between MCUR1 mRNA expression and the low appendicular lean mass index (ALMI), grip strength and time to stand up and walk, the *Pearson* correlation coefficient was calculated and showed a significantly positive correlation between MCUR1 mRNA and ALMI as well as MCUR1 mRNA and grip strength, while MCUR1 mRNA and stand up and walk were inversely correlated, meaning that with a lower MCUR1 mRNA level, time to stand up and walk increased. These parameters,

ALMI, grip strength and time to stand up and walk, were selected according to the AWGSOP criteria for the assessment of sarcopenia (Migliavacca et al., 2019). These results suggest an inverse correlation between MCUR1 mRNA expression levels and muscle performance.

To assess the potential link between MCUR1 downregulation and the mitochondrial Ca^{2+} homeostasis in aged individuals, protein expression of MCUR1 was depleted in primary adult myotubes using shRNA (**Figure 27A**). Subsequently, the effect of MCUR1 depletion was functionally validated by measuring mitochondrial Ca^{2+} uptake following stimulation with caffeine (**Figure 27B**, left panel).

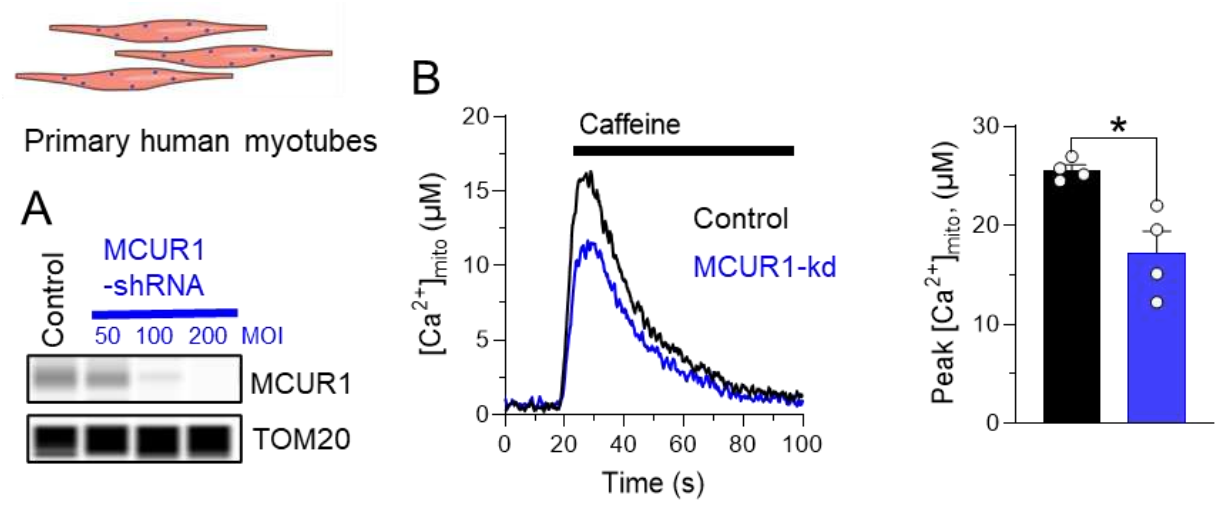

Figure 27. Knockdown of MCUR1 in HSMM reduces mitochondrial Ca^{2+} uptake.
(A) Shows gradual MCUR1 knockdown (MCUR1-kd) with different concentrations of control and MCUR1-shRNA (50, 100, 150 and 200 MOI) in HSMM validated by capillary Western blot using TOM20 as loading control. (B) Respective calibrated traces for control (black) and MCUR1-kd (blue) HSMM stimulated with 5 mM caffeine. Peak caffeine responses in control (black, n=4 samples) and MCUR1-kd (blue, n=4 samples) were statistically analyzed using a Student's *t*-test. Data are expressed as mean±SEM. Results are considered significant at a significance threshold of $\alpha < 0.05$; *$p < 0.05$.

Compared to control myotubes, MCUR1-knockdown (MCUR1-kd) myotubes had a significantly lower peak in caffeine-evoked mitochondrial Ca^{2+} uptake (**Figure 27B**, right panel), reflecting a similar trend to that observed in aged myotubes as shown in **Figure 25C**. Collectively, the findings suggest a functional connection between age-related skeletal muscle physiology, mitochondrial Ca^{2+} signaling and muscle function. As part of the collaboration with the University of Padova, this functional connection was also investigated in a preclinical model of aging. First, the relative expression of the mRNA of the subunits of the MCU complex (MCU, MCUb, EMRE, MICU1, MICU1.1, MICU2 and MCUR1) was measured in young (4 and 6 months) and old mice (24 months) (**Figure 28A**). The mouse model confirmed an age-related decrease in MCUR1 mRNA

expression. Old mice showed a significant decrease in mitochondrial Ca^{2+} uptake after stimulation with caffeine (40 mM) (**Figure 28B and C** right panel), whereas basal mitochondrial Ca^{2+} levels did not differ from those of young mice (**Figure 28C** left panel). When Ca^{2+} enters the mitochondria, it indirectly activates the PDH by activating PDP1. PDH is the major dehydrogenase of the TCA cycle and a rate-limiting enzyme for glucose oxidation (**Figure 28D**). While PDP1 activates PDH by dephosphorylation, pyruvate dehydrogenase kinase (PDK) inactivates PDH by phosphorylation. Ca^{2+}-dependent PDP1-induced activation of PDH feeds acetyl-CoA into the TCA cycle, enhancing the production of reducing equivalents and promoting mitochondrial energy metabolism through downstream stimulation of the respiratory chain (Gherardi et al., 2021). In aged mice, the ratio of inactive (phosphorylated) PDH to active (dephosphorylated) PDH (**Figure 28E**) was significantly higher than in young adult mice (**Figure 28F**), indicating a less active enzyme. These results are consistent with published data showing that a muscle-specific defect in the MCU in mice leads to a decrease in activated PDH, which is associated with impaired OCR (Gherardi et al., 2019b).

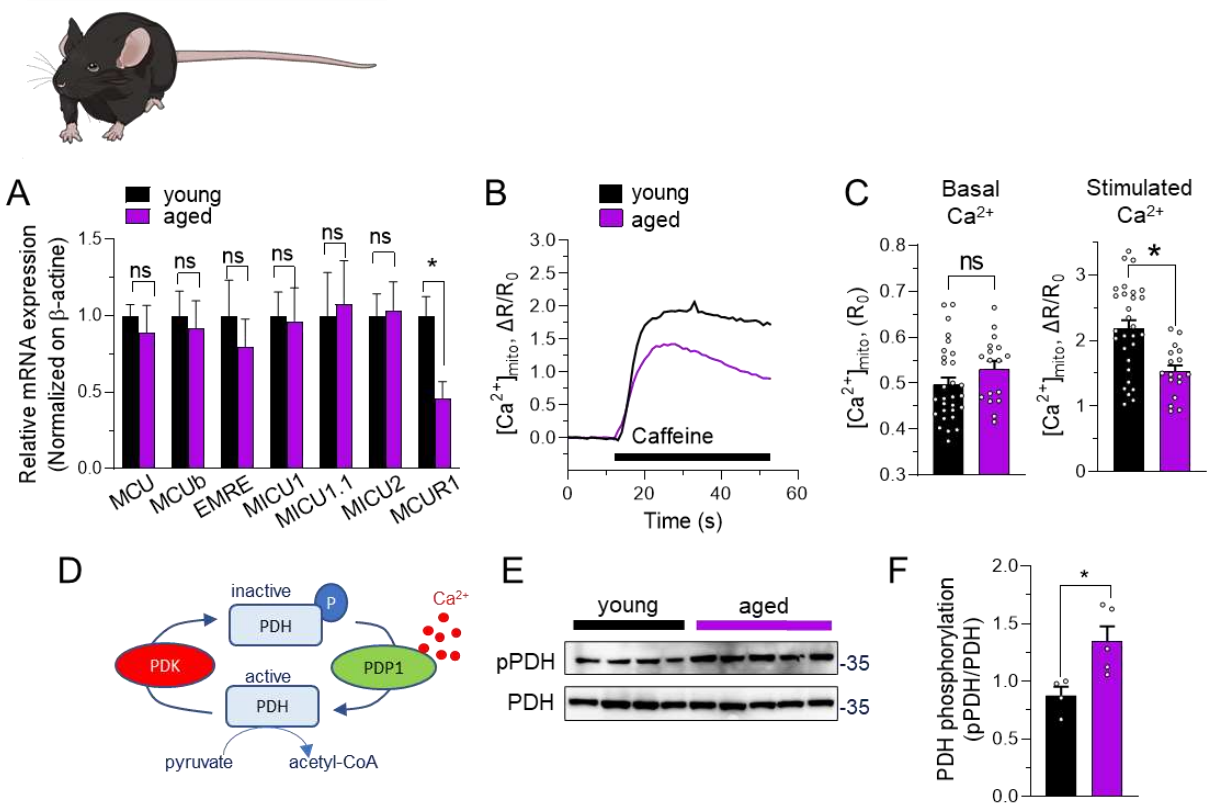

Figure 28. A naturally aged mouse model shows impaired mitochondrial Ca^{2+} uptake and PDH regulation. (A) Shows the relative qPCR results of MCU subunits (MCU, MCUb, EMRE, MICU1, MICU1.1, MICU2, MCUR1) in TA muscle from young (black, 4 months) and old mice (purple, 24 months). (B) Mitochondrial Ca^{2+} uptake triggered by caffeine (40 mM) is reduced in isolated muscle fibers from old mice (purple, 24 months) compared to young mice (black,

6 months). (C) Statistical analysis of young (black, 6 months, n=29 fibers) and old (purple, 24 months, n=17 fibers) isolated fibers after stimulation with caffeine (40 mM) and at rest (D). Scheme of activation (=dephosphorylation) of pyruvate dehydrogenase (PDH) by Ca^{2+}-dependent pyruvate dehydrogenase phosphatase 1 (PDP1), whose counterpart is pyruvate dehydrogenase kinase, which inactivates (=phosphorylates) PDH. PDH is the key enzyme of TCA and converts pyruvate to acetyl-CoA to increase NADH levels for downstream stimulation of the respiratory chain to increase bioenergetics. (E) Shows Western blot of phosphorylated and dephosphorylated PDH in muscle of young (black, 4 months) and old mice (purple, 24 months). (F) Statistical evaluation of the ratio of inactive (phosphorylated) to active (dephosphorylated) PDH from (E) in young (black, 4 months, n=4) and old (purple, 24 months, n=5) mice.

4.2.2. High-throughput screening of natural MCU activators identified oleuropein

Based on the functional link between mitochondrial Ca^{2+} metabolism and age-related skeletal muscle physiology, it was hypothesized that activation of MCU in skeletal muscle of the elderly could rescue mitochondrial energy metabolism and skeletal muscle function. Thus, it was decided to search for natural bioactives, present in food, capable of enhancing mitochondrial Ca^{2+} in skeletal muscle, and to develop an MCU-based nutritional solution to restore muscle function. For this purpose, an internal screening of 5571 natural compounds was performed at the NIHS in histamine-stimulated HeLa cells, with kaempferol serving as a positive control (**Figure 29A-D**). Kaempferol was chosen because of its property as a potent activator of mitochondrial Ca^{2+} uptake (Montero et al., 2004). After the primary screen, 78 positive hits (representing 1.4 % of positive hits) were orthogonally screened, of which 52 validated hits were used for counter-screening to ensure their effect on mitochondrial Ca^{2+} uptake was confined to mitochondria and did not alter cytosolic Ca^{2+} concentrations. A final selection of 43 compounds were confirmed as potent mitochondrial Ca^{2+} activators. Among them a compound present in olive plants and particularly in olive leaves was chosen, as it fulfills the criteria to be considered as a safe compound (Monteiro et al., 2021) regarding its use for a potential nutritional intervention and for regulatory reasons (self-affirmed GRAS status).

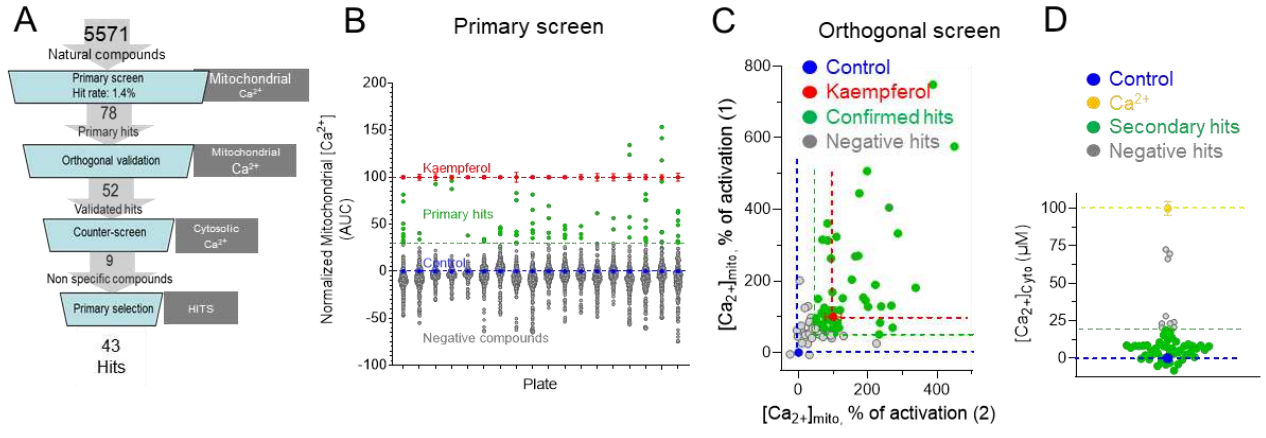

Figure 29. High-throughput screening in HeLa cells discovers mitochondrial Ca^{2+} activators.
(A) Shows a summary of the high-throughput screening of natural substances that activate mitochondrial Ca^{2+} uptake. (B) A total of 5571 natural compounds were tested in a primary screening for their effect in increasing mitochondrial Ca^{2+} uptake. Positive controls with 20 µM kaempferol were normalized to 100, and primary hits (green dots) were compounds, whose calculated AUC for mitochondrial Ca^{2+} uptake after stimulation with 100 µM histamine was above 25. (C) Orthogonal screening of the 78 primary hits from the previous step validated 52 compounds. (D) Counter-screening of the 52 compounds to exclude compounds that also increase cytosolic Ca^{2+} uptake. 100 mM extracellular Ca^{2+} served as negative control.

The compound of choice was the polyphenol oleuropein, which is present in glycosylated and non-glycosylated (aglycone) forms (**Figure 30A**). Its effect and specificity in modulating mitochondrial Ca^{2+} uptake was validated and statistically analyzed in histamine-stimulated HeLa cells. As shown in **Figures 30B-C**, oleuropein specifically enhanced mitochondrial but not cytosolic Ca^{2+} uptake in stimulated HeLa cells.

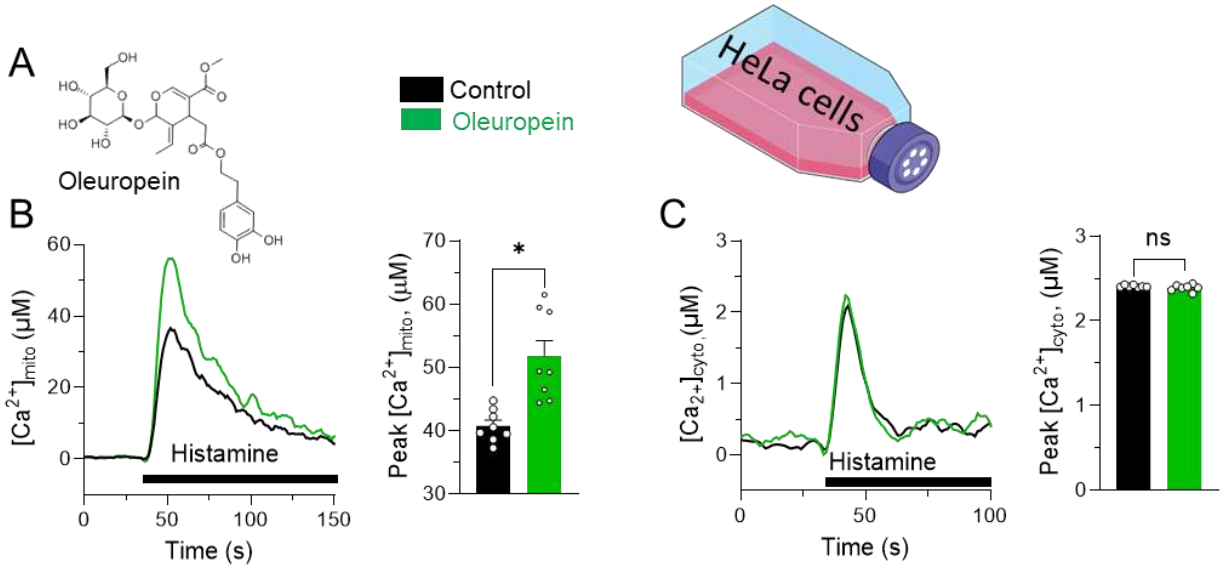

Figure 30. Validation of oleuropein as activator of Ca^{2+} uptake in mitochondria without affecting the cytosolic Ca^{2+} concentration.
(A) Shows chemical structure of the secoiridoid oleuropein. (B) Calibrated traces of control (black) and oleuropein treated (10 µM, green) HeLa cells after stimulation with histamine (100 µM). Statistical analysis of the peak response to histamine in control (black) and oleuropein treated (green) cells. (C) Validation of oleuropein as mitochondrial Ca^{2+} activator without impairing cytosolic Ca^{2+} concentrations. Statistics analyzed the peak response to histamine stimulation in control (black) and oleuropein treated (green) cells. Data are expressed as mean±SEM. Results are considered significant at a significance threshold of $\alpha < 0.05$; *$p < 0.05$; ns, not significant (Student's *t*-test to compare two groups).

During the ripening process of the olive plant, oleuropein gets transformed into its main metabolites the de-glycosylated oleuropein aglycone and hydroxytyrosol (**Figure 31A**). To investigate the effect of oleuropein and its metabolites in skeletal muscle, a respective dose-response in regard to mitochondrial Ca^{2+} uptake was conducted in caffeine-evoked C2C12 mouse

myotubes and identified oleuropein aglycone with the most potent half maximal effective concentration (**Figure 31B**).

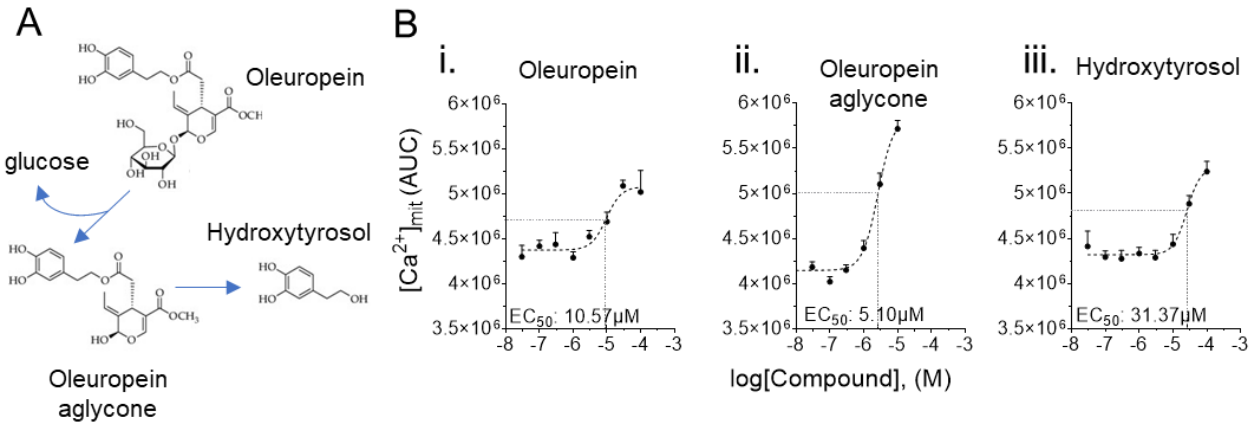

Figure 31. Oleuropein metabolites and their dose-response on mitochondrial Ca^{2+} increase in C2C12 myotubes. (A) During ripening process of olives, oleuropein gets metabolized first into oleuropein aglycone by removing the glucose moiety and finally into hydroxytyrosol by removing elenolic acid. (B) Shows dose response of oleuropein (i), oleuropein aglycone (ii) and hydroxytyrosol (iii) on mitochondrial Ca^{2+} elevation (AUC) after stimulation with 5 mM caffeine.

To determine whether the effect of oleuropein aglycone (**Figure 32A**) was a direct effect on the mitochondrial Ca^{2+} transport or an indirect effect, the compound was tested in semi-permeabilized HeLa cells (Basso et al., 2018), stimulated with free Ca^{2+} (**Figure 32B**). Statistical analysis of the slope (**Figure 32 C**), which is a direct measure of MCU activity, demonstrates that oleuropein aglycone directly activates mitochondrial Ca^{2+} transport.

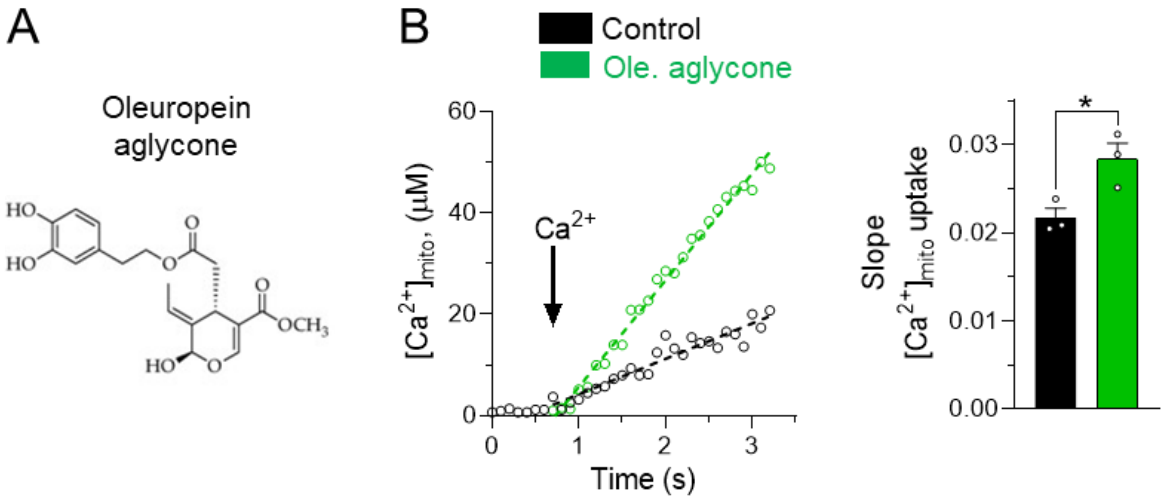

Figure 32. Validation of oleuropein aglycone as activator of mitochondrial Ca^{2+} uptake in semi-permeabilized HeLa cells.
(A) Shows chemical structure of the secoiridoid oleuropein-aglycone. (B) Calibrated slopes of control (black) and oleuropein aglycone treated (10 µM, green) HeLa cells after stimulation with free Ca^{2+} (4 µM). Statistical analysis of the slope values based on the response to free Ca^{2+} stimulation in control (black) and oleuropein aglycone treated (green) cells. Data are expressed as mean±SEM. Results are considered significant at a significance threshold of $\alpha < 0.05$; *p < 0.05; (Student's *t*-test to compare two groups).

4.2.3. Oleuropein enhances mitochondrial Ca^{2+} uptake and bioenergetics in human myotubes via the MCU subunit MICU1

The data obtained from the high-throughput screening and the subsequent validation of oleuropein and its aglycone supported their potential as natural bioactive compounds for interventions in balancing mitochondrial Ca^{2+} levels to restore muscle function. To study and provide evidence for the link between oleuropein, mitochondrial Ca^{2+} homeostasis and muscle function, the next step was to assess the effect of oleuropein and its metabolites on human muscle physiology. For this, oleuropein and its metabolites were tested in caffeine-stimulated primary human myotubes of adults to measure mitochondrial Ca^{2+} uptake (**Figure 33A-B**) which revealed oleuropein aglycone as the most potent mitochondrial Ca^{2+} activator without perturbing cytosolic Ca^{2+} concentrations (**Figure 33C**).

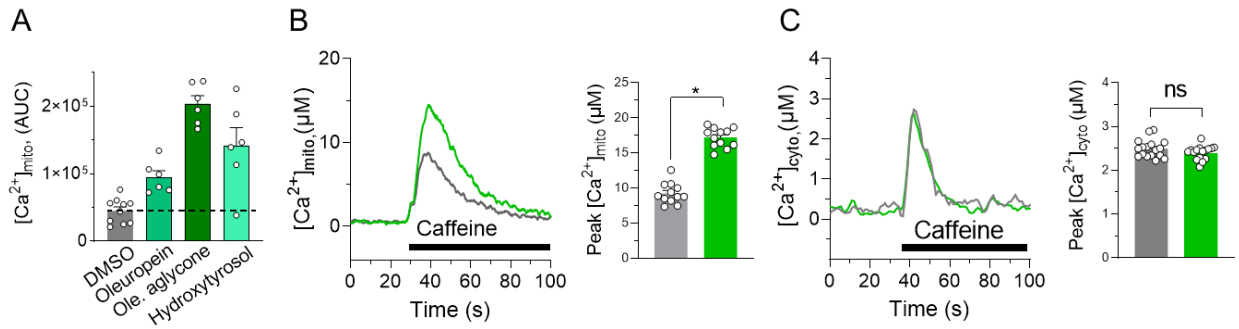

Figure 33. In human myotubes, oleuropein aglycone is the most potent mitochondrial Ca^{2+} activator without changing cytosolic Ca^{2+} levels.
(A) Effect of 10 µM oleuropein, oleuropein aglycone or hydroxytyrosol on mitochondrial Ca^{2+} uptake in human myotubes after stimulation with 5 mM caffeine. DMSO 1 % serves as control (grey bar). (B) Calibrated traces of control (grey, DMSO 1 %) and oleuropein aglycone treated (green, 10 µM) human myotube stimulated with 5 mM caffeine. Caffeine stimulated peak response on mitochondrial Ca^{2+} in control (grey) and oleuropein aglycone treated (green) myotubes was statistically analyzed using Student's t-test. (C) Respective traces for cytosolic Ca^{2+} increase in control (grey, DMSO 1 %) and oleuropein aglycone treated (green, 10 µM) human myotubes after caffeine stimulation. Right panel shows caffeine stimulated peak response on cytosolic Ca^{2+} in control (grey) and oleuropein aglycone treated (green) myotubes, statistically analyzed using Student's t-test. Data are expressed as mean±SEM. Results are considered significant at a significance threshold of $\alpha < 0.05$; *$p < 0.05$; ns, not significant.

To investigate the selectivity of oleuropein for interaction with the MCU channel, a model of primary human myotubes with an adenoviral shRNA-induced knockdown of MCU was used and first validated via capillary Western blot (**Figure 34A**, inset). The model was then functionally validated by measuring mitochondrial Ca^{2+} uptake after caffeine-stimulation (**Figure 34A**), which showed an impaired mitochondrial Ca^{2+} machinery in the MCU-kd. Next, oleuropein aglycone was tested in caffeine-evoked control and MCU-kd human myotubes, demonstrating that oleuropein aglycone exerts its effect on mitochondrial Ca^{2+} in an MCU-dependent manner. In human control myotubes, oleuropein enhanced mitochondrial Ca^{2+} uptake after caffeine-stimulation (**Figure 34B**, first and third panel), whereas this effect was completely attenuated in human MCU-kd myotubes (**Figure 34B**, second and third panel). When looking at cellular respiration, it can be seen that oleuropein aglycone treatment significantly increased ATP synthase-dependent OCR upon caffeine-stimulation in primary human control myotubes (**Figure 34C**, first panel), while oleuropein aglycone exerted no enhancing effect on mitochondrial respiration in MCU-kd myotubes (**Figure 34C**, second and third panel). These results indicate that MCU is required to promote the bioenergetics effects of oleuropein on mitochondrial Ca^{2+} uptake and coupled respiration.

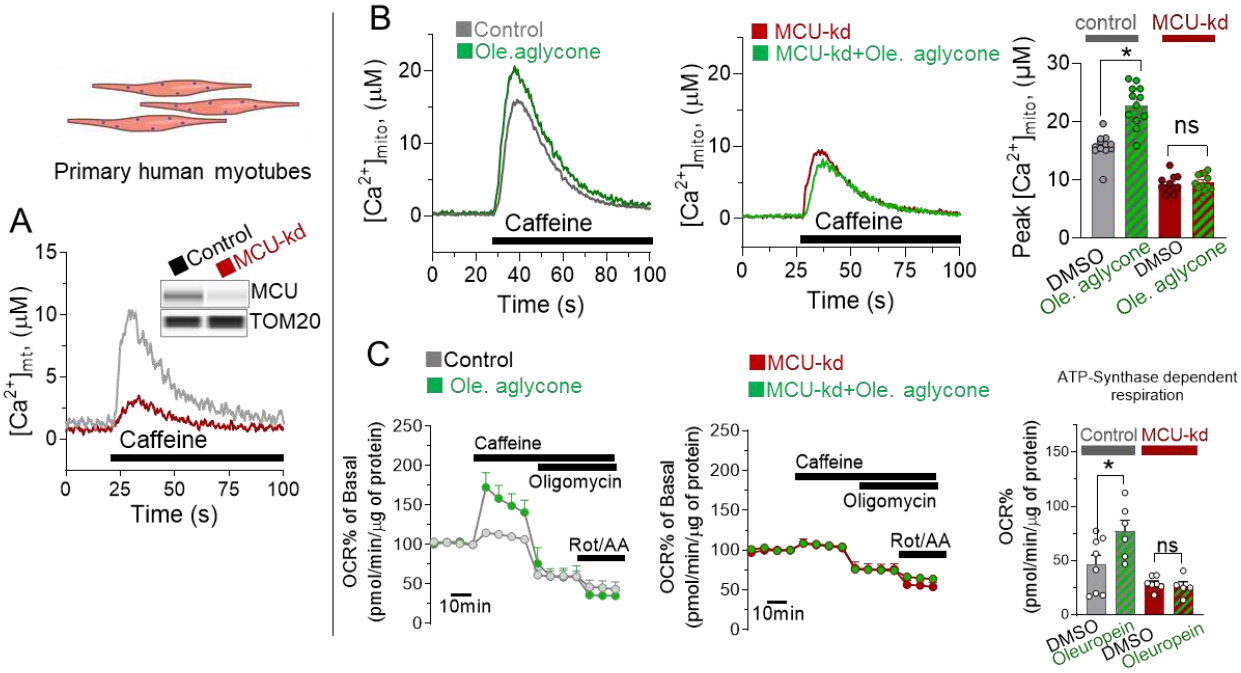

Figure 34. Oleuropein increases mitochondrial Ca^{2+} uptake via the MCU, promoting cellular respiration in human myotubes.
(A) Calibrated traces of control human myotubes infected with scrambled shRNA (grey) and myotubes infected with MCU-shRNA (red) to knockdown the MCU, after stimulation with 5 mM caffeine. MCU-knockdown (MCU-kd) was validated via capillary Western Blot and TOM20 was used as loading control. (B) Oleuropein aglycone (10 µM) increases mitochondrial Ca^{2+} uptake in caffeine stimulated (5 mM) control myotubes (left panel, green trace) compared to control myotubes treated with DMSO 1 % (grey trace). In MCU-kd myotubes treated with 10 µM oleuropein aglycone (center, green trace), treatment does not increase mitochondrial Ca^{2+} uptake compared to control MCU-kd myotubes treated with DMSO 1 % (red trace). Right panel provides statistical evaluation of caffeine evoked peak responses in mitochondrial Ca^{2+} uptake in control (grey) and MCU-kd (red) myotubes with (green diagonal strikes) and without (plain colored bars) 10 µM oleuropein aglycone. (C) Left panel displays oxygen consumption rate (OCR) in 5 mM caffeine stimulated control (grey) human myotubes, which increases after acute treatment with 10 µM oleuropein aglycone (green). In MCU-depleted myotubes (center, red trace), caffeine evoked respiratory capacity cannot be further increased with treatment of oleuropein aglycone (10 µM, green trace). Right panel shows summary of statistical analysis of the ATP-synthase dependent respiration in control with (grey-green strikes) and without (grey) oleuropein aglycone and in MCU-kd myotubes with (red-green strikes) and without (red) 10 µM oleuropein aglycone and represents the delta of maximal stimulation minus first measurement after addition of oligomycin. Data are expressed as mean±SEM. Results are considered significant at a significance threshold of $\alpha < 0.05$; *$p < 0.05$; ns, not significant (Student's *t*-test to compare two groups with normal distribution).

In a final approach, the effects of oleuropein aglycone on mitochondrial Ca^{2+} uptake, OCR and resistance to muscle fatigue in mouse myofibers were tested *ex-vivo*. For this purpose, isolated muscle fibers were acutely treated with oleuropein aglycone and mitochondrial Ca^{2+} uptake, OCR and resistance to muscle fatigue were measured after caffeine-stimulation (**Figure 35**). In all three experiments, acute treatment with oleuropein aglycone significantly enhanced caffeine-induced responses by increasing mitochondrial Ca^{2+} uptake, enhancing the OCR and improving resistance to fatigue compared to control muscle fibers.

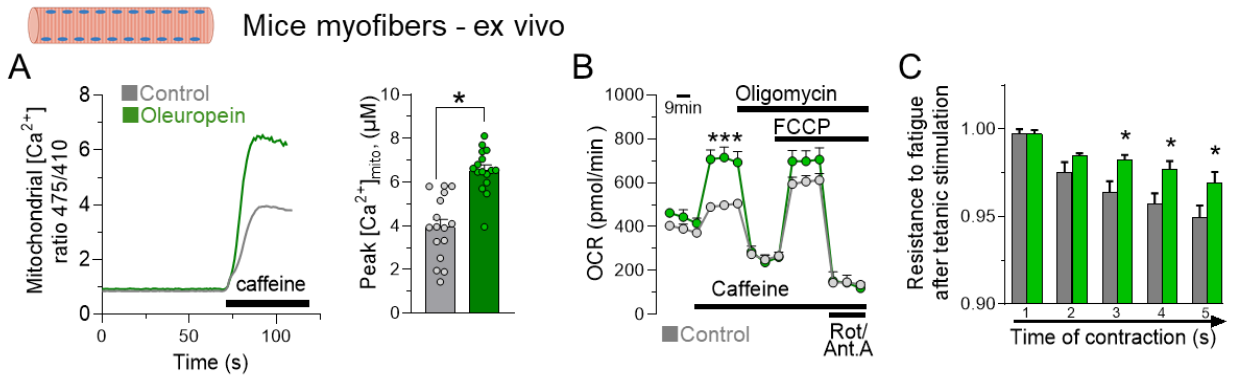

Figure 35. Oleuropein increases energy metabolism and performance in mouse myofibers, *ex-vivo.*
Shows mitochondrial Ca^{2+} uptake in control (grey, n=16 muscle fibers) and oleuropein aglycone treated (10 µM) FDB fibers (green, n=16 muscle fibers) after stimulation with 30 mM caffeine. Statistical evaluation of the peak values of mitochondrial Ca^{2+} uptake in control (grey) and oleuropein aglycone treated (green) FDB fibers. (B) Oxygen consumption rate (OCR) in control (grey, n=15) and oleuropein aglycone treated (green, n=15) FDB fibers after stimulation with 30 mM caffeine. (C) Shows resistance to fatigue after 120 tetanic contractions (100 Hz for 300 ms with 700 ms break, repeated every second) compared to initial force as a measure of muscle fatigue.

A recent study has demonstrated that some MCU inhibitors activate MCU by docking to the subunit MICU1 in adult C2C12 myotubes (Di Marco et al., 2020). It was hypothesized that a similar interaction could also be a potential mechanism for oleuropein (**Figure 36A**). To test this hypothesis, docking simulations were performed in collaboration with the Department of Pharmaceutical and Pharmacological Sciences of the University of Padova to investigate the *in silico* binding mode of oleuropein (both the glycosylated and aglycone forms were used) at the human MICU1 binding site. The results revealed a potential binding cleft within the MICU1 protein and a crucial binding site for both ligands, mediating the binding to MICU1 (**Figure 36B**). These docking simulations between MICU1 and oleuropein/oleuropein aglycone were assessed for strength, quality and stability of the ligand protein interaction using different scores (**Figure 36C**). The Chemplp Score/Norm assesses the strength of the protein ligand interaction with low values indicating a strong interaction and high values indicating a weak interaction. A more accurate score is the MMGBSA which assesses the quality of the ligand protein interaction. The last score is the Root Main Square Deviation of the coordinates (RMSD) and indicates the stability of the binding conformation. All scores have a reversed relationship and can be interpreted as the lower the value, the better the protein ligand communication.

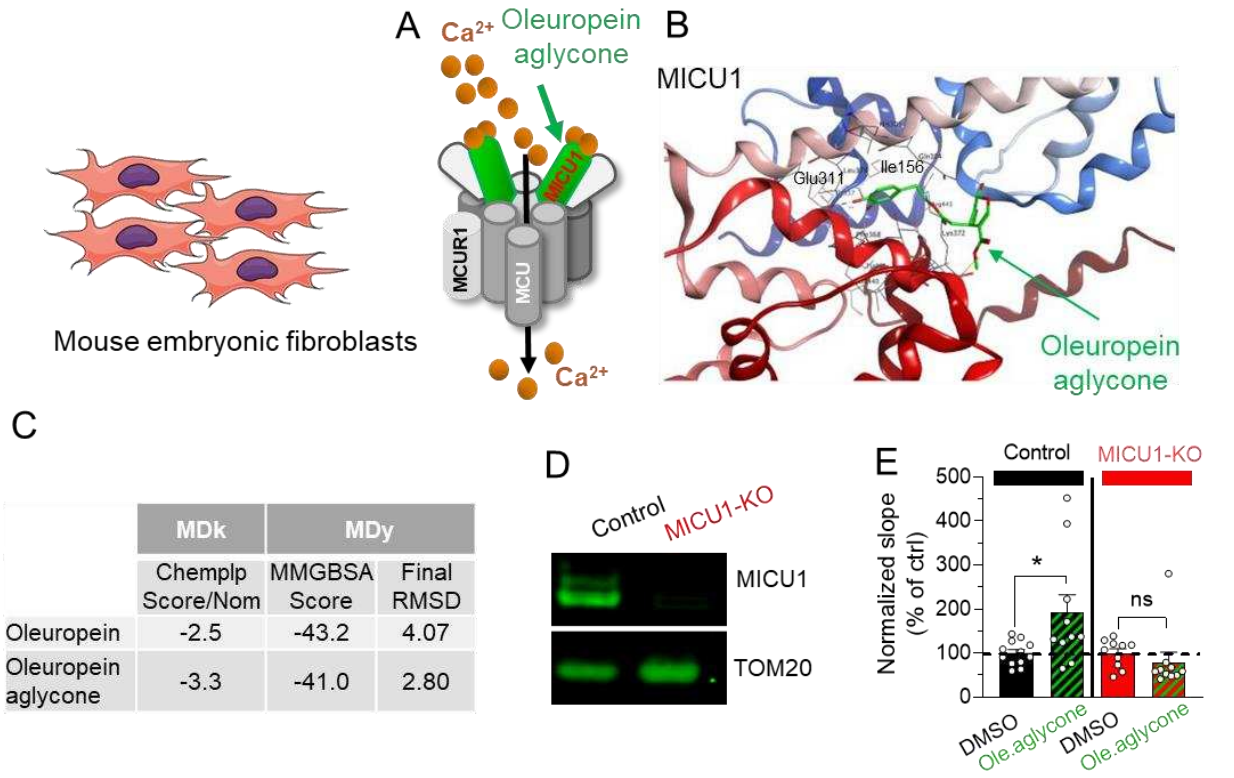

	MDk	MDy	
	Chemplp Score/Nom	MMGBSA Score	Final RMSD
Oleuropein	-2.5	-43.2	4.07
Oleuropein aglycone	-3.3	-41.0	2.80

Figure 36. The molecular mechanism of oleuropein in enhancing mitochondrial Ca^{2+} uptake depends on MICU1. (A) Shows the MCU complex and some subunits such as the pore forming MCU, the MCU regulator MCUR1 and the green highlighted subunit MICU1 which is the identified binding protein of oleuropein aglycone to exert its effect on mitochondrial Ca^{2+} uptake. (B) Displays the MICU1 binding pocket and the docking position of the ligand oleuropein aglycone. (C) Table containing molecular docking (MDk) and molecular dynamics (MDy) parameters describing strength, quality and stability of the ligand protein interaction. Chemplp Score/Norm represents a MDk score evaluating the strength of the interaction (the lower the value, the stronger the interaction). MDy simulations are used to evaluate the quality of the ligand protein interaction (MMGBSA score: the lower the value, the stronger the interaction) and the stability of the binding conformation (Root Main Square Deviation of the coordinates, RMSD: a low value, indicates a stable conformation). The MMGBSA score is slightly more accurate than the Chemplp Score/Nom. (D) Validation of the MICU1-KO model in mouse embryonic fibroblasts (MEF) cells via Western Blot, using TOM20 as loading control. (E) Statistical analysis of slope values of mitochondrial Ca^{2+} uptake in semi-permeabilized control (black, DMSO 1 %) and MICU1-KO (red, DMSO 1 %) MEF cells, with (green strikes) and without 10 µM oleuropein aglycone and stimulated with 4 µM free Ca^{2+}. Data are expressed as mean±SEM. Results are considered significant at a significance threshold of $\alpha < 0.05$; *$p < 0.05$; ns, not significant (Student's *t*-test to compare two groups).

The binding mode of oleuropein and its aglycone was marked by their chemical structure and size. The shared chemical moiety (the aglycone form) was positioned similarly in the MICU1 binding cleft, although the hydroxytyrosol moiety did not reach the deepest possible pocket. The hydroxytyrosol was able to form a hydrogen bond with Glu311 rather than Ile156. The elenolic group was facing both the N-lobe (216-220) and the C-lobe (loop 441-443). The glycosyl group of oleuropein was suspended in the solvent and probably interacted with the N-lobe as well as with the C-lobe via a network of hydrogen bonds (**Figure 37**). Although the glycosyl group might interact with the MICU1 pocket, its presence affected the stability of the conformation in the

binding site (RMSD higher than for the aglycone form), indicating that the aglycone can be better accommodated in the binding site.

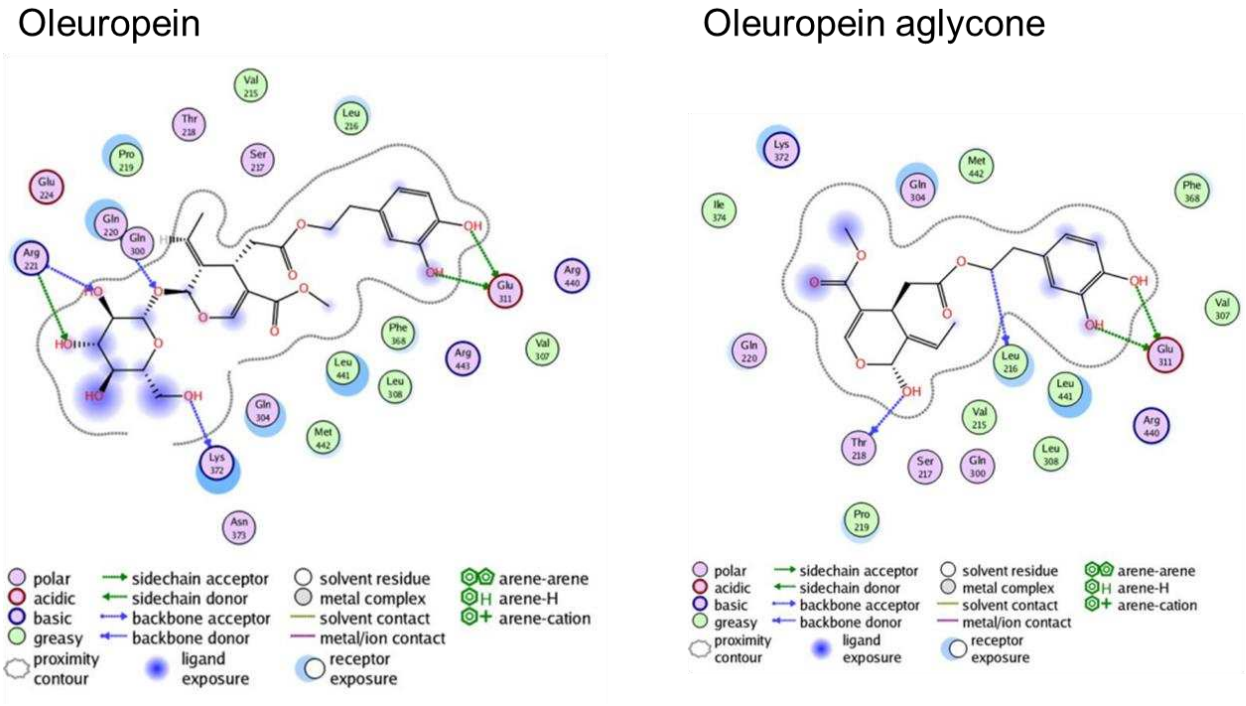

Figure 37. Binding modes of MICU1 and oleuropein and MICU1 and oleuropein aglycone.
Shows the interactions between MICU1 and oleuropein (left) and MICU1 and oleuropein aglycone (right). The common deglycosylated form of oleuropein and oleuropein aglycone shows a crucial hydrogen bond between hydroxytyrosol and Glu311 that facilitates binding.

The suggested MICU1-dependent mechanism of oleuropein action on mitochondrial Ca^{2+} modulation was investigated in mouse embryonic fibroblasts (MEFs) with a MICU1-KO (Antony et al., 2016). For this, the MICU1-KO MEFs were validated via Western blotting (**Figure 36D**). Functional analysis was performed in semi-permeabilized cells treated with oleuropein or DMSO as control after using free Ca^{2+} to evoke mitochondrial Ca^{2+} uptake in control and MICU1-KO cells. Statistical analysis of the slope values normalized to the DMSO-treated control cells proved the MICU1-dependency of oleuropein aglycone to enhance mitochondrial Ca^{2+} uptake (**Figure 36E**). These experiments demonstrate that the mechanism of action by which oleuropein promotes MCU activation is mediated by MICU1.

4.2.4. Intervention with an oleuropein-rich diet increases energy metabolism and improves performance in wild-type but not skeletal muscle-specific MCU-KO mice *in vivo*.

To validate the effect of oleuropein *in vivo*, a preclinical mouse model was used in collaboration with the Department of Biomedical Sciences of the University of Padova to develop a nutritional intervention with either olive leaf extract (OLE), containing 40% oleuropein processed into chow pellets or a control chow-diet. Myofibers were isolated and mitochondrial Ca^{2+} uptake was measured ratiometrically after caffeine-stimulation in control and chronic OLE-treated mouse samples (**Figure 38A**). Statistical analysis of peak mitochondrial Ca^{2+} uptake showed a significant increase in myofibers from OLE-treated mice (**Figure 38B**). When PDH phosphorylation was examined in TA muscle from control and OLE-treated mice, the latter group showed decreased PDH phosphorylation, implying mitochondrial Ca^{2+}-dependent activation of PDP1 (**Figure 38C**). In addition, the PDH activity was measured, which was increased in muscle fibers of OLE-treated mice compared to controls (**Figure 38H**). To evaluate the effect of OLE treatment on energy metabolism, OCR was measured and showed significantly increased mitochondrial respiration in the OLE group after stimulation with caffeine (**Figure 38E**). To investigate the effect of OLE on muscle performance, the running time on a treadmill was assessed after one bout of uphill exercise (10%) until the mice reached exhaustion. Mice treated with OLE showed a significantly longer running time (**Figure 38F**).

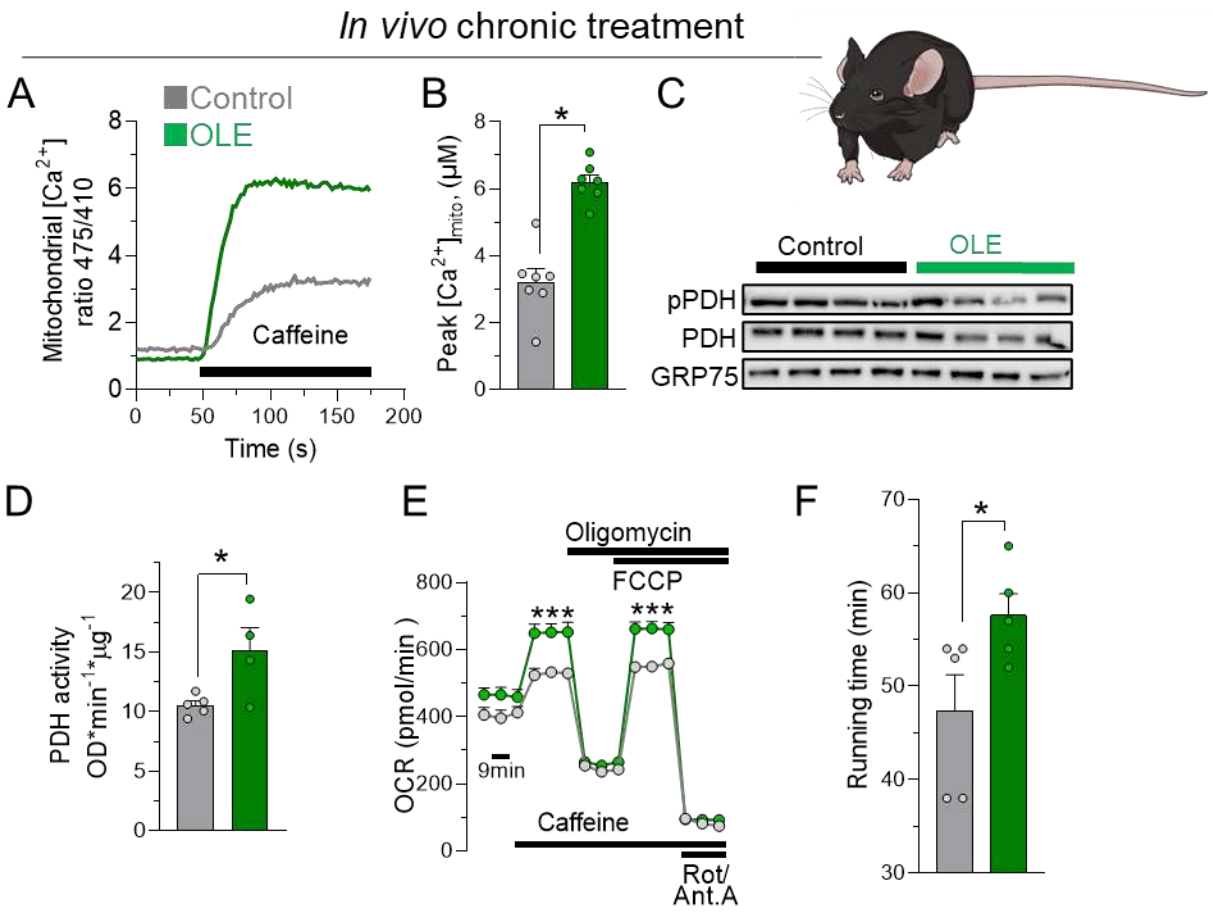

Figure 38. Chronic treatment with an OLE-containing diet boosts energy metabolism and muscle performance in young adult mice.
(A) Mitochondrial Ca^{2+} uptake in control (grey) and 1 month OLE-treated (green) mice after stimulation with caffeine (5 mM). (B) Statistical evaluation of (A) with control (grey, n=7) and OLE-treated (green, n=7) mice. (C) PDH phosphorylation levels in TA muscle fibers from control (n=4) and 1 month OLE-treated (n=4) mice with GRP75 as loading control. (D) PDH activity in control (grey, n=5) and OLE-treated (green, n=4) TA muscle samples. (E) OCR measurement in control (grey, n=10) and OLE-treated (n=10) isolated FDB myofibers after caffeine (5 mM) stimulation. Data are normalized to mean Calcein fluorescence. (F) Shows effect of 1 month OLE-diet (green, n=5) on running capacity compared to control (n=5) mice. Data are expressed as mean±SEM. Results are considered significant at a significance threshold of $\alpha < 0.05$; *p < 0.05; ns, not significant (Student's *t*-test to compare two groups).

Subsequently, in collaboration with the Department of Biomedical Sciences of the University of Padua, a genetically modified mouse model with a control mouse (MCU fl/fl) and a skeletal muscle-specific MCU-KO (skMCU-/-) was used to investigate the molecular mechanism of OLE-enriched diet on energy metabolism. For this purpose, OCR was examined after OLE treatment in mice with caffeine-stimulated FDB myofibers from MCU fl/fl and skMCU-/- mice. The result confirmed the positive effect of oleuropein on bioenergetics in MCU fl/fl mice (**Figure 39A**), which was attenuated in skMCU-/- mice (**Figure 39C**). With regard to muscle performance, the effect of the OLE-containing diet was studied by measuring running time on a treadmill after one run uphill

(10%) to exhaustion. Treatment with the OLE-containing diet resulted in a significant increase in running time in the control mice (**Figure 39B**), but not in the skMCU-/- mice (**Figure 39D**).

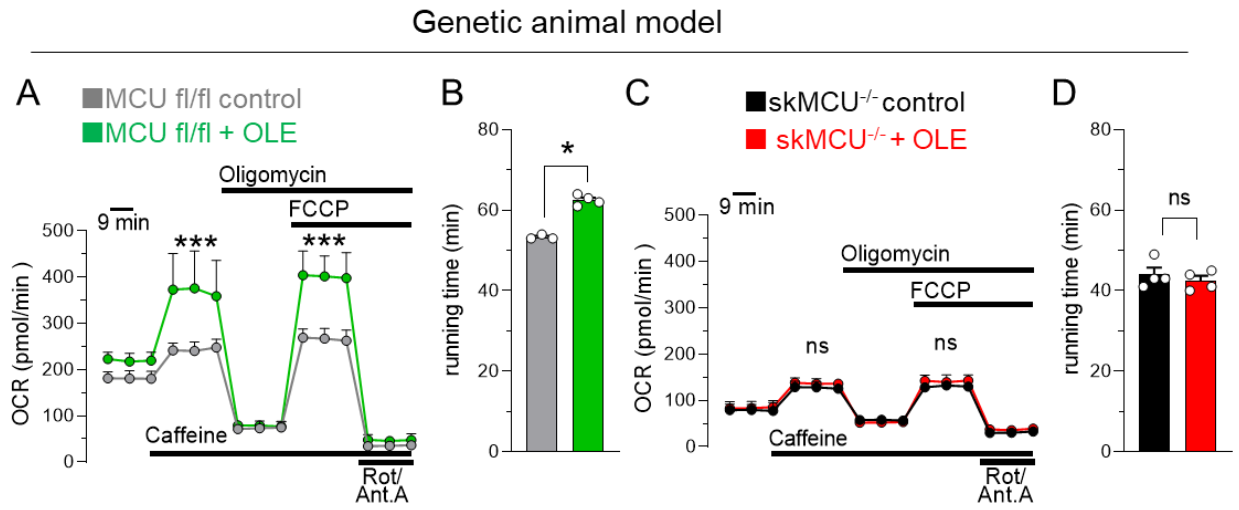

Figure 39. Oleuropein supplementation increases running performance and bioenergetics in adult control but not in skeletal muscle specific MCU-KO mice.
(A) Oxygen consumption rate (OCR) measured in control-diet MCU fl/fl FDB myofibers (grey, n=10 samples) and OLE-diet MCU fl/fl FDB myofibers (green, n=10 samples) from mice. Data was normalized to mean fluorescence of calcein. (B) Shows a single bout of treadmill running in control chow-diet (grey, n=3) and OLE-diet (green, n=4) fed MCU fl/fl mice. (C) In skMCU$^{-/-}$ samples, there was no enhancing effect of OLE (red) on OCR after caffeine stimulation compared to skMCU$^{-/-}$ control FDB myofibers (black). Data was normalized to mean fluorescence of calcein. (D) Shows a single bout of treadmill running in control chow-diet (black, n=4) and OLE-diet (red, n=4) fed skeletal muscle specific MCU-KO (skMCU$^{-/-}$) mice. Data are expressed as mean±SEM. Results are considered significant at a significance threshold of $\alpha < 0.05$; *$p < 0.05$; ns, not significant (Student's *t*-test to compare two groups).

Overall, the *in vivo* data described in this section confirmed the *in vitro* results and demonstrated the positive effects of oleuropein on energy metabolism and muscle performance. The effects were studied *in vivo* in young adult mice. In the next section, the oleuropein effects are investigated across different aging models, including mouse, rat and human.

4.2.5. Oleuropein aglycone improves skeletal muscle health in aged muscle

Based on the initial transcriptomic data obtained from elderly individuals suffering from sarcopenia, who were found to have significant downregulation of MCUR1, which strongly correlated with muscle dysfunction and based on the preclinical data on muscle aging in mice, the following objective was to investigate the efficacy of an intervention that could influence impaired muscle health during aging by affecting mitochondrial Ca^{2+} metabolism via oleuropein. To investigate the effect of oleuropein on mitochondrial Ca^{2+} metabolism in an aged human

muscle model, primary myotubes from three aged donors were studied. In aged human myotubes, oleuropein significantly elevated mitochondrial Ca^{2+} (**Figure 40A**). Next, the previously demonstrated shRNA induced MCUR1-kd model in adult primary human myotubes was used to assess the effect of oleuropein aglycone in the MCUR1 depleted model. While it has been shown previously that oleuropein action depends on the MCU complex and particularly on the MICU1 subunit, it can be seen in **Figure 40B**, that oleuropein aglycone works in the MCUR1-kd which makes it a promising compound for application in aged models. The statistical evaluation accordingly proved that oleuropein aglycone significantly increased the caffeine-induced peak response in MCUR1-kd myotubes. The data from this project convincingly show that oleuropein and its metabolites increase mitochondrial Ca^{2+} uptake and that this increase in mitochondrial Ca^{2+} activates PDP1, which in turn dephosphorylates PDH, thereby activating it (**Figure 40C**) to promote energy metabolism. At low mitochondrial Ca^{2+} levels, PDK does the opposite of PDP1 and keeps PDH phosphorylated (pPDH) and thus deactivated. To determine whether oleuropein can promote energy metabolism by activating PDH, oleuropein intervention was studied in 3-month-old rats and revealed marked dephosphorylation (activation) of PDH in gastrocnemius samples (**Figure 40D, E**). The downstream effect of activated PDH is increased formation of reducing equivalents within the TCA, which are supplied to the respiratory chain to increase mitochondrial respiration. To measure this effect, an aged mouse model was used with an OLE-based intervention for one month and showed a significantly increased OCR (**Figure 40F**). Next, the effect of the OLE-containing diet in aged mice was assessed by evaluating running time, which showed a significant extension compared to chow-fed controls (**Figure 40G**).

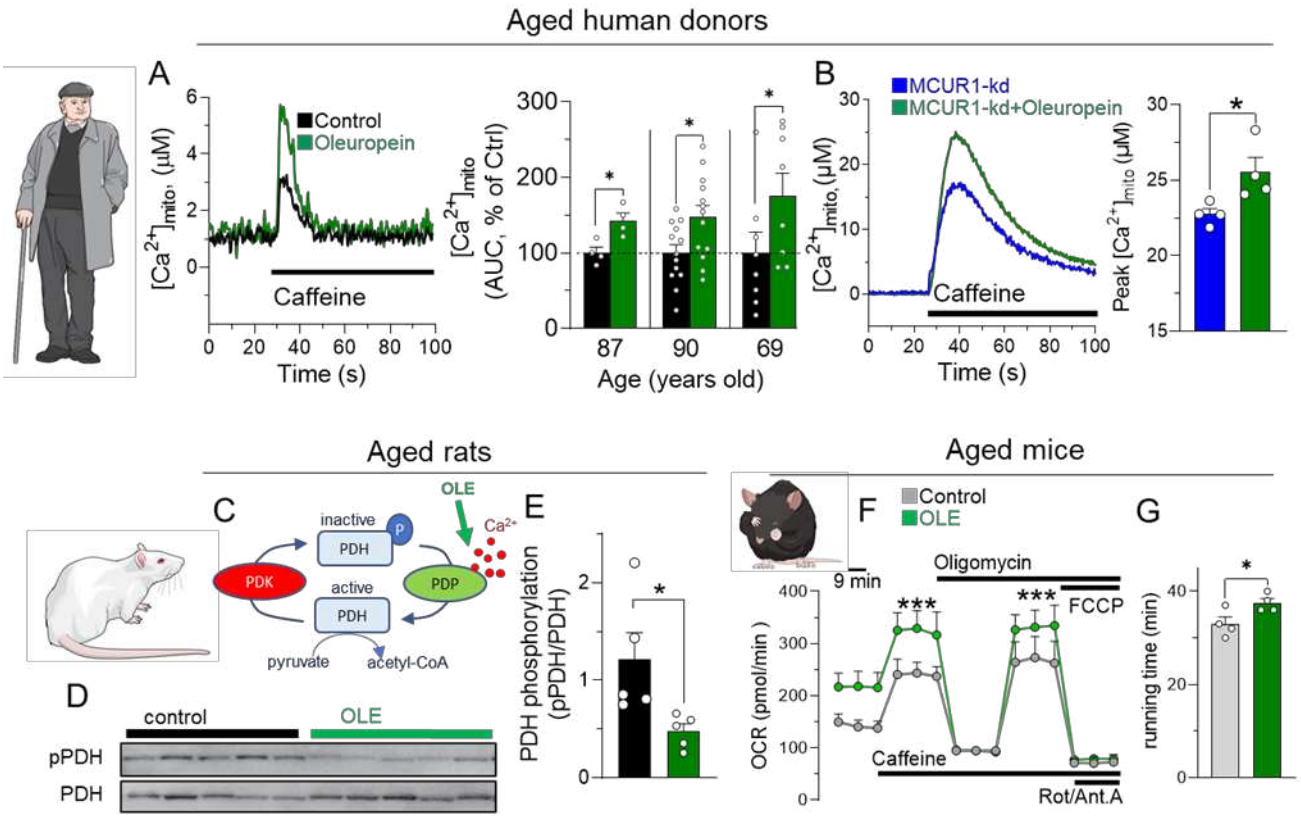

Figure 40. Treatment with oleuropein and its aglycone activates mitochondrial bioenergetics in aged models across species.
(A) Left panel shows calibrated traces of mitochondrial Ca^{2+} uptake in old primary human myotubes treated with 10 µM oleuropein aglycone (green) or DMSO 1 % as control (black) after stimulation with 5 mM caffeine. Right panel shows statistical analysis of three old donors of human myotubes without (black) and with oleuropein aglycone (green), normalized to each respective control and expressed as %. (B) In MCUR1-depleted primary human myotubes, acute oleuropein aglycone (10 µM) treatment (green trace) leads to an increase in mitochondrial Ca^{2+} uptake compared to DMSO (1 %) treated control MCUR1-kd myotubes (blue) after caffeine-stimulation (5 mM). Statistical analysis of mitochondrial Ca^{2+} peak responses to caffeine-stimulation in control MCUR1-kd myotubes (blue, n=4 samples) and oleuropein aglycone treated MCUR1-kd myotubes (green, n=4 samples). (C) Shows regulation mechanisms of pyruvate dehydrogenase (PDH). An active pyruvate dehydrogenase kinase (PDK) phosphorylates (=deactivates) the PDH, preventing the conversion of pyruvate into acetyl-CoA. The Ca^{2+} dependent PDH-phosphatase 1 (PDP1) dephosphorylates (=activates) the PDH and drives the conversion of pyruvate into acetyl-CoA, activating the TCA cycle. Since oleuropein aglycone increases mitochondria Ca^{2+} uptake upon stimulation with caffeine, oleuropein aglycone induces PDP1 activity and therefore PDH dephosphorylation. (D) Shows Western blot of PDH phosphorylation status of muscle samples of gastrocnemius from 3 months old control rats and rats treated with oleuropein. (E) Next panel displays the statistical analysis of the Western blot, showing the ratio of phosphorylated PDH (pPDH) to dephosphorylated PDH (PDH) in control (black, n=5) and oleuropein-rich diet treated (green, n=5) gastrocnemius samples of rats. (F) OCR in FDB myofibers of aged mice (24 months) treated with control-diet (grey, n=10 samples) or oleuropein-rich diet (green, n=10 samples) after caffeine stimulation (40 mM). Data was normalized to mean fluorescence of calcein. (G) Shows running time of 24 months old control mice (grey, n=4 animals) and 24 months old oleuropein treated mice (green, n=4 animals) after a single bout of exercise on a treadmill. Data are expressed as mean±SEM. Results are considered significant at a significance threshold of $\alpha < 0.05$; *$p < 0.05$; ns, not significant (Student's *t*-test and Mann-Whitney test to compare two groups).

The results obtained in the different aging models consistently showed positive effects of oleuropein treatment on impaired mitochondrial muscle metabolism and suggest that an

intervention with oleuropein may alleviate all age-related impairments in muscle. Together with the findings obtained in MCU-ablated models, it is proposed that oleuropein exerts its beneficial effects via the MCU and in particular the MICU1 subunit to promote skeletal muscle physiology (**Figure 41**).

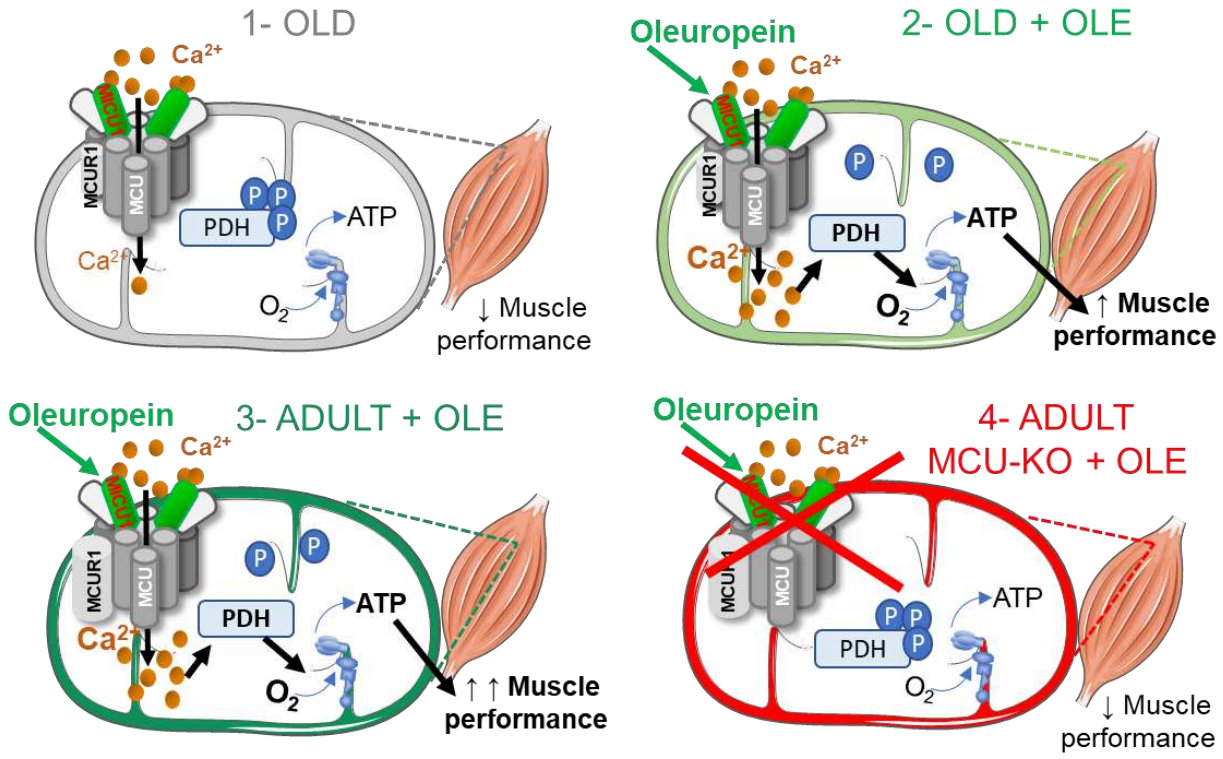

Figure 41. Proposed model of oleuropein and its beneficial effects on skeletal muscle health in aged and adult systems.
(1) Based on the results obtained, ageing has been shown to lead to increased pyruvate dehydrogenase (PDH) phosphorylation (=inactivation), which decreases NADH supply to the respiratory chain, resulting in decreased ATP synthesis associated with decreased muscle performance. (2) Nutritional intervention with the natural compound oleuropein increased mitochondrial Ca^{2+} uptake in aged models, leading to increased dephosphorylation (=activation) of PDH. Activated PDH drives TCA and stimulates downstream activation of oxidative phosphorylation, increasing ATP levels and improving muscle performance. (3) In young adult models, nutritional intervention with the natural compound oleuropein increased mitochondrial Ca^{2+} uptake, PDH activity and ATP-driven muscle performance. (4) In adult models with defective MCU, the effect of oleuropein on energy metabolism was abolished, demonstrating that oleuropein and its metabolites act as natural MCU activators.

4.3. Part III: Polyphenols require the MICU1 subunit to activate MCU, resulting in beneficial effects on energy metabolism and performance

Our discovery that the polyphenol oleuropein is a powerful and direct activator of MCU and previous reports in literature showing a positive effect of the polyphenol kaempferol on mitochondrial Ca^{2+} transport (Montero et al., 2004), emphasizes a close link between the polyphenol effects and MCU regulation. Next, the identification of the best polyphenolic compounds which activate MCU is described, as well as the validation of their benefit for mitochondrial respiration and their molecular mechanism of action. The results point to two different mechanisms of MCU activation depending on the polyphenol in question: one that is completely MICU1-dependent, and one that is only partially MICU1-dependent, suggesting that mechanisms other than MICU1 are involved.

4.3.1. A high-throughput screening reveals kaempferol and fisetin as potent MCU activators

To explore various polyphenols for effects on mitochondrial Ca^{2+} activation, a high-throughput screening developed at NIHS was employed in HeLa cells stimulated with histamine. A library of 897 polyphenols (pure compounds) was used, including flavones and flavonols, coumarins, hydroxycinnamic acid derivatives, flavanones and flavanonols, stilbenes, lignans and aurones (**Figure 42**).

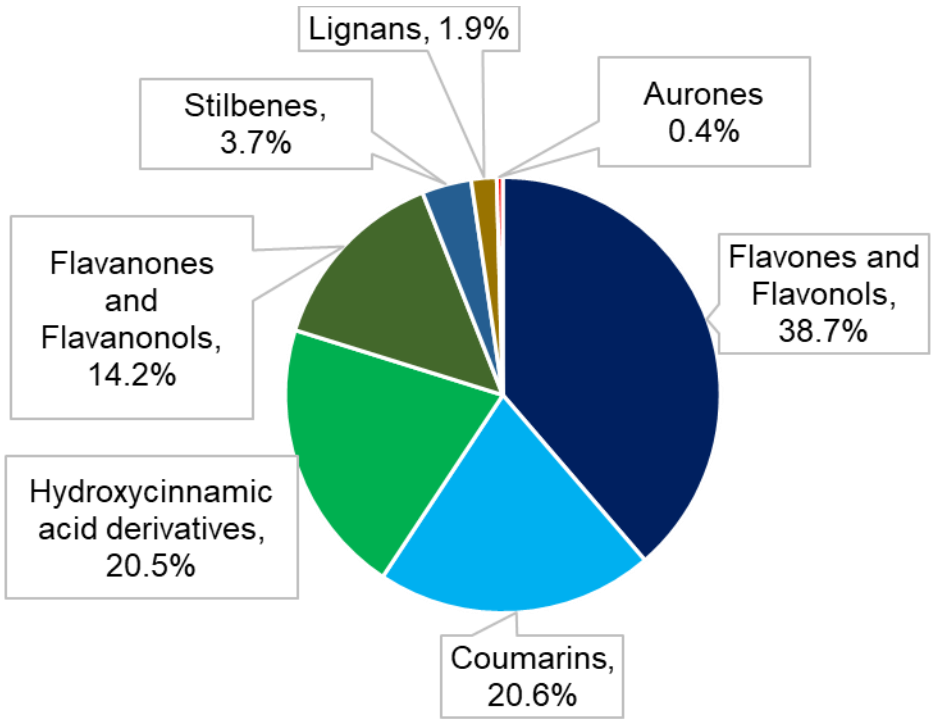

Figure 42. Relative proportions of polyphenolic classes tested to identify other natural MCU activators. Composition of the polyphenol library includes:38.7% are flavones and flavonols, 20.6 % coumarins, 20.5 % hydroxycinnamic acid derivatives, 14.2 % flavanones and flavanonols, 3.7% stilbenes, 1.9% lignans and 0.4% aurones.

We discovered that, the percentage of positive hits (2.7%, corresponding to 25 positive hits in 897 polyphenolic compounds) was greater than the percentage of positive hits in the complete library employed before (which was 1.4%; see **Figure 29A**, page 76). Specifically, the group of flavones and flavonols was most enriched with positive hits (4.0 %) compared to the other polyphenolic groups. (**Table 1**).

Table 1. The contributions of the different tested polyphenol classes to positive hits.

Group	Tested compounds	Positive hits	Positive hits %
Flavones and Flavonols	347	14	4.0
Coumarins	185	4	2.2
Flavanones and Flavanonols	127	1	0.8
Hydroxycinnamic acid derivatives	184	1	0.5
Stilbenes	33	2	-
Lignans	17	1	-
Aurones	4	2	-

Within the group of flavones and flavonols, kaempferol was the strongest MCU activator and formed the basis for a second screening focusing on kaempferol and its close analogues (**Figure 43**). As a result, 25 kaempferol-related analogues were tested in the mitochondrial Ca^{2+} screening and nine plant compounds were found to show robust effects on mitochondrial Ca^{2+} uptake during stimulation in an MCU-dependent manner. All those were also tested in cell lines other than HeLa and validated in C2C12 cells and primary human myotubes stimulated with caffeine (data not shown).

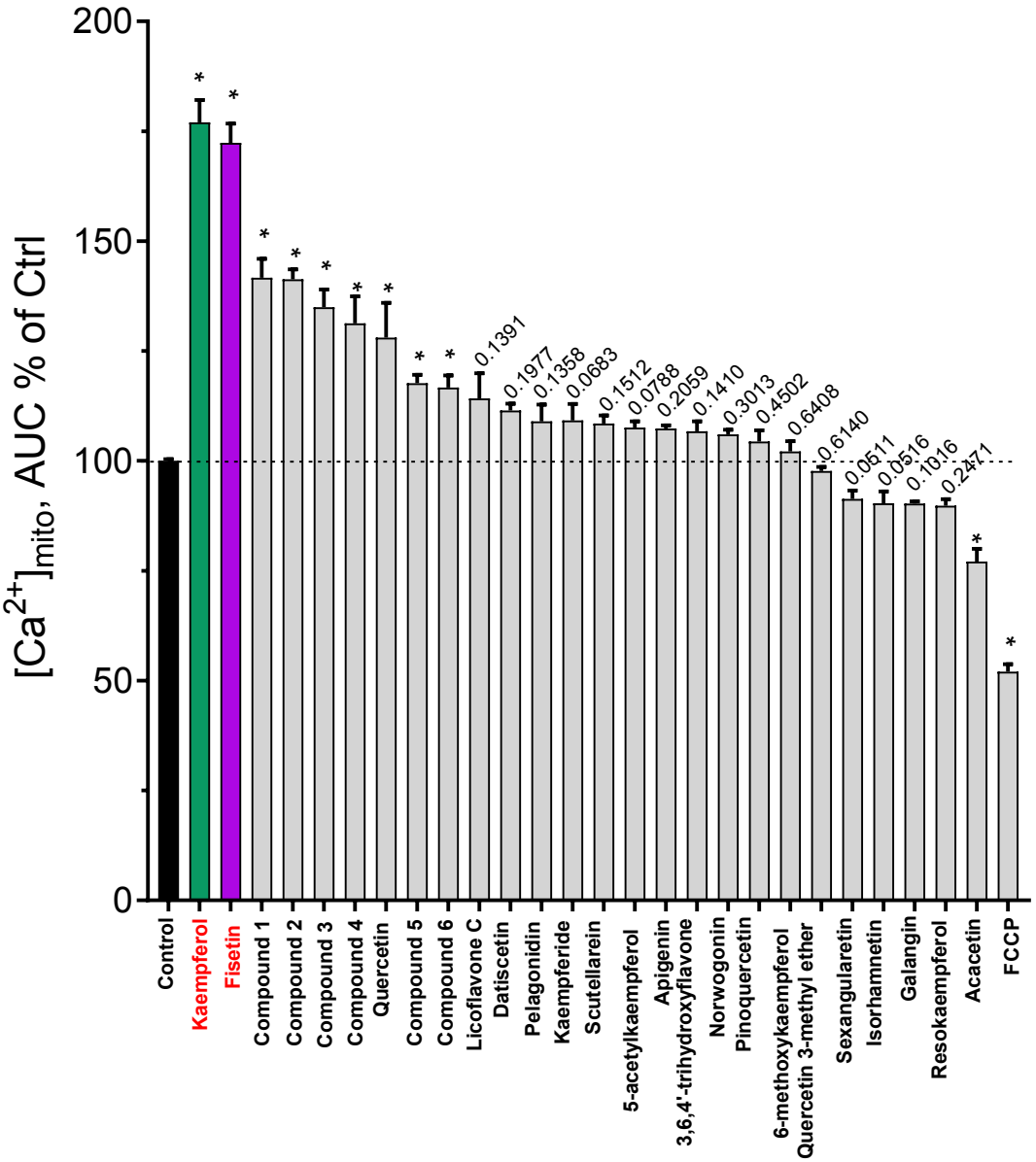

Figure 43. Screening results for 25 analogues compared to kaempferol in their effect on mitochondrial Ca^{2+} uptake.
Kaempferol and 25 analogues (10 µM) were tested in HeLa cells after stimulation with histamine (100 µM) for their effect on mitochondrial Ca^{2+} uptake. AUCs of n=3 experiments per compound were calculated and normalized to control cells treated with DMSO (1 %) and expressed in percentage. Data are presented as mean±SEM. Results are considered significant at a significance threshold of $\alpha < 0.05$; *$p < 0.05$; ns, not significant (Polyphenols were tested for normal distribution and compared to control using a Student's t-test).

The best hit, next to kaempferol, was fisetin (**Figure 44**), and those were used for further experiments to assess the mechanism for activating the MCU and to test their effect on *C. elegans* physiology *in vivo*.

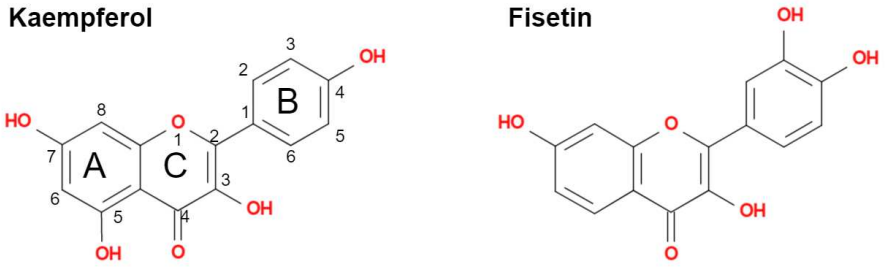

Figure 44. Chemical structure of the two best MCU activators: the flavonols kaempferol and fisetin.
The general nomenclature for phenolic compounds is highlighted in the chemical structure of kaempferol. The chemical structure of fisetin is shown on the right.

4.3.2. MCU subunits play different regulatory roles in mitochondrial Ca^{2+} transmission

To study the mechanism of MCU activation by kaempferol and fisetin, we considered the possibility that MCU activators require a specific subunit of the MCU complex. Thus, the role of relevant MCU subunits (MCU, MICU1, MCUR1, MCUb) in mitochondrial Ca^{2+} transport was characterized. Using HAP1 cells, CRISPR/Cas9-edited KOs were generated for further subunits of the MCU-complex, including the MICU1-subunit, the MCUR1-subunit and the MCUb-subunit. Isolated mitochondria of the respective cell lines were utilized to validate each KO cell line. The MCU-, MICU1- and MCUR1-KOs were verified via Western blot and the MCUb-KO cell line by PCR analysis due to the low specificity of MCUb-antibodies (**Figure 45**).

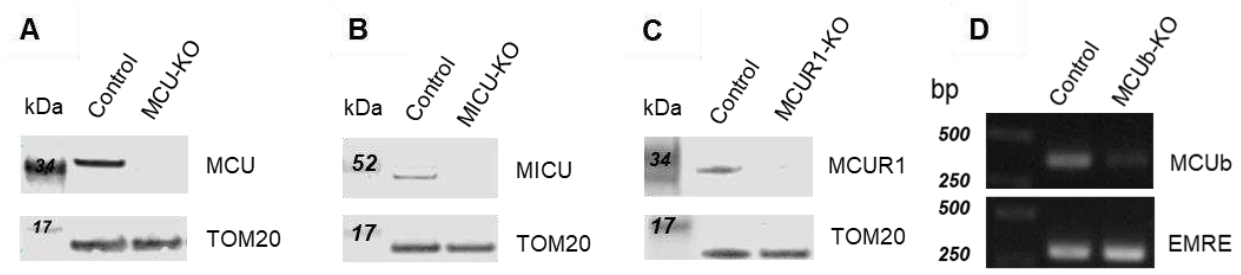

Figure 45. Validation of HAP1 KO cell lines via Western blot.
(A)-(C) Western blot of isolated mitochondria from MCU-, MICU1- and MCUR1-KO HAP1 cells using TOM20 as loading control. (D) RT-PCR of extracted RNA from MCUb-KO HAP1 cells using EMRE as control.

These cell lines were functionally validated by measuring ATP-induced mitochondrial Ca^{2+} uptake. For this purpose, a mitochondria-targeting aequorin probe as previously described was employed. The total mitochondrial Ca^{2+} elevation measured during ATP-stimulation was quantified as AUC in all HAP1 cell lines, normalized to control cells and expressed as a percentage (**Figure 46**).

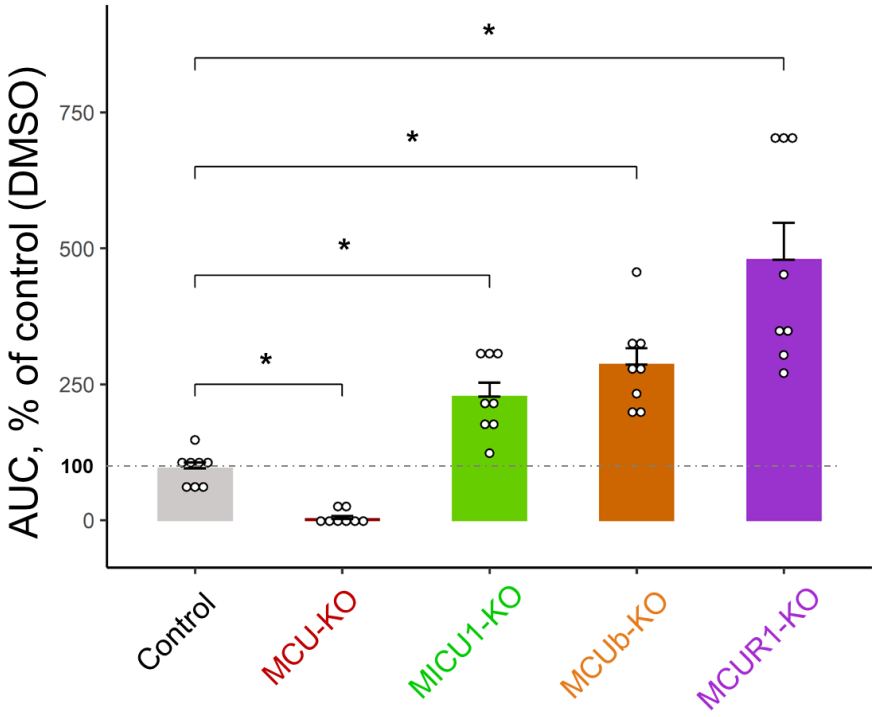

Figure 46. Mitochondrial Ca^{2+} uptake in control and HAP1 KO cell lines
Shows the AUC values of mitochondrial Ca^{2+} uptake measured in control and KO HAP1 cell lines after stimulation with ATP (1 mM). Mitochondrial Ca2+ uptake in KO cells is normalized to control cells and expressed as AUC %. For each group n=8. Data are expressed as mean±SEM. Results are considered significant at a significance threshold of $\alpha < 0.05$; *$p < 0.05$; (Student's t-test to compare two groups with normal distribution and one-way ANOVA to compare more than 2 groups).

Figure 46 demonstrated that ablation of MCU (MCU-KO cells) prevented the stimulated mitochondrial Ca^{2+} increase. In contrast, when the MCU down-regulator MCUb was ablated, mitochondrial Ca^{2+} increased as expected during stimulation. The same behaviour was observed in MICU1-ablated cells. Surprisingly, the greatest increase in mitochondrial Ca^{2+} was observed in MCUR1-ablated cells. The latter result was not expected, as the opposite effect was described in other models in literature (Mallilankaraman et al., 2012a) and also in our experiment with human myotubes. At this stage, we have no convincing explanation for this effect of MCUR1 in HAP1 cells; but it may be a celltype-specific phenomenon.

4.3.3. The MICU1 subunit is required the selected polyphenolic MCU activators in different ways to enhance mitochondrial Ca^{2+} uptake

To prove that kaempferol activates mitochondrial Ca^{2+} transport via MCU, control and MCU-KO HAP1 cells were stimulated with ATP and mitochondrial Ca^{2+} uptake was measured in cells acutely treated with DMSO or kaempferol (**Figure 47** shows traces and **Figure 48** statistics). Kaempferol increased stimulated mitochondrial Ca^{2+} uptake in control cells but not in MCU-KO cells, demonstrating that its effect is indeed mediated by MCU.

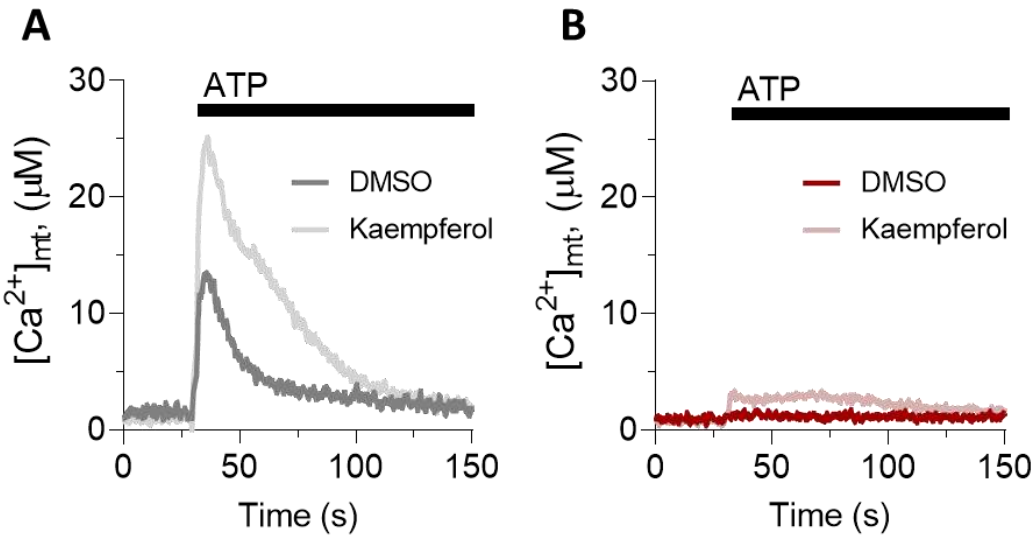

Figure 47. Kaempferol increases mitochondrial Ca^{2+} uptake in stimulated control but not in MCU-KO HAP1 cells.
(A) Shows calibrated mitochondrial Ca^{2+} traces of control (DMSO, light grey) and kaempferol (10 µM) treated control HAP1 cells (Kaempferol, dark grey) after stimulation with ATP (1 mM). (B) Shows calibrated mitochondrial Ca^{2+} traces of MCU-KO (DMSO, light red) and kaempferol (10 µM) treated MCU-KO HAP1 cells (Kaempferol, dark red) after stimulation with ATP (1 mM). The respective statistical assessment can be seen in **Figure 48**.

In a next step, the different HAP1-KO cell lines were treated with kaempferol to determine whether a specific subunit of the MCU-complex is required for the effect of the polyphenol. In control cells, kaempferol had the expected effect by increasing mitochondrial Ca^{2+} uptake, whereas this effect was completely prevented in MCU-KO cells (as expected). Kaempferol was still effective in all the other HAP1-KO systems except in MICU1-KO cells, where its effect was completely prevented, indicating a complete MICU1-dependency of MCU-activation by kaempferol (**Figure 48**).

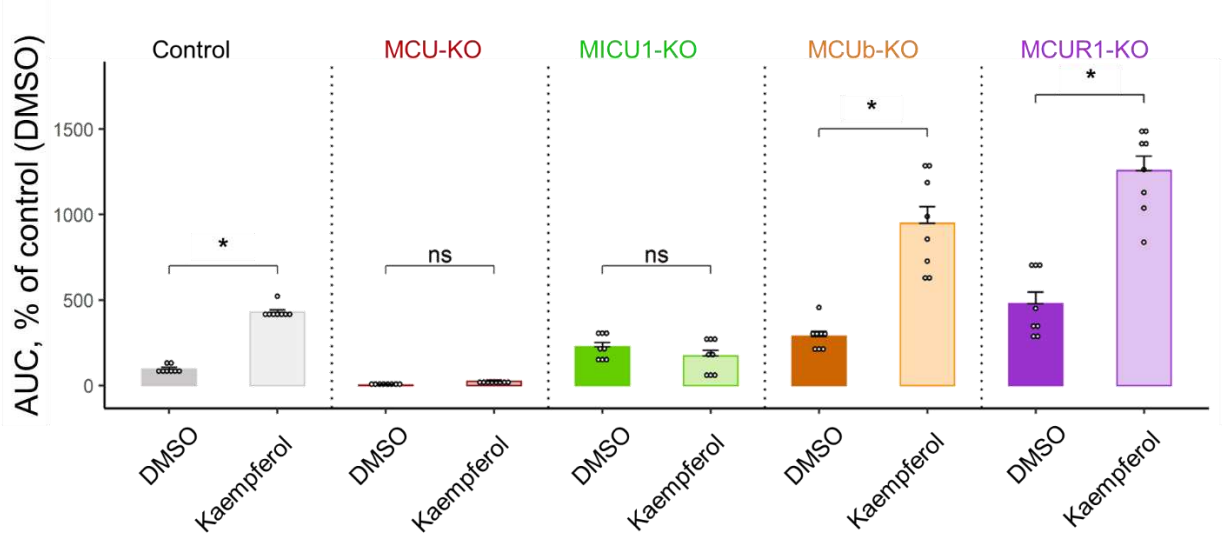

Figure 48. Mitochondrial Ca^{2+} uptake in control and KO cell lines treated with MCU activator kaempferol.
AUC values of mitochondrial Ca^{2+} uptake measured in control and KO cells treated with DMSO (1 %) or kaempferol (10 µM). Mitochondrial Ca^{2+} uptake in KO cells is normalized to control cells treated with DMSO and expressed as AUC %. For each group n=8. Data are expressed as mean±SEM. Results are considered significant at a significance threshold of $\alpha < 0.05$; *$p < 0.05$; (Student's *t*-test to compare two groups with normal distribution and one-way ANOVA to compare more than 2 groups).

The effect of fisetin was then also examined in control and MCU-KO HAP1 cells. The mitochondrial Ca^{2+} measurements for control and MCU-KO cells are shown in **Figure 49** and demonstrate an MCU-dependent increase in mitochondrial Ca^{2+} increase after stimulation with ATP in cells acutely treated with fisetin.

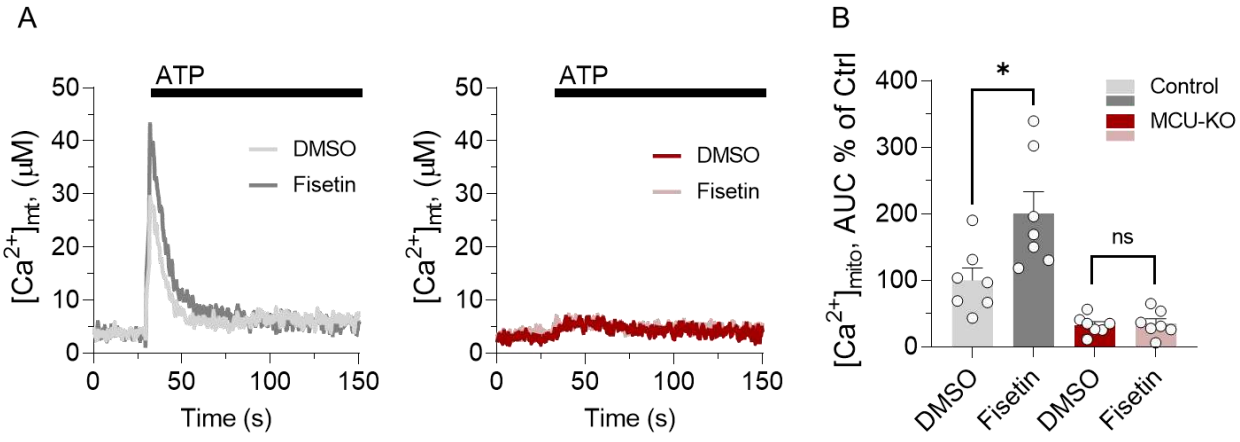

Figure 49. Fisetin enhances mitochondrial Ca^{2+} activation via MCU.
(A) Left panel shows calibrated mitochondrial Ca^{2+} traces of HAP1 control cells treated with DMSO (1 %, dark grey) or fisetin 10 µM (light grey) after stimulation with ATP (1 mM). Right panel depicts calibrated mitochondrial Ca^{2+} traces of HAP1 MCU-KO cells treated with DMSO (1 %, dark red) or fisetin 10 µM (light red) after stimulation with ATP (1 mM).

(B) Shows respective statistical analysis of mitochondrial Ca^{2+} uptake in KO cells, normalized to control cells treated with DMSO and expressed as AUC %. For each group n=7. Data are expressed as mean±SEM. Results are considered significant at a significance threshold of $\alpha < 0.05$; *p < 0.05; (Student's *t*-test to compare two groups with normal distribution).

The possible MICU1-dependency of the effect of fisetin was investigated and compared with the MICU1-dependency shown for kaempferol (**Figure 50**)**.** Chemically, fisetin is a compound with a high structural similarity to kaempferol, except for a different positioning of an -OH group. As can be seen in **Figure 50** (panel A), the activation of MCU by kaempferol was completely dependent on MICU1, as in MICU1-KO cells the effect of kaempferol was completely prevented (**Figure 50**, panel B). Conversely, the effect of fisetin was only partially dependent on MICU1, as its effect was not completely prevented in MICU1-KO cells (**Figure 50**, panel D). These results suggest that MCU activators may engage one or two different mechanisms to stimulate mitochondrial Ca^{2+} uptake. We therefore suggest with the current state of knowledge that two distinct mechanisms are involved in MCU activation by the identified compounds: one MICU1-dependent and one only partially MICU1-dependent.

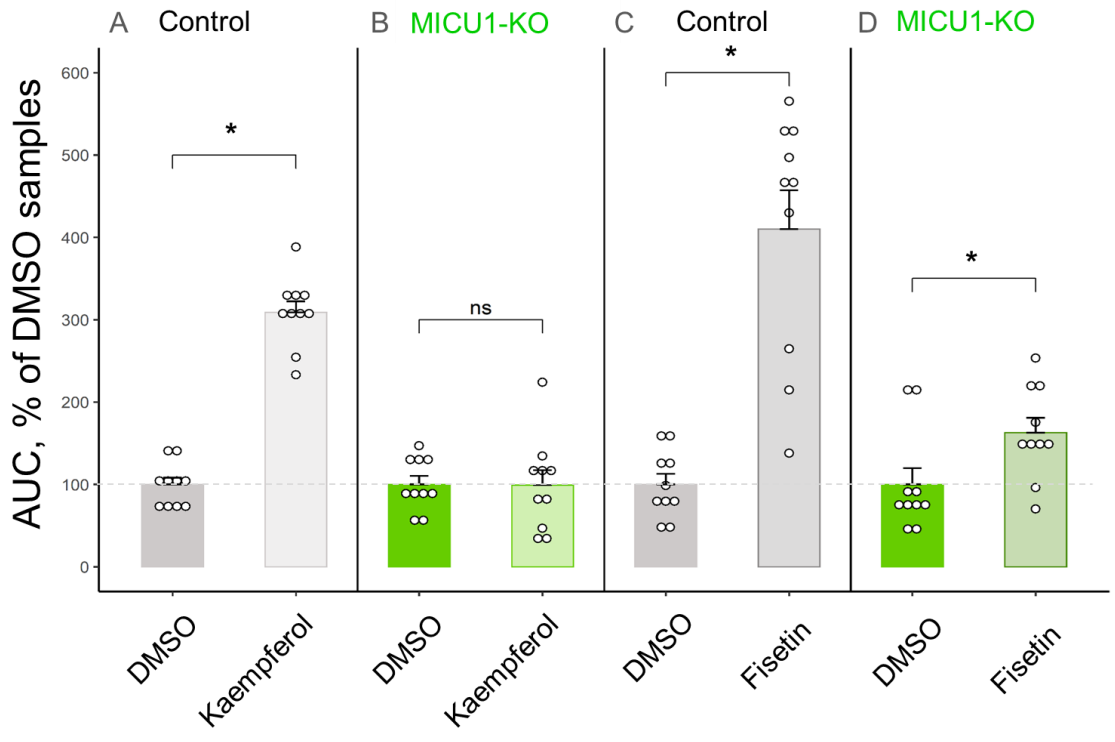

Figure 50. Mitochondrial Ca^{2+} uptake in control and MICU1-KO HAP1 cells treated with DMSO vs. kaempferol and fisetin.
Panel (A) shows ATP (1 mM) stimulated HAP1 control cells treated with DMSO (1%) and MCU activator kaempferol (10 µM) and normalized to the DMSO treated control cells. (B) Depicts ATP (1 mM) stimulated, DMSO (1 %) and

kaempferol (10 µM) treated MICU1-KO cells normalized to DMSO treated MICU1-KO cells. (C) – (D) Show the same set-up as (A) and (B) however cells were treated with fisetin (10 µM). Data are expressed as mean±SEM. For each group n=10. Results are considered significant at a significance threshold of $\alpha < 0.05$; *$p < 0.05$; (Student's *t*-test to compare two groups with normal distribution).

In the collaboration with the Department of Pharmaceutical and Pharmacological Sciences from the University of Padova the mechanism of interaction of the polyphenols with MICU1 was explored. Based on the crystal structure of MICU1 and the chemical structures of kaempferol and fisetin, it was possible to test whether or not polyphenols can bind to MICU1 to exert their effect on mitochondrial Ca^{2+} uptake. Molecular docking simulations were done to identify relevant amino acids that mediate the binding between kaempferol or fisetin and MICU1. The results revealed a binding cleft within the MICU1-protein for kaempferol and involved amino acid side-chains for this interaction. These amino acids are Leu308 and Tyr334 (**Figure 51A**, bold letters). The same analysis has been done for fisetin and the related amino acids with partial interaction between MICU1 and fisetin were as well Leu308 and Tyr334 (**Figure 51B**, bold letters).

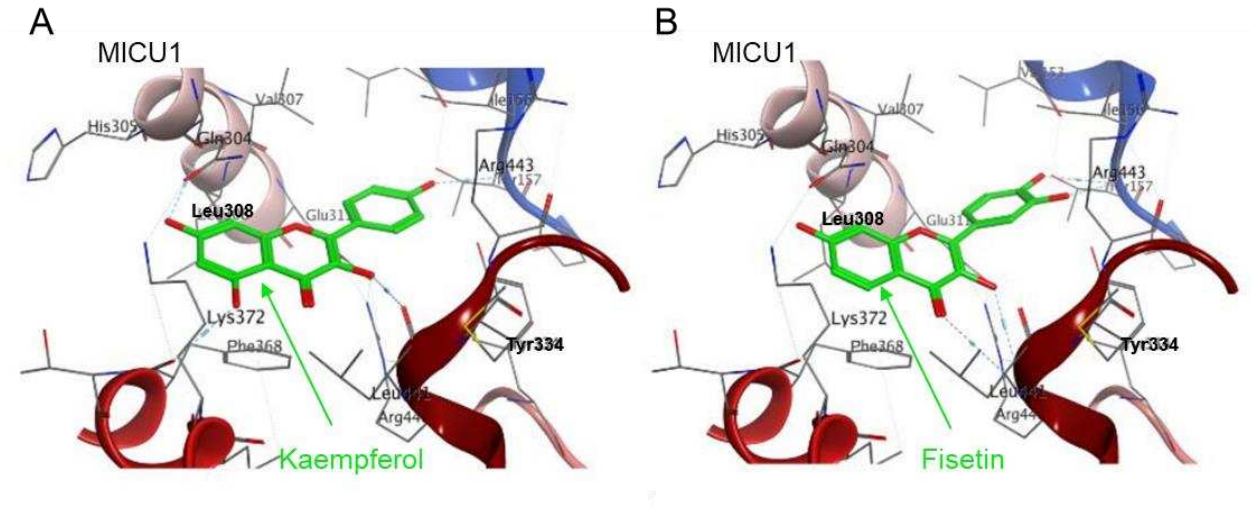

Figure 51. Molecular docking simulations identifies potential binding sites between MICU1 and polyphenols. (A) Depicts the binding interaction of MICU1 protein and kaempferol. Involved amino acids are Leu308 and Tyr334 (bold letters). (B) Shows the binding interaction between MICU1 protein and fisetin. Involved amino acids are Leu308 and Tyr334 (bold letters).

Based on the results obtained, the next objective was to introduce mutations into the identified potential binding sites and to express the control and mutated MICU1 proteins in a MICU1-KO system. These experiments should allow to determine the specificity of the identified amino acids for interaction and their effects on increasing mitochondrial Ca^{2+} uptake. For kaempferol and fisetin, the decision on which mutations should be introduced in MICU1 had to take into account

that most interactions are mediated by backbone atoms and do not involve many side chains of residues.

As a result, 3 possible strategies were identified:

(1) Mutating the residues with partial interaction with their own side chain Tyr334-> Ala (Y334A)

(2) Introducing a bulky amino acid in the binding site to sterically perturb the ligand accommodation Leu308 -> Trp (L308W) or Tyr334 -> Trp (Y334W) or a double mutant (L308W-Y334W)

(3) Monitoring the effect of dehydroxylated derivatives (scaffold search is a suitable database engine to check available vendors such as MolPort). For instance, galangin, flavonol and resokaempferol as starting candidates. Also, the replacement of the hydroxyl moieties with methoxy group could avoid/reduce the binding (e.g. artemetin).

The results of these studies are not completed and therefore not included in this thesis. To this end, several plasmids to express different versions of MICU1 in a human MICU1-KO system were designed. These different versions contain the normal MICU1-protein as control and MICU1-mutants carrying one or two mutations in amino acids previously identified in the molecular docking simulations. In total, 4 plasmids with MICU1-mutations (Mutant1-4) were generated, which are listed in **Table 2** and will be employed to measure mitochondrial Ca^{2+} uptake in the MICU1-rescue (hMICU1) and the different MICU1-mutants as controls or when exposed to kaempferol or fisetin. We expect to reproduce the effect of kaempferol (fisetin) on mitochondrial Ca^{2+} uptake in the MICU1-rescue cells. At the same time, we hope to find at least one mutant in which the potentiating effect of kaempferol (fisetin) cannot be restored. This mutant will help to identify the crucial amino acid(s) required for kaempferol (fisetin) binding and interaction with MICU1 to activate the MCU complex and increase mitochondrial Ca^{2+} uptake.

Table 2. List of plasmids to express mutated MICU1 proteins in HAP1 MICU1-KO cells to validate essential amino acids necessary to increase mitochondrial Ca^{2+} uptake.

Plasmid (based no pcDNA3.1)	Inserted protein
Control	hMICU1
Mutant 1	hMICU1-Y334A
Mutant 2	hMICU1-L308W
Mutant 3	hMICU1-Y334W
Mutant 4	hMICU1-L308W-Y334W

4.3.4. MICU1 is required by kaempferol and fisetin to enhance respiration in *C.elegans, in vivo*

The effect of kaempferol and fisetin on mitochondrial Ca^{2+} transport via MICU1 activation was next tested *in vivo* in *C.elegans* in which MICU1-expression was diminished. For this purpose, RNAi was used to decrease expression of MICU1 (MICU1-kd) which was validated using qPCR (**Figure 52A**). Subsequently, oxygen consumption was measured in worms (**Figure 52B**) after stimulation with carbachol, which is known to promote mitochondrial Ca^{2+} uptake, as shown by Alvarez et al (Álvarez-Illera et al., 2020). Statistical analysis of basal (**Figure -52C**) and NaN_3-dependent respiration (**Figure 52D**) showed a significant increase in both basal and NaN_3 synthase-dependent respiration in MICU1-kd worms compared to control worms. As MICU1 functions as a gatekeeper within the MCU-complex it was expected that a knockdown of the gatekeeper protein MICU1 causes an increased mitochondrial Ca^{2+} uptake after stimulation.

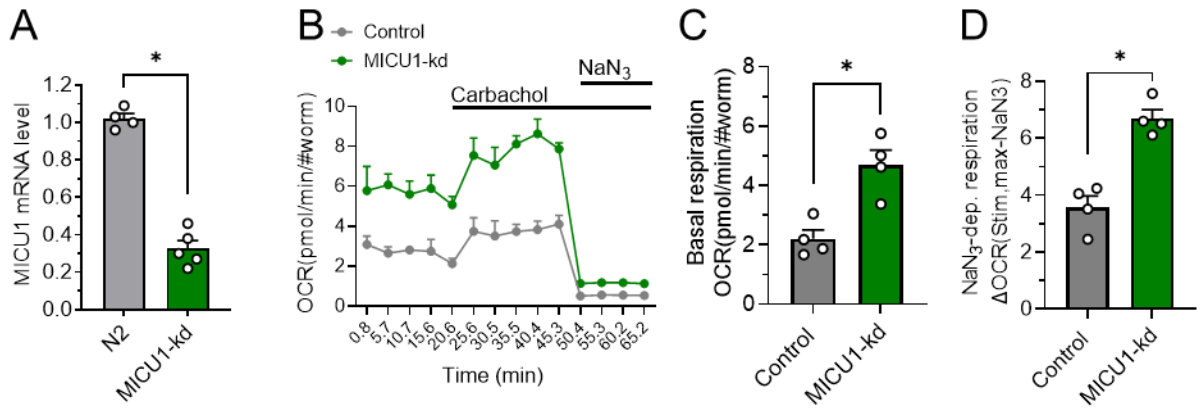

Figure 52. Knockdown of the MCU gatekeeper MICU1 causes increased oxygen consumption rate in *C.elegans*. (A) Validation of the MICU1-kd in L4 old *C.elegans* via RNAi feeding, n=5 experiments, each with a well populated 9 cm plate. MICU1 mRNA expression was corrected using *ama*-1 and *act*-1 as control genes. (B) Shows respiration profile in control (grey) and MICU1-kd (green) after stimulation with 10 mM carbachol followed by 40 mM sodium azide (NaN_3) to shut down the respiration by blocking complex V and IV. (C) Statistical analysis of basal respiration in control (grey) and MICU1-kd (green) after subtraction of non-mitochondrial respiration measured by adding NaN_3. (D) Statistical analysis of NaN_3-dependent respiration in control (grey) and MICU1-kd (green) after subtraction of non-mitochondrial respiration measured by adding NaN_3. Data are expressed as mean±SEM. For each group n=4 experiments, each with 25-50 worms. Results are considered significant at a significance threshold of $\alpha < 0.05$; *$p < 0.05$; (Student's *t*-test to compare two groups with normal distribution).

Next, the effect of kaempferol on cellular respiration in control and MICU1-kd worms was assessed. Worms were stimulated with carbachol and the respiration profile of kaempferol-treated control worms (**Figure 53A**) showed a significant increase in both basal (**Figure 53B**) and NaN_3-dependent respiration (**Figure 53D**). In MICU1-kd worms, these kaempferol-dependent effects were completely prevented (**Figure 53C, E**), indicating that the enhanced respiration profile of these MCU activators is mediated by MICU1.

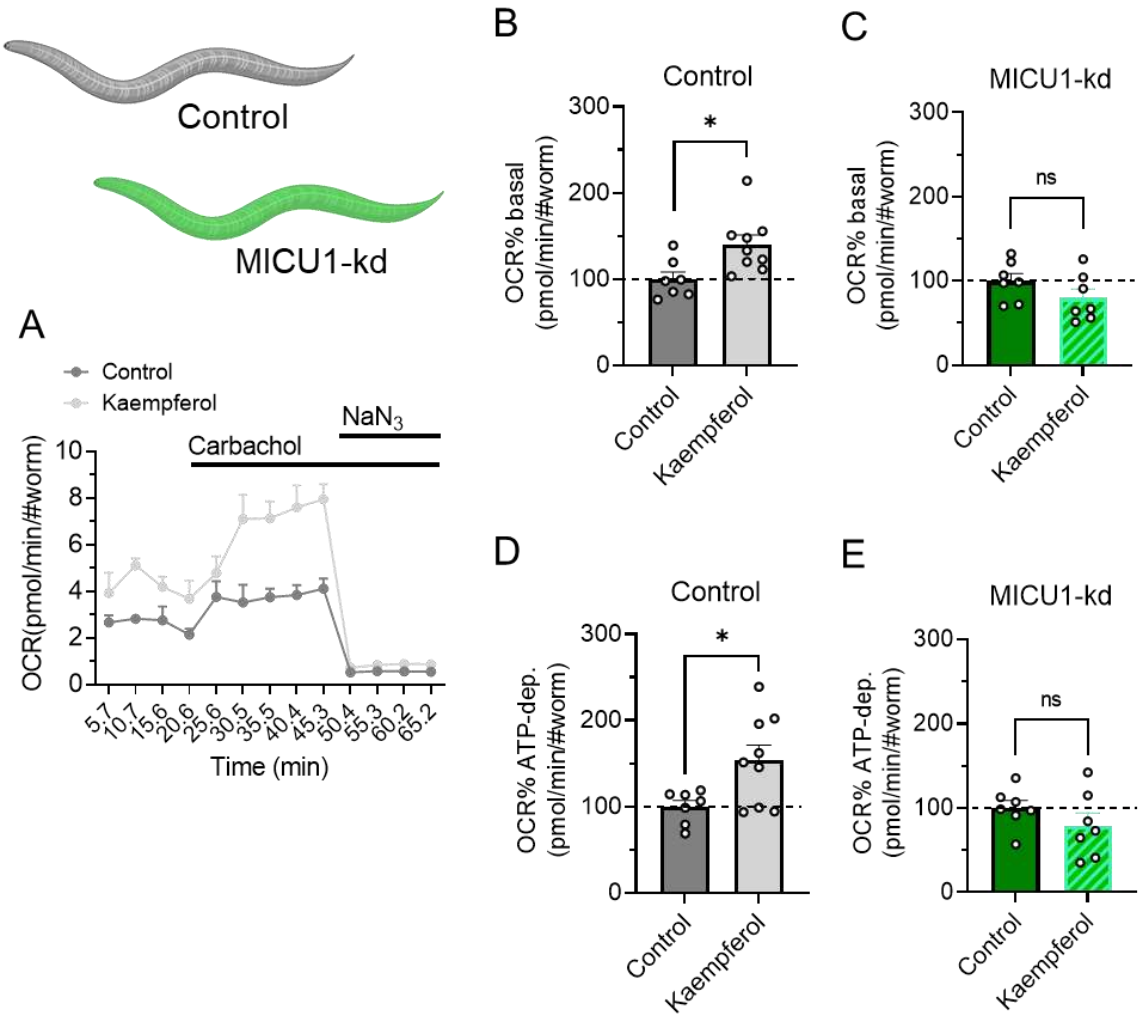

Figure 53. Effects of kaempferol on oxygen consumption rate in control and MICU1-kd *C.elegans*.
(A) Shows respiration profile in control worms treated with (light grey, n=9 experiments with 25-50 worms) or without (dark grey, n=7 experiments with 25-50 worms) kaempferol. Carbachol (10 mM) induced respiration was measured, followed by addition of NaN_3 (40 mM) to shut down respiration and assess non-mitochondrial respiration. (B-C) Statistical analysis of basal respiration in control (dark grey, n=7 experiments with 25-50 worms) and kaempferol treated (light grey, n=9 experiments with 25-50 worms) worms and in control MICU1-kd (dark green, n=7 experiments with 25-50 worms) and kaempferol treated (light green, n=7 experiments with 25-50 worms) MICU1-kd worms after subtraction of non-mitochondrial respiration. (D-E) Statistical analysis of NaN_3-dependent respiration in control (dark grey, n=7 experiments with 25-50 worms) and kaempferol treated (light grey, n=9 experiments with 25-50 worms) worms and in control MICU1-kd (dark green, n=7 experiments with 25-50 worms) and kaempferol treated (light green, n=7 experiments with 25-50 worms) MICU1-kd worms. Data are expressed as mean±SEM. Results are considered significant at a significance threshold of $\alpha < 0.05$; *$p < 0.05$; (Student's *t*-test to compare two groups with normal distribution).

Based on the positive hits from the high-throughput screening of putative MCU-activators, fisetin was next tested in *C.elegans* to see if its structural similarity to kaempferol also shows functional similarity. Therefore, the same conditions were used as described above to evaluate the effect of fisetin on cellular respiration in control and MICU1-kd worms. Compared to kaempferol, fisetin had no effect on basal respiration in control worms (**Figure 54A, B**). However, similar to

kaempferol, fisetin significantly increased NaN_3-dependent respiration after carbachol stimulation (**Figure 54D**). Much like kaempferol, the effect of fisetin was dependent on MICU1, as its effect was prevented in MICU1-kd worms (**Figure 54E**).

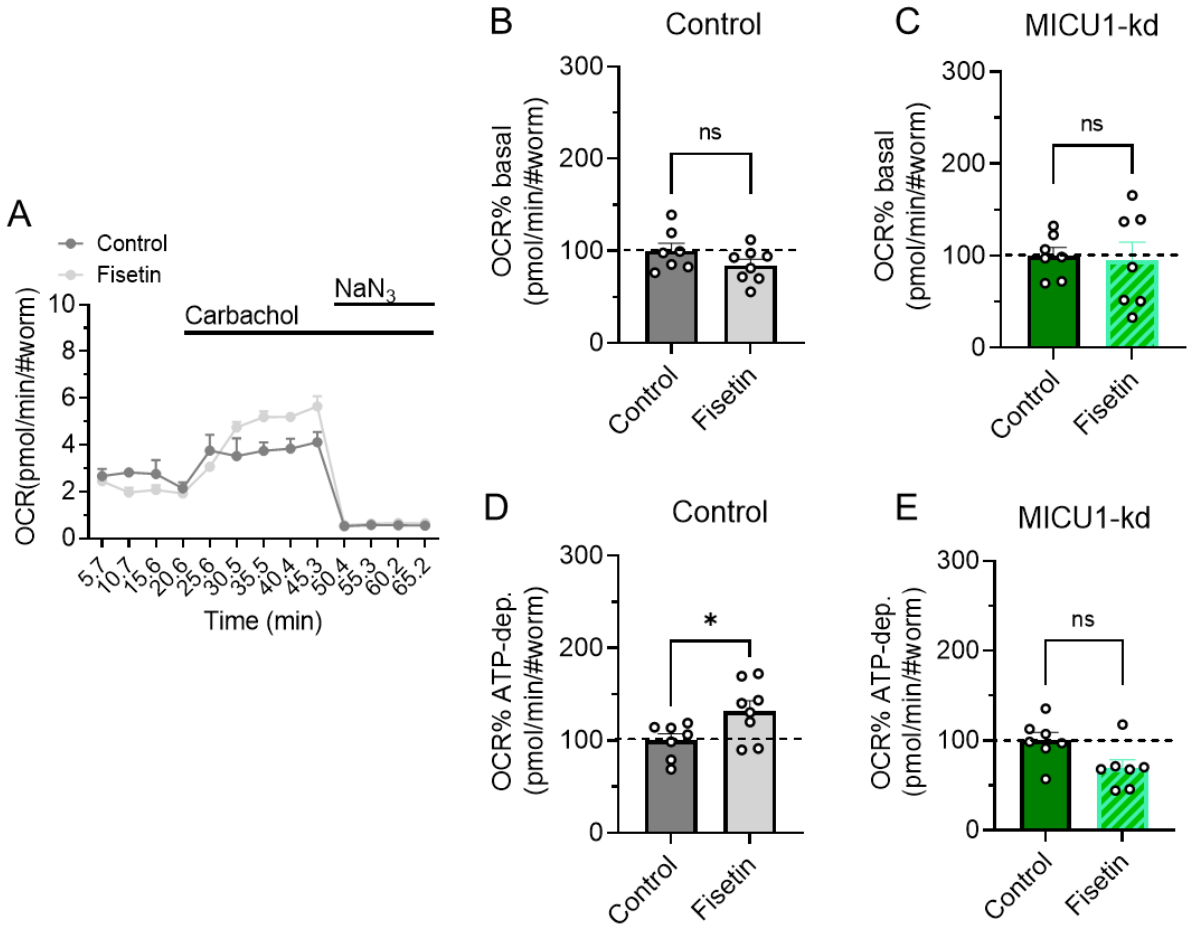

Figure 54. Polyphenols increase cellular respiration in N2 but not in MICU1-deficient *C. elegans*.
(A) Respiration profile in control worms treated with (light grey, n=8 experiments with 25-50 worms) or without (dark grey, n=7 experiments with 25-50 worms) fisetin. Carbachol (10 mM) induced respiration was measured, followed by addition of NaN_3 (40 mM) to shut down respiration and assess non-mitochondrial respiration. (B-C) Statistical analysis of basal respiration in control (dark grey, n=7 experiments with 25-50 worms) and fisetin treated (light grey, n=8 experiments with 25-50 worms) worms and in control MICU1-kd (dark green, n=7 experiments with 25-50 worms) and fisetin treated (light green, n=7 experiments with 25-50 worms) MICU1-kd worms after subtraction of non-mitochondrial respiration. (D-E) Statistical analysis of NaN_3- dependent respiration in control (dark grey, n=7 experiments with 25-50 worms) and fisetin treated (light grey, n=8 experiments with 25-50 worms) worms and in control MICU1-kd (dark green, n=7 experiments with 25-50 worms) and fisetin treated (light green, n=7 experiments with 25-50 worms) MICU1-kd worms. Data are expressed as mean±SEM. Results are considered significant at a significance threshold of $\alpha < 0.05$; *$p < 0.05$; (Student's *t*-test to compare two groups with normal distribution).

Section 5: Discussion

Three research gaps have been addressed within the overarching theme of the metabolic triad of MCU, mitochondrial redox biology, and polyphenol action underlying skeletal muscle health. With the results obtained, this work provides a unifying concept for the coupling of this triad and explores its implications for skeletal muscle health, including some novel approaches for targeted interventions to promote muscle functionality, particularly in advanced age. The discussion analyzes the implications of the findings described and places them in the context of the existing literature. Finally, this section concludes with a summary and an outlook for future experiments.

The first research gap to be filled addressed the link between Ca^{2+} and redox signaling in mitochondria. Both signaling pathways are central processes that play a role in various diseases, but no causality had been established. Mitochondrial Ca^{2+} signaling via MCU has been shown to be involved in key cellular processes such as intracellular Ca^{2+} signaling, cell death, proliferation, buffering of cytosolic Ca^{2+}, stimulation of muscle trophism and bioenergetics (De Stefani et al., 2015, Mammucari et al., 2015).

These established functions of MCU have now been extended to modulation of mitochondrial redox signaling. In the work presented here, it was discovered that MCU activation causes a net reduction in mitochondrial thiol groups and provides a causal link between Ca^{2+} and redox signaling in mitochondria of human leukemia cells (HAP1 cells) and primary human myotubes. Thiol groups have been identified as dynamic regulators of mitochondrial proteins that contain cysteine residues and are able to determine protein conformation and function, thus playing a central role in cell physiology and pathology (Mailloux et al., 2014, Riemer et al., 2015). The amount of redox-sensitive proteins in mitochondria is estimated to range between 60 and 90 mM, representing the largest group of reactive thiols in mitochondria (Requejo et al., 2010). MCU itself has been found to carry one redox-sensitive thiol group (cysteine-97) that enhances MCU activity upon oxidation (Dong et al., 2017). In this scenario, the current discovery may help explain that oxidation stimulates MCU activation, which in turn promotes a reduced mitochondrial redox state that prevents further increases in oxidation that could affect other mitochondrial metabolic pathways. Protein redox-sensitive thiol switches are modulated by oxidative and reductive processes. Mitochondria themselves are a source of ROS (Murphy, 2009) and have a repertoire of reducing moieties – predominantly GSH (approximately 5 mM) – that counteract on oxidizing reactions (Mailloux et al., 2014). An imbalanced redox state caused, for instance, by increased oxidative stress is one of the hallmarks of mitochondrial dysfunction, along with a decline in biogenesis, a reduced number of mitochondria and an impaired $\Delta\Psi m$ (Smith et al., 2012). The

present results suggest that MCU is a potentially novel way to counteract such disturbed redox states by modulating and eventually restoring a balanced redox state in mitochondria in favor of reduction.

Impaired redox signaling in mitochondria has been linked to numerous diseases, including a decline in muscle function (Calvani et al., 2013, Adhikari et al., 2021, Marzetti et al., 2013, O'Rourke et al., 2021, Ippolito et al., 2020). A recent paper highlighted MCU as an important key player in mediating skeletal muscle function and showed that a skeletal muscle-specific knockout of MCU in mice is linked to a severe decrease in bioenergetics, running capacity and tetanic muscle force (Gherardi et al., 2019b). However, a link to redox biology in relation to skeletal muscle health has not been investigated. The results presented in this work in human myotubes confirm the role of MCU as a redox modulator also in skeletal muscle, suggesting that its role as a redox modulator could be extended to other tissues. Indeed, MCU-mediated regulation of thiol groups would be particularly relevant in tissues with high Ca^{2+} and energy demands such as brain, heart, and endocrine pancreas (Mammucari et al., 2018).

Attempts to modulate mitochondrial redox state with various antioxidants have been investigated without finding significant health benefits (Theodorou et al., 2011). In addition, untargeted administration of antioxidants has been associated with negative health effects (Poljsak et al., 2013), as evidenced by its failure to mediate post-exercise muscle adaptations and its accelerating effect on lung cancer progression (Sayin et al., 2014, D'Autréaux and Toledano, 2007). In a more advanced approach, studies have linked antioxidants to the lipophilic cation triphenylphosphonium (TPP) to target the antioxidant to mitochondria. While several examples are provided in the Summary and Outlook section, it should be mentioned that targeting mitochondria is a step forward, but it is equally important to choose the right antioxidant because its molecular mechanism determines whether it can improve mitochondrial function or disrupt mitochondrial metabolic pathways (Broome et al., 2018). In the present work, the mitochondria-targeted antioxidants mitoTEMPO, mitoQ, and SkQ1 were tested, and none of the compounds had a marked effect on reducing mitochondrial thiol groups. Of the compounds tested, only mitoQ at a concentration of 0.25 µM appeared to have a mild effect on increasing reduced mitochondrial thiol groups. Furthermore, uncontrolled addition of cation-bound antioxidants will most likely affect the mitochondrial $\Delta\Psi m$, which must be considered depending on the physiological circumstances during administration.

In the present work, MCU activation was shown to exclusively target mitochondrial redox levels and not cytosolic redox levels without impairing mitochondrial $\Delta\Psi m$ (data not shown). These results pave the way for MCU-targeted interventions as opposed to antioxidant interventions.

One area in which the presented mechanism of MCU activation may play an important role is exercise. Although the focus of this work was not on exercise, mitochondrial Ca^{2+} metabolism is clearly linked to mitochondrial function, which is ultimately related to muscle function. In mice with a skeletal muscle-specific MCU-KO, there was a change in muscle fiber type from slow to fast muscle fibers, impaired muscle strength and performance, impaired glucose oxidation, a shift in fuel selection to fatty acid oxidation associated with lower PDH activity, and a lactate accumulation in the blood (Gherardi et al., 2019b). In this context, it could be speculated that the MCU-KO-induced compromised mitochondrial redox state could affect PDH activity and cause a switch from glucose to fatty acid utilization. Indeed, PDH has been found to have an attached thiol group that acts as a redox switch and inactivates the enzyme during oxidation (Gao et al., 2020)

A recent study showed that exercise increases cytosolic H_2O_2 production in humans and mice (Henriquez-Olguin et al., 2020) to mediate exercise-induced muscle adaptations, whereas in mitochondria, H_2O_2 production decreases during exercise. The authors did not provide an explanation for the decreased H_2O_2 production in mitochondria during exercise, but it could be speculated that this is caused by the mechanism of MCU activation demonstrated in this thesis, which causes a net reduction in the mitochondrial redox state (Henríquez-Olguin et al., 2019). In addition, the authors showed that exercise increases Prx3 concentration in mitochondria, which plays a crucial role in ROS detoxification. Interestingly, Prx3 concentrations decreased in elderly compared to young subjects. However, this decrease diminished after 6 weeks of aerobic exercise, suggesting that exercise improves mitochondrial redox metabolism. These results were presented at the International Biochemistry of Exercise Conference (IBEC) in Toronto in 2022 and have not yet been published. Interestingly, another study in older subjects showed that MCU protein expression is also upregulated after exercise, which could contribute to a profound reduction in mitochondrial redox state (Zampieri et al., 2016).

The second research line addressed the development of a therapeutic option for muscle health, especially during aging, by targeting MCU with a natural bioactive compound. Aging in muscle tissue has been associated with improper mitochondria and mitochondrial Ca^{2+} regulation, making MCU an interesting target for interventions. Moreover, MCU in its activity not only contributes to redox homeostasis, but evidently also has pronounced effects on mitochondrial energy metabolism, which decreases with age. In the current work, the natural bioactive oleuropein was identified which is present in food and enriched in olive leaf extracts, as a powerful MCU activator, that enhances – as demonstrated – also mitochondrial muscle energy metabolism in human myotubes. Furthermore, the *in vivo* data established these beneficial effects of the compound on

muscle function with a restoration of mitochondrial energy metabolism across species in aging models (mouse, rats and human). An oleuropein-rich diet administered to aged mice increased running performance, demonstrating the efficacy of the applied MCU-nutritional intervention on aging skeletal muscle.

This effect of oleuropein extends the list of reported health benefits of this polyphenol, such as anti-oncogenic and neuroprotective effects (Nediani et al., 2019). In the context of neurodegenerative diseases, oleuropein aglycone has been reported to reduce α-synuclein protein aggregation in muscle cells and improve mobility in Parkinson's disease models of *C. elegans* (Brunetti et al., 2020). Other studies suggested that oleuropein can increase mitochondrial biogenesis and reduce oxidative stress by upregulation of the cellular antioxidant defense mechanism via GSH and SOD2 (Blanco-Benítez et al., 2022). These results highlight the versatile role of oleuropein in different *in vitro* and *in vivo* models, although its mechanism of action for the beneficial effects had not been fully discovered. The results obtained here show a MICU1-dependent mechanism of oleuropein activity in mitochondria. That may be an important mechanism in how oleuropein induces the health benefits mentioned above, which may well go beyond skeletal muscle.

The reduced functionality in aged muscle tissue and sarcopenic elderly could be linked at the genetic level to a reduction in MCUR1-mRNA levels, which could well contribute to impaired MCU activity and the Ca^{2+}-dependent processes in redox-status and energy metabolism. Mimicking this MCUR1 down-regulation, found in biopsies obtained from sarcopenic patients, in human myotubes confirmed impaired mitochondrial Ca^{2+} regulation. Oleuropein-administration restored mitochondrial Ca^{2+} signaling in these conditions, extending its beneficial effects to human models of sarcopenia. Interestingly, a recent study demonstrated a comparable downregulation of MICU3 in aged mice and in senescent C2C12 mouse myotubes compared to young models (Yang et al., 2021), associated with impaired mitochondrial Ca^{2+} uptake, increased ROS levels, impaired differentiation and $\Delta\Psi m$, and a decrease in energy metabolism. These data essentially confirm the present findings for another subunit, but overall strongly support the functional link between MCU activity state and skeletal muscle aging. The experiments performed with the down-regulation of MCUR1 in primary human myotubes clearly demonstrated that this subunit is crucial and its lack could not be compensated by any of the other subunits – although there may be an evolutionary redundancy in the subunits for some functions of the large protein complex.

The final research line aimed to elucidate in detail the molecular mechanism by which oleuropein mediates its beneficial effects on mitochondrial energy metabolism. Since the current results, together with published data (Di Marco et al., 2020), demonstrated an essential role of MICU1 in

MCU regulation, the hypothesis was that the effects of oleuropein may be transmitted via this subunit. The analysis was also extended to two additional polyphenolic MCU activators, namely kaempferol and fisetin as the two best hits from the high-content screening of kaempferol analogues. As these two polyphenols do not yet have self-affirmed GRAS status, their use for intervention studies was not considered in this work.

The conclusion derived from all experiments conducted was that the three polyphenols can modulate MCU in two ways: via a fully MICU1-dependent pathway (oleuropein and kaempferol) and/or an only partially MICU1-dependent pathway (fisetin). This work is the first to demonstrate the molecular mechanism for MCU activators. Previous work had focused exclusively on MCU inhibitors and linked their mechanism to MICU1 (Di Marco et al., 2020). The employed *in vivo* model of *C. elegans* confirmed the positive effects of the polyphenols on mitochondrial respiration and their MICU1-dependence. Taken together, it is reasonable to conclude that the main effects of the tested polyphenols observed occur via MICU1.

The first indication that selected polyphenols might act via MCU was found in 2004 (Montero et al., 2004), but the molecular identity of MCU had not yet been described and was not published until 7 years later (Baughman et al., 2011, De Stefani et al., 2011). Over the years and with the genetic tools available, the MCU-dependent manner by which polyphenols can exert their effects has been shown, for instance, also in pancreatic β-cells (Bermont et al., 2020). A very recent study investigated MCU activators without exploring the detailed mechanism of MCU activation and found, among other compounds and polyphenols, the MCU activator amorolfine (De Mario et al., 2021). This compound is a morpholine antifungal drug and was identified in a screening of 1600 US Food and Drug Administration-approved drugs. It showed trophic effects on muscle *in vitro* and *in vivo*, as well as a beneficial effect on mitochondrial respiration *ex-vivo* (De Mario et al., 2021). The results from treatment with oleuropein presented here *in vivo* showed such effects for a food-constituent (with very low concentrations also in olive fruits) and, moreover, positive effects on muscle performance, such as prolonged running times as well as increased resistance to fatigue. To date, no studies have better characterized the mechanism by which MCU and MCU activators affect skeletal muscle performance and health as those presented here.

Kaempferol and fisetin were added to extend the analysis panel and proved helpful in elucidating the molecular interaction template. Kaempferol showed complete MICU1 dependence in increasing mitochondrial Ca^{2+}. It is of course interesting to ask how the polyphenols act on MICU1 and which amino acid residues in the subunit mediate the effects through ligand interaction. Possible residues for the interaction have been identified *in silico* in the human MICU1 protein, and work is underway to functionally test the proposed protein-ligand interaction structure

to fully uncover the underlying mechanisms. Since some beneficial effects of kaempferol and fisetin have been observed in *C. elegans* and the MICU1 protein is 55.26 (n) % conserved, it would be a first step to test whether some of the binding sites identified *in silico* are also present in the MICU1 sequence of *C. elegans*. If the ongoing MICU1 mutation experiments confirm the *in silico* hits and are present in *C.elegans*, it would be of interest to also construct MICU1-mutated worms and test whether loss of the binding site leads to a loss of MICU1-mediated effect of polyphenols on mitochondrial energy metabolism. In a further step, it would be of further interest to test whether these polyphenols affect mobility and, if so, whether this effect is lost in the respective MICU1-mutated worm.

In children, loss-of-function point mutations in MICU1 have been shown to cause deleterious neuromuscular effects such as muscle weakness, ataxia, and learning difficulties, and to cause mitochondrial Ca^{2+} dysregulation (Kohlschmidt et al., 2021, Logan et al., 2014). In the study by Kohlschmidt et al, patients with a MICU1 mutation showed higher mitochondrial Ca^{2+} clearance when semipermeabilized lymphoblastoid cells were stimulated with 3 µM Ca^{2+}, whereas high stimulation with 10 µM caused significantly reduced mitochondrial Ca^{2+} clearance in patients compared to controls. It would be of great interest to test the effect of MCU activators such as oleuropein, kaempferol, and fisetin as well as MCU inhibitors (Di Marco et al., 2020) in mutant worms that mimic the loss-of-function mutations in humans. In addition, it would be useful to assess mitochondrial redox status in MICU1 mutants, for example, using a redox sensor targeting *C. elegans* body wall muscle cell mitochondria (Johnson and Nehrke, 2010). If the redox state in the mutants is characterized by perturbations, it might be beneficial to test redox-active compounds that could help restore a physiological redox state in the mitochondria. In a final experiment, the effect of fuel utilization in the existing human patients could be measured by measuring the respiratory control ratio to get an impression of PDH activity. Subsequently, OCR and ECAR could be measured in MICU1 mutants of *C. elegans* and PDH activity determined. Because MICU1 mutations cause serious health problems in children, it is of utmost importance to advance in this field by investigating the underlying molecular mechanism and exploring potential treatments that can help regulate and improve mitochondrial, and thus muscle, function. In this way, the present work has provided evidence that MCU activation leads to a net reduction in mitochondrial redox state, which has been shown to be associated with a beneficial muscle energy metabolism and muscle function *in vivo*. As this is only one of the building blocks to gain deeper insight into mitochondrial Ca^{2+} regulation under pathophysiological conditions, it will be necessary to extend research to relevant pathologies such as MICU1 mutations in children.

Summary and outlook

Overall, the results described here in the dissertation clearly demonstrate that MCU has a coupled novel function as a mitochondrial redox modulator with downstream effects on muscle energy metabolism in addition to its Ca^{2+}-regulatory function. The activity state of MCU can be modulated by intervention with natural bioactive compounds, which may allow the development of nutritional products to improve muscle functionality, especially during aging, but also in the context of other conditions and diseases associated with de-regulated redox signaling in mitochondria. Because the natural bioactive oleuropein also acts in young muscle by improving muscle energy metabolism and muscle performance in rodents, it could also lead to nutritional solutions for improved muscle performance in humans. To investigate these effects, two human clinical trials are currently underway to evaluate the effect of oleuropein on muscle function in young and elderly people. A common pitfall in human studies examining the effects of polyphenols is their limited bioavailability. Data on plasma concentrations of oleuropein, oleuropein aglycone, and its metabolites are sparse and show high variability among study participants (de Bock et al., 2013, García-Villalba et al., 2014). De Bock et al. also showed that the bioavailability of oleuropein metabolites can be increased when administered in liquid form rather than capsules. Dose-response experiments for oleuropein aglycone in this work showed initial effects on mitochondrial Ca^{2+} uptake with 1 µM oleuropein aglycone, which is promising in light of ongoing human studies. Nevertheless, this limitation of bioavailability could be further addressed by testing the administration of oleuropein and its metabolites together with probiotics, which could potentially increase bioavailability.

MCU is a prime target for therapeutic intervention because it not only directly affects mitochondrial Ca^{2+} status, but also influences redox balance in mitochondria by promoting the reduction of thiol groups, which has been associated with various physiological benefits *in vitro* and *in vivo*, and by affecting energy metabolism and muscle performance. With the elucidation of the molecular mechanism of natural MCU activators, this research area offers promising avenues for treatment options that can be extended to cancer, cardiovascular and neurodegenerative research. Similarly, this natural compound-based approach offers a promising alternative or complement to pharmacological modulation of mitochondria. The latter has been proposed in three ways (Smith et al., 2012):

1) Direct drug accumulation in mitochondria (e.g. TPP moieties linked to a drug, Szeto–Schiller (SS) peptides, and mitochondrial-penetrating peptides (MPP)).

2) Non-targeted mitochondrial drugs (e.g. Cyclosporin A, which inhibits cyclophilin D and prevents opening of the MPTP).
3) Drugs that act outside of mitochondria and affect mitochondrial function by regulating transcription factors and their coactivators or kinases (e.g. AICAR, an AMPK agonist that stimulates mitochondrial biogenesis).

TPP-linked compounds have been tested *in vivo* in rodents and even in phase II of a human study (Snow et al., 2010, Gane et al., 2010) and have been shown to work through different modes of administration, including oral ingestion, intraperitoneal (IP), intravenous (IV) injection and eye drops, or ex vivo through organ infusion (Smith et al., 2012). Furthermore, oral administration of CsA showed beneficial effects in patients suffering from Bethlem myopathy and Ullrich congenital muscular dystrophy (Merlini and Bernardi, 2008), which are caused by a mutation in the collagen IV gene. These study results show promising ways to deliver and personalize mitochondria-targeted agents. Although progress in the field of mitochondria-targeted medicine is increasing, there are still some hurdles to overcome. One major problem is organ specificity: agents targeting mitochondria tend to accumulate in mitochondria-rich tissues, but even there they do not distribute evenly throughout the body, and as mentioned earlier, uncontrolled accumulation of TPP-linked compounds could disrupt mitochondrial $\Delta\Psi m$ and lead to disturbances in energy metabolism.

As highlighted in this work, mitochondrial function has a tremendous impact on the interface of physiology and pathology. Mitochondrial Ca^{2+} homeostasis, ATP synthesis, and redox biology have been identified as metabolic pillars that can stabilize or weaken each other. In the latter case, this can lead to cell death, either directly through impaired mitochondria or through pathological foci arising outside the mitochondria in diseases such as cancer, cardiovascular disease, myopathies, and diabetes. Hopefully, the future will reveal the potential of MCU activators and MCU inhibitors and whether it will be possible to achieve tissue-specific applications that ensure targeted and controlled accumulation of natural compounds that exert positive effects on human skeletal muscle function.

Section 6: References

ABELLAN VAN KAN, G. 2009. Epidemiology and consequences of sarcopenia. *JNHA - The Journal of Nutrition, Health and Aging,* 13**,** 708-712.

ADHIKARI, A., MONDAL, S., CHATTERJEE, T., DAS, M., BISWAS, P., GHOSH, R., DARBAR, S., ALESSA, H., ALTHAKAFY, J. T., SAYQAL, A., AHMED, S. A., DAS, A. K., BHATTACHARYYA, M. & PAL, S. K. 2021. Redox nanomedicine ameliorates chronic kidney disease (CKD) by mitochondrial reconditioning in mice. *Communications Biology,* 4**,** 1013.

AHAMAD, J., TOUFEEQ, I., KHAN, M. A., AMEEN, M. S. M., ANWER, E. T., UTHIRAPATHY, S., MIR, S. R. & AHMAD, J. 2019. Oleuropein: A natural antioxidant molecule in the treatment of metabolic syndrome. *Phytother Res,* 33**,** 3112-3128.

AKTERIN, S., COWBURN, R. F., MIRANDA-VIZUETE, A., JIMÉNEZ, A., BOGDANOVIC, N., WINBLAD, B. & CEDAZO-MINGUEZ, A. 2006. Involvement of glutaredoxin-1 and thioredoxin-1 in beta-amyloid toxicity and Alzheimer's disease. *Cell Death Differ,* 13**,** 1454-65.

ALEVRIADOU, B. R., PATEL, A., NOBLE, M., GHOSH, S., GOHIL, V. M., STATHOPULOS, P. B. & MADESH, M. 2021. Molecular nature and physiological role of the mitochondrial calcium uniporter channel. *American Journal of Physiology-Cell Physiology,* 320**,** C465-C482.

ALLEN, J. G. & TESSEM, J. S. 2022. Ca(2+) Sensors Assemble: Function of the MCU Complex in the Pancreatic Beta Cell. *Cells,* 11**,** 1993.

ÁLVAREZ-ILLERA, P., GARCÍA-CASAS, P., FONTERIZ, R. I., MONTERO, M. & ALVAREZ, J. 2020. Mitochondrial Ca2+ Dynamics in MCU Knockout C. elegans Worms. *International Journal of Molecular Sciences,* 21**,** 8622.

ALWAY, S. E. 2019. Chapter 27 - Antioxidants and Polyphenols Mediate Mitochondrial Mediated Muscle Death Signaling in Sarcopenia. *In:* WALRAND, S. (ed.) *Nutrition and Skeletal Muscle.* Academic Press.

ALWAY, S. E., MYERS, M. J. & MOHAMED, J. S. 2014. Regulation of Satellite Cell Function in Sarcopenia. *Frontiers in Aging Neuroscience,* 6.

ANSARI, M. A. & SCHEFF, S. W. 2010. Oxidative stress in the progression of Alzheimer disease in the frontal cortex. *J Neuropathol Exp Neurol,* 69**,** 155-67.

ANTONY, A. N., PAILLARD, M., MOFFAT, C., JUSKEVICIUTE, E., CORRENTI, J., BOLON, B., RUBIN, E., CSORDÁS, G., SEIFERT, E. L., HOEK, J. B. & HAJNÓCZKY, G. 2016. MICU1 regulation of mitochondrial Ca(2+) uptake dictates survival and tissue regeneration. *Nat Commun,* 7**,** 10955.

ARACENA-PARKS, P., GOONASEKERA, S. A., GILMAN, C. P., DIRKSEN, R. T., HIDALGO, C. & HAMILTON, S. L. 2006. Identification of cysteines involved in S-nitrosylation, S-glutathionylation, and oxidation to disulfides in ryanodine receptor type 1. *J Biol Chem,* 281**,** 40354-68.

ARDUINO, D. M. & PEROCCHI, F. 2018. Pharmacological modulation of mitochondrial calcium homeostasis. *The Journal of physiology,* 596**,** 2717-2733.

BARBA, F. J., ESTEVE, M. J. & FRÍGOLA, A. 2014. Chapter 11 - Bioactive Components from Leaf Vegetable Products. *In:* ATTA UR, R. (ed.) *Studies in Natural Products Chemistry.* Elsevier.

BARBARO, B., TOIETTA, G., MAGGIO, R., ARCIELLO, M., TAROCCHI, M., GALLI, A. & BALSANO, C. 2014. Effects of the Olive-Derived Polyphenol Oleuropein on Human Health. *International Journal of Molecular Sciences,* 15**,** 18508-18524.

BARCLAY, J. K. & HANSEL, M. 1991. Free radicals may contribute to oxidative skeletal muscle fatigue. *Can J Physiol Pharmacol,* 69**,** 279-84.

BASSO, E., RIGOTTO, G., ZUCCHETTI, A. E. & POZZAN, T. 2018. Slow activation of fast mitochondrial Ca(2+) uptake by cytosolic Ca(2). *The Journal of biological chemistry,* 293**,** 17081-17094.

BAUGHMAN, J. M., PEROCCHI, F., GIRGIS, H. S., PLOVANICH, M., BELCHER-TIMME, C. A., SANCAK, Y., BAO, X. R., STRITTMATTER, L., GOLDBERGER, O., BOGORAD, R. L., KOTELIANSKY, V. & MOOTHA, V. K.

2011. Integrative genomics identifies MCU as an essential component of the mitochondrial calcium uniporter. *Nature,* 476**,** 341-345.

BAZOTI, F. N., BERGQUIST, J., MARKIDES, K. E. & TSARBOPOULOS, A. 2006. Noncovalent interaction between amyloid-β-peptide (1–40) and oleuropein studied by electrospray ionization mass spectrometry. *Journal of the American Society for Mass Spectrometry,* 17**,** 568-575.

BEAS-JIMÉNEZ, J., LOPEZ-LLUCH, G., A, I., C, A., RODRIGUEZ BIES, E. & B, P. 2011. Sarcopenia: Implications of physical exercise in its pathophysiology, prevention and treatment. *Revista Andaluza de Medicina del Deporte,* 4**,** 158-66.

BERMONT, F., HERMANT, A., BENNINGA, R., CHABERT, C., JACOT, G., SANTO-DOMINGO, J., KRAUS, M. R.-C., FEIGE, J. N. & DE MARCHI, U. 2020. Targeting Mitochondrial Calcium Uptake with the Natural Flavonol Kaempferol, to Promote Metabolism/Secretion Coupling in Pancreatic β-cells. *Nutrients,* 12**,** 538.

BERNARDI, P. 1999. Mitochondrial transport of cations: channels, exchangers, and permeability transition. *Physiol Rev,* 79**,** 1127-55.

BERRIDGE, M. J., BOOTMAN, M. D. & LIPP, P. 1998. Calcium--a life and death signal. *Nature,* 395**,** 645-8.

BERRIDGE, M. J., BOOTMAN, M. D. & RODERICK, H. L. 2003. Calcium signalling: dynamics, homeostasis and remodelling. *Nat Rev Mol Cell Biol,* 4**,** 517-29.

BHATTI, J. S., BHATTI, G. K. & REDDY, P. H. 2017. Mitochondrial dysfunction and oxidative stress in metabolic disorders - A step towards mitochondria based therapeutic strategies. *Biochimica et biophysica acta. Molecular basis of disease,* 1863**,** 1066-1077.

BLANCO-BENÍTEZ, M., CALDERÓN-FERNÁNDEZ, A., CANALES-CORTÉS, S., ALEGRE-CORTÉS, E., URIBE-CARRETERO, E., PAREDES-BARQUERO, M., GIMENEZ-BEJARANO, A., DUQUE GONZÁLEZ, G., GÓMEZ-SUAGA, P., ORTEGA-VIDAL, J., SALIDO, S., ALTAREJOS, J., MARTÍNEZ-CHACÓN, G., NISO-SANTANO, M., FUENTES, J. M., GONZÁLEZ-POLO, R. A. & YAKHINE-DIOP, S. M. S. 2022. Biological effects of olive oil phenolic compounds on mitochondria. *Molecular & cellular oncology,* 9**,** 2044263-2044263.

BOENGLER, K., KOSIOL, M., MAYR, M., SCHULZ, R. & ROHRBACH, S. 2017. Mitochondria and ageing: role in heart, skeletal muscle and adipose tissue. *Journal of cachexia, sarcopenia and muscle,* 8**,** 349-369.

BONORA, M., GIORGI, C., BONONI, A., MARCHI, S., PATERGNANI, S., RIMESSI, A., RIZZUTO, R. & PINTON, P. 2013. Subcellular calcium measurements in mammalian cells using jellyfish photoprotein aequorin-based probes. *Nat Protoc,* 8**,** 2105-18.

BOSS, C., BOUCHE, N. & DE MARCHI, U. 2018. Encapsulated Optically Responsive Cell Systems: Toward Smart Implants in Biomedicine. *Advanced Healthcare Materials,* 7**,** 1701148.

BOYMAN, L., WILLIAMS, G. S., KHANANSHVILI, D., SEKLER, I. & LEDERER, W. J. 2013. NCLX: the mitochondrial sodium calcium exchanger. *J Mol Cell Cardiol,* 59**,** 205-13.

BRATIC, A. & LARSSON, N.-G. 2013. The role of mitochondria in aging. *The Journal of Clinical Investigation,* 123**,** 951-957.

BROOME, S. C., WOODHEAD, J. S. T. & MERRY, T. L. 2018. Mitochondria-Targeted Antioxidants and Skeletal Muscle Function. *Antioxidants,* 7**,** 107.

BRUNETTI, G., DI ROSA, G., SCUTO, M., LERI, M., STEFANI, M., SCHMITZ-LINNEWEBER, C., CALABRESE, V. & SAUL, N. 2020. Healthspan Maintenance and Prevention of Parkinson's-like Phenotypes with Hydroxytyrosol and Oleuropein Aglycone in C. elegans. *International journal of molecular sciences,* 21**,** 2588.

CALVANI, R., JOSEPH, A.-M., ADHIHETTY, P. J., MICCHELI, A., BOSSOLA, M., LEEUWENBURGH, C., BERNABEI, R. & MARZETTI, E. 2013. Mitochondrial pathways in sarcopenia of aging and disuse muscle atrophy. *Biological Chemistry,* 394**,** 393-414.

CASABURI, I., PUOCI, F., CHIMENTO, A., SIRIANNI, R., RUGGIERO, C., AVENA, P. & PEZZI, V. 2013. Potential of olive oil phenols as chemopreventive and therapeutic agents against cancer: A review of in vitro studies. *Molecular Nutrition & Food Research,* 57**,** 71-83.

CHANCE, B. & WILLIAMS, G. R. 1956. The respiratory chain and oxidative phosphorylation. *Adv Enzymol Relat Subj Biochem,* 17**,** 65-134.

CHAUDHURI, D., ARTIGA, D. J., ABIRIA, S. A. & CLAPHAM, D. E. 2016. Mitochondrial calcium uniporter regulator 1 (MCUR1) regulates the calcium threshold for the mitochondrial permeability transition. *Proceedings of the National Academy of Sciences of the United States of America,* 113**,** E1872-E1880.

CHEN, L., MAGLIANO, D. J. & ZIMMET, P. Z. 2011. The worldwide epidemiology of type 2 diabetes mellitus--present and future perspectives. *Nat Rev Endocrinol,* 8**,** 228-36.

CHEN, Y.-R., CHEN, C.-L., PFEIFFER, D. R. & ZWEIER, J. L. 2007. Mitochondrial Complex II in the Post-ischemic Heart: OXIDATIVE INJURY AND THE ROLE OF PROTEIN S-GLUTATHIONYLATION*. *Journal of Biological Chemistry,* 282**,** 32640-32654.

CHO, C. S., LEE, S., LEE, G. T., WOO, H. A., CHOI, E. J. & RHEE, S. G. 2010. Irreversible inactivation of glutathione peroxidase 1 and reversible inactivation of peroxiredoxin II by H2O2 in red blood cells. *Antioxid Redox Signal,* 12**,** 1235-46.

CHOUCHANI, E. T., METHNER, C., NADTOCHIY, S. M., LOGAN, A., PELL, V. R., DING, S., JAMES, A. M., COCHEMÉ, H. M., REINHOLD, J., LILLEY, K. S., PARTRIDGE, L., FEARNLEY, I. M., ROBINSON, A. J., HARTLEY, R. C., SMITH, R. A., KRIEG, T., BROOKES, P. S. & MURPHY, M. P. 2013. Cardioprotection by S-nitrosation of a cysteine switch on mitochondrial complex I. *Nat Med,* 19**,** 753-9.

CLAPHAM, D. E. 2007. Calcium Signaling. *Cell,* 131**,** 1047-1058.

CONDE DE LA ROSA, L., GARCÍA-RUIZ, C. & FERNÁNDEZ-CHECA, J. C. 2014. Glutathione in Mammalian Biology. *In:* LAHER, I. (ed.) *Systems Biology of Free Radicals and Antioxidants.* Berlin, Heidelberg: Springer Berlin Heidelberg.

COOPER, A. J. L., PINTO, J. T. & CALLERY, P. S. 2011. Reversible and irreversible protein glutathionylation: biological and clinical aspects. *Expert Opinion on Drug Metabolism & Toxicology,* 7**,** 891-910.

CRUZ-JENTOFT, A. J. & SAYER, A. A. 2019. Sarcopenia. *Lancet,* 393**,** 2636-2646.

D'AUTRÉAUX, B. & TOLEDANO, M. B. 2007. ROS as signalling molecules: mechanisms that generate specificity in ROS homeostasis. *Nature Reviews Molecular Cell Biology,* 8**,** 813-824.

DAVIES, K. J. A., QUINTANILHA, A. T., BROOKS, G. A. & PACKER, L. 1982. Free radicals and tissue damage produced by exercise. *Biochemical and Biophysical Research Communications,* 107**,** 1198-1205.

DE BOCK, M., THORSTENSEN, E. B., DERRAIK, J. G., HENDERSON, H. V., HOFMAN, P. L. & CUTFIELD, W. S. 2013. Human absorption and metabolism of oleuropein and hydroxytyrosol ingested as olive (Olea europaea L.) leaf extract. *Mol Nutr Food Res,* 57**,** 2079-85.

DE MARIO, A., TOSATTO, A., HILL, J. M., KRISTON-VIZI, J., KETTELER, R., VECELLIO REANE, D., CORTOPASSI, G., SZABADKAI, G., RIZZUTO, R. & MAMMUCARI, C. 2021. Identification and functional validation of FDA-approved positive and negative modulators of the mitochondrial calcium uniporter. *Cell Reports,* 35**,** 109275.

DE STEFANI, D., PATRON, M. & RIZZUTO, R. 2015. Structure and function of the mitochondrial calcium uniporter complex. *Biochimica et Biophysica Acta (BBA) - Molecular Cell Research,* 1853**,** 2006-2011.

DE STEFANI, D., RAFFAELLO, A., TEARDO, E., SZABÒ, I. & RIZZUTO, R. 2011. A forty-kilodalton protein of the inner membrane is the mitochondrial calcium uniporter. *Nature,* 476**,** 336-340.

DEBATTISTI, V., HORN, A., SINGH, R., SEIFERT, E. L., HOGARTH, M. W., MAZALA, D. A., HUANG, K. T., HORVATH, R., JAISWAL, J. K. & HAJNOCZKY, G. 2019. Dysregulation of Mitochondrial Ca(2+) Uptake and Sarcolemma Repair Underlie Muscle Weakness and Wasting in Patients and Mice Lacking MICU1. *Cell Rep,* 29**,** 1274-1286.e6.

DENTON, R. M. 2009. Regulation of mitochondrial dehydrogenases by calcium ions. *Biochim Biophys Acta,* 1787**,** 1309-16.

DEPONTE, M. & LILLIG, C. H. 2015. Enzymatic control of cysteinyl thiol switches in proteins. *Biol Chem,* 396**,** 401-13.

DHANASEKARAN, S., VENUGOPAL, D., AL-DAYAN, N., RAVINAYAGAM, V. & MOHAMMED, A. A. 2020. Emerging insights into mitochondria-specific targeting and drug delivering strategies: Recent milestones and therapeutic implications. *Saudi journal of biological sciences,* 27**,** 3581-3592.

DI MARCO, G., VALLESE, F., JOURDE, B., BERGSDORF, C., STURLESE, M., DE MARIO, A., TECHER-ETIENNE, V., HAASEN, D., OBERHAUSER, B., SCHLEEGER, S., MINETTI, G., MORO, S., RIZZUTO, R., DE STEFANI, D., FORNARO, M. & MAMMUCARI, C. 2020. A High-Throughput Screening Identifies MICU1 Targeting Compounds. *Cell Rep,* 30**,** 2321-2331.e6.

DIMAURO, I., PEARSON, T., CAPOROSSI, D. & JACKSON, M. J. 2012. In vitro susceptibility of thioredoxins and glutathione to redox modification and aging-related changes in skeletal muscle. *Free radical biology & medicine,* 53**,** 2017-2027.

DONG, Z., SHANMUGHAPRIYA, S., TOMAR, D., SIDDIQUI, N., LYNCH, S., NEMANI, N., BREVES, S. L., ZHANG, X., TRIPATHI, A., PALANIAPPAN, P., RIITANO, M. F., WORTH, A. M., SEELAM, A., CARVALHO, E., SUBBIAH, R., JAÑA, F., SOBOLOFF, J., PENG, Y., CHEUNG, J. Y., JOSEPH, S. K., CAPLAN, J., RAJAN, S., STATHOPULOS, P. B. & MADESH, M. 2017. Mitochondrial Ca(2+) Uniporter Is a Mitochondrial Luminal Redox Sensor that Augments MCU Channel Activity. *Mol Cell,* 65**,** 1014-1028.e7.

DRÖSE, S., BRANDT, U. & WITTIG, I. 2014. Mitochondrial respiratory chain complexes as sources and targets of thiol-based redox-regulation. *Biochim Biophys Acta,* 1844**,** 1344-54.

DUTTON, G. R. & LEWIS, C. E. 2015. The Look AHEAD Trial: Implications for Lifestyle Intervention in Type 2 Diabetes Mellitus. *Prog Cardiovasc Dis,* 58**,** 69-75.

ESPINOSA-DIEZ, C., MIGUEL, V., MENNERICH, D., KIETZMANN, T., SÁNCHEZ-PÉREZ, P., CADENAS, S. & LAMAS, S. 2015. Antioxidant responses and cellular adjustments to oxidative stress. *Redox Biology,* 6**,** 183-197.

ESSMANN, U., PERERA, L., BERKOWITZ, M. L., DARDEN, T., LEE, H. & PEDERSEN, L. G. 1995. A smooth particle mesh Ewald method. *The Journal of chemical physics,* 103**,** 8577-8593.

FENO, S., BUTERA, G., VECELLIO REANE, D., RIZZUTO, R. & RAFFAELLO, A. 2019. Crosstalk between Calcium and ROS in Pathophysiological Conditions. *Oxid Med Cell Longev,* 2019**,** 9324018.

FOSKETT, J. K. & MADESH, M. 2014a. Regulation of the mitochondrial Ca(2+) uniporter by MICU1 and MICU2. *Biochem Biophys Res Commun,* 449**,** 377-83.

FOSKETT, J. K. & MADESH, M. 2014b. Regulation of the mitochondrial Ca(2+) uniporter by MICU1 and MICU2. *Biochemical and biophysical research communications,* 449**,** 377-383.

FRONTERA, W. R. & OCHALA, J. 2015. Skeletal muscle: a brief review of structure and function. *Calcif Tissue Int,* 96**,** 183-95.

FROSALI, S., LEONINI, A., ETTORRE, A., DI MAIO, G., NUTI, S., TAVARINI, S., DI SIMPLICIO, P. & DI STEFANO, A. 2009. Role of intracellular calcium and S-glutathionylation in cell death induced by a mixture of isothiazolinones in HL60 cells. *Biochimica et Biophysica Acta (BBA) - Molecular Cell Research,* 1793**,** 572-583.

GANE, E. J., WEILERT, F., ORR, D. W., KEOGH, G. F., GIBSON, M., LOCKHART, M. M., FRAMPTON, C. M., TAYLOR, K. M., SMITH, R. A. & MURPHY, M. P. 2010. The mitochondria-targeted anti-oxidant mitoquinone decreases liver damage in a phase II study of hepatitis C patients. *Liver Int,* 30**,** 1019-26.

GAO, X.-H., LI, L., PARISIEN, M., WU, J., BEDERMAN, I., GAO, Z., KROKOWSKI, D., CHIRIELEISON, S. M., ABBOTT, D., WANG, B., ARVAN, P., CAMERON, M., CHANCE, M., WILLARD, B. & HATZOGLOU, M. 2020. Discovery of a Redox Thiol Switch: Implications for Cellular Energy Metabolism. *Molecular & cellular proteomics : MCP,* 19**,** 852-870.

GARCÍA-PRAT, L., MARTÍNEZ-VICENTE, M., PERDIGUERO, E., ORTET, L., RODRÍGUEZ-UBREVA, J., REBOLLO, E., RUIZ-BONILLA, V., GUTARRA, S., BALLESTAR, E., SERRANO, A. L., SANDRI, M. & MUÑOZ-CÁNOVES, P. 2016. Autophagy maintains stemness by preventing senescence. *Nature,* 529**,** 37-42.

GARCÍA-VILLALBA, R., LARROSA, M., POSSEMIERS, S., TOMÁS-BARBERÁN, F. A. & ESPÍN, J. C. 2014. Bioavailability of phenolics from an oleuropein-rich olive (Olea europaea) leaf extract and its acute effect on plasma antioxidant status: comparison between pre- and postmenopausal women. *Eur J Nutr,* 53**,** 1015-27.

GHERARDI, G., DE MARIO, A. & MAMMUCARI, C. 2021. Chapter Six - The mitochondrial calcium homeostasis orchestra plays its symphony: Skeletal muscle is the guest of honor. *In:* MARCHI, S. & GALLUZZI, L. (eds.) *International Review of Cell and Molecular Biology.* Academic Press.

GHERARDI, G., DI MARCO, G., RIZZUTO, R. & MAMMUCARI, C. 2019a. Crosstalk between Mitochondrial Ca²⁺ Uptake and Autophagy in Skeletal Muscle. *Oxidative Medicine and Cellular Longevity,* 2019**,** 1845321.

GHERARDI, G., NOGARA, L., CICILIOT, S., FADINI, G. P., BLAAUW, B., BRAGHETTA, P., BONALDO, P., DE STEFANI, D., RIZZUTO, R. & MAMMUCARI, C. 2019b. Loss of mitochondrial calcium uniporter rewires skeletal muscle metabolism and substrate preference. *Cell Death Differ,* 26**,** 362-381.

GLANCY, B. & BALABAN, R. S. 2012. Role of mitochondrial Ca2+ in the regulation of cellular energetics. *Biochemistry,* 51**,** 2959-73.

GRANATIERO, V., DE STEFANI, D. & RIZZUTO, R. 2017. Mitochondrial Calcium Handling in Physiology and Disease. *Adv Exp Med Biol,* 982**,** 25-47.

GRIFFITHS, I. W. 1997. J. J. Thomson — the Centenary of His Discovery of the Electron and of His Invention of Mass Spectrometry. *Rapid Communications in Mass Spectrometry,* 11**,** 2-16.

HALESTRAP, A. P. 2009. What is the mitochondrial permeability transition pore? *Journal of Molecular and Cellular Cardiology,* 46**,** 821-831.

HAMDI, H. K. & CASTELLON, R. 2005. Oleuropein, a non-toxic olive iridoid, is an anti-tumor agent and cytoskeleton disruptor. *Biochemical and Biophysical Research Communications,* 334**,** 769-778.

HANDY, D. E. & LOSCALZO, J. 2012. Redox regulation of mitochondrial function. *Antioxid Redox Signal,* 16**,** 1323-67.

HANSON, G. T., AGGELER, R., OGLESBEE, D., CANNON, M., CAPALDI, R. A., TSIEN, R. Y. & REMINGTON, S. J. 2004. Investigating Mitochondrial Redox Potential with Redox-sensitive Green Fluorescent Protein Indicators *. *Journal of Biological Chemistry,* 279**,** 13044-13053.

HARMAN, D. 2002. Aging: A Theory Based on Free Radical and Radiation Chemistry. *Science of Aging Knowledge Environment,* 2002**,** cp14-cp14.

HARPER, C., GOPALAN, V. & GOH, J. 2021. Exercise rescues mitochondrial coupling in aged skeletal muscle: a comparison of different modalities in preventing sarcopenia. *Journal of Translational Medicine,* 19**,** 71.

HARRINGTON, J. L. & MURPHY, E. 2015. The mitochondrial calcium uniporter: Mice can live and die without it. *Journal of Molecular and Cellular Cardiology,* 78**,** 46-53.

HENRÍQUEZ-OLGUIN, C., KNUDSEN, J. R., RAUN, S. H., LI, Z., DALBRAM, E., TREEBAK, J. T., SYLOW, L., HOLMDAHL, R., RICHTER, E. A., JAIMOVICH, E. & JENSEN, T. E. 2019. Cytosolic ROS production by NADPH oxidase 2 regulates muscle glucose uptake during exercise. *Nature Communications,* 10**,** 4623.

HENRIQUEZ-OLGUIN, C., MENESES-VALDES, R. & JENSEN, T. E. 2020. Compartmentalized muscle redox signals controlling exercise metabolism – Current state, future challenges. *Redox Biology,* 35**,** 101473.

HERRMANN, J. M. & DICK, T. P. 2012. Redox Biology on the rise. *Biological Chemistry,* 393**,** 999-1004.

HOLLOSZY, J. O. 1967. Biochemical Adaptations in Muscle: EFFECTS OF EXERCISE ON MITOCHONDRIAL OXYGEN UPTAKE AND RESPIRATORY ENZYME ACTIVITY IN SKELETAL MUSCLE. *Journal of Biological Chemistry,* 242**,** 2278-2282.

HORN, A., VAN DER MEULEN, J. H., DEFOUR, A., HOGARTH, M., SREETAMA, S. C., REED, A., SCHEFFER, L., CHANDEL, N. S. & JAISWAL, J. K. 2017. Mitochondrial redox signaling enables repair of injured skeletal muscle cells. *Sci Signal,* 10.

HUERTAS, J. R., CASUSO, R. A., AGUSTÍN, P. H. & COGLIATI, S. 2019. Stay Fit, Stay Young: Mitochondria in Movement: The Role of Exercise in the New Mitochondrial Paradigm. *Oxidative medicine and cellular longevity,* 2019**,** 7058350-7058350.

IPPOLITO, L., GIANNONI, E., CHIARUGI, P. & PARRI, M. 2020. Mitochondrial Redox Hubs as Promising Targets for Anticancer Therapy. *Front Oncol,* 10**,** 256.

JACKSON, M. J., POLLOCK, N., STAUNTON, C., JONES, S. & MCARDLE, A. 2022. Redox Control of Signalling Responses to Contractile Activity and Ageing in Skeletal Muscle. *Cells,* 11**,** 1698.

JADIYA, P., KOLMETZKY, D. W., TOMAR, D., DI MECO, A., LOMBARDI, A. A., LAMBERT, J. P., LUONGO, T. S., LUDTMANN, M. H., PRATICÒ, D. & ELROD, J. W. 2019. Impaired mitochondrial calcium efflux contributes to disease progression in models of Alzheimer's disease. *Nature Communications,* 10**,** 3885.

JENKINS, R. R. 1988. Free Radical Chemistry. *Sports Medicine,* 5**,** 156-170.

JI, L. L., DILLON, D. & WU, E. 1990. Alteration of antioxidant enzymes with aging in rat skeletal muscle and liver. *American Journal of Physiology-Regulatory, Integrative and Comparative Physiology,* 258**,** R918-R923.

JI, L. L., KANG, C. & ZHANG, Y. 2016. Exercise-induced hormesis and skeletal muscle health. *Free Radical Biology and Medicine,* 98**,** 113-122.

JOHNSON, D. & NEHRKE, K. 2010. Mitochondrial fragmentation leads to intracellular acidification in Caenorhabditis elegans and mammalian cells. *Molecular biology of the cell,* 21**,** 2191-2201.

JONES, D. P. 2002. Redox potential of GSH/GSSG couple: assay and biological significance. *Methods Enzymol,* 348**,** 93-112.

KAMER, K. J., GRABAREK, Z. & MOOTHA, V. K. 2017. High-affinity cooperative Ca(2+) binding by MICU1-MICU2 serves as an on-off switch for the uniporter. *EMBO reports,* 18**,** 1397-1411.

KAMER, K. J., JIANG, W., KAUSHIK, V. K., MOOTHA, V. K. & GRABAREK, Z. 2019. Crystal structure of MICU2 and comparison with MICU1 reveal insights into the uniporter gating mechanism. *Proceedings of the National Academy of Sciences,* 116**,** 3546-3555.

KARLSTAD, J., SUN, Y. & SINGH, B. B. 2012. Ca(2+) signaling: an outlook on the characterization of Ca(2+) channels and their importance in cellular functions. *Advances in experimental medicine and biology,* 740**,** 143-157.

KEMP, M., GO, Y.-M. & JONES, D. P. 2008. Nonequilibrium thermodynamics of thiol/disulfide redox systems: A perspective on redox systems biology. *Free Radical Biology and Medicine,* 44**,** 921-937.

KIM, A. 2014. A panoramic overview of mitochondria and mitochondrial redox biology. *Toxicological research,* 30**,** 221-234.

KOHLSCHMIDT, N., ELBRACHT, M., CZECH, A., HÄUSLER, M., PHAN, V., TÖPF, A., HUANG, K.-T., BARTOK, A., EGGERMANN, K., ZIPPEL, S., EGGERMANN, T., FREIER, E., GROß, C., LOCHMÜLLER, H., HORVATH, R., HAJNÓCZKY, G., WEIS, J. & ROOS, A. 2021. Molecular pathophysiology of human MICU1 deficiency. *Neuropathology and Applied Neurobiology,* 47**,** 840-855.

KOKOSZKA, J. E., WAYMIRE, K. G., LEVY, S. E., SLIGH, J. E., CAI, J., JONES, D. P., MACGREGOR, G. R. & WALLACE, D. C. 2004. The ADP/ATP translocator is not essential for the mitochondrial permeability transition pore. *Nature,* 427**,** 461-465.

KONDO, H., NAKAGAKI, I., SASAKI, S., HORI, S. & ITOKAWA, Y. 1993. Mechanism of oxidative stress in skeletal muscle atrophied by immobilization. *Am J Physiol,* 265**,** E839-44.

KOOPMAN, M., MICHELS, H., DANCY, B. M., KAMBLE, R., MOUCHIROUD, L., AUWERX, J., NOLLEN, E. A. & HOUTKOOPER, R. H. 2016a. A screening-based platform for the assessment of cellular respiration in Caenorhabditis elegans. *Nat Protoc,* 11**,** 1798-816.

KOOPMAN, M., MICHELS, H., DANCY, B. M., KAMBLE, R., MOUCHIROUD, L., AUWERX, J., NOLLEN, E. A. A. & HOUTKOOPER, R. H. 2016b. A screening-based platform for the assessment of cellular respiration in Caenorhabditis elegans. *Nature protocols,* 11**,** 1798-1816.

KORB, O., STÜTZLE, T. & EXNER, T. E. 2009. Empirical scoring functions for advanced protein-ligand docking with PLANTS. *J Chem Inf Model,* 49**,** 84-96.

KOROTKOV, S. M. & NOVOZHILOV, A. V. 2022. The Joint Influence of Tl(+) and Thiol-Modifying Agents on Rat Liver Mitochondrial Parameters In Vitro. *Int J Mol Sci,* 23.

KOTIADIS, V. N., DUCHEN, M. R. & OSELLAME, L. D. 2014. Mitochondrial quality control and communications with the nucleus are important in maintaining mitochondrial function and cell health. *Biochimica et Biophysica Acta (BBA) - General Subjects,* 1840**,** 1254-1265.

KREBS, J., AGELLON, L. B. & MICHALAK, M. 2015. Ca2+ homeostasis and endoplasmic reticulum (ER) stress: An integrated view of calcium signaling. *Biochemical and Biophysical Research Communications,* 460**,** 114-121.

KUMARI, A. 2018. Chapter 3 - Electron Transport Chain. *In:* KUMARI, A. (ed.) *Sweet Biochemistry.* Academic Press.

KWONG, JENNIFER Q., LU, X., CORRELL, ROBERT N., SCHWANEKAMP, JENNIFER A., VAGNOZZI, RONALD J., SARGENT, MICHELLE A., YORK, ALLEN J., ZHANG, J., BERS, DONALD M. & MOLKENTIN, JEFFERY D. 2015. The Mitochondrial Calcium Uniporter Selectively Matches Metabolic Output to Acute Contractile Stress in the Heart. *Cell Reports,* 12**,** 15-22.

LANDI, F., MARZETTI, E., MARTONE, A. M., BERNABEI, R. & ONDER, G. 2014. Exercise as a remedy for sarcopenia. *Curr Opin Clin Nutr Metab Care,* 17**,** 25-31.

LANE, N. 2011. The Costs of Breathing. *Science,* 334**,** 184-185.

LE MOAL, E., PIALOUX, V., JUBAN, G., GROUSSARD, C., ZOUHAL, H., CHAZAUD, B. & MOUNIER, R. 2016. Redox Control of Skeletal Muscle Regeneration. *Antioxidants & Redox Signaling,* 27**,** 276-310.

LE MOAL, E., PIALOUX, V., JUBAN, G., GROUSSARD, C., ZOUHAL, H., CHAZAUD, B. & MOUNIER, R. 2017. Redox Control of Skeletal Muscle Regeneration. *Antioxidants & redox signaling,* 27**,** 276-310.

LEE, Y., MIN, C. K., KIM, T. G., SONG, H. K., LIM, Y., KIM, D., SHIN, K., KANG, M., KANG, J. Y., YOUN, H. S., LEE, J. G., AN, J. Y., PARK, K. R., LIM, J. J., KIM, J. H., KIM, J. H., PARK, Z. Y., KIM, Y. S., WANG, J., KIM, D. H. & EOM, S. H. 2015. Structure and function of the N-terminal domain of the human mitochondrial calcium uniporter. *EMBO Rep,* 16**,** 1318-33.

LEWIS-SMITH, D., KAMER, K. J., GRIFFIN, H., CHILDS, A. M., PYSDEN, K., TITOV, D., DUFF, J., PYLE, A., TAYLOR, R. W., YU-WAI-MAN, P., RAMESH, V., HORVATH, R., MOOTHA, V. K. & CHINNERY, P. F. 2016. Homozygous deletion in MICU1 presenting with fatigue and lethargy in childhood. *Neurol Genet,* 2**,** e59.

LI, H. 2019. Mitochondria and the Future of Medicine: The Key to Understanding Disease, Chronic Illness, Aging, and Life Itself. *The Yale Journal of Biology and Medicine,* 92**,** 569-570.

LIAGHATI, A., PILEGGI, C. A., PARMAR, G., PATTEN, D. A., HADZIMUSTAFIC, N., CUILLERIER, A., MENZIES, K. J., BURELLE, Y. & HARPER, M.-E. 2021. Grx2 Regulates Skeletal Muscle Mitochondrial Structure and Autophagy. *Frontiers in Physiology,* 12.

LIN, J., WU, H., TARR, P. T., ZHANG, C.-Y., WU, Z., BOSS, O., MICHAEL, L. F., PUIGSERVER, P., ISOTANI, E., OLSON, E. N., LOWELL, B. B., BASSEL-DUBY, R. & SPIEGELMAN, B. M. 2002. Transcriptional co-activator PGC-1α drives the formation of slow-twitch muscle fibres. *Nature,* 418**,** 797-801.

LINDAHL, M., MATA-CABANA, A. & KIESELBACH, T. 2011. The Disulfide Proteome and Other Reactive Cysteine Proteomes: Analysis and Functional Significance. *Antioxidants & Redox Signaling,* 14**,** 2581-2642.

LIU, J. C., LIU, J., HOLMSTRÖM, K. M., MENAZZA, S., PARKS, R. J., FERGUSSON, M. M., YU, Z. X., SPRINGER, D. A., HALSEY, C., LIU, C., MURPHY, E. & FINKEL, T. 2016. MICU1 Serves as a Molecular Gatekeeper to Prevent In Vivo Mitochondrial Calcium Overload. *Cell Rep,* 16**,** 1561-1573.

LOGAN, C. V., SZABADKAI, G., SHARPE, J. A., PARRY, D. A., TORELLI, S., CHILDS, A. M., KRIEK, M., PHADKE, R., JOHNSON, C. A., ROBERTS, N. Y., BONTHRON, D. T., PYSDEN, K. A., WHYTE, T., MUNTEANU, I., FOLEY, A. R., WHEWAY, G., SZYMANSKA, K., NATARAJAN, S., ABDELHAMED, Z. A., MORGAN, J. E., ROPER, H., SANTEN, G. W., NIKS, E. H., VAN DER POL, W. L., LINDHOUT, D., RAFFAELLO, A., DE STEFANI, D., DEN DUNNEN, J. T., SUN, Y., GINJAAR, I., SEWRY, C. A., HURLES, M., RIZZUTO, R., DUCHEN, M. R., MUNTONI, F. & SHERIDAN, E. 2014. Loss-of-function mutations in MICU1 cause a brain and muscle disorder linked to primary alterations in mitochondrial calcium signaling. *Nat Genet,* 46**,** 188-93.

LUONGO, T. S., LAMBERT, J. P., YUAN, A., ZHANG, X., GROSS, P., SONG, J., SHANMUGHAPRIYA, S., GAO, E., JAIN, M., HOUSER, S. R., KOCH, W. J., CHEUNG, J. Y., MADESH, M. & ELROD, J. W. 2015. The Mitochondrial Calcium Uniporter Matches Energetic Supply with Cardiac Workload during Stress and Modulates Permeability Transition. *Cell Rep,* 12**,** 23-34.

MAILLOUX, R. J. 2020. Protein S-glutathionylation reactions as a global inhibitor of cell metabolism for the desensitization of hydrogen peroxide signals. *Redox Biology,* 32**,** 101472.

MAILLOUX, R. J., ADJEITEY, C. N., XUAN, J. Y. & HARPER, M. E. 2012. Crucial yet divergent roles of mitochondrial redox state in skeletal muscle vs. brown adipose tissue energetics. *Faseb j,* 26**,** 363-75.

MAILLOUX, R. J., JIN, X. & WILLMORE, W. G. 2014. Redox regulation of mitochondrial function with emphasis on cysteine oxidation reactions. *Redox Biol,* 2**,** 123-39.

MAILLOUX, R. J. & TREBERG, J. R. 2016. Protein S-glutathionlyation links energy metabolism to redox signaling in mitochondria. *Redox Biology,* 8**,** 110-118.

MALLILANKARAMAN, K., CÁRDENAS, C., DOONAN, P. J., CHANDRAMOORTHY, H. C., IRRINKI, K. M., GOLENÁR, T., CSORDÁS, G., MADIREDDI, P., YANG, J., MÜLLER, M., MILLER, R., KOLESAR, J. E., MOLGÓ, J., KAUFMAN, B., HAJNÓCZKY, G., FOSKETT, J. K. & MADESH, M. 2012a. MCUR1 is an essential component of mitochondrial Ca2+ uptake that regulates cellular metabolism. *Nature cell biology,* 14**,** 1336-1343.

MALLILANKARAMAN, K., DOONAN, P., CÁRDENAS, C., CHANDRAMOORTHY, H. C., MÜLLER, M., MILLER, R., HOFFMAN, N. E., GANDHIRAJAN, R. K., MOLGÓ, J., BIRNBAUM, M. J., ROTHBERG, B. S., MAK, D.-O. D., FOSKETT, J. K. & MADESH, M. 2012b. MICU1 is an essential gatekeeper for MCU-mediated mitochondrial Ca(2+) uptake that regulates cell survival. *Cell,* 151**,** 630-644.

MAMMUCARI, C., GHERARDI, G. & RIZZUTO, R. 2017. Structure, Activity Regulation, and Role of the Mitochondrial Calcium Uniporter in Health and Disease. *Frontiers in Oncology,* 7.

MAMMUCARI, C., GHERARDI, G., ZAMPARO, I., RAFFAELLO, A., BONCOMPAGNI, S., CHEMELLO, F., CAGNIN, S., BRAGA, A., ZANIN, S., PALLAFACCHINA, G., ZENTILIN, L., SANDRI, M., DE STEFANI, D., PROTASI, F., LANFRANCHI, G. & RIZZUTO, R. 2015. The Mitochondrial Calcium Uniporter Controls Skeletal Muscle Trophism In Vivo. *Cell Reports,* 10**,** 1269-1279.

MAMMUCARI, C., RAFFAELLO, A., VECELLIO REANE, D., GHERARDI, G., DE MARIO, A. & RIZZUTO, R. 2018. Mitochondrial calcium uptake in organ physiology: from molecular mechanism to animal models. *Pflügers Archiv - European Journal of Physiology,* 470**,** 1165-1179.

MÅRTENSSON, J. & MEISTER, A. 1989. Mitochondrial damage in muscle occurs after marked depletion of glutathione and is prevented by giving glutathione monoester. *Proceedings of the National Academy of Sciences,* 86**,** 471-475.

MARZETTI, E., CALVANI, R., CESARI, M., BUFORD, T. W., LORENZI, M., BEHNKE, B. J. & LEEUWENBURGH, C. 2013. Mitochondrial dysfunction and sarcopenia of aging: from signaling pathways to clinical trials. *Int J Biochem Cell Biol,* 45**,** 2288-301.

MAZUMDER, M., PADHAN, N., BHATTACHARYA, A. & GOURINATH, S. 2014. Prediction and analysis of canonical EF hand loop and qualitative estimation of Ca(2)(+) binding affinity. *PLoS One,* 9**,** e96202.

MCDONAGH, B., SAKELLARIOU, G. K., SMITH, N. T., BROWNRIDGE, P. & JACKSON, M. J. 2014. Differential Cysteine Labeling and Global Label-Free Proteomics Reveals an Altered Metabolic State in Skeletal Muscle Aging. *Journal of Proteome Research,* 13**,** 5008-5021.

MCLAIN, A. L., CORMIER, P. J., KINTER, M. & SZWEDA, L. I. 2013. Glutathionylation of α-ketoglutarate dehydrogenase: The chemical nature and relative susceptibility of the cofactor lipoic acid to modification. *Free Radical Biology and Medicine,* 61**,** 161-169.

MERLINI, L. & BERNARDI, P. 2008. Therapy of collagen VI-related myopathies (Bethlem and Ullrich). *Neurotherapeutics,* 5**,** 613-8.

MEYER, A. J. & DICK, T. P. 2010. Fluorescent Protein-Based Redox Probes. *Antioxidants & Redox Signaling,* 13**,** 621-650.

MIEYAL, J. J., GALLOGLY, M. M., QANUNGO, S., SABENS, E. A. & SHELTON, M. D. 2008. Molecular mechanisms and clinical implications of reversible protein S-glutathionylation. *Antioxidants & redox signaling,* 10**,** 1941-1988.

MIGLIAVACCA, E., TAY, S. K. H., PATEL, H. P., SONNTAG, T., CIVILETTO, G., MCFARLANE, C., FORRESTER, T., BARTON, S. J., LEOW, M. K., ANTOUN, E., CHARPAGNE, A., SENG CHONG, Y., DESCOMBES, P., FENG, L., FRANCIS-EMMANUEL, P., GARRATT, E. S., GINER, M. P., GREEN, C. O., KARAZ, S., KOTHANDARAMAN, N., MARQUIS, J., METAIRON, S., MOCO, S., NELSON, G., NGO, S., PLEASANTS, T., RAYMOND, F., SAYER, A. A., MING SIM, C., SLATER-JEFFERIES, J., SYDDALL, H. E., FANG TAN, P., TITCOMBE, P., VAZ, C., WESTBURY, L. D., WONG, G., YONGHUI, W., COOPER, C., SHEPPARD, A., GODFREY, K. M., LILLYCROP, K. A., KARNANI, N. & FEIGE, J. N. 2019. Mitochondrial oxidative capacity and NAD+ biosynthesis are reduced in human sarcopenia across ethnicities. *Nature Communications,* 10**,** 5808.

MISHINA, N. M., TYURIN-KUZMIN, P. A., MARKVICHEVA, K. N., VOROTNIKOV, A. V., TKACHUK, V. A., LAKETA, V., SCHULTZ, C., LUKYANOV, S. & BELOUSOV, V. V. 2011. Does cellular hydrogen peroxide diffuse or act locally? *Antioxid Redox Signal,* 14**,** 1-7.

MISHRA, J., JHUN, B. S., HURST, S., O-UCHI, J., CSORDÁS, G. & SHEU, S.-S. 2017. The Mitochondrial Ca(2+) Uniporter: Structure, Function, and Pharmacology. *Handbook of experimental pharmacology,* 240**,** 129-156.

MISHRA, P., VARUZHANYAN, G., PHAM, A. H. & CHAN, D. C. 2015. Mitochondrial Dynamics is a Distinguishing Feature of Skeletal Muscle Fiber Types and Regulates Organellar Compartmentalization. *Cell metabolism,* 22**,** 1033-1044.

MONTEIRO, M., SILVA, A. F. R., RESENDE, D., BRAGA, S. S., COIMBRA, M. A., SILVA, A. M. S. & CARDOSO, S. M. 2021. Strategies to Broaden the Applications of Olive Biophenols Oleuropein and Hydroxytyrosol in Food Products. *Antioxidants,* 10**,** 444.

MONTERO, M., LOBATÓN, CARMEN D., HERNÁNDEZ-SANMIGUEL, E., SANTODOMINGO, J., VAY, L., MORENO, A. & ALVAREZ, J. 2004. Direct activation of the mitochondrial calcium uniporter by natural plant flavonoids. *Biochemical Journal,* 384**,** 19-24.

MOUCHIROUD, L., SORRENTINO, V., WILLIAMS, E. G., CORNAGLIA, M., FROCHAUX, M. V., LIN, T., NICOLET-DIT-FÉLIX, A. A., KRISHNAMANI, G., OUHMAD, T., GIJS, M. A. M., DEPLANCKE, B. & AUWERX, J. 2016. The Movement Tracker: A Flexible System for Automated Movement Analysis in Invertebrate Model Organisms. *Curr Protoc Neurosci,* 77**,** 8.37.1-8.37.21.

MUROI, H., HORI, K., TOKUTAKE, Y., HAKAMATA, Y., KAWABATA, F., TOYOMIZU, M. & KIKUSATO, M. 2022. Oleuropein suppresses mitochondrial reactive oxygen species generation possibly via an activation of transient receptor potential V1 and sirtuin-1 in cultured chicken muscle cells. *Animal Science Journal,* 93**,** e13677.

MURPHY, M. P. 2009. How mitochondria produce reactive oxygen species. *Biochem J,* 417**,** 1-13.

MURPHY, M. P. 2011. Mitochondrial Thiols in Antioxidant Protection and Redox Signaling: Distinct Roles for Glutathionylation and Other Thiol Modifications. *Antioxidants & Redox Signaling,* 16**,** 476-495.

MURPHY, M. P., HOLMGREN, A., LARSSON, N. G., HALLIWELL, B., CHANG, C. J., KALYANARAMAN, B., RHEE, S. G., THORNALLEY, P. J., PARTRIDGE, L., GEMS, D., NYSTRÖM, T., BELOUSOV, V., SCHUMACKER, P. T. & WINTERBOURN, C. C. 2011. Unraveling the biological roles of reactive oxygen species. *Cell Metab,* 13**,** 361-366.

NAKAYAMA, S. & KRETSINGER, R. H. 1994. Evolution of the EF-hand family of proteins. *Annu Rev Biophys Biomol Struct,* 23**,** 473-507.

NEDIANI, C., RUZZOLINI, J., ROMANI, A. & CALORINI, L. 2019. Oleuropein, a Bioactive Compound from Olea europaea L., as a Potential Preventive and Therapeutic Agent in Non-Communicable Diseases. *Antioxidants (Basel, Switzerland),* 8**,** 578.

NEMANI, N., SHANMUGHAPRIYA, S. & MADESH, M. 2018. Molecular regulation of MCU: Implications in physiology and disease. *Cell calcium,* 74**,** 86-93.

NETTO, L. E., KOWALTOWSKI, A. J., CASTILHO, R. F. & VERCESI, A. E. 2002. Thiol enzymes protecting mitochondria against oxidative damage. *Methods Enzymol,* 348**,** 260-70.

NOH, Y. H., BAEK, J. Y., JEONG, W., RHEE, S. G. & CHANG, T.-S. 2009. Sulfiredoxin Translocation into Mitochondria Plays a Crucial Role in Reducing Hyperoxidized Peroxiredoxin III*. *Journal of Biological Chemistry,* 284**,** 8470-8477.

NOTKINS, A. L. & LERNMARK, A. 2001. Autoimmune type 1 diabetes: resolved and unresolved issues. *J Clin Invest,* 108**,** 1247-52.

O'ROURKE, B., ASHOK, D. & LIU, T. 2021. Mitochondrial Ca²⁺ in heart failure: Not enough or too much? *Journal of Molecular and Cellular Cardiology,* 151**,** 126-134.

O-UCHI, J., PAN, S. & SHEU, S.-S. 2012. Molecular identities of mitochondrial Ca²⁺ influx mechanism: Updated passwords for accessing mitochondrial Ca²⁺-linked health and disease. *The Journal of General Physiology,* 139**,** 435-443.

PAILLARD, M., CSORDÁS, G., HUANG, K.-T., VÁRNAI, P., JOSEPH, S. K. & HAJNÓCZKY, G. 2018. MICU1 Interacts with the D-Ring of the MCU Pore to Control Its Ca(2+) Flux and Sensitivity to Ru360. *Molecular cell,* 72**,** 778-785.e3.

PALLAFACCHINA, G., ZANIN, S. & RIZZUTO, R. 2018. Recent advances in the molecular mechanism of mitochondrial calcium uptake. *F1000Res,* 7.

PALLAFACCHINA, G., ZANIN, S. & RIZZUTO, R. 2021. From the Identification to the Dissection of the Physiological Role of the Mitochondrial Calcium Uniporter: An Ongoing Story. *Biomolecules,* 11.

PAN, X., LIU, J., NGUYEN, T., LIU, C., SUN, J., TENG, Y., FERGUSSON, M. M., ROVIRA, II, ALLEN, M., SPRINGER, D. A., APONTE, A. M., GUCEK, M., BALABAN, R. S., MURPHY, E. & FINKEL, T. 2013. The physiological role of mitochondrial calcium revealed by mice lacking the mitochondrial calcium uniporter. *Nat Cell Biol,* 15**,** 1464-72.

PATRON, M., GRANATIERO, V., ESPINO, J., RIZZUTO, R. & DE STEFANI, D. 2019. MICU3 is a tissue-specific enhancer of mitochondrial calcium uptake. *Cell Death Differ,* 26**,** 179-195.

PATRON, M., RAFFAELLO, A., GRANATIERO, V., TOSATTO, A., MERLI, G., DE STEFANI, D., WRIGHT, L., PALLAFACCHINA, G., TERRIN, A., MAMMUCARI, C. & RIZZUTO, R. 2013. The mitochondrial calcium uniporter (MCU): molecular identity and physiological roles. *J Biol Chem,* 288**,** 10750-8.

PAUPE, V., PRUDENT, J., DASSA, EMMANUEL P., RENDON, OLGA Z. & SHOUBRIDGE, ERIC A. 2015. CCDC90A (MCUR1) Is a Cytochrome c Oxidase Assembly Factor and Not a Regulator of the Mitochondrial Calcium Uniporter. *Cell Metabolism,* 21**,** 109-116.

PEARSON, T., KABAYO, T., NG, R., CHAMBERLAIN, J., MCARDLE, A. & JACKSON, M. J. 2014. Skeletal Muscle Contractions Induce Acute Changes in Cytosolic Superoxide, but Slower Responses in Mitochondrial Superoxide and Cellular Hydrogen Peroxide. *PLOS ONE,* 9**,** e96378.

PENDIN, D., NORANTE, R., DE NADAI, A., GHERARDI, G., VAJENTE, N., BASSO, E., KALUDERCIC, N., MAMMUCARI, C., PARADISI, C., POZZAN, T. & MATTAREI, A. 2019. A Synthetic Fluorescent

Mitochondria-Targeted Sensor for Ratiometric Imaging of Calcium in Live Cells. *Angewandte Chemie International Edition,* 58**,** 9917-9922.

PFEFFERLE, A., MAILLOUX, R. J., ADJEITEY, C. N.-K. & HARPER, M.-E. 2013. Glutathionylation of UCP2 sensitizes drug resistant leukemia cells to chemotherapeutics. *Biochimica et Biophysica Acta (BBA) - Molecular Cell Research,* 1833**,** 80-89.

PHILLIPS, C. B., TSAI, C.-W. & TSAI, M.-F. 2019. The conserved aspartate ring of MCU mediates MICU1 binding and regulation in the mitochondrial calcium uniporter complex. *eLife,* 8**,** e41112.

PINTON, P. 2018. Mitochondria-associated membranes (MAMs) and pathologies. *Cell Death & Disease,* 9**,** 413.

POLJSAK, B., ŠUPUT, D. & MILISAV, I. 2013. Achieving the balance between ROS and antioxidants: when to use the synthetic antioxidants. *Oxid Med Cell Longev,* 2013**,** 956792.

PRAKASH, Y. S., PABELICK, C. M. & SIECK, G. C. 2017. Mitochondrial Dysfunction in Airway Disease. *Chest,* 152**,** 618-626.

PRINCE, R. J. & SINE, S. M. 1999. Acetylcholine and Epibatidine Binding to Muscle Acetylcholine Receptors Distinguish between Concerted and Uncoupled Models*. *Journal of Biological Chemistry,* 274**,** 19623-19629.

PUGH, J. N., STRETTON, C., MCDONAGH, B., BROWNRIDGE, P., MCARDLE, A., JACKSON, M. J. & CLOSE, G. L. 2021. Exercise stress leads to an acute loss of mitochondrial proteins and disruption of redox control in skeletal muscle of older subjects: An underlying decrease in resilience with aging? *Free Radical Biology and Medicine,* 177**,** 88-99.

RAFFAELLO, A., FENO, S., REANE, D. V., MUNARI, F., VALLESE, F., VIOLA, A. & RIZZUTO, R. 2020. Role of Mitochondrial Calcium in the Maintenance of Skeletal Muscle Homeostasis. *The FASEB Journal,* 34**,** 1-1.

RAMOT, D., JOHNSON, B. E., BERRY, T. L., JR., CARNELL, L. & GOODMAN, M. B. 2008. The Parallel Worm Tracker: A Platform for Measuring Average Speed and Drug-Induced Paralysis in Nematodes. *PLOS ONE,* 3**,** e2208.

REGGIANI, C. 2021. Caffeine as a tool to investigate sarcoplasmic reticulum and intracellular calcium dynamics in human skeletal muscles. *Journal of Muscle Research and Cell Motility,* 42**,** 281-289.

REQUEJO, R., HURD, T. R., COSTA, N. J. & MURPHY, M. P. 2010. Cysteine residues exposed on protein surfaces are the dominant intramitochondrial thiol and may protect against oxidative damage. *Febs j,* 277**,** 1465-80.

RIEMER, J., SCHWARZLANDER, M., CONRAD, M. & HERRMANN, J. M. 2015. Thiol switches in mitochondria: operation and physiological relevance. *Biol Chem,* 396**,** 465-82.

RISTOW, M., ZARSE, K., OBERBACH, A., KLÖTING, N., BIRRINGER, M., KIEHNTOPF, M., STUMVOLL, M., KAHN, C. R. & BLÜHER, M. 2009. Antioxidants prevent health-promoting effects of physical exercise in humans. *Proc Natl Acad Sci U S A,* 106**,** 8665-70.

RIZZUTO, R., DE STEFANI, D., RAFFAELLO, A. & MAMMUCARI, C. 2012. Mitochondria as sensors and regulators of calcium signalling. *Nat Rev Mol Cell Biol,* 13**,** 566-78.

ROZEN, S. & SKALETSKY, H. 2000. Primer3 on the WWW for general users and for biologist programmers. *Methods Mol Biol,* 132**,** 365-86.

RYDSTRÖM, J. 2006. Mitochondrial NADPH, transhydrogenase and disease. *Biochimica et Biophysica Acta (BBA) - Bioenergetics,* 1757**,** 721-726.

RYU, S.-Y., BEUTNER, G., DIRKSEN, R. T., KINNALLY, K. W. & SHEU, S.-S. 2010. Mitochondrial ryanodine receptors and other mitochondrial Ca2+ permeable channels. *FEBS Letters,* 584**,** 1948-1955.

SABENS LIEDHEGNER, E. A., GAO, X.-H. & MIEYAL, J. J. 2012. Mechanisms of altered redox regulation in neurodegenerative diseases--focus on S--glutathionylation. *Antioxidants & redox signaling,* 16**,** 543-566.

SAKELLARIOU, G. K., VASILAKI, A., PALOMERO, J., KAYANI, A., ZIBRIK, L., MCARDLE, A. & JACKSON, M. J. 2013. Studies of mitochondrial and nonmitochondrial sources implicate nicotinamide adenine

dinucleotide phosphate oxidase(s) in the increased skeletal muscle superoxide generation that occurs during contractile activity. *Antioxid Redox Signal,* 18**,** 603-21.

SANTO-DOMINGO, J. & DEMAUREX, N. 2010. Calcium uptake mechanisms of mitochondria. *Biochimica et Biophysica Acta (BBA) - Bioenergetics,* 1797**,** 907-912.

SANTO-DOMINGO, J., WIEDERKEHR, A. & DE MARCHI, U. 2015. Modulation of the matrix redox signaling by mitochondrial Ca(2.). *World journal of biological chemistry,* 6**,** 310-323.

SANTOS, A. L., SINHA, S. & LINDNER, A. B. 2018. The Good, the Bad, and the Ugly of ROS: New Insights on Aging and Aging-Related Diseases from Eukaryotic and Prokaryotic Model Organisms. *Oxid Med Cell Longev,* 2018**,** 1941285.

SANTULLI, G. & MARKS, A. R. 2015. Essential Roles of Intracellular Calcium Release Channels in Muscle, Brain, Metabolism, and Aging. *Curr Mol Pharmacol,* 8**,** 206-22.

SARBISHEGI, M., MEHRAEIN, F. & SOLEIMANI, M. 2014. Antioxidant role of oleuropein on midbrain and dopaminergic neurons of substantia nigra in aged rats. *Iranian biomedical journal,* 18**,** 16-22.

SAYIN, V. I., IBRAHIM, M. X., LARSSON, E., NILSSON, J. A., LINDAHL, P. & BERGO, M. O. 2014. Antioxidants accelerate lung cancer progression in mice. *Sci Transl Med,* 6**,** 221ra15.

SCHINDELIN, J., ARGANDA-CARRERAS, I., FRISE, E., KAYNIG, V., LONGAIR, M., PIETZSCH, T., PREIBISCH, S., RUEDEN, C., SAALFELD, S., SCHMID, B., TINEVEZ, J.-Y., WHITE, D. J., HARTENSTEIN, V., ELICEIRI, K., TOMANCAK, P. & CARDONA, A. 2012. Fiji: an open-source platform for biological-image analysis. *Nature Methods,* 9**,** 676-682.

SCHWARZLANDER, M., DICK, T. P., MEYER, A. J. & MORGAN, B. 2016. Dissecting Redox Biology Using Fluorescent Protein Sensors. *Antioxid Redox Signal,* 24**,** 680-712.

SEN, C. K. 1995. Oxidants and antioxidants in exercise. *Journal of Applied Physiology,* 79**,** 675-686.

SHASHA, B. & LEIBOWITZ, J. 1959. Oleuropeic Acid: a New Compound from Olea europæa. *Nature,* 184**,** 2019-2020.

SHUTT, T., GEOFFRION, M., MILNE, R. & MCBRIDE, H. M. 2012. The intracellular redox state is a core determinant of mitochondrial fusion. *EMBO reports,* 13**,** 909-915.

SIES, H. 2017. Hydrogen peroxide as a central redox signaling molecule in physiological oxidative stress: Oxidative eustress. *Redox Biol,* 11**,** 613-619.

SMITH, R. A. J., HARTLEY, R. C., COCHEMÉ, H. M. & MURPHY, M. P. 2012. Mitochondrial pharmacology. *Trends in Pharmacological Sciences,* 33**,** 341-352.

SNOW, B. J., ROLFE, F. L., LOCKHART, M. M., FRAMPTON, C. M., O'SULLIVAN, J. D., FUNG, V., SMITH, R. A., MURPHY, M. P. & TAYLOR, K. M. 2010. A double-blind, placebo-controlled study to assess the mitochondria-targeted antioxidant MitoQ as a disease-modifying therapy in Parkinson's disease. *Mov Disord,* 25**,** 1670-4.

ST-PIERRE, J., DRORI, S., ULDRY, M., SILVAGGI, J. M., RHEE, J., JÄGER, S., HANDSCHIN, C., ZHENG, K., LIN, J., YANG, W., SIMON, D. K., BACHOO, R. & SPIEGELMAN, B. M. 2006. Suppression of Reactive Oxygen Species and Neurodegeneration by the PGC-1 Transcriptional Coactivators. *Cell,* 127**,** 397-408.

STEWART, J. J. P. 2007. Optimization of parameters for semiempirical methods V: Modification of NDDO approximations and application to 70 elements. *Journal of Molecular Modeling,* 13**,** 1173-1213.

SZENTESI, P., CSERNOCH, L., DUX, L. & KELLER-PINTÉR, A. 2019. Changes in Redox Signaling in the Skeletal Muscle with Aging. *Oxidative medicine and cellular longevity,* 2019**,** 4617801-4617801.

TANGANELLI, F., MEINKE, P., HOFMEISTER, F., JARMUSCH, S., BABER, L., MEHAFFEY, S., HINTZE, S., FERRARI, U., NEUERBURG, C., KAMMERLANDER, C., SCHOSER, B. & DREY, M. 2021. Type-2 muscle fiber atrophy is associated with sarcopenia in elderly men with hip fracture. *Experimental Gerontology,* 144**,** 111171.

TARASOV, A. I., SEMPLICI, F., RAVIER, M. A., BELLOMO, E. A., PULLEN, T. J., GILON, P., SEKLER, I., RIZZUTO, R. & RUTTER, G. A. 2012. The Mitochondrial Ca2+ Uniporter MCU Is Essential for Glucose-Induced ATP Increases in Pancreatic β-Cells. *PLOS ONE,* 7**,** e39722.

TERRITO, P. R., MOOTHA, V. K., FRENCH, S. A. & BALABAN, R. S. 2000. Ca(2+) activation of heart mitochondrial oxidative phosphorylation: role of the F(0)/F(1)-ATPase. *Am J Physiol Cell Physiol,* 278**,** C423-35.

THEODOROU, A. A., NIKOLAIDIS, M. G., PASCHALIS, V., KOUTSIAS, S., PANAYIOTOU, G., FATOUROS, I. G., KOUTEDAKIS, Y. & JAMURTAS, A. Z. 2011. No effect of antioxidant supplementation on muscle performance and blood redox status adaptations to eccentric training. *Am J Clin Nutr,* 93**,** 1373-83.

TOMAR, D., DONG, Z., SHANMUGHAPRIYA, S., KOCH, DIANA A., THOMAS, T., HOFFMAN, NICHOLAS E., TIMBALIA, SHRISHIV A., GOLDMAN, SAMUEL J., BREVES, SARAH L., CORBALLY, DANIEL P., NEMANI, N., FAIRWEATHER, JOSEPH P., CUTRI, ALLISON R., ZHANG, X., SONG, J., JAÑA, F., HUANG, J., BARRERO, C., RABINOWITZ, JOSEPH E., LUONGO, TIMOTHY S., SCHUMACHER, SARAH M., ROCKMAN, M. E., DIETRICH, A., MERALI, S., CAPLAN, J., STATHOPULOS, P., AHIMA, REXFORD S., CHEUNG, JOSEPH Y., HOUSER, STEVEN R., KOCH, WALTER J., PATEL, V., GOHIL, VISHAL M., ELROD, JOHN W., RAJAN, S. & MADESH, M. 2016. MCUR1 Is a Scaffold Factor for the MCU Complex Function and Promotes Mitochondrial Bioenergetics. *Cell Reports,* 15**,** 1673-1685.

TRAYNOR, J. R. 1998. Epibatidine and pain. *British Journal of Anaesthesia,* 81**,** 69-76.

VAIS, H., TANIS, J. E., MULLER, M., PAYNE, R., MALLILANKARAMAN, K. & FOSKETT, J. K. 2015. MCUR1, CCDC90A, Is a Regulator of the Mitochondrial Calcium Uniporter. *Cell Metab,* 22**,** 533-5.

VECELLIO REANE, D., CERQUA, C., SACCONI, S., SALVIATI, L., TREVISSON, E. & RAFFAELLO, A. 2022. The Splicing of the Mitochondrial Calcium Uniporter Genuine Activator MICU1 Is Driven by RBFOX2 Splicing Factor during Myogenic Differentiation. *International Journal of Molecular Sciences,* 23.

VECELLIO REANE, D., VALLESE, F., CHECCHETTO, V., ACQUASALIENTE, L., BUTERA, G., DE FILIPPIS, V., SZABÒ, I., ZANOTTI, G., RIZZUTO, R. & RAFFAELLO, A. 2016. A MICU1 Splice Variant Confers High Sensitivity to the Mitochondrial Ca²⁺ Uptake Machinery of Skeletal Muscle. *Molecular Cell,* 64**,** 760-773.

VISIOLI, F., DE LA LASTRA, C. A., ANDRES-LACUEVA, C., AVIRAM, M., CALHAU, C., CASSANO, A., D'ARCHIVIO, M., FARIA, A., FAVÉ, G., FOGLIANO, V., LLORACH, R., VITAGLIONE, P., ZORATTI, M. & EDEAS, M. 2011. Polyphenols and human health: a prospectus. *Crit Rev Food Sci Nutr,* 51**,** 524-46.

WANG, L., YANG, X., LI, S., WANG, Z., LIU, Y., FENG, J., ZHU, Y. & SHEN, Y. 2014. Structural and mechanistic insights into MICU1 regulation of mitochondrial calcium uptake. *The EMBO journal,* 33**,** 594-604.

WANG, Y., LUO, S., LUO, J., QU, J., FENG, S., CHEN, T., ZHOU, L., YUAN, M., YANG, H., LI, T., LAN, B. & DING, C. 2021. Preparation of Hydroxytyrosol by Acid Hydrolysis from Olive Leaves. *Separations,* 8**,** 159.

WEISER, A., FEIGE, J. N. & DE MARCHI, U. 2021. Mitochondrial Calcium Signaling in Pancreatic β-Cell. *International journal of molecular sciences,* 22**,** 2515.

WEYER, C., BOGARDUS, C., MOTT, D. M. & PRATLEY, R. E. 1999. The natural history of insulin secretory dysfunction and insulin resistance in the pathogenesis of type 2 diabetes mellitus. *J Clin Invest,* 104**,** 787-94.

XIONG, Y., UYS, J. D., TEW, K. D. & TOWNSEND, D. M. 2011. S-glutathionylation: from molecular mechanisms to health outcomes. *Antioxidants & redox signaling,* 15**,** 233-270.

XU, S. & CHISHOLM, A. D. 2014. C. elegans epidermal wounding induces a mitochondrial ROS burst that promotes wound repair. *Dev Cell,* 31**,** 48-60.

YAN, L.-J., SUMIEN, N., THANGTHAENG, N. & FORSTER, M. J. 2013. Reversible inactivation of dihydrolipoamide dehydrogenase by mitochondrial hydrogen peroxide. *Free Radical Research,* 47**,** 123-133.

YANG, Y.-F., YANG, W., LIAO, Z.-Y., WU, Y.-X., FAN, Z., GUO, A., YU, J., CHEN, Q.-N., WU, J.-H., ZHOU, J. & XIAO, Q. 2021. MICU3 regulates mitochondrial Ca2+-dependent antioxidant response in skeletal muscle aging. *Cell Death & Disease,* 12**,** 1115.

YOO, S.-Z., NO, M.-H., HEO, J.-W., PARK, D.-H., KANG, J.-H., KIM, S. H. & KWAK, H.-B. 2018. Role of exercise in age-related sarcopenia. *Journal of exercise rehabilitation,* 14**,** 551-558.

ZAMPIERI, S., MAMMUCARI, C., ROMANELLO, V., BARBERI, L., PIETRANGELO, L., FUSELLA, A., MOSOLE, S., GHERARDI, G., HÖFER, C., LÖFLER, S., SARABON, N., CVECKA, J., KRENN, M., CARRARO, U., KERN, H., PROTASI, F., MUSARÒ, A., SANDRI, M. & RIZZUTO, R. 2016. Physical exercise in aging human skeletal muscle increases mitochondrial calcium uniporter expression levels and affects mitochondria dynamics. *Physiological reports,* 4**,** e13005.

ZHAO, Y., HU, X., LIU, Y., DONG, S., WEN, Z., HE, W., ZHANG, S., HUANG, Q. & SHI, M. 2017. ROS signaling under metabolic stress: cross-talk between AMPK and AKT pathway. *Molecular Cancer,* 16**,** 79.

ZIAALDINI, M. M., MARZETTI, E., PICCA, A. & MURLASITS, Z. 2017. Biochemical Pathways of Sarcopenia and Their Modulation by Physical Exercise: A Narrative Review. *Frontiers in medicine,* 4**,** 167-167.

ZURLO, F., LARSON, K., BOGARDUS, C. & RAVUSSIN, E. 1990. Skeletal muscle metabolism is a major determinant of resting energy expenditure. *J Clin Invest,* 86**,** 1423-7.

Section 7: Appendix

7.1. List of Figures

7.2. List of Tables

7.4. List of Abbreviations

∆Ψm	Mitochondrial membrane potential
AChR	Acetylcholine receptor
Aldh2	Aldehyde-dehydrogenase 2
ALMI	Low appendicular lean mass index
AMPK	Adenosine monophosphate-activated protein kinase
ANT	Adenine nucleotide translocase
AntiA	Antimycin A
AUC	Area under the curve
BCATm	Mitochondrial branched-chain amino transferase
Ca2+	Calcium
cADPR	Cyclic ADP ribose
Cyp-D	Cyclophilin D
DTT	Dithiothreitol
EMRE	Essential mitochondrial Ca^{2+} uniporter regulator
ER	Endoplasmic reticulum
ETC	Electron transport chain
FMN	Flavin mononucleotide
GPCR	G-protein coupled receptor
GPx	Glutathione-peroxidase
GR	Glutathione reductase
Grx	Glutaredoxin
GSH	Reduced glutathione
GSNO	Nitrosoglutathione
GSSG	Oxidized glutathione
H_2O_2	Hydrogen peroxide
HCX	Proton-calcium exchanger
IC-DH	Isocitrate dehydrogenase
IMM	Inner mitochondrial membrane
IMS	Intermembrane space
IP3	Inositol-trisphosphate
IP3R	IP3-Receptor
Letm1	Leucine-zipper-EF hand-containing transmembrane region
MAMs	Mitochondrial associated membranes

MAPK	Mitogen activated protein kinase
MCU	Mitochondrial calcium uniporter
MCU-kd	MCU knockdown
MCU-KO	MCU knockout
MCUR1	Mitochondrial calcium uniporter regulator 1
MCUR1-kd	MCUR1-knockdown
MDk	Molecular docking
MDy	Molecular dynamics
MEF	Mouse embryonic fibroblasts
Mfn	Mitofusin
MICU	Mitochondrial calcium uptake
MICU1-kd	MICU1 knockdown
MICU1-KO	MICU1 knockout
MPTP	Mitochondrial permeability transition pore
mRyR1	Mitochondrial type 1 ryanodine receptor
mtDNA	Mitochondrial DNA
mtPQ	Mitochondrial paraquat
NaN_3	Sodium azide
NCLX	Sodium-calcium exchanger
NIHS	Nestlé Institute of Health Sciences
NMDA	N-methyl-D-aspartate receptor
NNT	Nicotinamide-nucleotide-transhydrogenase
NO	Nitric oxide
NOX/DUOX	NADPH oxidase enzymes
NRF2	Nuclear respiratory factor2
OCR	Oxygen consumption rate
Oligo	Oligomycin
OMM	Outer mitochondrial membrane
$ONOO^{\bullet-}$	Peroxynitrite anion
PDH	Pyruvate dehydrogenase
PDK	Pyruvate dehydrogenase kinase
PDP1	Pyruvate dehydrogenase phosphatase isoform 1
PGC-1α	Peroxisome proliferator-activated receptor gamma coactivator-1 alpha
PLC	Phospholipase C
PMCA	Plasma membrane calcium ATPases

Prx	Peroxiredoxin
RaM	Rapid mode of calcium uptake
RET	Respiratory complex I-mediated reverse electron transfer
RMSD	Root Main Square Deviation
roGFP	Reduction-oxidation-sensitive green fluorescent protein
ROS	Reactive oxygen species
Rot	Rotenone
rxYFP	Reduction-oxidation-sensitive yellow fluorescent protein
RyR	Ryanodine receptor
SERCA	Sarco-/endoplasmic reticulum calcium ATPases
SOCE	Store-operated calcium entry
SOD1	Cytosolic and IMS sodium dismutase
SOD2	Mitochondrial superoxide dismutase
SR	Sarcoplasmic reticulum
Srx	Sulfiredoxin
STIM	Stromal interaction molecule
T2D	Type 2 diabetes
TCA	Tricarboxylic acid cycle
TDH	Proton translocating transhydrogenase
TPP	Trophenylphosphonium
TRPC	Transient receptor potential channels
Trx_{ox}/Trx_{red}	$Thioredoxin_{ox}/thioredoxin_{red}$
TrxR	Selenoprotein thioredoxin reductase
UCP	Uncoupling protein
VDAC	Voltage dependent anion carrier
VOCC	Voltage-operated calcium channels
XO	Xanthine oxidase
αKG-DH	α-ketoglutarate dehydrogenase